A study of fibroblast-mediated contraction in ocular scarring: gene expression profiling and the role of small GTPases in Matrix Metalloproteinase 1 (MMP1) regulation

He Li

This thesis is submitted to University College London for the degree of Doctor of Philosophy in Cell Biology

2017

Supervisors:

Dr. Maryse Bailly

Prof. Sir. Peng Tee Khaw

UCL Institute of Ophthalmology

11-43 Bath Street,

London EC1V 9EL

Declaration

I, He Li, confirm that the work presented in this thesis is my own. Where information has been derived from other sources, I confirm that this has been indicated in the thesis.

Abstract

Understanding the molecular mechanisms involved in fibroblast-mediated tissue contraction is essential for developing future therapeutics for anti-scaring and fibrosis treatment not only for eyes, but also for a wide range of fibrotic diseases. The small Rho GTPase Rac1 is a master regulator of actin dynamics, which plays an essential role in protrusive activity, tissue repair and wound healing. A genome wide microarray study was performed with/without the transient treatment of human conjunctival fibroblasts with Rac1 inhibitor NSC23766 in a collagen gel contraction model to unveil the signalling events underlying contractile activity and the contribution of Rac1 activation. Through a comprehensive analysis that combined a pilot parallel study of scarring in an *in vivo* model in rabbit following glaucoma filtration surgery, and previously obtained microarray data of human ocular fibrotic diseases (including trachoma and thyroid-associated orbitopathy), it was identified that the contraction process consisted of two phases: an early phase that exhibited a classic serum/wound response profile with upregulation of genes related to inflammation, matrix remodelling, and transcription activation; and a late stage when the hyperactive signal receded and the gene profile progressed to promote fibrosis. The transient treatment with NSC23766 altered gene expression, and the early inhibition of Rac1 blocked the fibroblasts from entering the contractile phenotype as a whole. Interestingly, NSC23766 did not supress the mRNA expression of Matrix Metalloproteinase (MMP) 1, 3 and 10 during contraction, but reduced their enzymatic activity. The link between the activation of the Rho GTPase and MMP expression was subsequently investigated using MMP1 as an example. The results showed Rac1, Cdc42 and RhoA differently regulated MMP1 expression and secretion in fibroblasts during contraction, suggesting that the rate-limiting step for

modulating MMP is the release in the extracellular medium rather than expression levels, drawing some interesting new prospects for therapies.

Acknowledgments

I would like to thank both of my primary and secondary supervisors, Dr. Maryse Bailly and Prof. Sir. Peng T. Khaw, for providing ultimate support, guidance, and mentoring throughout my PhD. Many thanks to Lady Peggy Khaw who very kindly provided help and guidance. I much appreciate Dr. Victoria Tovell's contribution to the samples preparation work for the human conjunctival fibroblasts microarray. My thanks to Dr. David Simpson (Queen's University Belfast) for advice on techniques to analyse the microarray data. Thanks to Dr. Daniel Paull who performed the *in vivo* microarray and Dr. Jian-Liang Li (Sanford Burnham Prebys Medical Discovery Institute) who analysed the *in vivo* data. Many thanks to Ms. Diana Sefic-Svara who helped me a lot with the microscopy work. Thanks to Dr. Y. Itoh (University of Oxford) who kindly provided the in-house produced anti-MMP1 antibody. Thanks to Prof. Gregg B. Fields (Florida Atlantic University) who kindly provided the full-length MMP1 vector. Thanks to all of my group members (past and current) including Dr. Caroline Fittchet, Ms. Kasia Kozdon, Dr. Cynthia Yu-Wai-Man and Dr. Y-Hui Yang for the general support and help kindly provided. I would especially like to thank Dr. Zanetta Kechagia and Dr. Garima Sharma--without your company, those late nights and weekends in the lab would have been so long and lonely.

Thanks to my parents, without whose love and support I would not be able to do anything. Thanks to Jun who is so supportive to my work and life.

Table of Contents

Abbreviations

2D	Two-dimensional space
3D	Three-dimensional space
Akt	Protein Kinase B
APMA	4-aminophenylmercuric acetate
BSA	Bovine serum albumin
cDNA	Complementary DNA
CID	Corrected integrated density
CNS	Central nervous system
DAVID	The Database for Annotation, Visualization and Integrated Discovery
DMSO	Dimethyl sulfoxide
DNA	Deoxyribonucleic acid
DPBS	Dulbecco's phosphate-buffered saline
ECM	Extracellular matrix
EGF	Epidermal growth factor
ELISA	Enzyme-linked immunosorbent assay
ERK	Extracellular-signal-regulated kinase
FBS	Fetal bovine serum
FES	Floppy eye syndrome
GAP	GTPase-activating proteins
GDI	Guanine nucleotide dissociation inhibitor
gDNA	Genomic DNA
GDP	Guanosine diphosphate
GEF	Guanine nucleotide exchange factors
GFP	Green fluorescent protein
GFS	Glaucoma filtration surgery
GTP	Guanosine triphosphate
His-tag	Polyhistidine-tag
HTF	Human Tenon's fibroblast
IC50	The half maximal inhibitory concentration
IOP	Intraocular pressure
mAChRs	Muscarinic acetylcholine receptors
MAPK	Mitogen-activated protein kinase
MMP	Matrix metalloproteinase
mRNA	Messenger RNA
mTORC2	Mammalian target of rapamycin complex 2
PBS	Phosphate buffered saline
PCA	Principal component analysis
PCR	Polymerase chain reaction
PDGF	Platelet-derived growth factor
PI3K	Phosphatidylinositol-4,5-bisphosphate 3-kinase
RMA	Robust multi-array average
ROCK	Rho-associated protein kinase
qPCR	Quantitative real time polymerase chain reaction

SEM	The standard error of the mean
TBS	Tris-buffered saline
TBS-T	Tris-buffered saline, 0.1% Tween 20
TED	Thyroid-associated orbitopathy
TGFα	Transforming growth factor alpha
TGFβ	Transforming growth factor beta

List of Figures

Chapter 1

Chapter 3

Chapter 4

Chapter 5

Chapter 6

List of Tables

Chapter 1

Chapter 2

Chapter 3

Chapter 4

Chapter 5

Chapter 1 Introduction

1.1 Wound healing

Wound healing is the process by which body tissue repairs itself after injury. It is a complicated but well-organised process. With the goal of restoring tissue homeostasis and architecture after insult, tissue repair starts immediately after wounding by synthesising a fibrous extracellular matrix (ECM) to replace lost or damaged tissue. The newly deposited ECM is then re-modelled over time to emulate normal tissue. The process is an orchestrated biological phenomena that consists of three sequential and predictable phases: blood clotting (homeostasis) and inflammation, tissue growth (proliferation), and tissue remodelling (maturation) (**Figure 1.1**) (Clark, 1996, Stadelmann et al., 1998, Singer and Clark, 1999).

1.1.1 Blood clotting and inflammation

Immediately after wounding, platelets in the blood are activated upon contact with the collagen exposed from damaged endothelium. They stick to the injury site by binding to the extracellular matrix via their collagen-specific glycoprotein surface receptors. The platelets change into amorphous shape and aggregate to form a plug to prevent further bleeding. A series of clotting factors released by platelets trigger the activation of the zymogen prothrombin into thrombin, which in turn catalyses the conversion of the soluble plasma protein fibrinogen into insoluble fibrous fibrin. The polymerized fibrin forms a mesh of fibres around the platelet plug to build a temporary clot (Pallister and Watson, 2011). The clot is also the main structural support for the wound until the deposition of newly formed collagen, which

serves to induce homeostasis and provides a matrix for the inflammatory cells. Meanwhile, platelets release mediators into the blood, including growth factors such as epidermal growth factor (EGF), platelet-derived growth factor (PDGF), transforming growth factor beta (TGFβ) and numerous cytokines, which promote the recruitment of inflammatory leukocytes from the bloodstream to the site of injury. Within an hour of wounding, infiltrating neutrophils are attracted to the site. They phagocytose debris, remove contaminating bacteria by releasing free radicals, and cleanse the wound by producing proteases that break down the damaged tissue. Thereafter, they undergo apoptosis or are phagocytosed by macrophages, which are differentiated from monocytes and play important roles in amplifying inflammatory response and tissue debridement. Two days after injury, macrophages become the predominant cells in the wound, where they stimulate the re-epithelialisation process, initiate the development of granulation tissue and release a variety of pro-inflammatory cytokines. These cytokines include IL-1 and IL-6, and growth factors such as fibroblast growth factor (FGF), EGF, TGFβ and PDGF, which lead to the next stage of the wound healing process (Rasche, 2001, Versteeg et al., 2013, Midwood et al., 2004, Martin and Leibovich, 2005, Greenhalgh, 1998).

1.1.2 Tissue growth (Proliferation)

The proliferation phase commences even before the inflammatory phase has ended. In this stage, re-epithelialisation, neovascularisation, granulation tissue formation, collagen deposition and wound contraction occur. Following the release of growth factors and cytokines at the wound site, the epithelial cells migrate and proliferate, resulting in re-epithelialisation to achieve wound closure. Neovascularisation, which is the process of angiogenesis, starts concurrently with the migration and proliferation of fibroblasts, endothelial cells, and macrophages. The vascular endothelial growth factor (VEGF) and FGF secreted by macrophages

promote the formation of new blood vessels by endothelial cells. Neovascularisation is imperative for other stages in wound healing, as it provides the oxygen and nutrients that are required by active fibroblasts and epithelial cells.

Simultaneously with angiogenesis, the formation of granulation tissue starts approximately four days after injury. Fibroblasts are attracted by the growth and chemotactic factors produced by macrophage and mast cells, and they infiltrate and accumulate at the site of the wound. Their numbers peak at one to two weeks post-wounding, and eventually they become the main residential cells in the site. By depositing fibronectin and collagen, fibroblasts grow and form a new, provisional ECM that not only allows all the cells involved in the process to attach to, grow and differentiate, but also facilitates their further migration. Later this provisional matrix will be replaced with a matrix that closely resembles the previous non-injured tissue. At the same time, fibroblasts also secrete growth factors to attract other cell types to the wound site.

A key phase of wound healing is contraction, which occurs approximately a week after injury, and initially starts without the involvement of myofibroblasts. Later on, upon the induction of TGFβ and PDGF, fibroblasts phenotypically differentiate into myofibroblasts that express alpha smooth muscle actin (α-SMA), which is normally found in smooth muscle cells. Myofibroblasts move along the fibronectin/fibrin provisional ECM to reach the wound borders, where they align themselves and form connections to the ECM to generate a constrictive mechanical force to cause wound closure, while fibroblasts continue to lay down collagen to reinforce the wound. At this stage, the wound closes more quickly due to the presence of myofibroblasts than it does in the first, non-differentiated fibroblast-dependent stage. Finally, the

wound edges are pulled together as the synthesis of new collagen and the degradation of the old matrix become equal, and the tensional homeostasis is restored. Fibroblasts gradually stop contracting and undergo apoptosis, which signals the beginning of the maturation phase (Falanga, 2005, Kondo and Ishida, 2010, Chang et al., 2004, Stadelmann et al., 1998, Ruszczak, 2003, Mirastschijski et al., 2004, Deodhar and Rana, 1997, Hinz, 2006, Greenhalgh, 1998).

1.1.3 Tissue remodelling (maturation)

During the maturation period, the granulation tissue formed in the tissue growth is replaced by a framework of collagen and elastin fibres, which are saturated with proteoglycans and glycoproteins. The tissue then remodels with the synthesis of new collagen, and the rearrangement of the originally disorganised collagen fibres that are cross-linked and aligned along tension lines. The final product of this procedure is scar tissue, which is formed as a result of the continued synthesis and catabolism of collagen. The key regulators of the collagen degradation are matrix metalloproteinases (MMPs), which are secreted by macrophages, epidermal cells, and endothelial cells, as well as fibroblasts. The maturation phase lasts from a few weeks to a year or longer, depending on the type of the wound (Morton and Phillips, 2016, Kondo and Ishida, 2010, Sethi et al., 2002).

These steps of wound healing do not occur in series but rather considerably overlap with each other. Recently, a parallel model has been suggested that divides the wound healing process into two stages: an early phase that leads to the homeostasis and formation of the provisional matrix, and a cellular phase in which the multiple cell types work together to order inflammation, re-epithelisation and remodelling (Orgill, 2009).

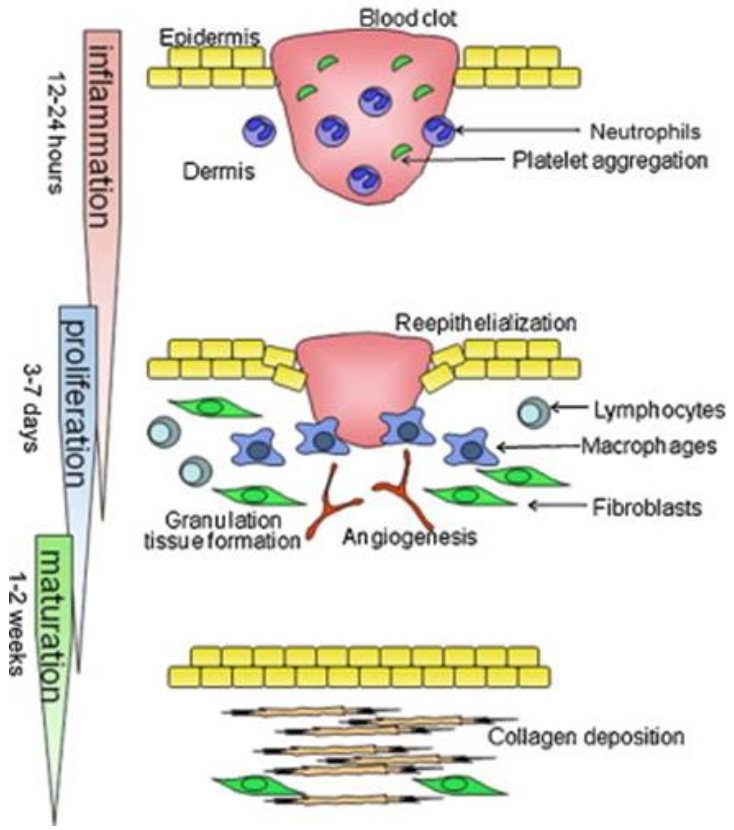

Figure 1.1 The phases of wound healing process.

Wound healing is a complicated but well-organised process including inflammation, proliferation, and maturation, with a number of cells and many cytokines, growth factors and proteases closely involved. The final product of this procedure is scar tissue, which forms as a result of the formation and contraction of a new fibrous extracellular matrix that replaces the previous lost or damaged tissue (figure adapted from (Kondo and Ishida, 2010)).

1.2 Fibrosis and scarring

Fibrosis is characterised by the production and accumulation of excessive fibrous connective tissue in response to wounding, and can be a reactive, benign, or pathological state (Birbrair et al., 2014). Derived through exaggerated wound

healing process, fibrosis causes the formation of scar tissue that is rich in extracellular matrix proteins, such as collagens and fibronectin, affecting normal tissue architecture and obstructing organ function (Neary et al., 2015). Currently a significant number of the world population is suffering from fibroproliferative diseases including pulmonary fibrosis, systemic sclerosis, liver cirrhosis, cardiovascular disease, progressive kidney disease and other chronic inflammation diseases. Fibrotic tissue remodelling can also promote cancer metastasis and increase chronic graft rejection in transplant recipients (Wynn, 2007, Wynn, 2008). In the developed world, these fibrotic-driven diseases account for up to 45% of all deaths (Lim and Kim, 2008). In the eye alone, deregulated tissue contraction and scarring are involved in either directly causing or failure of treatment of virtually every major blinding disease, for example glaucoma, cataract, macular degeneration and diabetes (Dahlmann et al., 2005, Friedlander, 2007). However, despite its enormous impact on human health, the detailed mechanisms by which 'the wound healing gone awry' and whether fibrosis and scarring can be therapeutically perturbed are still poorly understood. A thorough investigation of the cellular components and underlying molecular mechanisms is urgently required to identify cures for the often devastating health conditions.

1.2.1 Molecular mechanisms of fibrosis

Tissue fibrosis is determined by two major processes: the synthesis and the degradation of the ECM, which regulate the net increase or decrease of the collagen within a wound (Pardo and Selman, 2006). During skin homeostasis, both processes are in balance but can be shifted under specific conditions, for example towards ECM synthesis upon wound healing. The molecular mechanisms of ECM synthesis are addressed in the current section (**Figure 1.2**). The other critical part of

the tissue remodelling—ECM degradation, and the central effector cell in fibrosis—fibroblast, will be described in details in the later sections.

1.2.1.1 Chronic infections

Persistent infection with bacteria, viruses, fungi or multicellular parasites drives chronic inflammation and the development of fibrosis. It triggers marked alterations in the activation status of fibroblasts and M2 macrophages, which are key cells involved in the remodelling process. The conserved pathogen-associated molecular patterns (PAMPs) are pathogen by-products including lipoproteins, bacterial DNA and double-stranded RNA that are recognised by pattern recognition receptors (PRRs) found on a wide variety of cells, including fibroblasts. The interactions between PAMPs and PRRs activate numerous pro-inflammatory cytokine and chemokine pathways, which maintain the cells at a state of activation as well as promoting fibroblasts to differentiate into collagen-producing myofibroblasts (Akira and Takeda, 2004, Meneghin and Hogaboam, 2007, Wynn, 2004).

1.2.1.2 Origins of myofibroblasts

Myofibroblasts can be derived from multiple sources, including resident mesenchymal fibroblasts, epithelial cells in the process of epithelial-mesenchymal transition (EMT) and endothelial cells through endothelial-mesenchymal transition (EndMT) (Willis et al., 2006, Zeisberg et al., 2007, Kalluri and Neilson, 2003). Furthermore, it is reported that bone marrow stem cells can differentiate into a unique circulating fibroblast-like cell type that has a fibroblast/myofibroblast-like phenotype and are now commonly called fibrocyte (Ebihara et al., 2006, Russo et al., 2006). Also, in liver fibrosis, the resident hepatic stellate cells (HSC) are found to contribute to the primary source of myofibroblasts (Iredale, 2007). With the induction

of the CXC chemokine receptor family such as chemokine receptor 4 (CXCR4), CC chemokine receptor 7 (CCR7) and the pro-fibrotic chemokine CC Motif Chemokine Ligand 2 (CCL2), these cells travel to the site of injury and participate with the resident mesenchymal cells in the reparative process (Phillips et al., 2004, Strieter et al., 2007, Moore et al., 2005).

1.2.1.3 Cytokines and growth factors

Cytokines are important cell signalling molecules, which include chemokines, interferons, interleukins, lymphokines and tumour necrosis factors. They are produced by a broad range of cells such as macrophages, lymphocytes, and mast cells, as well as endothelial cells, fibroblasts and various stromal cells (Thomson and Lotze, 2003). Many cytokines possess the ability to induce fibrogenesis. For instance, the pro-inflammatory cytokine interleukin 6 (IL-6) is involved in the pathogenesis of many fibrogenic diseases, due to its ability of regulating the synthesis of a broad spectrum of acute phase proteins (Choi et al., 1994, Klee et al., 2016, Kobayashi et al., 2015). Moreover, the production of the pro-fibrotic cytokines including interleukin 13 (IL-13) and interleukin 4 (IL-4) is found to closely associate with the CC chemokine activity, which is also important in mediating fibrosis (Blease et al., 2000, Gao et al., 1997). IL-4 is showed to augment collagen expression in fibroblasts with a higher efficiency than TGFβ (Fertin et al., 1991). IL-13 shares many functional activities with IL-4, it can regulate fibrosis independently of IL-4Ra/Stat6 signalling pathways and is identified as a dominant effector cytokine of fibrosis in several models of fibrosis (Zurawski et al., 1993, Blease et al., 2001, Jakubzick et al., 2004, Joshi et al., 2006). Similarly, interleukin 5 (IL-5), interleukin 17 (IL-17) and interleukin 21 (IL-21) are found to perform distinct roles in the regulation of tissue remodelling and fibrosis (Emad and Emad, 2008, Gharaee-Kermani and Phan, 1997, Brodeur et al., 2015, Lei et al., 2015).

Chemokines are leukocyte chemoattractants that function together with pro-fibrotic cytokines during fibrogenesis to recruit fibroblasts, macrophages and other key effector cells to the wounding site. Numerous chemokine signalling pathways, especially the CC and CXC chemokine receptor families, play important roles in the regulation of fibrosis. For example, monocyte chemotactic and activating factor (CCL2) and macrophage inflammatory protein 1α (CCL3) are chemotactic for mononuclear phagocytes including macrophages and epithelial cells, which are crucial pro-fibrotic mediators (Zhu et al., 2002, Smith et al., 1995). Other chemokines, such as macrophage inflammatory protein 1-β (CCL4), macrophage inflammatory protein 3α (CCL20), eosinophil chemotactic protein (CCL11) and macrophage-derived chemokine (CCL22), are all found to participate in the pathogenesis of fibrosis (Belperio et al., 2002, Ma et al., 2004).

The transforming growth factor β (TGFβ) signalling is the major inducer of collagen synthesis by activated fibroblasts and myofibroblasts (Hinz, 2015). TGFβ is the most intensively investigated ECM regulator, which is linked to the development of fibrosis in numerous diseases (Sato et al., 2003, Border et al., 1992, Hills and Squires, 2011, Meng et al., 2012). It has three isotypes in mammals including TGFβ1, -2 and -3, all exhibit similar biological activity (Gorelik and Flavell, 2002). TGFβ is produced by a variety of cell types, with circulating monocytes and macrophages being the predominant cellular sources. The tissue fibrosis is primarily attributed to the TGFβ1 isoform (Letterio and Roberts, 1998). Upon binding to its type I and II receptors, TGFβ activates the canonical Smad3/4, the non-canonical TAK1/p38/JNK (Leask and Abraham, 2004, Trojanowska, 2009) and the NOX4/ROS pathways (Liao et al., 2001, Yan et al., 2009), resulting in the induction of fibrogenic genes including α-SMA (ACTA2), ECM components including collagen

type I (COL1A1) and matricellular proteins such as the connective tissue growth factor (CTGF) that increase the mechanical tension of the matrix (Cucoranu et al., 2005, Leask, 2010). TGFβ induces fibroblasts to differentiate into myofibroblasts in an integrin-dependent fashion (Thannickal et al., 2003).

Other potent matrix regulators, such as platelet-derived growth factor (PDGF), also play important roles in tissue fibrogenesis. PDGF is a growth factor that regulates cell growth and division. It in particular contributes to angiogenesis (Hannink and Donoghue, 1989). PDGF is also a vital mitogen for cells of mesenchymal origin, especially fibroblasts (Heldin, 1992). It is found to stimulate fibroblast-mediated contraction (Rhee and Grinnell, 2006), significantly enhance TGFβ1 synthesis *in vitro* (Zhao et al., 2013) and work together with TGFβ to promote fibrosis (Zhao et al., 2013). Both TGFβ and PDGF are found to be upregulated in normal wound healing (Kane et al., 1991, Andrae et al., 2008), and increase considerably in a variety of pathological fibrotic conditions (Bottinger and Bitzer, 2002, Wang et al., 2005, van Steensel et al., 2010).

1.2.1.4 Other factors

A pro-fibrotic hormone to mention is the final product of the renin-angiotensin-aldosterone system, angiotensin II (ANG II), which is found to play important roles in cardiac, renal and hepatic fibrosis (Watanabe et al., 2005, Mezzano et al., 2001). ANG II is produced by activated macrophages and fibroblasts. It induces NADPH oxidase activity, stimulates TGFβ1 production and triggers fibroblasts proliferation and secretion of collagen via binding to their angiotensin II type1 (AT1) receptor (Rosenkranz, 2004, Bataller et al., 2003). ANG II augments ECM accumulation by increasing TGFβ1 signalling via enhancing SMAD2 levels, amplifying the nuclear

translocation of phosphorylated SMAD3, and through an autocrine TGFβ activation (Rosenkranz et al., 2002, Tomasek et al., 2002).

Furthermore, uncontrolled vascular proliferation, which often occurs prior to the development of fibrosis, is characterised in many fibrotic diseases, especially ocular fibrosis (Rattner and Nathans, 2006, Friedlander, 2007). Signalling pathways, for example the Wnt-b-catenin signalling, has been suggested as a major pathway leading to fibrosis. The increased expression and activity of its family member Wnt family member 10b (Wnt10b) has been detected in multiple fibrogenic models *in vitro* and *in vivo* (Wei et al., 2011, Wei et al., 2012).

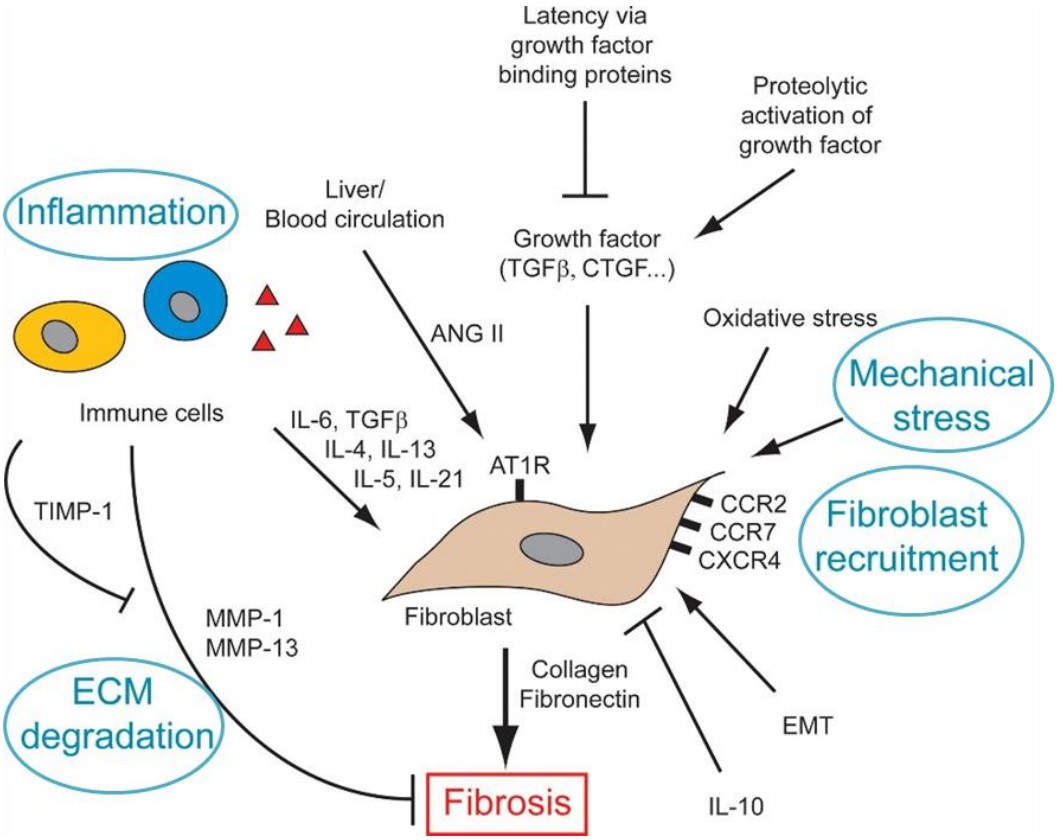

Figure 1.2 Regulators of fibrosis.

This figure illustrates the multiple contributors participating in the development of fibrosis. All of them converge onto fibroblast representing the central effector cell in the process. Fibroblasts can be derived from resident mesenchymal fibroblasts, which are recruited via their chemokine receptors. Fibroblasts can also transform from cells such as endothelial or epidermal cells, in the process of EMT. Oxidative stress, mechanical tension, pro-fibrotic and pro-inflammatory cytokines and growth factors all induce ECM synthesis in fibroblasts. Furthermore, immune cells are an important source of pro-fibrotic mediators. ECM deposition can be suppressed by MMP secretion. ANG II: angiotensin II, AT1R: angiotensin II type I receptor, CCR: CC chemokine receptor, CTGF: connective tissue growth factor, CXCR: CXC chemokine receptor, ECM: extracellular matrix, EMT: epithelial-to-mesenchymal transition, IL: interleukin, MMP: matrix metalloproteinase, TIMP: tissue inhibitor of metalloproteinases, TGFβ: transforming growth factor β (figure adapted from (Do and Eming, 2016)).

1.2.2 Ocular Scarring

Similar to the tissues elsewhere in the body, the presence of the normal vasculature, ECM and various cell types maintain the homeostasis in the eye. Following infection, inflammation or metabolic diseases, such homeostasis is disturbed and the consequent event is often fibrosis. Fibrosis in the eye is used to describe the wound-healing responses and the associated scar formation mediated by fibroblasts in the non-CNS (central nervous system) tissues. In the CNS, of which the neuro-retina is a part, the similar processes are mediated by glial cells and usually termed gliosis. Nevertheless, abnormal wound healing can lead to disastrous consequences for vision, as a result of mechanical disruption of the highly ordered tissue architecture and/or biological malfunctioning in the eye. For example, fibrosis of the cornea that occurs after corneal injury, surgery or secondary to infection causes corneal opacification and thereby loss of vision. Uncontrolled retinal angiogenesis, induced by diabetes-associated retinal hypoxia, leads to diabetic retinopathy (DR) with retinal fibrosis and traction retinal detachment. In the neuro-retina, similar fibrosis can occur due to the pathogenesis of age-related macular degeneration (AMD) (Friedlander, 2007, Yu-Wai-Man and Khaw, 2016). Moreover, conjunctival fibrosis is the major determinant of the surgical success after glaucoma filtration surgery (GFS) (Dahlmann et al., 2005). It is also the consequence of *Chlamydia trachomatis* infection that causes trichiasis (inward-turned eyelids) and permanent blindness in trachoma (Resnikoff et al., 2004, Rajak et al., 2012). Collectively, these conditions of ocular fibrosis result in vision loss in millions of individuals worldwide.

1.2.2.1 Glaucoma and glaucoma filtration surgery (GFS)

Glaucoma is a progressive optic neuropathy affecting retinal ganglion cells and optic nerve axons (Nuzzi and Tridico, 2017). It is defined by characteristic optic disc

damage and visual field loss for that the intraocular pressure (IOP), which is the fluid pressure inside the eye, is a major modifiable risk factor. It can progress at variable rates and afflict all age groups, and is a significant global health problem and the second leading cause of blindness worldwide after cataract. Based on the status of the internal drainage system, the disease can be characterised into two major subtypes: the open-angle and closed-angle glaucomas, with the former being the most common type with a prevalence in the USA of 1.55% (Coleman and Brigatti, 2001). Risk factors for open-angle glaucoma are family history, IOP, aging, increased cup-to-disc ratio and thinner central corneas; and for closed-angle glaucoma are hyperopia, female gender and Asian ethnicity (Mantravadi and Vadhar, 2015).

The underlying causes of glaucoma are still unclear. In a normal eye, the aqueous humour first flows from the ciliary processes into the posterior chamber, bounded posteriorly by the lens and anteriorly by the iris. It then goes through the pupil of the iris into the anterior chamber, bounded posteriorly by the iris and anteriorly by the cornea. Eventually, it drains through the trabecular meshwork via the scleral venous sinus (Schlemm's canal) into the scleral plexuses and general blood circulation (Walker et al., 1990). In open-angle glaucoma, due to the degeneration and obstruction of the trabecular meshwork, the flow of aqueous humour out of the eye is reduced, which results in a rise of the intraocular pressure (IOP). In closed-angle glaucoma, the aqueous fluid is not able to flow out of the trabecular network, as the iridocorneal angle is completely closed, which results in an increase of IOP that can be acute and associated with pain (Mozaffarieh et al., 2008) (**Figure 1.3**).

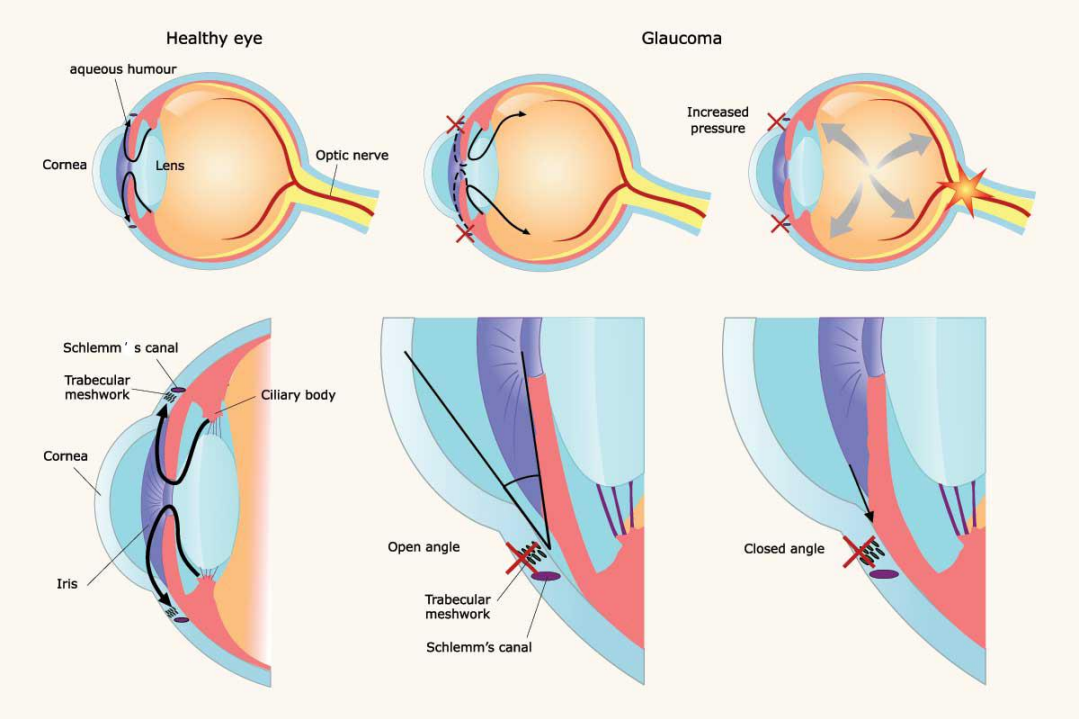

Figure 1.3 The pathogenesis of glaucoma (outflow mechanism) compared to normal eye.

The figure illustrates the pathogenesis of glaucoma aqueous outflow compared to a normal eye, in which the aqueous humour flow is not able to drain through the trabecular meshwork via the Schlemm's canal into scleral plexuses and general blood circulation, so that it accumulates and increases the intraocular pressure (IOP), which results in damage to the optic nerve and eventually causes vision loss. In open-angle glaucoma, IOP is caused by the blockage of the trabecular meshwork; in close-angle glaucoma, the blockage occurs at the contact between the iris and trabecular meshwork, which obstructs outflow of the aqueous humour (figure cited from http://www.maskelloptometrists.com/glaucoma/).

Glaucoma can be managed by topical and oral medical therapies, laser modalities and surgeries with the goal of lowering IOP to avoid optical nerve damage (Parikh et al., 2008). The most commonly performed glaucoma filtration surgery (GFS) is the trabeculectomy, which aims to create a permanent drainage outflow channel for aqueous humour that connects the anterior chamber to the sub-Tenon's space. Herein, a partial thickness flap with its base at the corneoscleral junction is made in the scleral wall, and a window opening is produced under the flap to remove a portion of the sclera, Schlemm's canal and trabecular meshwork. The flab is then sutured loosely back in place forming a 'bleb' on the surface of the eye, which allows fluid to flow out (Wells et al., 2004) (**Figure 1.4**).

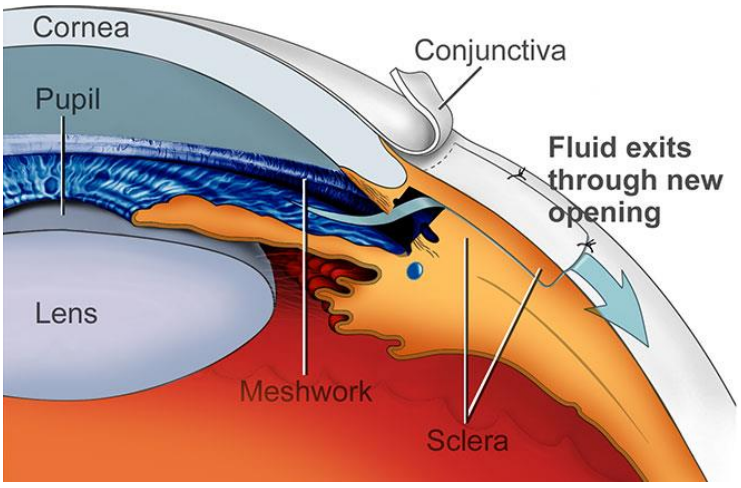

Figure 1.4 Graphic illustration of glaucoma filtration surgery (GFS).

The glaucoma filtration surgery (GFS) creates a new opening that connects the anterior chamber to the sub-Tenon's space, which allows the aqueous humour to leave the eye and therefore decrease the intraocular pressure (IOP) (figure cited from http://www.allaboutvision.com/conditions/glaucoma-surgery.htm).

1.2.2.2 Conjunctival scarring after GFS

Subconjunctival fibrosis and scarring at either the level of scleral flap or the ostium of the newly created drainage channel is the main reason that glaucoma filtration surgery (GFS) fails (Khaw et al., 2012). The successful prevention of the scarring after GFS determines the percentage of patients who achieve low final intraocular pressure (IOP) and virtually no disease progression. Fibroblasts from Tenon's capsule are known to play an essential part in conjunctival scarring following the GFS, by their ability of remodelling the extracellular matrix (ECM) via both direct cell-mediated contractile activity and matrix metalloproteinases (MMPs)-mediated matrix degradation (Martin-Martin et al., 2011, Daniels et al., 2003). However, signalling events that regulate fibroblast-driven matrix contraction and remodelling remain unclear. The current anti-metabolites treatment used after GFS to inhibit fibrosis and scarring of trabeculectomy blebs are anti-cancer agents, such as mitomycin-C (MMC) and 5-fluorouracil (5-Fu). Unfortunately they are associated with severe complications including non-specific cytotoxicity, tissue damage, breakdown and infections, all of which are linked to sight-threatening risks (Yu-Wai-Man and Khaw, 2015). Still there is a large unmet need to better understand the mechanisms underlying conjunctival fibrosis and scarring following ocular wound healing. The development of such anti-fibrotic therapies in the eye will also benefit other pathological conditions associated with contractile scarring.

1.3 Fibroblast-mediated contraction

1.3.1 Fibroblasts

Fibroblasts are ubiquitous mesenchymal cells in the stroma of all epithelial organs. They are known to play an essential role in organ development, inflammation,

wound healing and fibrosis. In each anatomic site of the body, fibroblasts differentiate in a site-specific way and display distinct and characteristic transcriptional patterns, suggesting that they perform important duties in establishing and maintaining the positional identity in tissues and organs (Chang et al., 2002). Normal human fibroblasts require growth factors for proliferation in culture, which are usually supplied by fetal bovine serum (FBS). In the events of injury, upon exposure to the specific physiological signals within the soluble fraction of coagulated blood, serum, fibroblasts are activated and programmed to perform a broadly coordinated and multifaceted program including regulation of homeostasis, cell cycle progression, epithelial cell migration, inflammation, and angiogenesis (Iyer et al., 1999, Chang et al., 2004). With the help of other cellular participants, they not only execute central effector roles in the process of wound repair, but also act as the main regulator of fibrosis. At the end of the healing process, fibroblasts remodel the extracellular matrix via direct cell-mediated contractile activity, as well as degradation and synthesis to bring the margins of the wound together, leading to the formation of scar tissue. The initiation and maintenance of the fibrotic responses of contracting fibroblasts result from a complicated interaction among a network of growth factors, cytokines and hormones, and the cellular microenvironment that promotes the pathological responses to these stimuli, though the molecular mechanisms underneath remain unclear (Leask, 2010).

1.3.2 Cell-mediated contraction

Tissue contraction is a fundamental part of many important biological processes, including wound healing, in which abnormal contraction leads to fibrosis and scarring that associate with a wide range of debilitating pathological conditions. The resident fibroblasts are believed to play a key role in controlling this process, by generating substantial contractile forces on the extracellular matrix that are in part

regulated by the mechanical loading in the environment in which they reside. To maintain an active tensional homeostasis, fibroblasts consistently react to modify the endogenous matrix tension in the opposite direction to externally applied loads by changing in cell shape and attachment in a predictable manner (Eastwood et al., 1998, Brown et al., 1998). However, the mechanisms by which they remodel their environment are still unclear. Bell's introduction of the fibroblast-populated collagen lattice (FPCL) has become the most commonly used *in vitro* model to study the reciprocal and adaptive interactions that occur between fibroblasts and surrounding matrix in the tissue-like environment (Bell et al., 1979, Grinnell, 2003). To create such a pseudo-physiological 3D environment, a suspension of trypsinised fibroblasts are added to pH neutralised type-I collagen solution with concentrated medium. After the collagen polymerises, the fibroblasts are dispersed throughout the resulting gel-like matrix, which is then allowed to free-float in the medium containing tissue culture dish. Stimulated by the serum or growth factors contained in the culture medium, the cells contract the matrix by applying force to the neighbouring collagen fibres. Through cycles of extension and retraction, they structurally reorganise the collagen architecture down to a fraction of its original size. The speed of contraction depends on the cell type, density and collagen concentration (Tomasek et al., 2002) (**Figure 1.5**).

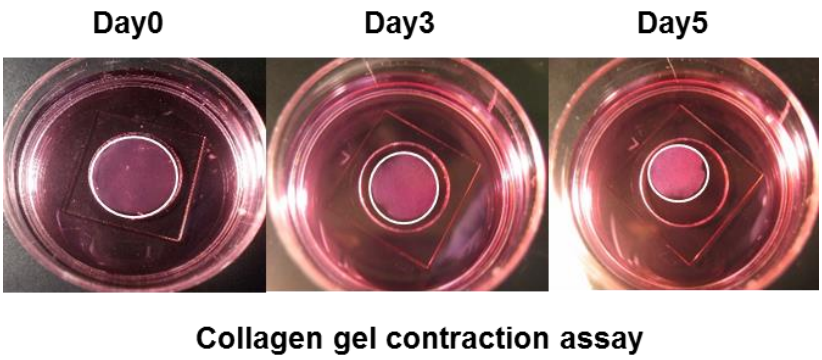

Figure 1.5 The free-floating fibroblast-populated collagen gel contraction assay.

Collagen gel contraction assay with human conjunctival fibroblasts HTF7071 at Day0, 3 and 5 in culture medium with 10% FBS (the contracting collagen gel at the centre of the well is labelled with white circle).

There are three main cellular mechanisms proposed to be responsible for generating the FPCL contraction (Dallon and Ehrlich, 2008). The first one is cell tractional forces that are how fibroblasts generate sufficient force in order to bend individual collagen fibres bound to their surface to allow cell spreading and migration, which relate to cell migration or locomotion. The assumption is that these tractional forces are distributed throughout the matrix via the cross-linked collagen fibres, which lead to global remodelling and contraction of the whole environment (Meshel et al., 2005, Roy et al., 1997). Nevertheless, challenging data suggested that tractional forces may not be sufficient to induce matrix contraction *in vitro* as well as wound closure *in vivo* (Ehrlich and Rajaratnam, 1990, Roy et al., 1999).

Another possible mechanism is that through differentiation into α-smooth muscle actin rich stress fibres expressing myofibroblast phenotype, the 'modified' cells enhance their contractility and become the 'icon of fibrosis' (Tomasek et al., 2002).

The myofibroblast was first defined by Gabbiani's group in 1971 in an experimental animal model of wound healing (Gabbiani et al., 1971, Majno et al., 1971). Subsequently, their presence has been identified in a variety of pathological connective tissue conditions including cancer and has been intensively studied (Gabbiani, 1992, Gabbiani, 1999, Desmouliere et al., 2004). However, myofibroblasts only appear at the later stage of wound healing *in vivo*, and differentiation into myofibroblasts *in vitro* requires specific conditions such as TGFβ, tension, and most importantly, time (Arora and McCulloch, 1994, Hinz, 2015, Grinnell et al., 1999, Desmouliere et al., 1993). Hence the transformation of myofibroblasts is unlikely to be the reason of early matrix contraction of FPCL *in vitro* and early wound closure *in vivo* (Grinnell, 1994, Dahlmann-Noor et al., 2007).

The third mechanism of cell-mediated contraction proposed is the traction generated by cell protrusive activity without association with net cell locomotion. Previous studies have demonstrated that through the dynamic extension and retraction of pseudopodial extensions, non-motile cells can produce local tension in the matrix that leads to contraction (Roy et al., 1997, Sawhney and Howard, 2002, Sawhney and Howard, 2004). By performing protrusions and retractions by lamellipodia in the typical “hand-over-hand” cycle, fibroblasts can also reposition the individual collagen fibres placed on their upper surface in such case (Meshel et al., 2005). The molecular machinery contributes to the process including assembly of actin filaments, myosin activity, as well as microtubules depolymerizing (Sawhney and Howard, 2004). Furthermore, the macroscopic matrix contraction has been linked to the stochastic nature of cell elongation initiation and of the time required for cells to reach a final morphology, but not cell migration (Freyman et al., 2001).

The host laboratory have investigated the cellular mechanisms underlying force generation and matrix contraction using primary human ocular fibroblasts in the standard collagen matrix. The former studies have identified factors that affect early matrix contraction including cell size, intrinsic level of actin dynamics and genuine contractile force, dynamic cell protrusive activity, and net pericellular matrix displacement. It was reported that protrusive activity is the main cell behaviour observed within the first 24 hrs of matrix deformation (Dahlmann-Noor et al., 2007). Furthermore, it has been proposed that fibroblasts remodel the collagen matrix by two major mechanisms, one via local active collagen fibre alignment through cellular protrusive activity, and the other through matrix degradation. We found that cells with a rounded morphology and proliferative profile display low intrinsic cellular force, whereas those with an elongated morphology express higher levels of protrusive activity that leads to efficient matrix remodelling and contraction (Martin-Martin et al., 2011).

1.3.3 Matrix degradation

1.3.3.1 Matrix metalloproteinases (MMPs)

The degradation of the excessive ECM during tissue remodelling is tightly controlled by the production of matrix metalloproteinases (MMPs) and their regulators by multiple stromal cells, including fibroblasts (Kessenbrock et al., 2010). Dysregulation of such procedure causes fibrosis or non-healing wounds. MMPs are a family of zinc-dependent endopeptidases that were first described more than half a century ago in the tail of a tadpole undergoing metamorphosis (Gross and Lapiere, 1962). They are collectively capable of cleaving essentially all ECM components, thus play a crucial role in almost every physiological process that involving matrix remodelling throughout the mammalian life span, from embryo implantation (Alexander et al., 1996) to cell death or necrosis (Egeblad and Werb, 2002, Currie et al., 2007). Also,

they perform a primary function in wound healing and tissue repair, organ development, regulation of inflammatory processes and in pathological conditions such as cancer metastasis and tumour invasion (Page-McCaw et al., 2007, Parks et al., 2004, Egeblad and Werb, 2002). The expression of MMPs is transcriptionally regulated by growth factors, hormones, cytokines and cellular transformation (Nagase and Woessner, 1999).

MMPs are secreted from the cells or anchored to the cell surface, in order to catalyse membrane proteins and proteins in the secretory pathway or extracellular space (Parks et al., 2004). To date, 24 different vertebrate MMPs have been identified, of which 23 are found expressed in humans. Structurally, MMPs generally consist of three domains that are common to almost all of them, which include a pro-peptide, a catalytic domain and a hemopexin-like C-terminal domain that is linked to the catalytic domain via a flexible hinge region (Visse and Nagase, 2003) (**Figure 1.6**). Initially, MMPs are expressed in an enzymatically inactive state as 'pro-MMP', due to a cysteine residue of the pro-domain that binds the zinc ion of the catalytic site. Upon breaking down of this interaction by a mechanism called 'cysteine switch', which usually occurs as a result of the proteolytic removal of the pro-domain, or chemical modification of the cysteine residue, the pro-enzyme becomes a proteolytically active 'active-MMP'. The pro-domain has a consensus sequence that can be proteolytically cleaved by convertases, which happens intracellularly by furin, extracellularly by other MMPs or serine proteinases, depending on the difference of the sequences (Sternlicht and Werb, 2001).

Based on the specificity, sequence similarity and domain organisation, vertebrate MMPs can be divided into six groups. These are (1) Collagenases, including MMP1,

8, 12 and 18 that are able to cleave interstitial collagens I, II, and III. (2) Gelatinases, such as MMP2 and 9 that digest the denatured collagens—gelatins. (3) Stromelysins, including MMP3 and 10, which have similar substrate specificities and digest ECM components. MMP3 activates several pro-MMPs, whose action is important for the generation of fully active MMP-1 (Suzuki et al., 1990). (4) Matrilysins, including MMP7 and 26 that are also called endometase, which do not have a hemopexin domain. Apart from ECM components, MMP7 also processes a number of cell surface molecules such as pro–α-defensin, Fas-ligand, pro–tumour necrosis factor (TNF)-α and E-cadherin. (5) Membrane-type (MT) MMPs, such as MMP14, 15, 16, 24, 17 and 25 can also digest a number of ECM molecules. MMP14 (MT1-MMP) exhibits collagenolytic activity on type I, II and III collagens, and plays a critical role in angiogenesis, tumour invasion and metastatic cancer cell migration (Ohuchi et al., 1997, Pepper, 2001, Friedl and Wolf, 2008). (6) Other MMPs, including MMP12, 19, 20, 22, 23 and 28 that are not classified in the former categories. MMP12 is mostly expressed by macrophages and is essential for macrophage migration (Shipley et al., 1996). MMP28 is mainly expressed in keratinocytes, which may play a role in tissue homeostasis and wound repair (Marchenko and Strongin, 2001, Lohi et al., 2001, Saarialho-Kere et al., 2002).

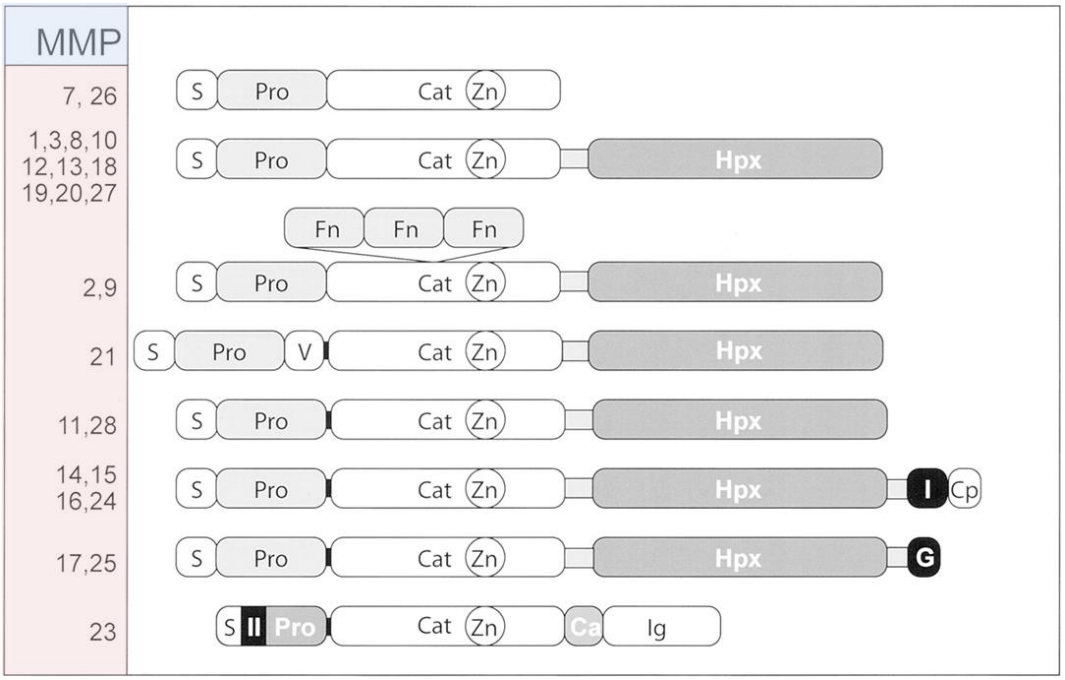

Figure 1.6 The domain structural characterisation of the MMPs.

The structural features of matrix metalloproteinases (MMPs) are illustrated, showing the minimal domain structures. S, signal peptide; Pro, pro-domain; Cat, catalytic domain; Zn, active-site zinc; Hpx, hemopexin-like C-terminal domain; Fn, fibronectin domain; V, vitronectin insert; I, type I transmembrane domain; II, type II transmembrane domain; G, a glycosylphosphatidylinositol (GPI) anchor; Cp, cytoplasmic domain; Ca, cysteine array region; Ig, IgG-like domain. The black band between pro-domain and catalytic domain represents the furin cleavage (figure adapted from (Visse and Nagase, 2003)).

In the eye, overexpression of MMPs has been shown to associate with aberrant wound healing and scarring diseases in all ocular structures from the anterior segment to the retina, which include corneal endothelium, stroma, lens, trabecular meshwork, uveoscleral outflow and conjunctiva (Wong et al., 2002) (**Table 1.1**). It has been reported that application of the broad-range MMP inhibitor GM6001 efficiently prevented human conjunctival fibroblast-mediated collagen lattice contraction *in vitro,* as well as reducing the production of collagen by those fibroblasts (Daniels et al., 2003). Also, in the *in vivo* rabbit model of glaucoma filtration surgery, inhibition of MMPs led to a dramatic reduction of scarring, with retention of normal tissue morphology (Wong et al., 2003). Furthermore, previous studies have demonstrated that treatment with GM6001 consistently decreased cell dynamics in 3D-culture, which correlated with a significant reduction of early matrix contraction *in vitro* and *ex vivo* (Martin-Martin et al., 2011, Tovell et al., 2011). These results suggest that MMP inhibition potentially prevents conjunctival fibroblast-mediated tissue contraction and scarring.

Table 1.1 MMPs expression in the different structures of the eye (Wong et al., 2002).

** Bovine corneal endothelium.*

MMPs expression in the Anterior Segment

Ocular structures	MMPs
Tear Film	MMP-1, -2, -8, -9
Cornea	n/a
Epithelium*	MMP-1, -9, -10, -12, -13, -14
Stroma	MMP-1, -2, -3, -14
Endothelium	MMP-2, -9
Aqueous Humour	MMP-2, -3, -9
Lens	MMP-2, -9, -14
Trabecular Meshwork	MMP-2, -3, -9
Uveoscleral Outflow	MMP-1, -2, -3, -9
Conjunctiva	MMP-1, -2, -3

1.3.3.1.1 MMP1

MMP1 (Collagenase-1) is the founding member of the MMPs family, which was first purified to homogeneity as a protein in 1962 (Gross and Lapiere, 1962). It cleaves interstitial collagens I, II and III at a specific site three-fourths from the N-terminus, and also digests a number of other ECM and non-ECM molecules (Visse and Nagase, 2003). It is not only involved in the breakdown of ECM in numerous normal physiological processes, but also exaggeratedly accumulated in many pathological conditions. Elevated expression of MMP1 has been implicated in diseases characterised by excessive ECM degradation, such as chronic ulcerations (Saarialho-Kere et al., 1993, Pilcher et al., 1997, Pilcher et al., 1999), rheumatoid arthritis (Walakovits et al., 1992, Mateos et al., 2012) and lung emphysema (Mercer et al., 2004, Imai et al., 2001); as well as in the fibrotic conditions, which by contrast associate to over-deposition of ECM substrates, including pulmonary fibrosis (Zuo et al., 2002, Pardo and Selman, 2006, Herrera et al., 2013) and various of cancers (McColgan and Sharma, 2009, Tao et al., 2015, Nguyen et al., 2015, Pietruszewska et al., 2016).

The mechanism by which MMP1 is produced and expressed by the cell is not clear. The expression of MMP1 is inducible under certain circumstances, not only by soluble factors such as growth factors, cytokines and chemical agents, but also through cell-matrix and cell-cell interactions. For example, via ligation of the $\alpha_2\beta_1$ integrin with collagen, MMP1 is largely expressed in migrating keratinocytes, which therefore becomes a reliable marker of activated keratinocytes in wounded human skin in a variety of conditions (Rohani et al., 2014). Particular signalling pathways also lead to expression of MMP1, such as blocking of $\alpha_5\beta_1$ integrin by soluble antibody, which results in a disruption of the actin cytoskeleton and an augmented expression of MMP1 in rabbit synovial fibroblasts (Werb et al., 1989). This is due to

the activation of the small Rho GTPase Rac1 that induces the activation of NF-kB by generating reactive oxygen species (ROS), which further results in an induction of IL1A, an autocrine inducer of MMP1 (Kheradmand et al., 1998). Furthermore, MAP kinase pathways also play a role in the regulation of MMP1, as ERK1/2, stress-activated protein kinase (SAPK)/JNK and p38 MAPK that all independently trigger the expression of MMP1 in human skin fibroblasts (Reunanen et al., 1998).

MMP1 is significantly expressed by fibroblasts during tissue contraction. Increased mRNA level of MMP1 is detected in the conjunctiva of patients with recurrent trichiasis one year after trachoma surgery (Burton et al., 2010). In primary trachoma fibroblast-mediated collagen gel contraction, MMP1 is found to be dramatically upregulated comparing to other MMPs (Li et al., 2013). Most importantly, MMP1 was found to be significantly upregulated during conjunctival fibroblast-mediated contraction *in vitro* (Tovell et al., 2012).

1.4 Small Rho GTPases

1.4.1 Small Rho GTPases and their regulators

The family of small Rho GTPases belong to the Ras superfamily and are highly conserved in all eukaryotic organisms. In mammals 22 Rho GTPases are identified that are related in primary sequence. Each one of them acts as a molecular switch to control distinct biochemical pathways. They contribute to various cellular activities including regulation of gene transcription, cell cycle, microtubule dynamics, vesicle transport and numerous enzymatic activities, as well as controlling the assembly of filamentous actin and the organisation of the actin cytoskeleton (Ridley, 2006).

Most of the Rho GTPases bind to guanosine triphosphate (GTP) and guanosine diphosphate (GDP), and have intrinsic GTPase activity. In their GDP-bound conformation they are generally assumed to be inactive, as they do not bind effector proteins; whilst when bound to GTP they are active and able to transduce signals through interacting with downstream target proteins. This inter-conversion is tightly regulated by guanine nucleotide exchange factors (GEFs), GTPase-activating proteins (GAPs) and guanine nucleotide dissociation inhibitors (GDIs). Generic Rho GTPases anchor to the membrane with a prenyl group near the carboxyl terminus. GEFs and GAPs are often constitutively or inducibly associated with membranes. GEFs promote the release of GDP to allow binding of GTP on monomeric GTPases, thus playing an activation role; whereas GAPs accelerate the hydrolysis of GTP to GDP that turns the GTPases' activity off. The GDIs bind to the C-terminal lipid groups on GTPases to prevent their membrane binding and interaction with the membrane-associated proteins, thus also performing an inhibitory role (Tybulewicz and Henderson, 2009) (**Figure 1.7**).

There are 85 Rho GTPases' GEFs identified in the mammalian genome. Many of them were originally characterised as oncogenes after transfection of immortalized fibroblast cell lines with cDNA expression libraries (Cerione and Zheng, 1996). Most of the GEFs belong to the Dbl subfamily, which contain a Dbl homology (DH) domain that has catalytic activity. Other subgroups include the Dock family whose catalytic activity resides in a Dock homology region 2 (DHR2), and those do not contain either of the domain (Cote and Vuori, 2002, Schmidt and Hall, 2002). Similarly, a large family of GAPs are identified that are typified by a conserved RhoGAP domain, which contains the catalytic activity of the enzymes (Tcherkezian and Lamarche-Vane, 2007). The reasons for the large number of GEFs and GAPs relative to Rho GTPases are unclear. Some GEFs or GAPs are specific for only one

or a few GTPases respectively, whereas others have a broader specificity. How GEFs and GAPs are themselves regulated is still unknown, which is very likely the key point of understanding the mechanisms that underlie the spatial and temporal activation of GTPases within a cell in response to outside influence.

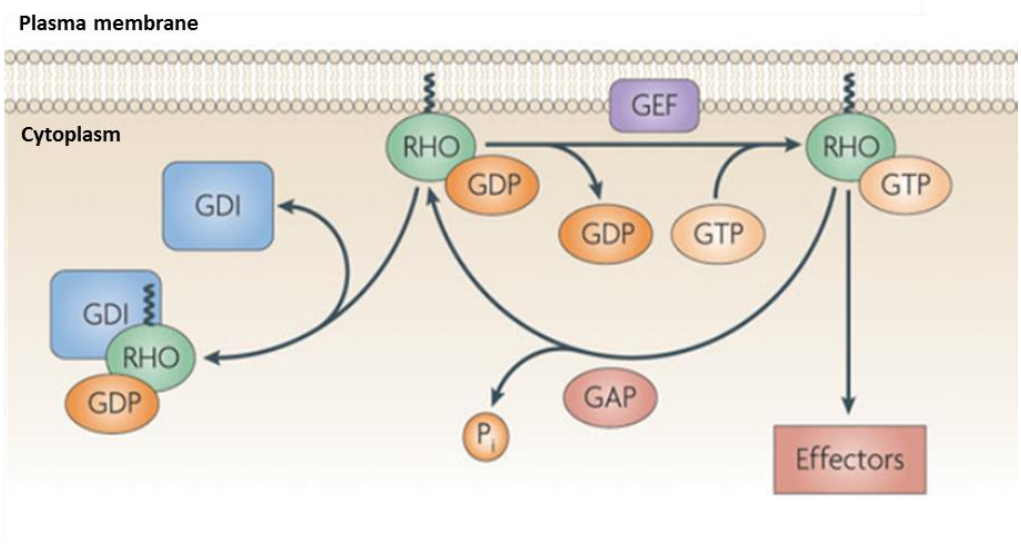

Figure 1.7 The regulations of Rho GTPases by GEF, GAP and GDI.

GEFs (Guanine nucleotide exchange factors) activate Rho GTPases by accelerating their GDP/GTP exchange rates. GAPs (GTPase-activating proteins) increase the intrinsic activity of Rho GTPases, causing GTP to be hydrolysed to GDP and phosphate (Pi). GDIs (Rho guanine nucleotide dissociation inhibitors) to the prenyl group of Rho GTPases' thereby inhibit their membrane-binding and interaction with effector proteins (figure adapted from (Tybulewicz and Henderson, 2009)).

1.4.2 Rac1, Cdc42 and RhoA

The best-known members of the Rho GTPases family are Rac1, Cdc42 and RhoA, originally identified through their effect on actin polymerisation. Each of them controls a signalling pathway that associates with membrane receptors to the assembly and disassembly of actin cytoskeleton and of linking integrin adhesion complexes. Rac1 induces plasma membrane protrusions known as lamellipodia, Cdc42 triggers filopodial extensions at the cell periphery, and RhoA stimulates focal adhesion and formation of stress fibres. Therefore they play vital regulatory roles in any cellular process that involves the activity of filamentous actin (Hall, 1998, Hall, 2005).

Regulation of the actin cytoskeleton downstream of Rac1, Cdc42 and RhoA is mediated by several effector proteins (**Figure 1.8**). Rac1 activates the WASP (Wiskott–Aldrich syndrome protein)-related WAVE (WASP-family verprolin homologous protein) family of proteins that lead to new actin polymerisation branching off from the sides of existing filaments through the ARP2/3 protein complex. Cdc42 activates the same pathway through the WASP. Both Rac1 and Cdc42 activate DIAP3 (members of the Diaphanous-related formins, also known as mDIA2), which causes the nucleation and extension of non-branching actin filaments. Also, these two GTPases activate the PAK (p21 activated kinases) family kinases, which in turn phosphorylate and activate LIMK (LIM domain kinase), a kinase that phosphorylates and inhibits cofilin, an actin depolymerising protein. The inhibition of cofilin promotes the stability of polymerized actin. LIMK is also activated by ROCK (Rho-associated protein kinase), a kinase effector that is downstream of RhoA. ROCK phosphorylates and suppresses the myosin light chain phosphatase (MLCP), which as a result leads to an increased phosphorylation of the myosin light chain (MLC), which strengthens the association between MLC and actin filaments.

MLC can also be phosphorylated via inhibition of the MLC kinase (MLCK) by PAK (Millard et al., 2004, Hall, 2005, Tybulewicz and Henderson, 2009, Taylor et al., 2011).

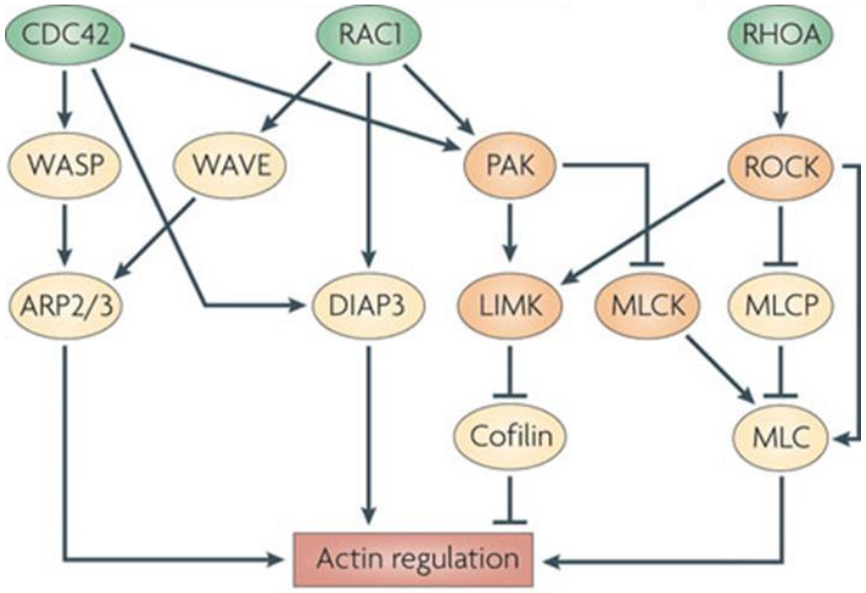

Figure 1.8 Rac1, Cdc42 and RhoA regulate actin cytoskeleton via their downstream effector proteins.

The downstream effectors of Rac1, Cdc42 and RhoA including: WASP (Wiscott-Aldrich syndrome protein)-WAVE (WASP-family verprolin-homologous protein) proteins, DIAP3 (Diaphanous-related formins, also known as mDIA proteins), and kinases such as PAKs (p21 activated kinases) and ROCK (RHO-associated protein kinases). WASP-WAVE proteins stimulate the activation of the ARP2/3 complex, lead to the branching of new actin filaments. Activation of DIAP3 stimulates the extension of parallel actin filaments. PAKs and ROCKs contribute to the stabilization of actin filaments via phosphorylation of LIMKs (LIM domain kinases), which in turn inactivate cofilin, ROCK also stimulates the phosphorylation of myosin regulatory light chain (MLC) via suppressing MLCP (myosin light chain phosphatase), thus contributes to the contractility of actin–myosin (figure adapted from (Tybulewicz and Henderson, 2009)).

In contracting fibroblasts, the cytoskeletal components are reorganized in order to produce a tensile strength (Ehrlich and Rajaratnam, 1990). Rac1 is shown to promote the assembly of a peripheral actin meshwork in these cells, which causes membrane protrusions (lamellipodia/membrane ruffles) in response to growth factors stimulation such as PDGF (platelet-derived growth factor) or insulin (Ridley and Hall, 1992, Ridley et al., 1992). The activity of Rac1 is reported to be required for controlling cell mobility, tissue repair, wound healing and fibrogenic responses *in vitro* and *in vivo* (Liu et al., 2009, Nobes and Hall, 1999). The expression of Rac1 was shown to associate with matrix remodelling in fibroblasts in the context of tumour-promoting stroma and fibrotic diseases, whilst its inactivation reversed the elevated contractile phenotype of cancer-associated fibroblasts (Hooper et al., 2010, Xu et al., 2009), suggesting that signalling through Rac1 is one of the major components in fibroblast-mediated contraction. Recently, it was demonstrated that transient inhibition of Rac1 by its inhibitor NSC23766 dramatically reduced human conjunctival fibroblasts mediated contraction *in vitro*, as well as *ex vivo* tissue contraction, suggesting a critical role for Rac1 in early matrix contraction and ocular scarring (Tovell et al., 2012).

Cdc42 induces peripheral actin-rich microspikes (filopodia) through a number of kinase and non-kinase effector proteins (Nobes and Hall, 1995, Kozma et al., 1995). It regulates the myotonic dystrophy kinase-related Cdc42-binding kinases (MRCKs), which are key regulators of the actin stress fibre contractility (Zhao and Manser, 2015). Interacting through the Par polarity complex and other targets, Cdc42 performs vital functions in cell migration by establishing cell migratory polarity and migratory persistence (Ridley, 2015). Also, it is in particular involved in fibroblasts migrating in 3D matrix, which is driven by localised protrusions known as invadopodia, via acting through its target N-WASP and several Cdc42 GEFs (Spuul

et al., 2014). In primary mouse embryonic fibroblast-mediated matrix remodelling, Cdc42 deficiency reduced the collagen gel contraction that associated with cell morphological changes, decreased focal adhesion complex formation, blocked MMP9 production and altered fibronectin deposition patterning, suggesting that it plays an essential role in regulating cell-matrix interaction (Sipes et al., 2011).

RhoA is shown to promote the assembly of contractile actin and myosin filaments (stress fibres) in fibroblasts in response to LPA (lysophosphatidic acid) addition (Ridley and Hall, 1992). The RhoA-ROCK pathway plays important roles in the formation of actin stress fibres and focal adhesions, as well as regulating actomyosin cytoskeletal organisation, cell adhesion, morphology, motility, contraction and cytokinesis (Takai et al., 1995). The anti-scarring property of the ROCK inhibitor has been tested in the human conjunctival fibroblast-populated collagen lattice *in vitro* and rabbit glaucoma filtration surgery model *in vivo,* which showed promising results in preventing fibroblasts contractile activity and increasing the survival rate of the GFS blebs compared to the control ones (Honjo et al., 2007).

Moreover, Rac1, Cdc42 and RhoA contribute to modulate multiple aspects of wound healing including matrix degradation. They have been reported to participate in the regulation of MMP1 expression in various fibroblast cells, though the effects appeared to be cell-type and origin dependent. For example, activation of Rac1 or RhoA induced the expression of MMP1 through the ROS/NF-kB/IL1A pathway in response to the integrin-mediated disruption of actin cytoskeleton in rabbit synovial fibroblasts (Kheradmand et al., 1998, Werner et al., 2001, Werner and Werb, 2002); and silencing of Cdc42, but not that of Rac1 or RhoA, induced a significant increase of MMP1 secretion in human skin fibroblasts, which was dependent on ERK1/2

pathways (Deroanne et al., 2005). However, these studies were all performed with fibroblasts cultured in 2D format. No studies have explored the regulations of Rac1, Cdc42 or RhoA on MMP1 expression and secretion in the model of 3D-cultured contracting fibroblasts.

1.5 Aims and objectives

In a previous study, it was found that transient inhibition of small Rho GTPase Rac1 by its inhibitor NSC23766 significantly prevented tissue contraction and matrix degradation during fibroblast-mediated contraction *in vitro* and *ex vivo* (Tovell et al., 2012), suggesting that Rac1 could be a master regulator of contractile scarring. Therefore, the main aim of the study is to identify the regulatory roles that Rac1 performs in the contraction, which includes three objectives:

1. To characterise the gene expression profiles underlying fibroblast-mediated contraction and the involvement of Rac1, comparing it to *in vivo* studying and published studies of human ocular fibrotic diseases.

2. To evaluate the anti-scarring potential of a range of Rac inhibitors and further explore the regulatory roles of Rho GTPases Rac1, Cdc42, RhoA, and Rac2, and their regulators in contraction.

3. To investigate the connection between Rho GTPases' activation and MMP expression using MMP1 as an example.

Chapter 2 Material and methods

2.1 Fibroblast cell culture

2.1.1 Human conjunctival samples

Human conjunctival fibroblasts were isolated from conjunctival biopsy samples or whole eye globes in accord with the tenets of the Declaration of Helsinki and with local ethics approval. The conjunctival biopsies were kept in sterile culture medium and refrigerated prior of processing, and processed within 48 hrs of sample arrival. The whole eye globes were incubated in 1000 IU/ml penicillin and 1000µg/ml streptomycin (Invitrogen) in sterile PBS for 10-20 min, and then dissected to obtain conjunctival tissue. The primary fibroblast cells used in this study and the originated donors' information are listed in **Table 2.1**.

Table 2.1 Isolated primary conjunctival fibroblasts and their donors' information.

**HTF7071 was established by Dr. Victoria Tovell. **HTF2320, the age and sex of its donor are not known.*

Cell line	Age	Gender	Isolated from
HTF9154	62	male	whole eye globe
HTF7071*	56	male	conjunctiva biopsy
HTF1785R	49	female	whole eye globe
HTF0041	39	female	conjunctiva biopsy
HTF1818	83	male	conjunctiva biopsy
HTF2493	65	male	conjunctiva tissue
HTF2489	40	male	conjunctiva tissue
HTF0401	53	female	conjunctiva tissue
HTF2320**	n/a	n/a	conjunctiva tissue
HTF0748-1	84	male	whole eye globe

2.1.2 Cell culture

The biopsies were transferred to a sterile flat surface (15cm diameter tissue culture dish) and cut into small pieces, which were then placed in the 3cm diameter tissue culture dishes and incubated with 100-200µl of 0.05% collagenase in DPBS (Gibco, Thermo Fisher Scientific) for 10-20 min at 37ºC with 5% CO_2. To prevent the tissue fragments from floating in the culture medium, a sterile coverslip was placed on top of them, and 0.8ml of Dulbecco's modified Eagle's medium (DMEM) with high glucose (Gibco, Thermo Fisher Scientific), supplemented with 10% fetal bovine serum (FBS) (Sigma-Aldrich), 100 IU/ml penicillin, 4.5g/L l-Glutamine and 100µg/ml streptomycin (Invitrogen) was added to the dish. The medium was changed 2-3 times per week, until the cells have expanded to over 50% confluency (usually in 2-4 weeks).The cells were then trypsinised with trypsin-EDTA 0.25% (Gibco, Thermo Fisher Scientific) and plated into a T25 tissue culture flask (Corning, Sigma-Aldrich) with 5ml of medium (passage 1). The cells were passaged again 1:3 when the confluency reached 80-90%. Stock of cells at passage 2 to 6 were kept in liquid nitrogen in 10% DMSO v/v (Sigma-Aldrich) in FBS. The fibroblast cells used in this study were aged from passage 3 to 8.

2.2 Collagen contraction assay

The collagen contraction assay was performed to characterise the ability of fibroblasts to contract the extracellular matrix (ECM). $1x10^5$ fibroblast cells were suspended in 100µl of serum free medium (DMEM with 100 IU/ml penicillin, 4.5g/L l-Glutamine and 100µg/ml streptomycin), and added to a mixture of 1ml type I collagen solution (2.05 mg/ml in 0.6% acetic acid, First Link Ltd) and 160µl concentrated medium (10x DMEM, Sigma-Aldrich, l-Glutamine, Invitrogen, sodium bicarbonate 0.75%, Sigma-Aldrich), which had been adjusted to pH 7.2 by addition of 80-90µl of sterile 1M NaOH (Sigma-Aldrich). And then, the cell-collagen solution

was quickly casted into the inner well of MatTek dish (MatTek Corporation) as 150µl/well and set at 37ºC with 5% CO_2 for 10-15 min. The polymerized gels were detached from the edge of the well by sliding a pipette tip around it to allow free floating, and 2ml of culture medium with/without treatment was added per dish. Gel contraction was monitored daily for 3-5 days depended on experimentation by digital photography. Gel areas were measured using ImageJ software (http://rsb.info.nih.gov/ij/), and the contraction was plotted as a percentage of gel area normalised to original area (day 0 measurement).

2.2.1 Contraction assay with inhibitors

The inhibitors were added in the culture medium of the contraction assay after the initial gel polymerisation. For treatment within a specific time, the medium with inhibitor as well as the control medium were replaced with fresh culture medium after the time. The inhibitors used in this study are listed in **Table 2.2**:

Table 2.2 The inhibitors and their concentrations used in the study.

Inhibitor	Supplier	Concentration
NSC23766	TOCRIS bioscience	50µM
Ehop-016	Merck Millipore	10µM
EHT1864	TOCRIS bioscience	50µM
Z62954982	Merck Millipore	50µM
W56	TOCRIS bioscience	20µM
Simvastatin	TOCRIS bioscience	50µM
GM6001	Enzo life sciences	100µM
H1152	Merck Millipore	10µM
U0126	Sigma-Aldrich	10µM
SB203580	Selleckchem	10µM
Ly294002	Cell Signaling	25µM
Dynasore	Sigma-Aldrich	80µM

2.2.2 Cell viability assay

The alamarBlue reagent (Thermo Fisher Scientific) was used to evaluate cell viability. It contains resazurin, which is a blue dye that is cell permeable and non-fluorescent. Upon entering cells, resazurin is reduced to resorufin that produces very bright red fluorescence via the reduction reactions of metabolically active cells. Viable cells continuously convert resazurin to resorufin, thereby generating a quantitative measure of cell viability. The alamarBlue reagent was added to the gel contraction culture as 10% of the total volume (200µl in 2ml medium), and followed by an incubation at 37ºC for 4 hrs. And then, 100µl of the medium was taken from each sample and transferred to a 96-well plate. The fluorescence intensity was measured at Ex/Em=530/590nM using a plate reader (Fluostar Optima). Each experiment was performed with triplicate wells.

2.3 Real-time PCR

2.3.1 RNA isolation

Contraction gels with/without transient 24hrs treatment of NSC23766 were harvested at day0, 3 and 5, and placed straight into TRIzol Reagent (Invitrogen) at 4°C for 1 hr (3 gels:1ml TRIzol). The day0 gels were obtained after 1hr of initial gel polymerisation in serum free medium. After the gels were completely dissolved with vortexing if necessary, 0.2 mL of chloroform per 1ml TRIzol was added and the solution was incubated for 2-3 min at room temperature after a vigorously shaking by hand for 15 sec. The samples were then centrifuged at 12000 x g for 15 min at 4°C to achieve phase separation. The aqueous phase that contained RNA was transferred to a new 1.5ml tube (Eppendorf) and 2 volumes of 100% ethanol (Sigma-Aldrich) was added. The mixture was transferred to an RNeasy spin column placed in a 2 ml collection tube (RNeasy Kit; Qiagen) and spun for 15s at 8000 x g

at room temperature. After discarding the flow-through, 700µl of Buffer RW1 and 500µl of Buffer RPE were added to the column respectively, each following a 15s centrifugation at 8000 x g at room temperature. A final wash of 500µl Buffer RPE was repeated, and the column was spin again for 2 min at 8000 x g to thoroughly wash the membrane. The column was placed in a new 1.5 ml collection tube (Qiagen) and 40µl of RNase-free water (Qiagen) was added directly to the column membrane. After a short incubation of 3-5 min at room temperature, the column was centrifuged for 1 min at 8000 x g to elute the RNA. The concentration of the RNA samples was measured using NanoDrop Spectrophotometer (Thermo Fisher Scientific).

2.3.2 Reverse transcription

Reverse transcription was carried out using QuantiTect Reverse Transcription Kit (Qiagen) to obtain cDNA samples. The RNA samples were briefly incubated in gDNA Wipeout Buffer at 42°C for 2 min to remove remaining genomic DNA. And then, a reverse-transcription master mix that contained Quantiscript Reverse Transcriptase, 5x Quantiscript RT Buffer, and RT Primer Mix was added to the template RNA according to manufacturer's instructions. The reactions were incubated at 42°C for 30 min, and 95°C for 3 min to inactivate the transcriptase. The cDNA samples obtained were proceed directly to real-time PCR, or stored at -80°C for long-term storage.

2.3.3 qPCR

The mRNA expression levels of the genes of interest were measured by qPCR using Taqman Gene Expression Assays (Thermo Fisher Scientific) (**Table 2.3**), which rely on the 5´-3´ exonuclease activity of Taq polymerase to cleave a dual-

labelled probe during hybridization to the complementary target sequence and fluorophore-based detection. 10ng of cDNA was added into the reaction mix made of 12.5µl of Taqman gene expression master mix (Thermo Fisher Scientific), 1.25µl of Taqman assays (identification numbers listed below), and 6.25µl of RNase free water (Qiagen) to achieve a final volume of 25µl on the MicroAmp optical 96-well reaction Plate (Applied Biosystems). The plate was sealed with MicroAmp optical adhesive film (Applied Biosystems) and read in the HT7900 Fast Real-Time PCR system (Applied Biosystems) using the standard protocol: hold at 50°C for 2 min, hold at 95°C for 10 min, followed by repeating 40 cycles of 95°C for 15 sec for annealing and 60°C for 1 min for elongation. The reactions were performed in triplicate wells and the HPRT1 gene (hypoxanthine phosphoribosyl transferase 1) was used as an endogenous control for normalizing the sample concentration. The 2(-ΔΔCT) method was applied to quantify the mRNA expression levels (Livak and Schmittgen, 2001).

Table 2.3 Taqman Gene Expression Assays used in the qPCR experiments.

	Taqman Gene Expression Assay
Gene name	**Identification number**
IL8	Hs00174103_m1
IL1A	Hs00174092_m1
HBEGF	Hs00181813_m1
MMP1	Hs00899658_m1
MMP3	Hs00968305_m1
MMP10	Hs00233987_m1
PMEPA1	Hs00375306_m1
TNFAIP6	Hs01113602_m1
LIMCH1	Hs00405524_m1
KCND2	Hs01054873_m1
PLXDC2	Hs00262350_m1
ATRNL1	Hs00827146_m1
FAM213A	Hs00800009_s1
GAS6	Hs01095852_s1
GBP3	Hs00544385_m1
SLC20A1	Hs00965587_m1
CCND1	Hs00765553_m1
HRPT1	Hs02800695_m1

2.4 Microarrays

2.4.1 The *in vitro* microarray

Independent parallel sets of RNA samples isolated from contraction gels of conjunctival fibroblast cells HTF7071 at day0, 3 and 5 were prepared as described previously. Day0 gels were cultured in serum free medium and harvested 1 hour after gel polymerization. The gels harvested at day3 and 5 were cultured in normal medium with 10% serum (FBS) and treated with/without transient treatment of NSC23766 for the first 24 hours after gel polymerization. Accordingly, the sample groups were labelled as Day0, Day3 and Day5, and Day3NSC and Day5NSC. Initially all the samples were triplicated and processed by Dr. Tovell. However, two replicates from Day0 and Day5 group respectively had inadequate amount of RNA, thus were re-prepared by myself. Nevertheless, the replacement samples that I processed were isolated from gels made with serum containing medium, thus exhibited a different gene expression profile comparing to the Tovell's ones due to the early serum stimulation. Therefore, the final analysis was performed with only Tovell's samples in which the Day0 and Day5 groups only had duplicate replicates.

The samples were assessed for quality, integrity, quantity and purity using a bioanalyser (QC model 2100; Aglient, Santa Clara, CA) and reverse-transcribed to cDNA, labelled and hybridised to the array chip, and then analysed on the GeneChip Human Gene 1.0 ST transcriptome-level cDNA platform (Affymetrix, Santa Clara, CA) at the UCL Genomics microarray laboratory, Institute of Child Health (London, UK) following the standard Affymetrix protocols. Arrays were scanned on a GeneChip 3000 7G Scanner (Affymetrix) and the '.DAT' files collected were converted to '.CEL' files using 2100 Bioanalyzer (Agilent), which were subsequently processed using the Robust Multi-array Average (RMA) normalization

methodology (Irizarry et al., 2003). Due to the small sample size, a moderate t-test was conducted. The gene expression levels, annotations, the principal component analysis (PCA), and clustering heatmaps were obtained by analysing the '.CEL' files through Altanalyze v2.0.9 (http://www.altanalyze.org/) (Emig et al., 2010). Genes that were differently expressed were filtered as fold change>1.2 times and a significance of $p<0.05$. The identification of the functional-related enrichment gene clusters was carried out by the Database for Annotation, Visualization and Integrated Discovery Bioinformatics v6.8 (DAVID; http://david.abcc.ncifcrf.gov/) (Huang da et al., 2009a, Huang da et al., 2009b).

2.4.2 The *in vivo* microarray

The raw data of the microarray profiling of *in vivo* wounding model in rabbit was obtained from Dr. Daniel Paull who performed the study using rabbits (2-2.5kg, 12-14 weeks old, Harlan UK) that underwent glaucoma filtration surgery (GFS) on the left eye, and with the right eye used as un-operated control. GFS created a fornix-based conjunctival flap with a drainage channel that connected the anterior chamber to the sub-Tenon's space underneath, together those formed a 'bleb' on the surface of the eye. Five days after surgery, conjunctival samples (approximately 2 × 2mm in size) of both eyes were taken from the centre of the bleb and RNA was extracted using the RNeasy Mini Kit (Qiagen) following the manufacturer's instructions as described before. The quality was assessed using the 2100 Bioanalyzer (Agilent) and RNA 6000 Nano Chip Kit (Agilent), and then the samples were hybridised to the arrays all following Agilent standard protocols. The microarray was undertaken using a custom designed, rabbit specific, Agilent 8 × 15k 60-mer oligonucleotide arrays (Agilent AMADID# 017130). The data was analysed with the Limma package with Bioconductor (Ritchie et al., 2015), which

applied a modified t-test using a Bayesian approach. Genes that were differently expressed were filtered as fold change>1.2 times and a significance of $p<0.05$.

2.5 MMP activity assay

The total (both pro and active forms) and active (only active form) activities of the MMPs' in the contraction medium were determined using the MMP activity assay kit (Abcam ab112147). It uses a fluorescence resonance energy transfer (FRET) peptide as a MMP substrate, which upon cleavage by MMPs releases the fluorescence. 25µl of culture medium was removed from each control and NSC23766 treated gel contraction culture at Day0, Day3 and Day5, and added to 96-well plate that contained 25µl of 2mM APMA (4-aminophenylmercuric acetate) working solution that activates the pro MMPs or 25 µl of Assay buffer as non-stimulated control and incubated at 37°C for 3hrs. And then, 50µl of the MMP Red Substrate was added to the reaction and incubated at room temperature for 1hr. The fluorescence intensity was measured at Ex/Em=540/590nM using a plate reader (Fluostar Optima). The assay was performed in triplicate wells.

2.6 MMP1 ELISA

The MMP1 protein secreted into the culture medium by fibroblasts was measured using MMP1 Human ELISA (Enzyme-Linked Immunosorbent Assay) Kit (Abcam ab100603) that quantitatively measured the Human MMP1 pro and active forms in cell culture supernatants. 100µl of the culture medium was removed from gel contraction culture at desired time points and eight MMP1 protein standards ranging from 0 to 18000 pg/ml were added into the ELISA plate respectively for incubation for 2.5hrs. The solution was discarded and the wells were washed with 300 µl of wash solution/well for 4 times. And then, 100 µl of Biotinylated MMP1 Detection

Antibody and 100µl of HRP-streptavidin solution were added to each well respectively and each incubated for 1hr with a washing step followed as previously described. 100µl/well of the one-step TMB-ELISA substrate solution was added to the plate and incubated for 30 min in the dark. Finally, 50µl of stop solution was added to each well and the absorbance was read immediately at 450 nm on the plate reader (Fluostar Optima). The whole experiment was performed at room temperature and each sample was assessed in triplicate wells. The plate was incubated with gentle shaking on a plate shaker.

2.7 siRNA

The silencing of the genes of interest was achieved using siRNA SMARTpools (Dharmacon) that contained a mixture of 4 siRNAs targeting the same human gene. Either HiPerfect Transfection Reagent (Qiagen) or Lipofectamine RNAiMAX Transfection Reagent (Thermo Fisher Scientific) was used depending on the gene of target. Two non-target (NT) siRNAs were initially tested as negative control, including the Allstars negative control siRNA (Qiagen), and the siGENOME non-targeting siRNA #1 (Dharmacon). However, each of them had their own side-effects, for example the siGENOME one decreased the contractile activity of fibroblasts, and the Allstars one slightly increased MMP1 production in the cells. In the end, the Allstars NT siRNA (Qiagen) was applied in most of the experiments. The details of the siRNAs and their working concentrations used are listed in **Table 2.4**. The concentration and transfection reagent used for NT siRNA were matching the ones applied for the target siRNA. The cells were transfected with the fast-forward transfection method. Firstly, $0.8x10^5$ cells were seeded on 6cm petri dish in 4ml of culture medium. When the cells were attached to the bottom of the dish (2-3hrs after the seeding), a transfection complex that consisted of siRNA, transfection reagent and serum-free culture medium (or Opti-MEM (Thermo Fisher Scientific) if

using RNAiMAX) was added drop-wise on the cell culture. The petri dish was gently swirled to ensure uniform distribution of the complex. The cells were incubated at 37ºC with 5% CO_2 and medium unchanged. 72 hrs after transfection, cells were harvested and seeded into collagen contraction assay, as well as lysed for immunoblotting to confirm the protein downregulation.

Table 2.4 List of siRNA used for the gene silencing study, with the catalogue number, working concentration and the transfection reagent applied.

Gene	Cat. No.	Concentration	Reagent
Rac1	M-003560-06-0005	10nM	HiPerfect
Cdc42	L-005057-00-0005	20nM	HiPerfect
RhoA	M-003860-03-0005	10nM	RNAiMAX
MMP1	M-005951-01-0005	10nM	HiPerfect
Rac2	M-007741-01-0005	10nM	HiPerfect
Arhgap5	M-009580-01-0005	10nM	HiPerfect
Racgap1	M-008650-00-0005	10nM	HiPerfect
Arhgef3	M-013243-00-0005	5nM	RNAiMAX
Allstars Non-target (NT)	SI03650318	5-20nM	Accordingly
siGENOME Non-Targeting #1	D-001206-13-05	5-20nM	Accordingly

2.8 Protein extraction

2.8.1 Protein extraction from 2D culture

Total protein extraction of cells seeded on tissue culture plate (2D format) was performed by lysing cells in ice cold Radioimmunoprecipitation assay (RIPA) buffer (150mM NaCl, 0.1% Triton X-100, 0.5% sodium deoxycholate, 0.1% sodium dodecyl sulphate (SDS), 50mM Tris-HCl pH8.0 (all from Sigma-Aldrich), cOmplete protease inhibitor cocktail (Roche)) on ice. The cells were then scraped from the plate using a cell scraper (VWR) and lysing on ice for 15-20 min, followed by a centrifugation at 11000 rpm at 4 ºC for 15 min. The insoluble pellet was discarded and the supernatant was stored at -80 ºC.

2.8.2 Protein extraction from 3D culture

To extract protein from cells seeded in collagen gels (3D format), the gel was first digested. Triplicate collagen gels from contraction assay were carefully transferred to a 15ml conical centrifuge tube (Sigma-Aldrich) that contained 500µl of 0.05% Collagenase D (Roche) in DPBS (Thermo Fisher Scientific) using pipette tip. The tube was placed in the incubator at 37 ºC for no longer than 30 min until the gels were just dissolved. 3ml of DPBS was added to the tube to dilute the collagenase and the solution was centrifuged at 1400 rpm at 4 ºC for 7 min. The supernatant was carefully aspirated without disturbing the cell pellet. Finally, the cells were resuspend in 50µl of ice cold RIPA buffer, lysed on ice for 10 min, centrifuged at 11000 rpm at 4 ºC for 15 min, and the supernatant containing the cellular protein was stored at -80 ºC.

2.9 Western blotting

The concentrations of the protein samples were determined using the bicinchoninic acid (BCA) assay (Thermo Fisher Scientific). 10µl of the protein samples and protein standards (ranging from 0.125 to 2mg/ml) were added to 50µl of assay reagent on flat-bottom 96-well plate (Thermo Fisher Scientific) and incubated at 37 ºC for 30 min. The absorbance was read at 562nm using a plate reader (Fluostar Optima). The protein samples were then normalised to same concentration by adding RIPA buffer, and 5x sample buffer (Thermo Fisher Scientific) and boiled in the heat block at 90 ºC for 5 min for denaturation. 5µg of the samples were loaded on 8-16% precast polyacrylamide Tris-Glycine or 4-12% Bis-Tris Plus mini gels (Thermo Fisher Scientific) and ran with Tris-HEPES SDS or MOPS SDS running buffer (Thermo Fisher Scientific) respectively depending on the size of the protein of interest at 200V for 20-40 min until optimal separation obtained. The wet transfer method was applied to transfer the proteins on the gel to polyvinylidene difluoride

(PVDF) membrane (Thermo Fisher Scientific). The membrane was soaked in methanol (VWR) for activation for a few seconds, then quickly rinsed in water, and equilibrated in transfer buffer (25mM Tris-HCl pH8.3, 192mM Glycine, 20% v:v methanol) with filter paper (Thermo Fisher Scientific) and foam pads (Bio-Rad). The transfer sandwich was assembled in the order of foam pads/filter paper/PVDF membrane/gel/filter paper/foam pads, which was subsequently placed in the Mini Trans-Blot cell apparatus (Bio-Rad) and transferred at 110V for 1hr. The membrane was blocked in Blotto buffer (5% reduced-fat milk in TBS-T (0.1% Tween-20 in Tris-buffered saline)) for 1hr at room temperature and followed by overnight incubation at 4 ºC in primary antibody (**Table 2.5**). Then, after 3 times x10 min each washing in TBS-T, the membrane was incubated in secondary horseradish peroxidase (HRP)-conjugated antibody (Jacksons ImmunoResearch) (**Table 2.6**) in Blotto buffer for 2hrs, followed with 3 times x10 min each washing in TBS-T. Lastly, the membrane was placed in the transparent plastic layflat sheet (Scientific Laboratory Supplies), incubated in Pierce ECL Plus Substrate (Thermo Fisher Scientific) for 3-5 min, and developed in the dark room using Fujifilm Corporation RX NIF Sheet X-ray Film (Thermo Fisher Scientific) in the X-ray developer with varied exposure time depending on the signal strength. The film was scanned with a high resolution scanner and image was analysed using ImageJ software (http://rsb.info.nih.gov/ij/).

Table 2.5 Primary antibodies used in the Western blot experiments.

Antibody	Cat. No	Supplier	Dilution
anti-MMP1	ab38929	Abcam	1/1000
anti-Rac1	ARC03	Cytoskeleton	1/500
anti-cdc42	sc-8401	Santa Cruz	1/500
anti-RhoA	sc-179	Santa Cruz	1/1000
anti-Rac2	sc-293429	Santa Cruz	1/1000
anti-Arhgap5	611612	BD Biosciences	1/1000
anti-Racgap1	ab2270	Abcam	1/1000
anti-Arhgef3	ab154263	Abcam	1/1000
anti-Gapdh	ab9485	Abcam	1/3300

Table 2.6 Secondary antibodies used in the Western blot experiments.

Antibody	Cat. No	Supplier	Dilution
Donkey Anti-Goat IgG (H+L)	705-035-003-JIR	Jacksons ImmunoResearch	1/5000
Goat Anti-Rabbit IgG (H+L)	111-035-003-JIR	Jacksons ImmunoResearch	1/5000
Donkey Anti-Mouse IgG (H+L)	715-035-150-JIR	Jacksons ImmunoResearch	1/5000

2.10 Subcellular fractionation

Parallel sets of fibroblast cells were seeded as $1.2x10^5$ cells/dish on 6cm petri dish in 4ml of culture medium with/without the treatment of 50µM NSC23766 for the first 24hrs and cultured for 3 days. To separate nucleus and cytoplasm, cells were typsinised, spun down and resuspended in 300µl of ice-cold fractionation buffer (sucrose 250mM, HEPES PH7.4 20mM, KCl 10mM, MgCl2 2mM, EDTA 1mM, EGTA 1mM, DTT 5mM (all from Sigma-Aldrich), cOmplete™ protease inhibitor cocktail (Roche)). The cells suspension was passed through a 25 gauge needle for 10 times using a 1ml syringe, and then left on ice for 20 min, following by centrifugation at 3000 rpm at 4 ºC for 5 min to separate the nuclei and the cytoplasm components. The cytoplasm components in the supernatant were clarified by centrifugation at 8000 rpm at 4 ºC for 10 min to discard any insoluble pellet. The nuclear pellet remained was washed with 500µl of ice cold fractionation buffer, and dispersed with a pipette and passed through a 25 gauge needle for 10

times, followed by a centrifugation at 3000 rpm at 4 ºC for 10 min to remove any cytoplasm contamination. The supernatant was discarded and the pellet was resuspended in 300µl of ice cold RIPA buffer added with 10% glycerol, and then sonicated briefly for 10 sec. It was subsequently centrifuged again at 8000 rpm at 4 ºC for 10 min to discard any insoluble pellet. The whole cell lysate was obtained by lysing equal number of cells in 600µl of ice cold RIPA buffer according to the standard protein extraction protocol describe previously. The sample loading of whole cell, nuclear and cytoplasmic lysates for electrophoresis was equal in volume (20µl for each sample).

2.11 Cell staining and microscopy

2.11.1 2D fluorescent imaging

Three 13mm diameter coverslips (VWR) were placed in 3cm tissue culture dish, and treated with 1M HCl for 5 min, washed with sterile PBS, followed by incubation of 70% ethanol for 5 min, and a final wash in sterile PBS. $1x10^5$ cells were seeded per dish in 2ml of culture medium, and cultured at 37ºC with 5% CO_2 overnight. The next day, the medium was aspirated and the dish was rinsed quickly with warm PBS, followed by fixation in 3.7% formaldehyde (Sigma-Aldrich) in PBS for 7 min, permeabilization in 0.5% Triton-X100 (Sigma-Aldrich) in PBS for 20 min, and incubation in 0.1M Glycine (Sigma-Aldrich) in PBS for 10 min. The dish was then washed with 1% BSA (Thermo Fisher Scientific) in TBS pH8.0 for 5 min, and the coverslips were transferred onto a glass plate covered with parafilm and blocked with 50µl of rhodamine-phalloidin (Thermo Fisher Scientific) 1:50 in 1% BSA plus 1% FBS in TBS pH8.0 in a humidified chamber in the dark for 20 min. Then, the phalloidin block was replaced with 50µl of primary antibody (anti-MMP1 antibody) 1:50 in 1% BSA in TBS pH8.0 and incubated for 1hr in the dark. The coverslips

were washed for 30 min with 1% BSA in TBS pH8.0 with a minimum of 3 changes of buffer, followed by incubation of 50µl of secondary antibody (Alexa Fluor® 488-AffiniPure Donkey Anti-Rabbit IgG (H+L), Stratech) 1:50 in 1% BSA in TBS pH8.0 for 1hr in the dark, and wash again for 30 min with 1% BSA in TBS pH8.0 as previously described. After carefully blotting the extra liquid, the coverslips were inverted onto the Fluoroshield mounting medium (Abcam ab1041135) drop on the glass slide (VWR) using forceps, and the edges were sealed by nail polish. The slides were stored at 4ºC in the dark and images were carried out on a Nikon Ti-E microscope with CoolSNAP HQ2 camera (Photometrics, Tucson, AZ, USA), using a x20 air objective (20x Plan Fluor ELWD ADM with correction collar). The images were imported into ImageJ software and the cells were manually traced for the calculation of cell area and integrated density. Corrected integrated density (CID) was calculated based on the equation: CID=Integrated density - (cell area x background integrated density).

2.11.2 Collagen gel imaging

Collagen contraction assays were terminated at the desired time point. The culture medium was removed by aspirating, and the gels were fixed with pre-warmed (37ºC) 3.7% formaldehyde (Sigma-Aldrich) in PBS for 30 min, followed with permeabilisation with 2ml of 0.5% Triton-X100 (Sigma-Aldrich) in PBS for 30 min, and 1 time rinse and incubation with 0.1M Glycine (Sigma-Aldrich) in PBS for 30 min. The gels were then transferred into eppendorf tubes (Eppendorf) with 50µl of 0.5µM labelled phalloidin (Thermo Fisher Scientific) (approximately 1:20 of the stock phalloidin) in TBS pH8.0 with 1% BSA plus 1% FBS, and incubated in the dark for 30 min. The gels were transferred to another eppendorf tube with 50µl of 1:50 anti-MMP1 primary antibody (ab38929, Abcam; or in-house produced anti-MMP1 antibody provided by Dr. Yoshi Itoh from Oxford University) in TBS pH8.0 with 1%

BSA, and incubated overnight at 4ºC in the dark. The primary antibody was removed by gentle pipetting, and the eppendorf tubes were filled with TBS pH8.0 with 1% BSA, and placed in a 50ml centrifuge tube (Thermo Fisher Scientific) that wrapped in foil paper on the rotating wheel for 10 min washes for 3 times. The gels were then transferred to fresh eppendorf tubes with 50µl 1:50 of the secondary antibody (Alexa Fluor® 488-AffiniPure Donkey Anti-Rabbit IgG (H+L), Thermo Fisher Scientific) in TBS pH8.0 with 1% BSA and incubated for 2-3 hrs in the dark at room temperature, following with 3 x 15 min washes as described previously. The last wash was made in TBS pH8.0 instead of TBS pH8.0 with 1% BSA. The gels were placed back to the centre of the original Mattek dishes, and mounted by adding 200µl of Fluoroshield mounting medium (Abcam ab1041135) or freshly made mounting medium (N-propyl gallate 6g/L in glycerol 50% in TBS pH8.0) and covered with coverslip.

The gels were imaged using Biorad Radiance confocal microscope (Zeiss Axiovert S100/Biorad Radiance 2000) with a long working distance objective (ZEISS LD plan- Neofluoar 63x0.75) to visualise cells (red, green HeNe laser 540/565nm) and matrix (confocal reflection microscopy). The 3D re-construction was processed using Volocity software (PerkinElmer). In addition, imaging of the gels was also performed using Nikon Ti-E microscope with CoolSNAP HQ2 camera (Photometrics, Tucson, AZ, USA) with 20x objective (20x S Plan Fluor ELWD 0.45 Ph1). The composite images were captured with a z-stacking of 2µm per layer and the projection process was performed using the Nikon NIS elements software.

2.12 Statistical analysis

The statistical analysis was performed using Microsoft Excel 2013. Data is presented as means averaged from at least triplicate experiments ± standard error of the mean (SEM). Student's t-test was performed using 2-tailed paired tests to establish significant differences and individual p value was displayed. In the case of different experimental value applied, it is indicated in the figure's legend.

Chapter 3 The 'molecular portrait' of fibroblast-mediated contraction *in vitro*

3.1 Gene expression profiling reveals global but transient gene activation during contraction

To identify the molecular pathways underlying fibroblast-mediated matrix contraction following serum stimulation, and the role of small Rho GTPase Rac1 in contraction, a microarray platform (Affymetrix human gene 1.0 ST) was used to analyse the gene expression profiles of human conjunctival fibroblasts during contraction at time point day0 (30min after initial gel polymerisation in the serum free condition), day3 (peak contraction rate) and day5 (contraction plateau) with/without transient treatment with Rac1 inhibitor NSC23766 for 24 hrs in the standard free-floating collagen gel contraction assay (Tovell et al., 2011). As explained in **Chapter 2** (**2.4.1**), all the groups contained triplicate samples, except Day0 and Day5 those had duplicate samples. The raw Affymetrix CEL files were processed using the Robust Multi-array Average (RMA) normalization methodology (Irizarry et al., 2003), and data analysis was performed using AltAnalyze 2.0.9 (http://www.altanalyze.org/). A moderated t-test was conducted due to the small sample size. The data was evaluated to be of high quality according to the density plot that showed the distribution of normalised log2 probe set intensity values of the samples (**Figure 3.1**). It confirmed a very good overlapping to allow comparisons that in line with the principle of "lower variability data with all other things being equal, should be judged to be of higher quality" (Gentleman, 2005). The Principal Component Analysis (PCA), which uses an orthogonal transformation to convert

samples of possibly correlated variables into a set of values of linearly uncorrelated variables, also demonstrated a very good level of similarities between the experimental replicates. The PCA plot also indicated that the Day3 samples were clearly separated from the others, whilst the NSC23766 treated ones were very close to the Day5 samples. Furthermore, little variation was shown between the Day5NSC and Day5 untreated samples (**Figure 3.2**). The gene expression patterns across all the samples were visualised by hierarchical clustering, which suggested a similar result to the PCA plot: among the three time points tested, the Day3 samples exhibited a strikingly strong and altered gene expression profile that implicated massive gene changes, which receded at day5. However, with NSC23766 treatment, this hyperactive gene cascade was supressed (**Figure 3.3**).

The differentially expressed genes among the contraction at day0, 3 and 5 non-treated group were compared by drawing a Venn diagram, which is an interactive tool for comparing lists with Venn Diagrams. There were over 10,000 genes being differentially regulated during the whole contraction process ($p<0.05$, fold change >1.2 times). Approximately half of the genes that went up from day0 to day3 (1672 of a total of 3162) also went down from day3 to day5 (1672 of a total of 2721). The same was true for the 1656 genes that both went down during day0 to day3 and backed up later on from day3 to day5, suggesting a major but transient activation of the fibroblasts during contraction, which receded after 3 days (**Figure 3.4**).

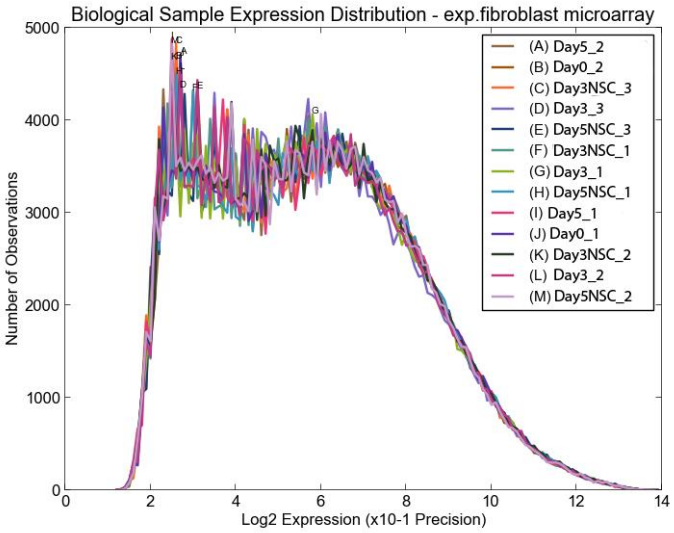

Figure 3.1 The distribution of normalised log2 probe set intensity values of the samples.

The density plot showed the density of the probe intensities was of good overlapping between the samples. Each line represented a different array in the experiment (Day0--J, B; Day3--G, L, D; Day5--J, A; Day3NSC--F, K, C; Day5NSC--H, K, M).

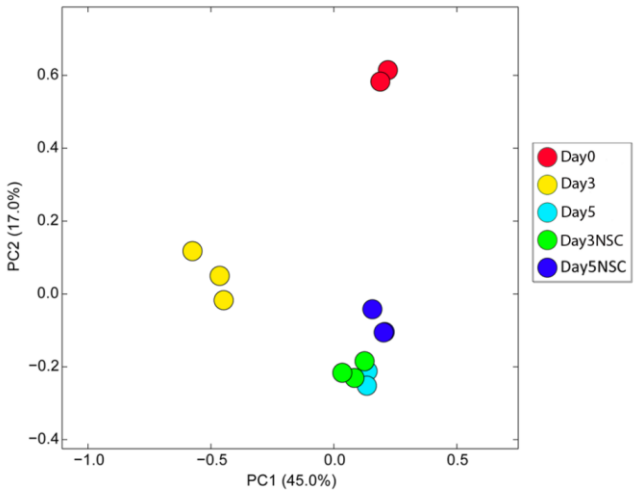

Figure 3.2 Principal Component Analysis (PCA) plot showing the separation of individual samples.

The PCA plot demonstrated a very good level of similarities between the experimental replicates. In terms of sample variation, Day3 samples were the most separated among all, whilst the Day3NSC, Day5NSC, and Day5 samples sit in a similar position. The Day0 samples showed a modest variability from the others.

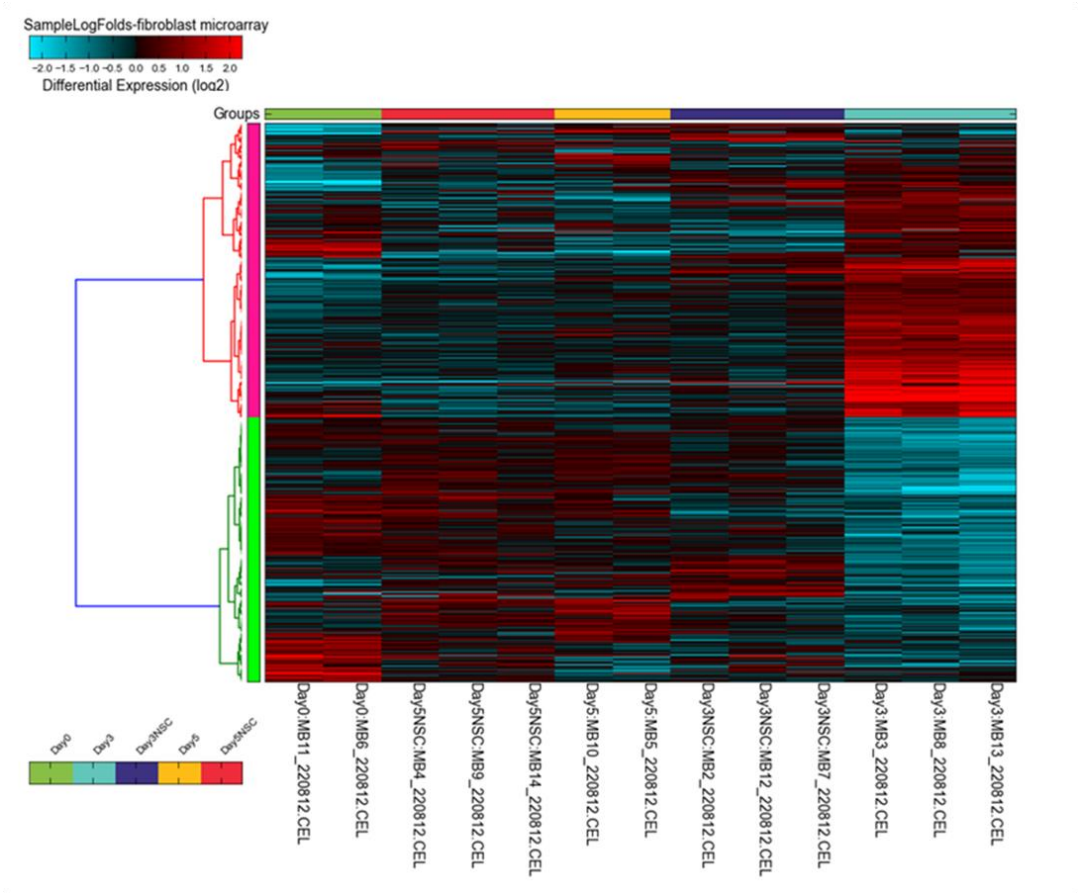

Figure 3.3 Hierarchical clustering heatmap showing the differential gene expressions (log2 fold) during contraction at the time points day0, 3 and 5 with/without NSC23766 treatment.

The expression pattern of each gene is displayed as a horizontal strip. The gene expression level (log2 fold) in each sample replicate is represented by a colour, according to the colour scale at the top left. Each column of the heatmap represents the expression pattern of a sample replicate, with the sample name labelled at the bottom. The sample groups are represented by the colour bar on the top of the heatmap, according to the colour scale at the bottom left. The figure illustrates that the Day3 sample group showed a strikingly strong and altered gene expression profile that exhibited a massive gene regulation towards opposite direction comparing to the others, whereas with the treatment of NSC23766, this hyperactive regulation was receded.

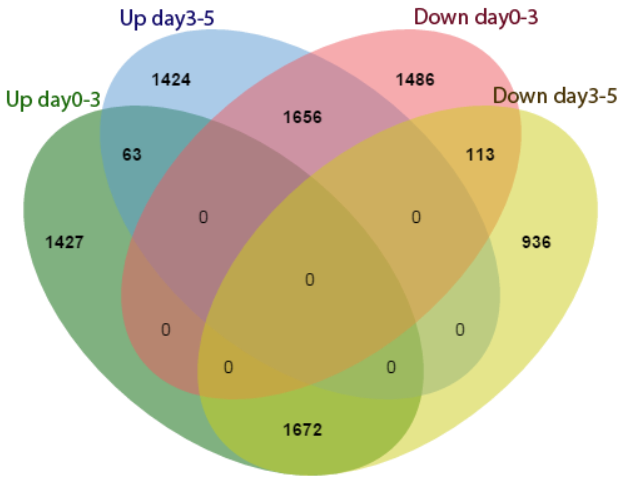

Figure 3.4 Paired comparisons of genes differentially expressed among day0, 3 and 5 during the in vitro contraction.

During the 5-day serum stimulated in vitro contraction, over 10,000 genes were captured during the process. More than 3000 genes were regulated up and down dynamically, with 1672 genes being upregulated from day0 to 3 changed to the opposite direction from day3 to 5, whilst 1656 downregulation genes from day0 to 3 reactivated again at day3 to 5.

3.2 Early contraction: a classical wound healing/serum response

According to the gene expression profiles, the fibroblast-mediated *in vitro* contraction was divided into two stages: early contraction (from day0 to 3) and late contraction (from day3 to 5). The most dramatic gene expression changes (over 60 times) were observed in the early contraction upregulation profile, which included inflammatory factors (F2EL1, LIF, PTGS2), cytokines (IL8, IL36B, IL11), growth factors (HBEGF, PTHLH) and matrix metalloproteinases (MMPs) (MMP1, MMP10), underlying a classical “response to wounding” profile (Iyer et al., 1999) (**Table 3.1**). Meanwhile, genes related to cell migration (CD34, PEX2, TGFBR3) and membrane integrity (ADAM22, FGFR2, LDLR) were found greatly suppressed, with the most downregulated gene being affected less than 20 fold (**Table 3.2**).

Table 3.1 The symbol, definition and fold change of the first 100 genes upregulated in the early contraction from day0 to 3 (fold change>2 times, p value<0.05). 75 of them were downregulated at day3 in the NSC23766 treated samples comparing to the untreated control samples. 25 genes that did not show downregulation were coloured in blue. The serum response genes that were identified in a study of transcriptional profile of human foreskin fibroblasts in response to serum (Iyer et al., 1999) were labelled in bold character (12 genes).

Symbol	Definition	FoldChng
IL1RN	interleukin 1 receptor antagonist	63.56
CXCR4	chemokine (C-X-C motif) receptor 4	62.13
SERPINB2	serpin peptidase inhibitor, clade B (ovalbumin), member 2	60.46
F2RL1	coagulation factor II (thrombin) receptor-like 1	47.90
MMP1	matrix metallopeptidase 1 (interstitial collagenase)	38.73
RNA5SP242	RNA, 5S ribosomal pseudogene 242	34.76
IL8	interleukin 8	29.98
CYP1A1	cytochrome P450, family 1, subfamily A, polypeptide 1	29.46
CYP19A1	cytochrome P450, family 19, subfamily A, polypeptide 1	28.78
HBEGF	heparin-binding EGF-like growth factor	27.53
TFPI2	tissue factor pathway inhibitor 2	25.80
RAD54L	RAD54-like (S. cerevisiae)	25.25
KRTAP3-2	keratin associated protein 3-2	25.21
LSMEM1	leucine-rich single-pass membrane protein 1	23.49
CD163L1	CD163 molecule-like 1	23.22
MMP10	matrix metallopeptidase 10 (stromelysin 2)	22.09
MFSD2A	major facilitator superfamily domain containing 2A	21.00
ITGA2	integrin, alpha 2 (CD49B, alpha 2 subunit of VLA-2 receptor)	20.46
TSPAN13	tetraspanin 13	20.36
LPXN	leupaxin	20.00
ANGPTL4	angiopoietin-like 4	18.87
HS3ST2	heparan sulfate (glucosamine) 3-O-sulfotransferase 2	18.43
LIF	leukaemia inhibitory factor	18.31
UPP1	uridine phosphorylase 1	16.98
C12orf50	chromosome 12 open reading frame 50	16.81
PAX8-AS1	PAX8 antisense RNA 1	16.63
HAS2	hyaluronan synthase 2	15.56
TEX26	testis expressed 26	15.46
RNU6ATAC2P	RNA, U6atac small nuclear 2, pseudogene	14.52
ZNF267	zinc finger protein 267	13.09
VTRNA1-3	vault RNA 1-3	13.07
LEKR1	leucine, glutamate and lysine rich 1	12.79
RNU6ATAC3P	RNA, U6atac small nuclear 3, pseudogene	12.40
ADTRP	androgen-dependent TFPI-regulating protein	12.24
MT1G	metallothionein 1G	11.79
MIR222	microRNA 222	11.61
PTHLH	parathyroid hormone-like hormone	11.54
GEM	GTP binding protein overexpressed in skeletal muscle	11.46
FCGR1B	Fc fragment of IgG, high affinity Ib, receptor (CD64)	11.35

CDCP1	CUB domain containing protein 1	11.27
PMEPA1	prostate transmembrane protein, androgen induced 1	11.27
STC1	stanniocalcin 1	11.23
SLC16A6	solute carrier family 16, member 6 (monocarboxylic acid transporter 7)	11.08
PRSS3	protease, serine, 3	10.99
RP11-170L3.8	n/a	10.71
USP38	ubiquitin specific peptidase 38	10.63
C5orf45	chromosome 5 open reading frame 45	10.51
ABCC2	ATP-binding cassette, sub-family C (CFTR/MRP), member 2	10.49
LIMD1-AS1	LIMD1 antisense RNA 1	10.48
TMEM100	transmembrane protein 100	10.45
PDK4	pyruvate dehydrogenase kinase, isozyme 4	10.44
SIK1	salt-inducible kinase 1	10.13
TNC	tenascin C	10.08
CCL20	chemokine (C-C motif) ligand 20	9.91
MT1H	metallothionein 1H	9.80
PRSS3P2	protease, serine, 3 pseudogene 2	9.77
NCKAP1L	NCK-associated protein 1-like	9.75
GABARAP	GABA(A) receptor-associated protein	9.71
S100A2	S100 calcium binding protein A2	9.71
MT1F	metallothionein 1F	9.68
MIR31HG	MIR31 host gene (non-protein coding)	9.64
E2F7	E2F transcription factor 7	9.58
SLC39A14	solute carrier family 39 (zinc transporter), member 14	9.51
MT1M	metallothionein 1M	9.29
CSRNP1	cysteine-serine-rich nuclear protein 1	9.27
CREB5	cAMP responsive element binding protein 5	9.20
SLC22A3	solute carrier family 22 (extraneuronal monoamine transporter), member 3	9.19
SCUBE2	signal peptide, CUB domain, EGF-like 2	9.07
TEX35	testis expressed 35	9.00
IL36B	interleukin 36, beta	9.00
BCL2L10	BCL2-like 10 (apoptosis facilitator)	8.96
RYBP	RING1 and YY1 binding protein	8.95
DGKI	diacylglycerol kinase, iota	8.92
SEL1L2	sel-1 suppressor of lin-12-like 2 (C. elegans)	8.87
LINC01270	long intergenic non-protein coding RNA 1270	8.85
IL11	interleukin 11	8.84
C3orf67	chromosome 3 open reading frame 67	8.84
HIST2H3C	histone cluster 2, H3c	8.82
MIR103A2	microRNA 103a-2	8.73
DEFB107A	defensin, beta 107A	8.70
DEFB107B	defensin, beta 107B	8.70
PTPRR	protein tyrosine phosphatase, receptor type, R	8.67
DACT1	dapper, antagonist of beta-catenin, homolog 1 (Xenopus laevis)	8.65

NFATC2	nuclear factor of activated T-cells, cytoplasmic, calcineurin-dependent 2	8.62
PTGS2	prostaglandin-endoperoxide synthase 2 (prostaglandin G/H synthase and cyclooxygenase)	8.39
ACTN2	actinin, alpha 2	8.34
RCAN1	regulator of calcineurin 1	8.29
ETV4	ets variant 4	8.21
PLEK2	pleckstrin 2	8.20
ADNP2	ADNP homeobox 2	8.10
C3orf35	chromosome 3 open reading frame 35	8.07
CXCL1	chemokine (C-X-C motif) ligand 1 (melanoma growth stimulating activity, alpha)	8.03
KLF10	Kruppel-like factor 10	8.01
RNU6ATAC10P	RNA, U6atac small nuclear 10, pseudogene	8.00
TAGLN3	transgelin 3	7.99
PLAUR	plasminogen activator, urokinase receptor	7.91
TMEM217	transmembrane protein 217	7.84
IER3	immediate early response 3	7.83
IDI2	isopentenyl-diphosphate delta isomerase 2	7.81
DEC1	deleted in esophageal cancer 1	7.61

Table 3.2 The symbol, definition and fold change of the first 100 genes downregulated in the early contraction from day0 to 3 (fold change>2 times, p value<0.05). 58 of them were upregulated at day3 in the NSC23766 treated samples comparing to the untreated control samples. The genes that did not show upregulation were coloured in blue. The serum response genes that were identified in a study of transcriptional profile of human foreskin fibroblasts in response to serum (Iyer et al., 1999) were labelled in bold character (9 genes).

Symbol	Definition	FoldChng
C10orf10	chromosome 10 open reading frame 10	-16.46
GOLGA8O	golgin A8 family, member O	-12.71
FMO2	flavin containing monooxygenase 2 (non-functional)	-11.21
SLC40A1	solute carrier family 40 (iron-regulated transporter), member 1	-10.70
LANCL1	LanC lantibiotic synthetase component C-like 1 (bacterial)	-10.33
LMO3	LIM domain only 3 (rhombotin-like 2)	-10.26
ALPK1	alpha-kinase 1	-9.56
TFAP2B	transcription factor AP-2 beta (activating enhancer binding protein 2 beta)	-9.47
SLC25A27	solute carrier family 25, member 27	-9.15
VWA5A	von Willebrand factor A domain containing 5A	-9.12
OSR2	odd-skipped related 2 (Drosophila)	-8.76
IFIT1	interferon-induced protein with tetratricopeptide repeats 1	-8.61
SKP2	S-phase kinase-associated protein 2, E3 ubiquitin protein ligase	-7.90
BTN3A3	butyrophilin, subfamily 3, member A3	-7.52
NCAPH	non-SMC condensin I complex, subunit H	-7.27
ARHGAP28	Rho GTPase activating protein 28	-7.20
KLF2	Kruppel-like factor 2 (lung)	-7.08
RASSF4	Ras association (RalGDS/AF-6) domain family member 4	-7.07
KIT	v-kit Hardy-Zuckerman 4 feline sarcoma viral oncogene homolog	-7.07
HLTF	helicase-like transcription factor	-6.81
HNMT	histamine N-methyltransferase	-6.78
ADAM22	ADAM metallopeptidase domain 22	-6.76
EYA2	eyes absent homolog 2 (Drosophila)	-6.73
FANCA	Fanconi anemia, complementation group A	-6.65
AL953854.2	n/a	-6.36
PRUNE2	prune homolog 2 (Drosophila)	-6.35
DENND3	DENN/MADD domain containing 3	-6.34
CC2D2A	coiled-coil and C2 domain containing 2A	-6.23
SPEG	SPEG complex locus	-6.21
TRPM3	transient receptor potential cation channel, subfamily M, member 3	-6.20
LRIG3	leucine-rich repeats and immunoglobulin-like domains 3	-6.13
CRELD1	cysteine-rich with EGF-like domains 1	-6.12
OSBPL5	oxysterol binding protein-like 5	-6.01
DMAP1	DNA methyltransferase 1 associated protein 1	-5.96
RNY3P6	RNA, Ro-associated Y3 pseudogene 6	-5.94

NLGN1	neuroligin 1	-5.88
ABCA8	ATP-binding cassette, sub-family A (ABC1), member 8	-5.84
PPP1R12B	protein phosphatase 1, regulatory subunit 12B	-5.81
ARHGEF3	Rho guanine nucleotide exchange factor (GEF) 3	-5.81
MRVI1	murine retrovirus integration site 1 homolog	-5.73
DBC1	deleted in bladder cancer 1	-5.70
RIMS1	regulating synaptic membrane exocytosis 1	-5.68
MPP7	membrane protein, palmitoylated 7 (MAGUK p55 subfamily member 7)	-5.68
TMEM14E	transmembrane protein 14E	-5.61
IRAK1BP1	interleukin-1 receptor-associated kinase 1 binding protein 1	-5.52
CABLES1	Cdk5 and Abl enzyme substrate 1	-5.50
LDLR	low density lipoprotein receptor	-5.49
AC025171.1	n/a	-5.48
PPM1K	protein phosphatase, Mg2+/Mn2+ dependent, 1K	-5.47
ADH1B	alcohol dehydrogenase 1B (class I), beta polypeptide	-5.43
GCNT1	glucosaminyl (N-acetyl) transferase 1, core 2	-5.40
PRKG2	protein kinase, cGMP-dependent, type II	-5.38
RN7SKP56	RNA, 7SK small nuclear pseudogene 56	-5.36
ANG	angiogenin, ribonuclease, RNase A family, 5	-5.35
ACACB	acetyl-CoA carboxylase beta	-5.31
TMEM182	transmembrane protein 182	-5.30
PRELP	proline/arginine-rich end leucine-rich repeat protein	-5.14
C11orf74	chromosome 11 open reading frame 74	-5.14
ABCA9	ATP-binding cassette, sub-family A (ABC1), member 9	-5.13
PARP9	poly (ADP-ribose) polymerase family, member 9	-5.10
CCBE1	collagen and calcium binding EGF domains 1	-5.03
DTX3L	deltex 3-like (Drosophila)	-5.02
PEX2	peroxisomal biogenesis factor 2	-5.01
IFIT2	interferon-induced protein with tetratricopeptide repeats 2	-4.97
FGFR2	fibroblast growth factor receptor 2	-4.93
LMOD1	leiomodin 1 (smooth muscle)	-4.91
CCDC7	coiled-coil domain containing 7	-4.90
ACAD11	acyl-CoA dehydrogenase family, member 11	-4.87
TTLL1	tubulin tyrosine ligase-like family, member 1	-4.81
INVS	inversin	-4.80
LPIN1	lipin 1	-4.80
LPCAT3	lysophosphatidylcholine acyltransferase 3	-4.79
SELENBP1	selenium binding protein 1	-4.77
SLC9A9	solute carrier family 9, subfamily A (NHE9, cation proton antiporter 9), member 9	-4.74
UBL4B	ubiquitin-like 4B	-4.73
MAN1C1	mannosidase, alpha, class 1C, member 1	-4.69
ANXA3	annexin A3	-4.69
PGAP2	post-GPI attachment to proteins 2	-4.67
MTMR4	myotubularin related protein 4	-4.64

RTP4	receptor (chemosensory) transporter protein 4	-4.64
ATL3	atlastin GTPase 3	-4.63
JUP	junction plakoglobin	-4.62
SNORD48	small nucleolar RNA, C/D box 48	-4.53
C2CD5	C2 calcium-dependent domain containing 5	-4.51
C5orf30	chromosome 5 open reading frame 30	-4.50
GLRB	glycine receptor, beta	-4.50
KANK2	KN motif and ankyrin repeat domains 2	-4.49
CCL28	chemokine (C-C motif) ligand 28	-4.49
PARP4	poly (ADP-ribose) polymerase family, member 4	-4.49
CD34	CD34 molecule	-4.46
CRYZ	crystallin, zeta (quinone reductase)	-4.45
CCDC158	coiled-coil domain containing 158	-4.42
ALDH7A1	aldehyde dehydrogenase 7 family, member A1	-4.41
TGFBR3	transforming growth factor, beta receptor III	-4.40
TLR3	toll-like receptor 3	-4.40
GOLGA8M	golgin A8 family, member M	-4.39
ZMYM1	zinc finger, MYM-type 1	-4.37
MITF	microphthalmia-associated transcription factor	-4.37
DMKN	dermokine	-4.37
ZNF277	zinc finger protein 277	-4.35

To identify the important biological pathways underlying early contraction, DAVID (the Database for Annotation, Visualization and Integrated Discovery v6.8) functional annotation analysis was performed on the first 1000 genes up/downregulated respectively from day0 to 3. The top functional clusters of the upregulated genes according to enrichment score ($p<0.01$) included ion binding, response to wounding, regulation of transcription, cell motion and cytokine activity (**Figure 3.5a**); and the ones of the downregulated genes included cofactor binding, sterol metabolism and metal ion binding (**Figure 3.5b**).

Fibroblast-mediated gel contraction is reliant on the presence of serum or growth factors (Winkles, 1998, Cordeiro et al., 2000, Denk et al., 2003). Previous study has shown that fibroblasts in response to serum stimulation at least partially

recapitulated a classical wound response *in vitro* (Iyer et al., 1999). To evaluate the contribution of serum stimulation to the contraction profile of our model, we compared the early contraction gene expression profile to the transcriptional profile of human foreskin fibroblasts in response to serum (517 genes captured in total, with 479 of which with known annotation) (Iyer et al., 1999). We found that nearly half of the serum response genes (228 out of 479 genes) were captured in our early contraction gene expression profile, with 87 of which (44 within the first 1000 most upregulated genes) showing upregulation and 141 (60 within the first 1000 most downregulated genes) showing downregulation (**Figure 3.6**). These included the top up/downregulated genes in the *in vitro* profile, such as SERPINB2, IL8 and TFPI2 (fold change 60, 30, and 26 times respectively), as well as IFIT1, KIT and HLTF (fold change -9, -7, and -6.8 times respectively) (**Table 3.1**, **Table 3.2**). It suggested that the dramatic gene expression changes occurred during the early contraction were at least partly due to a response to serum. Nevertheless, the majority of the genes in the early contraction profile were not related to the serum response, suggesting that they were specifically related to contractile activity.

Figure 3.5 Functional annotation by DAVID of the first 1000 genes up/downregulated during early contraction from day0 to 3.

(a) The top 10 functional clusters of the first 1000 upregulation genes during early contraction according to enrichment score (p<0.01). (b) The top 10 functional clusters of the first 1000 downregulation genes during early contraction according to enrichment score (p<0.01). The first 10 most regulated genes of each cluster were listed below the score bar.

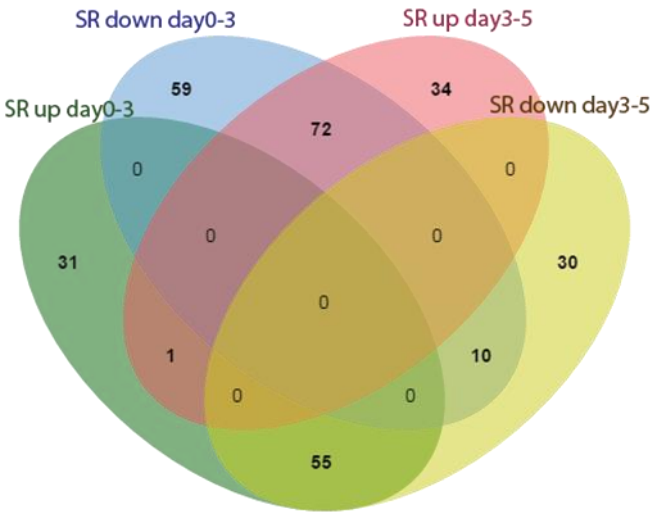

Figure 3.6 Paired comparisons of the fibroblast serum responsive (SR) genes (genes that were identified in a study of transcriptional profile of human foreskin fibroblasts in response to serum (Iyer et al., 1999)) that were regulated dynamically during the in vitro contraction.

87 and 141 SR genes were up/downregulated in the early contraction from day0 to 3, whilst 107 and 95 SR genes were up/downregulated in the late contraction from day3 to 5 respectively. 55 genes upregulated from day0 to 3 were downregulated from day3 to 5, and 72 genes downregulated from day0 to 3 were upregulated from day3 to 5. 1 gene that was upregulated consistently was CYP1B1, and 10 genes that were downregulated consistently were FOS, SYNPO2, PARD3B, SVEP1, ARID5B, C1R, MID1, ZFP36L2, CRABP2 and DAAM1.

3.3 Late contraction gene expression profile

In the later contraction from day3 to 5, the hyperactive early activation profile clearly receded. 3143 genes were found upregulated and 2721 downregulated during this stage. More than half of the genes were the ones that being up or downregulated from day0 to 3 going back to their original expression levels from day3 to 5 (**Figure 3.4**). The first 100 genes up/downregulated during late contraction are listed in (**Table 3.3**) and (**Table 3.4**), which showed that most of the extremely upregulated

genes in early contraction were downregulated, and those that significantly downregulated from day0 to 3 were upregulated again. Also, 202 serum response genes were found expressed in the late contraction. More than half of them (127 genes) were up or downregulated in the early contraction and being regulated to the opposite direction in the late contraction (**Figure 3.6**), suggesting that the active serum stimulation response rested. One serum response gene that was upregulated throughout the contraction was CYP1B1, which relates to oxidative homeostasis, ultrastructural organisation and the function of trabecular meshwork tissue in the eye (Bejjani et al., 1998). Ten genes that were downregulated consistently included FOS, SYNPO2, PARD3B, SVEP1, ARID5B, C1R, MID1, ZFP36L2, CRABP2 and DAAM1.

The functional annotation analysis of the first 1000 genes up/downregulated during late contraction by DAVID showed a reverse image of that of the early contraction. Gene groups that related to cytokine and growth factors, wound healing response, protein kinase and transcription activities were largely turned down, and the ones that related to oxidation reduction, steroid biosynthesis, mitochondrion and peroxisome were re-activated. Moreover, 63 genes were upregulated and 113 downregulated respectively in the early contraction from day0 to 3, and in the late contraction from day3 to 5 (**Figure 3.4**). The genes that involved in collagen degradation (MMP1, 3, 16), modulation of extracellular space (VEGFC, SERPINE2, AKR1B1) and vesicle mediated transport (NEDD4, SYTL5, PCLO) were promoted all the time; and the ones that related to glycoprotein (A2M, PZP, MASP1), EGF-like calcium binding (MATN2, F10, SVEP1) and cell adhesion (MATN2, COL14A1, TNXB) were supressed consistently (**Figure 3.7**).

Table 3.3 The symbol, definition and fold change of the first 100 genes upregulated in the late contraction from day3 to 5 (fold change>2 times, p value<0.05). 67 of them were the reverse-backs from the downregulation genes in the early contraction. The ones that were not regulated in the early contraction (fold change≤2 times, p value<0.05) were coloured in blue. The serum response genes (genes that were identified in a study of transcriptional profile of human foreskin fibroblasts in response to serum (Iyer et al., 1999)) were labelled in bold character (5 genes).

Symbol	Definition	FoldChng
TAC1	tachykinin, precursor 1	12.36
AKR1B10	aldo-keto reductase family 1, member B10 (aldose reductase)	9.37
GLRB	glycine receptor, beta	8.35
C5orf30	chromosome 5 open reading frame 30	8.12
ENPP5	ectonucleotide pyrophosphatase/phosphodiesterase 5 (putative)	7.75
DHCR7	7-dehydrocholesterol reductase	7.55
GPR125	G protein-coupled receptor 125	7.26
EYA2	eyes absent homolog 2 (Drosophila)	6.92
PTGR2	prostaglandin reductase 2	6.65
SKP2	S-phase kinase-associated protein 2, E3 ubiquitin protein ligase	6.62
ZNF737	zinc finger protein 737	6.60
NFXL1	nuclear transcription factor, X-box binding-like 1	6.54
SC5D	sterol-C5-desaturase	6.24
KCND2	potassium voltage-gated channel, Shal-related subfamily, member 2	6.16
CCRL1	chemokine (C-C motif) receptor-like 1	6.16
RGS12	regulator of G-protein signaling 12	6.16
TMEM155	transmembrane protein 155	6.13
RP3-509I19.1	n/a	6.13
TM7SF2	transmembrane 7 superfamily member 2	6.10
CEP57L1	centrosomal protein 57kDa-like 1	6.05
SLC6A6	solute carrier family 6 (neurotransmitter transporter, taurine), member 6	6.05
B3GALNT1	beta-1,3-N-acetylgalactosaminyltransferase 1 (globoside blood group)	5.81
DTNB	dystrobrevin, beta	5.79
PCBP4	poly(rC) binding protein 4	5.75
DEPTOR	DEP domain containing MTOR-interacting protein	5.71
OSBPL10	oxysterol binding protein-like 10	5.69
AFP	alpha-fetoprotein	5.69
CC2D2A	coiled-coil and C2 domain containing 2A	5.61
CLGN	calmegin	5.56
HLTF	helicase-like transcription factor	5.37
PARP4	poly (ADP-ribose) polymerase family, member 4	5.35
GPR63	G protein-coupled receptor 63	5.28
COG6	component of oligomeric golgi complex 6	5.21
FAM8A1	family with sequence similarity 8, member A1	5.20

PIR	pirin (iron-binding nuclear protein)	5.18
ZNF141	zinc finger protein 141	5.18
CNP	2',3'-cyclic nucleotide 3' phosphodiesterase	5.09
DCDC1	doublecortin domain containing 1	5.01
ANG	angiogenin, ribonuclease, RNase A family, 5	4.99
SGCD	sarcoglycan, delta (35kDa dystrophin-associated glycoprotein)	4.95
PGAP2	post-GPI attachment to proteins 2	4.94
ENOX1	ecto-NOX disulfide-thiol exchanger 1	4.91
TTC5	tetratricopeptide repeat domain 5	4.91
PEX2	peroxisomal biogenesis factor 2	4.89
TNFRSF11B	tumour necrosis factor receptor superfamily, member 11b	4.89
PLSCR4	phospholipid scramblase 4	4.85
MSMO1	methylsterol monooxygenase 1	4.82
TFAP2B	transcription factor AP-2 beta (activating enhancer binding protein 2 beta)	4.82
IMPACT	impact RWD domain protein	4.78
DDIT4L	DNA-damage-inducible transcript 4-like	4.76
RIN2	Ras and Rab interactor 2	4.74
PTPN13	protein tyrosine phosphatase, non-receptor type 13 (APO-1/CD95 (Fas)-associated phosphatase)	4.74
GPSM2	G-protein signaling modulator 2	4.70
SNCA	synuclein, alpha (non A4 component of amyloid precursor)	4.69
NFRKB	nuclear factor related to kappaB binding protein	4.65
PDGFRL	platelet-derived growth factor receptor-like	4.65
PLXDC2	plexin domain containing 2	4.64
C14orf1	chromosome 14 open reading frame 1	4.63
USF1	upstream transcription factor 1	4.60
ARRDC1	arrestin domain containing 1	4.56
RFX5	regulatory factor X, 5 (influences HLA class II expression)	4.54
GALNT5	UDP-N-acetyl-alpha-D-galactosamine:polypeptide N-acetylgalactosaminyltransferase 5 (GalNAc-T5)	4.53
COLEC12	collectin sub-family member 12	4.53
HIBCH	3-hydroxyisobutyryl-CoA hydrolase	4.51
TMEM97	transmembrane protein 97	4.48
ADAM22	ADAM metallopeptidase domain 22	4.47
UFSP2	UFM1-specific peptidase 2	4.46
TP53TG1	TP53 target 1 (non-protein coding)	4.45
FKBP7	FK506 binding protein 7	4.42
SMIM11	small integral membrane protein 11	4.40
MMP3	matrix metallopeptidase 3 (stromelysin 1, progelatinase)	4.40
NAALADL1	N-acetylated alpha-linked acidic dipeptidase-like 1	4.37
TMEM62	transmembrane protein 62	4.34
DTWD2	DTW domain containing 2	4.33
SPATA20	spermatogenesis associated 20	4.32
APEH	N-acylaminoacyl-peptide hydrolase	4.31
CLCC1	chloride channel CLIC-like 1	4.30
CNTN3	contactin 3 (plasmacytoma associated)	4.29

ACACB	acetyl-CoA carboxylase beta	4.27
KDELR3	KDEL (Lys-Asp-Glu-Leu) endoplasmic reticulum protein retention receptor 3	4.25
ACN9	ACN9 homolog (S. cerevisiae)	4.19
CHSY3	chondroitin sulfate synthase 3	4.14
COL10A1	collagen, type X, alpha 1	4.13
HIST1H1C	histone cluster 1, H1c	4.13
GOLGA8O	golgin A8 family, member O	4.11
ARHGAP18	Rho GTPase activating protein 18	4.11
ATRNL1	attractin-like 1	4.11
TRIM2	tripartite motif containing 2	4.10
GPX8	glutathione peroxidase 8 (putative)	4.09
BCR	breakpoint cluster region	4.08
GLDN	gliomedin	4.06
AKR1B1	aldo-keto reductase family 1, member B1 (aldose reductase)	4.05
TMEM182	transmembrane protein 182	4.04
AK5	adenylate kinase 5	4.04
LMO3	LIM domain only 3 (rhombotin-like 2)	4.04
KIT	v-kit Hardy-Zuckerman 4 feline sarcoma viral oncogene homolog	4.04
GPER	G protein-coupled estrogen receptor 1	4.03
ZNF14	zinc finger protein 14	4.02
CRYZ	crystallin, zeta (Quinone reductase)	4.01
TIMD4	T-cell immunoglobulin and mucin domain containing 4	4.00

Table 3.4 The symbol, definition and fold change of the first 100 genes downregulated in the late contraction from day3 to 5 (fold change>2 times, p value<0.05). Remarkably 84 of them were the reverse-backs from the upregulation genes in the early contraction. The ones that were not regulated in the early contraction (fold change⩽2 times, p value<0.05) were coloured in blue. The serum response genes (genes that were identified in a study of transcriptional profile of human foreskin fibroblasts in response to serum (Iyer et al., 1999)) were labelled in bold character (10 genes).

Symbol	Definition	FoldChng
IL8	interleukin 8	-18.31
NR4A2	nuclear receptor subfamily 4, group A, member 2	-17.21
CXCR4	chemokine (C-X-C motif) receptor 4	-15.81
MFSD2A	major facilitator superfamily domain containing 2A	-15.53
CYP1A1	cytochrome P450, family 1, subfamily A, polypeptide 1	-13.68
LSMEM1	leucine-rich single-pass membrane protein 1	-13.51
RAD54L	RAD54-like (S. cerevisiae)	-13.48
SERPINB2	serpin peptidase inhibitor, clade B (ovalbumin), member 2	-13.24
C12orf50	chromosome 12 open reading frame 50	-13.04
KIAA0226L	KIAA0226-like	-13.03
RASGRF1	Ras protein-specific guanine nucleotide-releasing factor 1	-12.58
IL33	interleukin 33	-12.54
FOS	FBJ murine osteosarcoma viral oncogene homolog	-12.47
ICAM1	intercellular adhesion molecule 1	-12.29
LIMD1-AS1	LIMD1 antisense RNA 1	-11.89
FCGR1B	Fc fragment of IgG, high affinity Ib, receptor (CD64)	-11.80
ATF3	activating transcription factor 3	-11.34
ISG20	interferon stimulated exonuclease gene 20kDa	-11.01
RN7SL184P	RNA, 7SL, cytoplasmic 184, pseudogene	-10.48
SCUBE2	signal peptide, CUB domain, EGF-like 2	-10.13
POLG2	polymerase (DNA directed), gamma 2, accessory subunit	-9.81
KRTAP3-2	keratin associated protein 3-2	-9.69
NR4A3	nuclear receptor subfamily 4, group A, member 3	-9.35
INHBA	inhibin, beta A	-9.32
SLC22A3	solute carrier family 22 (extraneuronal monoamine transporter), member 3	-9.19
GUCY2C	guanylate cyclase 2C (heat stable enterotoxin receptor)	-9.15
EGR1	early growth response 1	-8.96
CCL20	chemokine (C-C motif) ligand 20	-8.72
TSLP	thymic stromal lymphopoietin	-8.70
TEX35	testis expressed 35	-8.49
RNU4ATAC	RNA, U4atac small nuclear (U12-dependent splicing)	-8.31
REL	v-rel reticuloendotheliosis viral oncogene homolog (avian)	-8.21

EGR3	early growth response 3	-8.16
ACTN2	actinin, alpha 2	-7.98
PPP4R1L	protein phosphatase 4, regulatory subunit 1-like	-7.97
KB-1732A1.1	n/a	-7.95
RNA5SP242	RNA, 5S ribosomal pseudogene 242	-7.93
CYP19A1	cytochrome P450, family 19, subfamily A, polypeptide 1	-7.87
RNU6ATAC33P	RNA, U6atac small nuclear 33, pseudogene	-7.52
NCKAP1L	NCK-associated protein 1-like	-7.43
RNU6ATAC3P	RNA, U6atac small nuclear 3, pseudogene	-7.38
NFATC2	nuclear factor of activated T-cells, cytoplasmic, calcineurin-dependent 2	-7.36
LMCD1	LIM and cysteine-rich domains 1	-7.29
A2M	alpha-2-macroglobulin	-7.29
C5orf45	chromosome 5 open reading frame 45	-7.27
BCL2L10	BCL2-like 10 (apoptosis facilitator)	-7.21
C9	complement component 9	-7.17
HBEGF	heparin-binding EGF-like growth factor	-7.15
LRMP	lymphoid-restricted membrane protein	-7.06
UTS2B	urotensin 2B	-7.01
RNU6ATAC2P	RNA, U6atac small nuclear 2, pseudogene	-7.00
IDI2-AS1	IDI2 antisense RNA 1	-6.97
CXCL1	chemokine (C-X-C motif) ligand 1 (melanoma growth stimulating activity, alpha)	-6.87
DUSP5	dual specificity phosphatase 5	-6.83
POPDC2	popeye domain containing 2	-6.83
PIK3CG	phosphatidylinositol-4,5-bisphosphate 3-kinase, catalytic subunit gamma	-6.79
NEB	nebulin	-6.78
TMEM100	transmembrane protein 100	-6.74
SORBS2	sorbin and SH3 domain containing 2	-6.73
LIF	leukaemia inhibitory factor	-6.69
MIR103A2	microRNA 103a-2	-6.61
DERL3	derlin 3	-6.53
HIST2H3C	histone cluster 2, H3c	-6.49
CYP27B1	cytochrome P450, family 27, subfamily B, polypeptide 1	-6.47
PSG2	pregnancy specific beta-1-glycoprotein 2	-6.46
PRKCH	protein kinase C, eta	-6.40
IDI2	isopentenyl-diphosphate delta isomerase 2	-6.38
EGR2	early growth response 2	-6.37
TAGLN3	transgelin 3	-6.30
GEM	GTP binding protein overexpressed in skeletal muscle	-6.28
CREB5	cAMP responsive element binding protein 5	-6.27
CSPG4	chondroitin sulfate proteoglycan 4	-6.22
MT1G	metallothionein 1G	-6.20

PLEKHA8P1	pleckstrin homology domain containing, family A member 8 pseudogene 1	-6.16
SIK1	salt-inducible kinase 1	-6.15
SNHG1	small nucleolar RNA host gene 1 (non-protein coding)	-6.11
BACH2	BTB and CNC homology 1, basic leucine zipper transcription factor 2	-6.10
MIR222	microRNA 222	-6.07
MTFR2	mitochondrial fission regulator 2	-6.06
RCC1	regulator of chromosome condensation 1	-6.02
ZC3H12C	zinc finger CCCH-type containing 12C	-6.02
HSPA6	heat shock 70kDa protein 6 (HSP70B')	-6.01
SLC30A1	solute carrier family 30 (zinc transporter), member 1	-5.96
RPL31P57	ribosomal protein L31 pseudogene 57	-5.92
RP3-393E18.2	n/a	-5.91
FCGR1C	Fc fragment of IgG, high affinity Ic, receptor (CD64), pseudogene	-5.91
PLEK2	pleckstrin 2	-5.86
CCDC15	coiled-coil domain containing 15	-5.84
TNRC6C	trinucleotide repeat containing 6C	-5.82
TNFAIP3	tumour necrosis factor, alpha-induced protein 3	-5.81
MOGAT1	monoacylglycerol O-acyltransferase 1	-5.79
ZC3H4	zinc finger CCCH-type containing 4	-5.78
RNU6ATAC10P	RNA, U6atac small nuclear 10, pseudogene	-5.78
LINC01270	long intergenic non-protein coding RNA 1270	-5.78
KDM6B	lysine (K)-specific demethylase 6B	-5.70
HOMER1	homer homolog 1 (Drosophila)	-5.70
STX11	syntaxin 11	-5.68
MAP7D2	MAP7 domain containing 2	-5.68
FOSB	FBJ murine osteosarcoma viral oncogene homolog B	-5.64
SYPL2	synaptophysin-like 2	-5.63

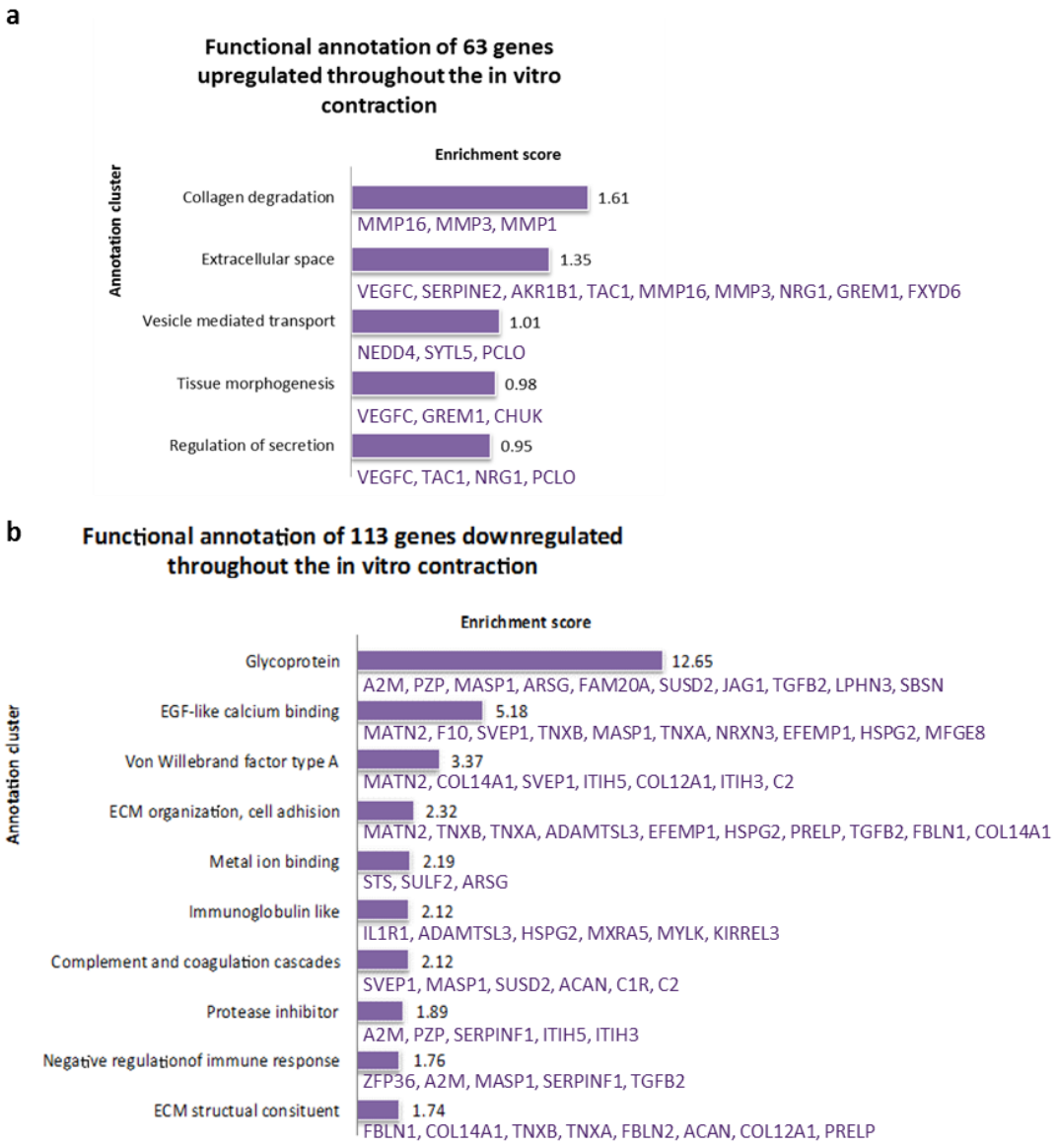

Figure 3.7 Functional annotation of the genes regulated throughout the whole contraction process.

Functional annotation analysis by DAVID showing the top 5 gene clusters upregulated (a) and 10 downregulated (b) throughout the in vitro contraction according to enrichment score. The most regulated genes (or the first 10 of them) of each cluster were listed below the score bar.

3.4 Gene expression profile changes induced by NSC23766 treatment

Previous study showed that transient treatment with the Rac1 inhibitor NSC23766 was sufficient to block long-term tissue contraction *in vitro* and ex vivo (Tovell et al., 2012), suggesting that the inhibitor could block a major activation signal that is necessary for the fibroblasts to engage in the contraction process. Importantly, this activation signal appeared to be transient, suggesting that it could be linked to a short, temporary activation of signalling pathways downstream of small GTPases. Indeed, the above analysis of the gene expression changes during the early and late contraction phases confirmed the transient nature of the contraction activation signal. It was also clear from the PCA plot (**Figure 3.2**) and the hierarchical clustering heatmap (**Figure 3.3**) that the NSC23766 treated samples, and particularly Day3NSC, clustered close to the untreated samples at day 5 where the transient hyperactivation phase has receded. Looking at the individual gene profiles, there was a strong overlap between the genes upregulated during early contraction and the genes downregulated by NSC23766 treatment at day3, and the genes downregulated during early contraction and the genes upregulated by NSC23766 treatment at Day3, respectively (**Figure 3.8**). The significantly up/downregulated genes were particularly affected (**Table 3.1**, **Table 3.2**), indicating that most of the early contraction signals were suppressed by NSC23766.

To further characterise the gene modulation upon NSC23766 treatment, DAVID functional annotation analysis was performed on the first 500 genes up/downregulated in early contraction respectively and those that were reversely regulated by NSC23766 at day3. Notably, a major downregulation of gene function by NSC23766 was focused on the transcription activity, and the upregulation modulation was made on oxidation-reduction, coenzyme metabolism and ion binding (**Figure 3.9**).

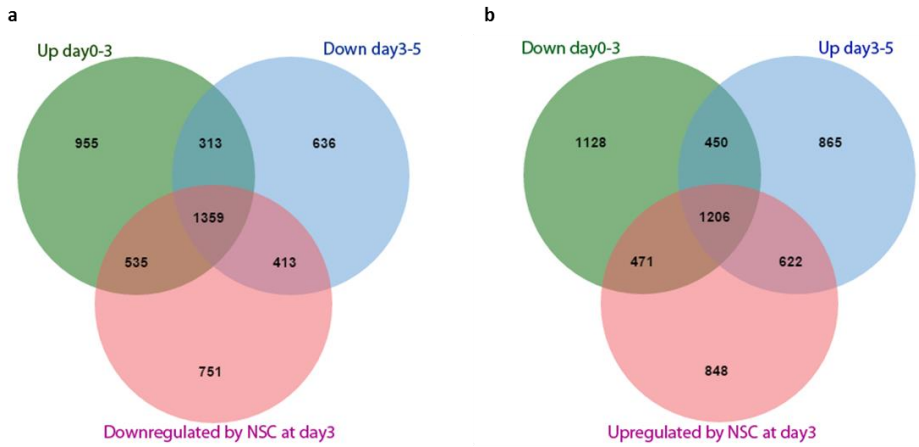

Figure 3.8 Venn diagrams showing that majority of the early contraction gene signalling were suppressed by NSC23766 treatment.

(a) 1894 out of 2849 upregulation genes in the early contraction were downregulated by NSC23766 treatment. (b) 1677 out of 2805 downregulation genes in the early contraction were upregulated by NSC23766 treatment.

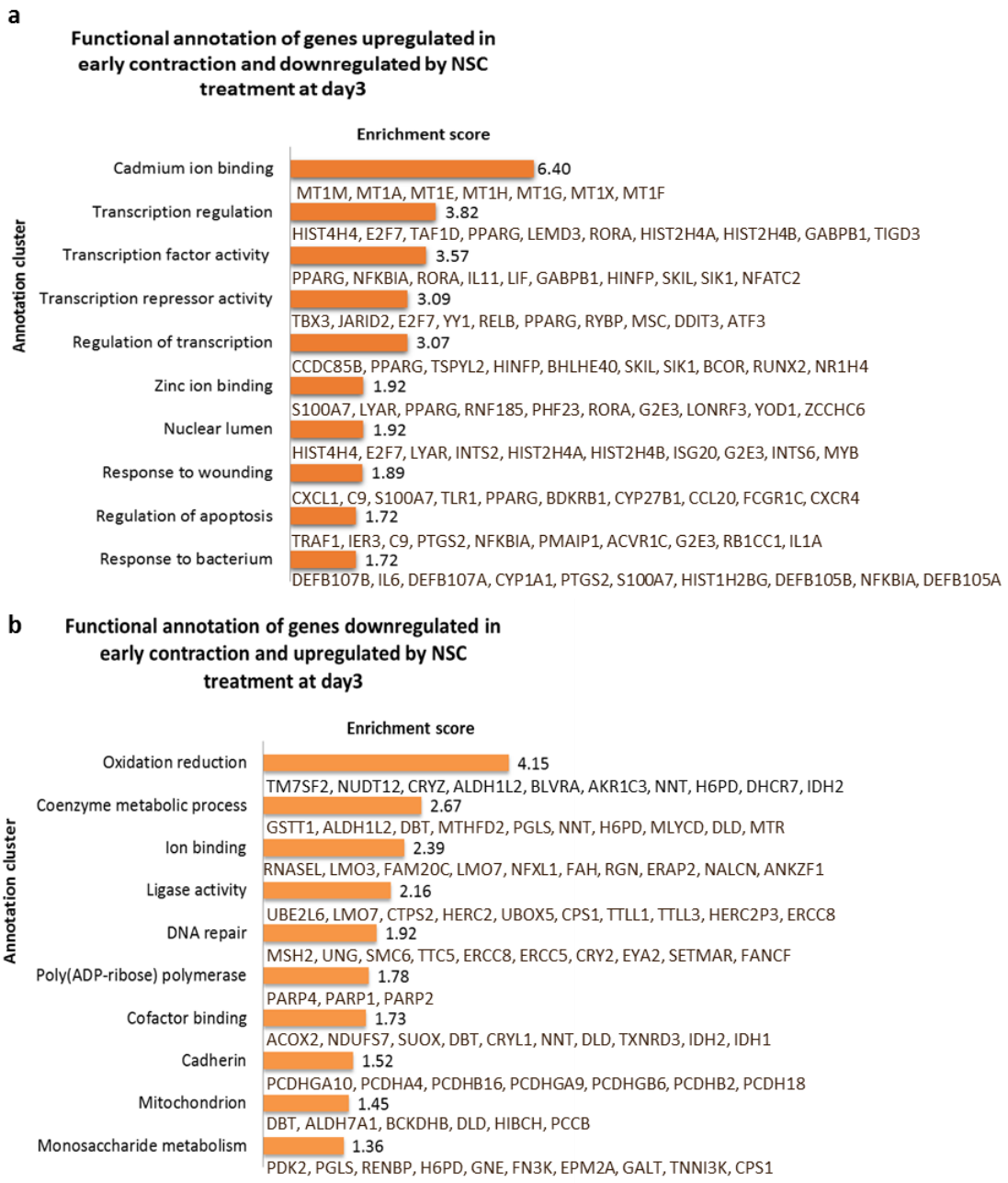

Figure 3.9 Functional annotation analysis by DAVID showing the modulations of NSC23766 made on the early contraction gene signalling.

(a) The top 10 gene functional clusters of the first 500 upregulation genes in the early contraction that were suppressed by NSC23766 treatment at day3. (b) The top 10 gene functional clusters of the first 500 downregulation genes in early contraction that were upregulated by NSC23766 treatment at day3. The most regulated genes (or the first 10 of them) of each cluster were listed below the score bar.

3.5 Relevance to *in vivo* contraction profile

The fibroblast-populated collagen lattices have been used widely as a classical model for tissue contraction in the context of ocular scarring, providing invaluable insights into disease mechanisms as well as a tool for identifying drugs with anti-scarring potential (Ehrmann and Gey, 1956, Porter et al., 1998, Daniels et al., 2003, Kottler et al., 2005). However, there is little information on how well this *in vitro* assay recapitulates the *in vivo* scarring. To further assess the compatibility and reliability of the gene expression profile of our *in vitro* contraction model to a real wounding event, we compared it to the raw data obtained from a pilot microarray study in the classical model of conjunctival scarring in rabbits following glaucoma filtration surgery. Conjunctiva samples were taken from un-operated control eye and operated eye respectively on the same rabbit 5 days after the surgery (stage of active wound response), and RNA was extracted from the samples for the subsequent microarray. The array was performed with the Agilent two-colour microarray system using a custom designed rabbit chip (Agilent AMADID# 017130) with 7328 annotated genes. The data was analysed by the LIMMA package within Bioconductor (Ritchie et al., 2015), and a modest t-test was applied using a Bayesian approach (the *in vivo* microarray was performed by Dr. Daniel Paull, and the data analysis was performed by Dr. Jian-Liang Li).

As a result, 479 genes were found upregulated in the operated samples comparing to the control ones, and 459 genes were downregulated (fold change >1.2 times, p value<0.05). DAVID functional annotation analysis was applied on these genes respectively and identified that gene clusters including cytoplasmic vesicle, protein folding and response to wounding were upregulated, whilst the ones related to oxidation reduction, vesicular fraction, ion binding and cofactor binding being downregulated (**Figure 3.10**). Notably, the functional clusters of ‘respond to

wounding' and 'cofactor binding' were also observed in the *in vitro* early contraction up and downregulation profiles respectively.

Also, the comparison between the *in vivo* and *in vitro* array profiles indicated that about one third of the genes altered during the *in vivo* wound healing were common to the ones observed in the *in vitro* profiles, with a slightly stronger similarity to the early contraction profile, matching the expected wound response (**Figure 3.11**). It suggested that the *in vitro* contraction model mimics well the wound healing response *in vivo* and possibly the very early stage of scarring. The main genes whose expression increased dramatically in the *in vitro* early contraction including IL1A, TNFAIP6, MMP1 and PMEPA1, as well as those that decreased significantly such as FMO2, LANCL1 and NLGN1 were also found up or downregulated respectively in the *in vivo* profile (**Table 3.5,Table 3.6**). Notably, 5 genes regulated consistently in the same way throughout the *in vitro* contraction were also presented in the *in vivo* profile, including MMP1 and MMP3 that were upregulated all the time; and A2M, IL1R1 and ACE, which were downregulated constantly *in vitro* and *in vivo*.

297 upregulated and 298 downregulated genes were expressed exclusively in the *in vivo* profile (**Figure 3.11**), with an expression profile particularly matched to epithelium or inflammatory cells. For example, the epithelial markers KRT6A and GKN1, lymphoblast marker HBB, neuron-derived factor C4or31, dendritic cell marker LILRA4 and immune response regulators S100A8/9 were found upregulated (**Table 3.7**). The muscle proteins including MYL1, TNNI2, ACTA1 and LPL, neuron filament NEFL, leukocyte derived chemotaxin LECT1 and the cytochrome P450 superfamily of monooxygenases were downregulated (**Table 3.8**).This expression profile was expected as the *in vivo* samples contained a mixture of cells and with

the presence of inflammation, and they possibly had contaminations of epithelium and muscle. In addition, the gene expression profile of the *in vivo* array and the profile of human fibroblasts in response to serum (Iyer et al., 1999) were also compared. However, only 4% genes from the *in vivo* array (23 upregulated genes and 18 downregulated genes, data not shown) matched the serum stimulation profile, suggesting that our 3D collagen contraction model was a better match to the *in vivo* wounding behaviour than the 2D serum stimulation model.

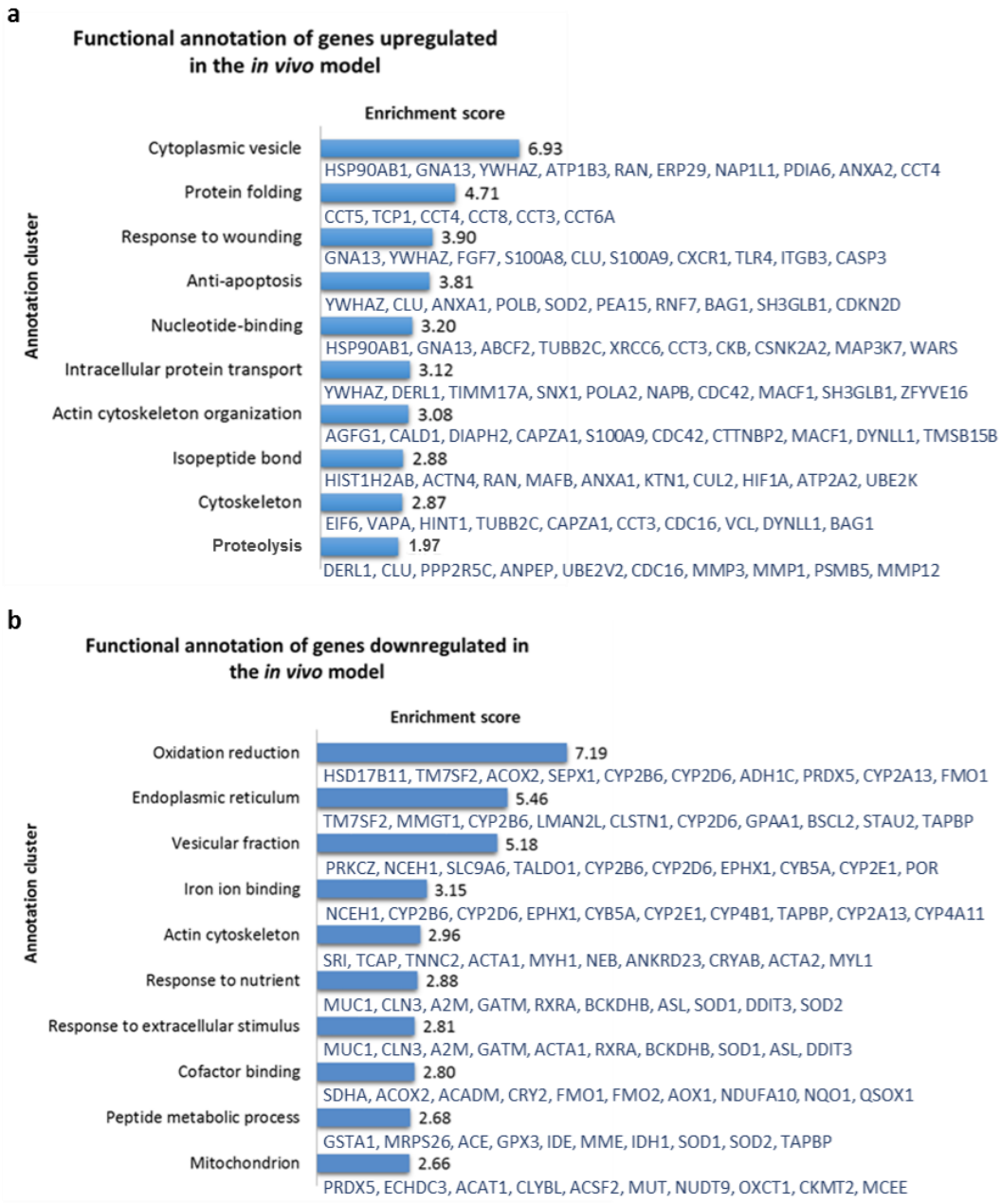

Figure 3.10 Characterisation of the functional gene clusters regulated during the in vivo wound healing study.

(a) The top 10 functional gene clusters upregulated in the in vivo wound healing study analysed by DAVID functional annotation analysis according to the enrichment score. (b) The top 10 functional gene clusters downregulated in the in vivo wound healing study analysed by DAVID functional annotation analysis according to the enrichment score. The most regulated genes (or the first 10 of them) of each cluster were listed below the score bar.

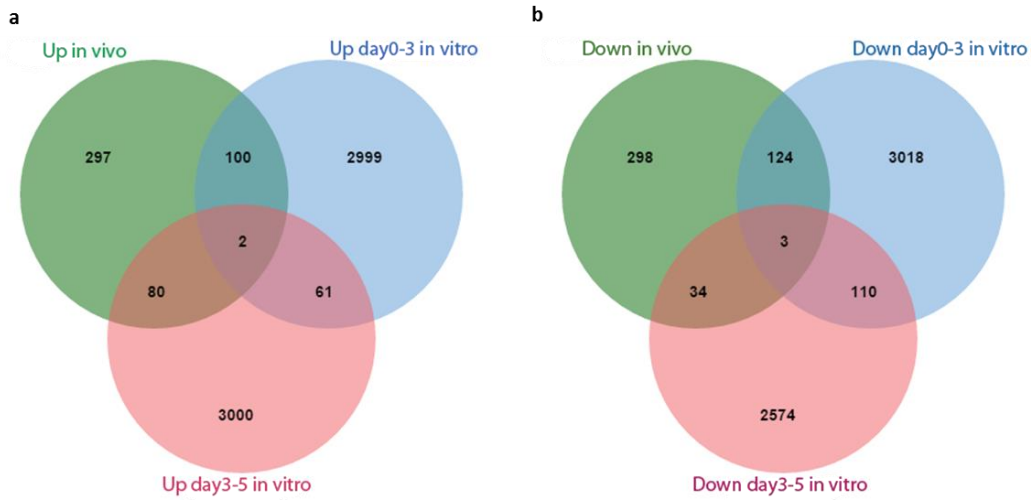

Figure 3.11 Paired comparisons of the gene expression profiles of the in vivo and in vitro wounding models.

(a*) 102 and 82 out of 479 upregulation genes in the in vivo microarray were in common with the in vitro early and late contraction upregulation profiles respectively. The two genes upregulated both in vivo and throughout the in vitro contraction were MMP1 and MMP3. (b) 127 and 37 out of 459 downregulation genes in the in vivo microarray were in common with the in vitro early and late contraction downregulation profiles respectively. The three genes downregulated both in vivo and throughout the in vitro contraction were A2M, IL1R1 and ACE.*

Table 3.5 The gene symbol, definition and fold changes of the first 20 common upregulation genes in the in vitro early contraction and in vivo profiles (fold change>1.2, p<0.05).

Gene	Defination	Fold Change *in vitro* Day0-3	*in vivo*
IL1RN	Interleukin 1, alpha	63.56	1.84
SERPINB2	Serpin peptidase inhibitor, clade B (ovalbumin), member 2	60.46	3.03
MMP1	Matrix metallopeptidase 1 (interstitial collagenase)	38.73	4.88
HAS2	Hyaluronan synthase 2	15.56	2.97
PMEPA1	Prostate transmembrane protein, androgen induced 1	11.27	4.00
NCKAP1L	NCK-associated protein 1-like	9.75	1.86
TAGLN3	Transgelin 3	7.99	1.31
TNFAIP6	Tumor necrosis factor, alpha-induced protein 6	7.02	9.03
MMP3	Matrix metallopeptidase 3 (stromelysin 1, progelatinase)	5.31	3.01
IL1A	Interleukin 1 receptor antagonist	4.40	23.18
CARD10	Caspase recruitment domain family, member 10	4.15	1.21
KBTBD2	Kelch repeat and BTB (POZ) domain containing 2	3.96	1.74
KCNAB1	Potassium Voltage-Gated Channel Subfamily A Regulatory Beta Subunit 2	3.63	1.63
EDNRB	Endothelin receptor type B	3.58	3.18
PTPN12	Protein tyrosine phosphatase, non-receptor type 12	3.49	1.67
TDG	Thymine-DNA glycosylase	3.20	1.45
PPARG	Peroxisome Proliferator Activated Receptor Gamma	3.13	1.46
TCEB3	Transcription Elongation Factor B Subunit 3	3.10	1.43
ART4	ADP-Ribosyltransferase 4 (Dombrock Blood Group)	2.97	2.35
SAT1	Spermidine/spermine N1-acetyltransferase 1	2.92	1.68

Table 3.6 The gene symbol, definition and fold changes of the first 20 common downregulation genes in the in vitro early contraction and in vivo profiles (fold change>1.2, p<0.05).

Gene	Defination	Fold Change *in vitro* Day0-3	*in vivo*
FMO2	Flavin containing monooxygenase 2	-11.21	-4.35
LANCL1	LanC Like 1	-10.33	-1.72
NLGN1	Neuroligin 1	-5.88	-2.01
ABCA8	ATP-binding cassette, sub-family A (ABC1), member 8	-5.84	-1.31
LPIN1	Lipin 1	-4.80	-1.83
CCPG1	Cell cycle progression 1	-4.34	-1.46
PDGFRL	Platelet-derived growth factor receptor-like	-4.31	-2.19
WBSCR27	Williams Beuren syndrome chromosome region 27	-4.21	-1.46
TM7SF2	Transmembrane 7 superfamily member 2	-4.08	-1.24
ACOX2	Acyl-Coenzyme A oxidase 2, branched chain	-4.07	-1.35
SNRPN	Small nuclear ribonucleoprotein polypeptide N	-3.76	-1.42
DHCR7	7-Dehydrocholesterol Reductase	-3.71	-1.62
AMOT	Angiomotin	-3.57	-2.0
CYP27A1	Cytochrome P450 Family 27 Subfamily A Member 1	-3.55	-1.79
IMPACT	Impact RWD Domain Protein	-3.41	-1.41
CLDN11	Claudin 11	-3.41	-2.47
BCKDHB	Branched Chain Keto Acid Dehydrogenase E1, Beta Polypeptide	-3.37	-1.55
IGSF10	Immunoglobulin Superfamily Member 10	-3.36	-1.8
HIBCH	3-hydroxyisobutyryl-CoA hydrolase	-3.34	-1.74
DBT	Dihydrolipoamide branched chain transacylase E2	-3.25	-1.62

Table 3.7 The gene symbol, definition and fold change of the first 20 upregulated genes expressed exclusively in the in vivo wounding model (fold change>2, p<0.05).

Gene	Defination	Fold Change *in vivo*
CXCL5	Chemokine (C-X-C motif) ligand 5	8.83
SAA1	Serum amyloid A1	7.28
MMP13	Matrix metallopeptidase 13 (collagenase 3)	6.36
COL4A1	Collagen, type IV, alpha 1	5.72
S100A9	S100 calcium binding protein A9	5.68
COL12A1	Collagen, type XII, alpha 1	5.47
KRT6A	Keratin 6A	5.39
GKN1	Gastrokine 1	5.25
GPR115	G protein-coupled receptor 115	5.23
THBS1	Thrombospondin 1	5.14
CRISP3	Cysteine-rich secretory protein 3	5.03
HBB	Hemoglobin Subunit Beta	4.97
ACTA2	Actin, Alpha 2, Smooth Muscle, Aorta	4.57
S100A8	S100 calcium binding protein A8	4.51
ARHGAP24	Rho GTPase activating protein 24	4.14
ARG1	Arginase 1	3.93
LILRA4	Leukocyte Immunoglobulin Like Receptor A4	3.69
C4orf31	Neuron-Derived Neurotrophic Factor	3.65
NKAIN1	Na+/K+ Transporting ATPase Interacting 1	3.59
NID2	Nidogen 2	3.50

Table 3.8 The gene symbol, definition and fold change of the first 20 downregulated genes expressed exclusively in the in vivo wounding model (fold change>2, p<0.05).

Gene	Defination	Fold Change *in vivo*
MYL1	Myosin Light Chain 1	-19.79
EIF2C2	Argonaute 2, RISC Catalytic Component	-11.49
NEFL	Neurofilament, light polypeptide	-10.15
MYH1	Myosin, heavy chain 1, skeletal muscle, adult	-9.90
CKMT2	Creatine Kinase, Mitochondrial 2	-8.64
ACTA1	Actin, alpha 1, skeletal muscle	-7.79
C4orf49	Mitochondria Localized Glutamic Acid Rich Protein	-7.01
DUSP26	Dual specificity phosphatase 26 (putative)	-6.78
CYP4A11	Cytochrome P450 Family 4 Subfamily A Member 11	-6.45
CYP2B6	Cytochrome P450 Family 2 Subfamily B Member 6	-6.30
TNNI2	Troponin I2, Fast Skeletal Type	-5.53
LPL	Lipoprotein lipase	-5.29
CYP2E1	Cytochrome P450 Family 2 Subfamily E Member 1	-5.20
COL2A1	Collagen, type II, alpha 1	-5.14
LECT1	Leukocyte Cell Derived Chemotaxin 1	-4.49
BEX2	Brain Expressed X-Linked 2	-4.45
CYP2A13	Cytochrome P450 Family 2 Subfamily A Member 13	-4.20
WDR76	WD Repeat Domain 76	-4.04
CYP4B1	Cytochrome P450 Family 4 Subfamily B Member 1	-3.96
MT3	Metallothionein 3	-3.95

3.6 Relevance to ocular fibrotic disease profile

To further characterise the relevance of our *in vitro* contraction gene expression profile to a real wounding/fibrotic event, the early and late contraction profiles were compared to the profiles of human ocular fibrotic diseases including trachoma (Kechagia et al., 2016) and thyroid-associated orbitopathy (TED) (Ezra et al., 2012), both of which are associated to fibroblast-mediated contractile scarring (**Figure 3.12**). Trachoma is a conjunctiva scarring disease, whose scarring consequences are characterised by the presence of a highly fibrotic conjunctiva/tarsal plate with increased matrix deposition and a compact a-vascular stroma, mainly composed of fibroblasts and inflammatory cells (Abu el-Asrar et al., 1998). TED is caused by thyroid autoimmune disease, with manifestations including extraocular muscle inflammation and fibrosis, upper eyelid retraction and proptosis. Orbital fibroblasts are believed to play important roles in the TED, as they produce proinflammatory cytokines that activate genes regulating adipocyte proliferation (Naik et al., 2010, Kumar et al., 2004).

As a result, over one third of the genes upregulated in trachoma were also found in the *in vitro* profile, including 18 genes upregulated in the early contraction, including the inflammatory-responsible genes IL6, TNFSF4, PTGER3 and OLR1, apoptosis related genes RASGRF2, GATA6 and HSPB8, and transcription regulators TSHZ2 and DUXA. 23 trachoma signature genes were found upregulated in the late contraction, for example SEMA6A, DMD and UCHL1 (morphogenesis), KCND2, PLOD2, PLXDC2 and FLT1 (signal transduction), and MAP6 and APBB1IP (cytoskeleton) (**Table 3.9**). Meanwhile, more than half of the downregulated genes in trachoma were found downregulated in the *in vitro* model, such as glycoproteins CPM, NOG, KCNT2 and COLEC12 that were downregulated in early contraction, and signal peptides MYOC, WISP3 and SERPINA3, which were downregulated in

late contraction. Also, CLEC3B, which regulates fibrinolysis and related to calcium ion binding, was found to be suppressed both in trachoma and *in vitro* contraction (**Table 3.10**).

Moreover, for the gene expression profile of the thyroid-associated orbitopathy (TED), over one third of the upregulated genes were captured in the *in vitro* profile, including SGK1, IL7R, JUN and SLC2A14 that were transiently activated in early contraction and receded in the late contraction; and SLC20A1, CLEC11A and ST8SIA4, which were upregulated exclusively in the late contraction (**Table 3.11**). Two thirds of the downregulated genes of the disease were also downregulated *in vitro*, which included 13 genes that decreased in the early contraction and six of which reactivated later at day5, such as CMBL, FOXL2 and FABP4; and genes that were only downregulated in the early contraction, such as ADH1B, IGSF10, ERAP2 and ITGBL1. In addition, five downregulated genes of the TED were recorded in the late contraction, with three of which were suppressed consistently throughout the *in vitro* contraction, involving COL12A1, SFRP4 and DAAM1; and C14orf180 and IGFBP6 that were only downregulated from day3 to 5 (**Table 3.12**). The functional annotation clustering analysis of these common up/downregulated genes between the *in vitro* contraction and trachoma, and the ones of the *in vitro* contraction and TED suggested that the gene expression features of the inflammation and fibrotic progressions of the diseases' are replicated in the *in vitro* contraction model (**Figure 3.13**).

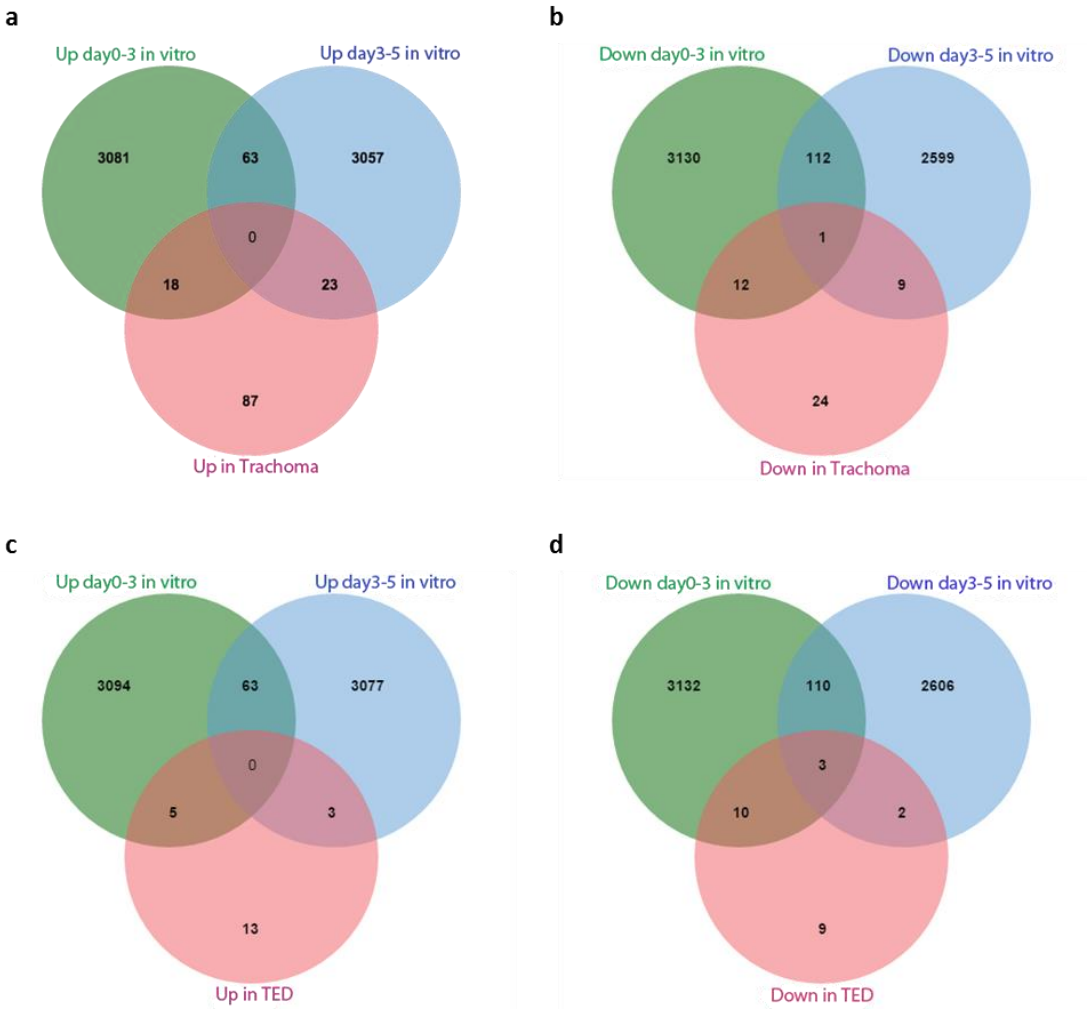

Figure 3.12 Venn diagrams showing the common genes expressed between the in vitro contraction and trachoma, and the in vitro contraction and the thyroid-associated orbitopathy (TED).

(a) *47 out of 128 upregulations and (b) 22 out of 46 downregulation genes in Trachoma were expressed in the in vitro contraction profile. (c) 8 out of 21 upregulations and (d) 15 out of 24 downregulation genes in the thyroid-associated orbitopathy (TED) were captured in the in vitro profile.*

Table 3.9 The gene expression profiles of the common upregulated trachoma signature genes (genes that were identified to be expressed significantly in trachoma (Kechagia et al., 2016)) in the in vitro early (day0-3) and late (day3-5) contraction stages (fold change>1.2 times, p<0.05). '—' represents no gene expression change detected.

		Fold change		
Gene	**Definition**	**day0-3**	**day3-5**	**Trachoma**
PMEPA1	Prostate Transmembrane Protein, Androgen Induced 1	11.27	-1.99	2.48
IL6	Interleukin 6	7.15	-3.73	6.18
AP1S3	Adaptor Related Protein Complex 1 Sigma 3 Subunit	6.69	-3.85	3.44
HSPB8	Heat Shock Protein Family B (Small) Member 8	5.44	–	2.55
LRRC15	Leucine Rich Repeat Containing 15	4.21	–	3.10
GATA6	GATA Binding Protein 6	2.65	-1.58	3.59
CLIC6	Chloride Intracellular Channel 6	2.15	-1.83	3.78
OLR1	Oxidized Low Density Lipoprotein Receptor 1	2.12	-2.29	6.78
TNFSF4	Tumor Necrosis Factor Superfamily Member 4	2.11	-2.02	4.31
RASGRF2	Ras Protein Specific Guanine Nucleotide Releasing Factor 2	2.06	–	2.59
PRR5L	Proline Rich 5 Like	2.01	–	2.19
OSGIN2	Oxidative Stress Induced Growth Inhibitor Family Member 2	1.99	–	2.13
TSHZ2	Teashirt Zinc Finger Homeobox 2	1.92	-2.08	3.62
PTGER3	Prostaglandin E Receptor 3	1.78	–	4.09
MCOLN3	Mucolipin 3	1.72	–	2.03
DUXA	Double Homeobox A	1.61	–	3.59
LIPH	Lipase H	1.60	-1.36	2.61
FBLN7	Fibulin 7	1.41	-1.67	2.10
KCND2	Potassium Voltage-Gated Channel Subfamily D Member 2	-4.15	6.16	2.79
DEPTOR	DEP Domain Containing MTOR-Interacting Protein	-2.78	5.71	2.92
PLXDC2	Plexin Domain Containing 2	–	4.64	2.14
NCAPH	Non-SMC Condensin I Complex Subunit H	-7.27	4.00	2.08
FAM213A	Family With Sequence Similarity 213 Member A	-2.84	3.22	2.04
TFAP2A	Transcription Factor AP-2 Alpha	-2.62	3.19	10.52
MAP6	Microtubule Associated Protein 6	–	3.04	2.35
CALCRL	Calcitonin Receptor Like Receptor	–	3.03	2.98
DPM2	Dolichyl-Phosphate Mannosyltransferase Polypeptide 2, Regulatory Subunit	–	2.67	2.11
APBB1IP	Amyloid Beta Precursor Protein Binding Family B Member 1 Interacting Protein	-2.04	2.48	2.25
SESN3	Sestrin 3	-3.18	2.42	2.44
PRKG2	Protein Kinase, CGMP-Dependent, Type II	-5.38	2.39	2.84
EYA4	EYA Transcriptional Coactivator And Phosphatase 4	-1.99	2.36	4.49
PLOD2	Procollagen-Lysine,2-Oxoglutarate 5-Dioxygenase 2	–	2.26	2.03
FLT1	Fms Related Tyrosine Kinase 1	-1.67	2.23	2.32
PCDHB2	Protocadherin Beta 2	-2.44	2.22	2.04
SEMA6A	Semaphorin 6A	-2.30	2.03	2.46
BDH1	3-Hydroxybutyrate Dehydrogenase, Type 1	-3.57	1.98	2.45
RASSF4	Ras Association Domain Family Member 4	-7.07	1.98	2.23
DMD	Dystrophin	-1.70	1.66	3.37
PCDHGA10	Protocadherin Gamma Subfamily A, 10	-3.41	1.65	2.38
UCHL1	Ubiquitin C-Terminal Hydrolase L1	–	1.58	2.32
ST3GAL6	ST3 Beta-Galactoside Alpha-2,3-Sialyltransferase 6	–	1.40	2.34

Table 3.10 The gene expression profiles of the common downregulated trachoma signature genes (genes that were identified to be expressed significantly in trachoma (Kechagia et al., 2016)) in the in vitro early (day0-3) and late (day3-5) contraction stages (fold change>1.2 times, p<0.05). '—' represents no gene expression change detected. One gene that was downregulated consistently in trachoma and in vitro is highlighted in pink.

		Fold change		
Gene	**Definition**	**day0-3**	**day3-5**	**Trachoma**
FAM129A	Family With Sequence Similarity 129 Member A	-3.57	1.62	-2.53
PPL	Periplakin	-2.96	–	-2.01
PLK1S1	Kizuna Centrosomal Protein	-2.63	2.57	-2.02
KCNT2	Potassium Sodium-Activated Channel Subfamily T Member 2	-2.19	–	-2.13
SCRG1	Stimulator Of Chondrogenesis 1	-2.09	–	-7.97
CPM	Carboxypeptidase M	-2.06	–	-4.18
OLFML2A	Olfactomedin Like 2A	-1.98	–	-2.39
PTPRD	Protein Tyrosine Phosphatase, Receptor Type D	-1.95	1.71	-2.56
ROBO3	Roundabout Guidance Receptor 3	-1.94	3.41	-2.55
CA12	Carbonic Anhydrase 12	-1.82	–	-2.37
COLEC12	Collectin Subfamily Member 12	-1.59	4.53	-3.09
NOG	Noggin	-1.49	1.43	-2.26
CLEC3B	C-Type Lectin Domain Family 3 Member B	-2.34	-4.41	-2.13
MYOC	Myocilin	–	-3.88	-8.21
SERPINA3	Serpin Family A Member 3	–	-2.76	-2.92
NDUFA4L2	NADH Dehydrogenase (Ubiquinone) 1 Alpha Subcomplex, 4-Like 2	–	-2.54	-2.35
C1QTNF1	C1q And Tumor Necrosis Factor Related Protein 1	1.42	-2.04	-2.08
WISP3	WNT1 Inducible Signaling Pathway Protein 3	1.56	-1.86	-6.66
ARHGAP26	Rho GTPase Activating Protein 26	–	-1.80	-2.90
IL31RA	Interleukin 31 Receptor A	–	-1.58	-3.66
EBF3	Early B-Cell Factor 3	1.78	-1.52	-2.41
HMOX1	Heme Oxygenase 1	4.38	-1.42	-2.08

Table 3.11 The gene expression profiles of the common upregulated thyroid-associated orbitopathy (TED) signature genes (genes that were identified to be expressed significantly in the TED (Ezra et al., 2012)) in the in vitro early (day0-3) and late (day3-5) contraction stages (fold change>1.2 times, p<0.05). '—' represents no gene expression change detected.

		Fold change		
Gene	**Definition**	**day0-3**	**day3-5**	**TED**
SGK1	Serum/Glucocorticoid Regulated Kinase 1	3.89	-3.16	2.75
CTSC	Cathepsin C	1.89	–	2.05
IL7R	Interleukin 7 receptor	1.74	-3.41	3.89
JUN	Jun Proto-Oncogene	1.69	-2.84	2.19
SLC2A14	Solute Carrier Family 2 Member 14	1.53	-2.69	2.38
SLC20A1	Solute Carrier Family 20 Member 1	–	1.88	2.01
CLEC11A	C-Type Lectin Domain Family 11 Member A	–	1.65	2.12
ST8SIA4	ST8 Alpha-N-Acetyl-Neuraminide Alpha-2,8-Sialyltransferase 4	–	1.58	2.14

Table 3.12 The gene expression profiles of the common downregulated thyroid-associated orbitopathy (TED) signature genes (genes that were identified to be expressed significantly in the TED (Ezra et al., 2012)) in the in vitro early (day0-3) and late (day3-5) contraction stages (fold change>1.2 times, p<0.05). '—' represents no gene expression change detected. Genes that were downregulated consistently in the TED and in vitro contraction were highlighted in pink.

		Fold change		
Gene	**Definition**	**day0-3**	**day3-5**	**TED**
ADH1B	Alcohol Dehydrogenase 1B (Class I), Beta Polypeptide	-5.43	–	-7.68
IGSF10	Immunoglobulin Superfamily Member 10	-3.76	–	-2.01
ERAP2	Endoplasmic Reticulum Aminopeptidase 2	-2.76	–	-2.51
CMBL	Carboxymethylenebutenolidase Homolog (Pseudomonas)	-2.73	2.49	-2.69
AKR1C1	Aldo-Keto Reductase Family 1, Member C1	-2.30	1.55	-3.73
FOXL2	Forkhead Box L2	-1.76	1.69	-2.41
GSTM5	Glutathione S-Transferase Mu 5	-1.73	3.11	-2.03
FABP4	Fatty Acid Binding Protein 4	-1.59	1.58	-5.85
FZD7	Frizzled Class Receptor 7	-1.57	2.13	-2.02
ITGBL1	Integrin Subunit Beta Like 1	-1.56	–	-2.38
COL12A1	Collagen Type XII Alpha 1	-1.99	-1.66	-2.26
DAAM1	Dishevelled Associated Activator Of Morphogenesis 1	-1.48	-1.47	-2.31
SFRP4	Secreted Frizzled Related Protein 4	-1.34	-2.34	-2.93
C14orf180	Chromosome 14 Open Reading Frame 180	–	-1.64	-4.28
IGFBP6	Insulin-like growth factor binding protein 6	–	-1.48	-2.16

a

Trachoma

Up day0-3 *in vitro*	**Up day3-5 *in vitro***
Inflammatory response	Cell projection morphogenesis
Regulation of transcription	Membrane, Glycoprotein
Metal ion binding	Cytoskeleton
	Synaptic transmission, Calcium binding

Down day0-3 *in vitro*	**Down day3-5 *in vitro***
Glycoprotein	Extracellular region
Secreted	Secreted
Glycosylation site, membrane	Regulation of cellular biosynthetic process
Metal ion binding	Defense response

b

TED

Up *in vitro*	**Down *in vitro***
Glycoprotein	Cytoplasm
Glycosylation site, memberane	Extracellular region
	Integral component of membrane

Figure 3.13 Annotated gene functional clusters (analysed by DAVID) of the common up/downregulated genes between the in vitro contraction and trachoma (a), and the ones of the in vitro contraction and TED (b).

3.7 Validation of the *in vitro* contraction profile signatures

To validate the signature gene profiles of the early and late contraction stages, a number of gene candidates were selected from the *in vitro* and *in vivo* microarray analysis, and in combination with the expression profiles of human ocular fibrotic diseases trachoma (Kechagia et al., 2016), thyroid-associated orbitopathy (TED) (Ezra et al., 2012) and floppy eye syndrome (FES) (Ezra et al., 2010). The early contraction signature candidates were selected because they were significantly upregulated *in vitro* from day0 to 3, and/or upregulated *in vivo* (**Table 3.13**). Similarly, the late contraction signature genes were chosen for validation as they were significantly upregulated from day3 to 5 *in vitro*; and/or upregulated in trachoma, thyroid-associated orbitopathy (TED) or floppy eyelid syndrome (FES) (**Table 3.14**), as we hypothesised that genes upregulated after the receding of the hyperactivation early phase would be involved in the acquisition of the fibrotic phenotype. The gene expression profiles were validated using qPCR with conjunctival fibroblast line HTF7071 (the original line used in the *in vitro* microarray study) and HTF9154 (another primary fibroblast line from a different donor) in the standard collagen contraction culture at day0, 3 and 5. All the early contraction candidate genes showed clear upregulation from day0 to 3 in both fibroblast cells, with MMP1, 3 and 10, and IL8 being the most upregulated genes (**Figure 3.14**). The expression levels of the gene candidates of the late contraction were also validated using qPCR with HTF7071 and HTF9154 at day0, 3 and 5 during contraction. In HTF9154 all the genes were upregulated from day0 to 3, and increased further from day3 to 5; whilst in HTF7071 the genes were upregulated from day0 to 3, and most of which kept around the similar expression levels from day3 to 5 (**Figure 3.15**), suggesting that the expression levels of these genes can vary between fibroblasts from different donors.

Table 3.13 Early contraction gene candidates selected for validation.

Early contraction gene candidates for validation

Fold Change (day0-3 *in vitro*)	Expression pattern	Gene	Description
38.7	Up day0-3 *in vitro* Up day3-5 *in vitro* Up *in vivo*	**MMP1**	matrix metallopeptidase 1 (interstitial collagenase)
30.0	Up day0-3 *in vitro* Up *in vivo* Down day3-5 *in vitro*	**IL8**	interleukin 8
27.5	Up day0-3 *in vitro* Up *in vivo* Down day3-5 *in vitro*	**HBEGF**	heparin-binding EGF-like growth factor
22.1	Up day0-3 *in vitro* Down day3-5 *in vitro*	**MMP10**	matrix metallopeptidase10 (stromelysin 2)
11.3	Up day0-3 *in vitro* Down day3-5 *in vitro* Up in Trachoma	**PMEPA1**	prostate transmembrane protein, androgen induced 1
7.0	Up day0-3 *in vitro* Up *in vivo*	**TNFAIP6**	tumor necrosis factor, alpha-induced protein 6
5.3	Up day0-3 *in vitro* Up day3-5 *in vitro* Up *in vivo*	**MMP3**	matrix metallopeptidase 3 (stromelysin 1, progelatinase)
4.4	Up day0-3 *in vitro* Up *in vivo*	**IL1A**	interleukin 1, alpha

Table 3.14 Late contraction gene candidates selected for validation.

Late contraction gene candidates for validation

Fold Change (day3-5 *in vitro*)	Expression pattern	Gene	Description
6.2	Up day3-5 *in vitro* Down day0-3 *in vitro* Up in Trachoma	**KCND2**	potassium voltage-gated channel, Shal-related subfamily, member 2
4.6	Up day3-5 *in vitro* Up in Trachoma	**PLXDC2**	plexin domain containing 2
4.1	Up day3-5 *in vitro* Down day0-3 *in vitro*	**ATRNL1**	attractin-like 1
3.2	Up day3-5 *in vitro* Down day0-3 *in vitro* Up in Trachoma	**FAM213A**	Family With Sequence Similarity 213 Member A
1.8	Up day3-5 *in vitro* Down day0-3 *in vitro* Up in FES	**GAS6**	growth arrest-specific 6
2.1	Up day3-5 *in vitro* Down day0-3 *in vitro*	**GBP3**	guanylate binding protein 3
1.9	Up day3-5 *in vitro* Up in TED	**SLC20A1**	solute carrier family 20 (phosphate transporter), member 1
1.5	Up day3-5 *in vitro* Up in FES	**CCND1**	cyclin D1

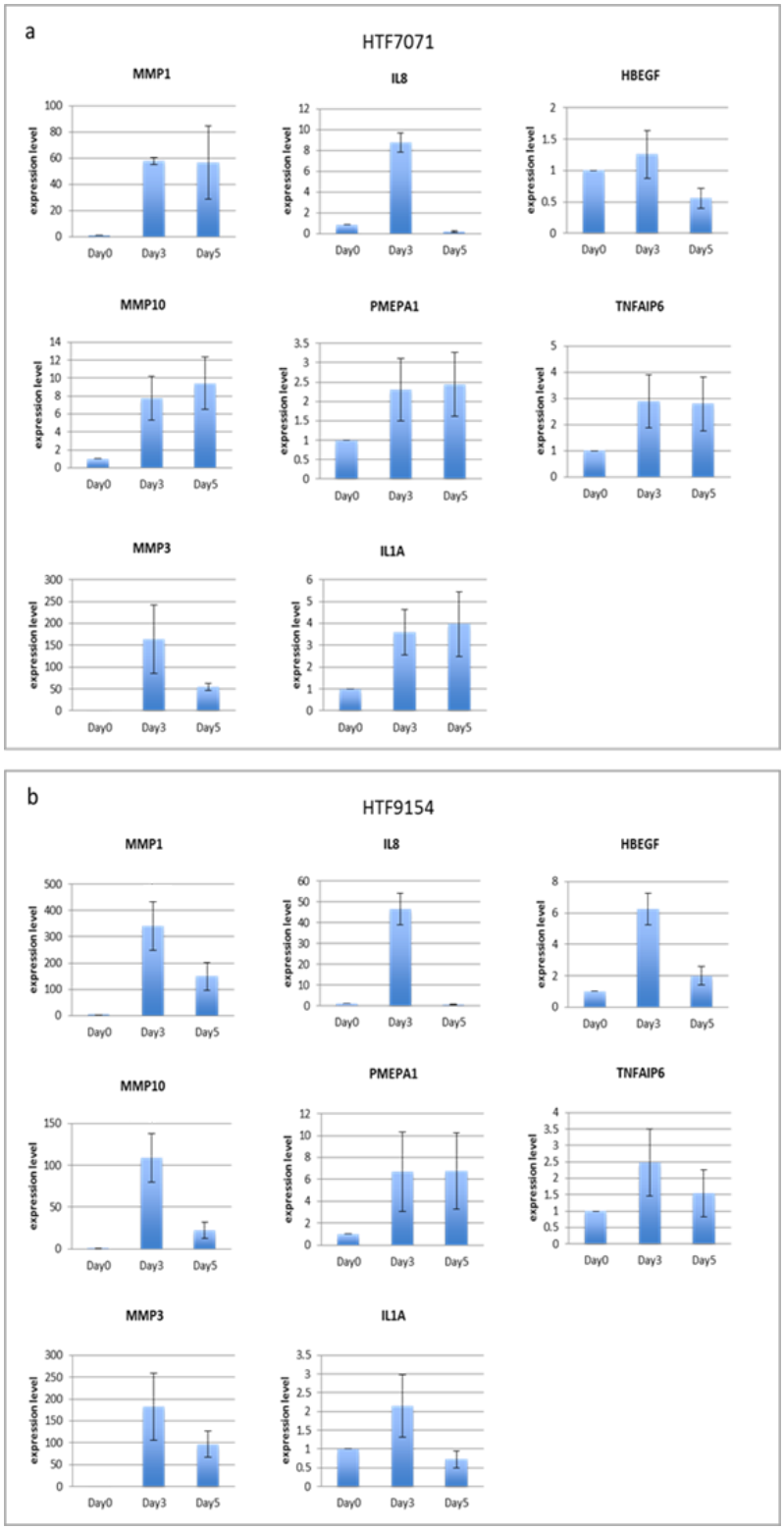

Figure 3.14 Validation of the in vitro early contraction profile signatures by qPCR. *qPCR validation of the early contraction candidates in two human conjunctival fibroblasts (a) HTF7071 and (b) HTF9154 (n≥2 experiments ± SEM). All the genes showed clear upregulation from day0 to 3 in both fibroblasts, with MMP1, 3 and 10, and IL8 being the most upregulated genes.*

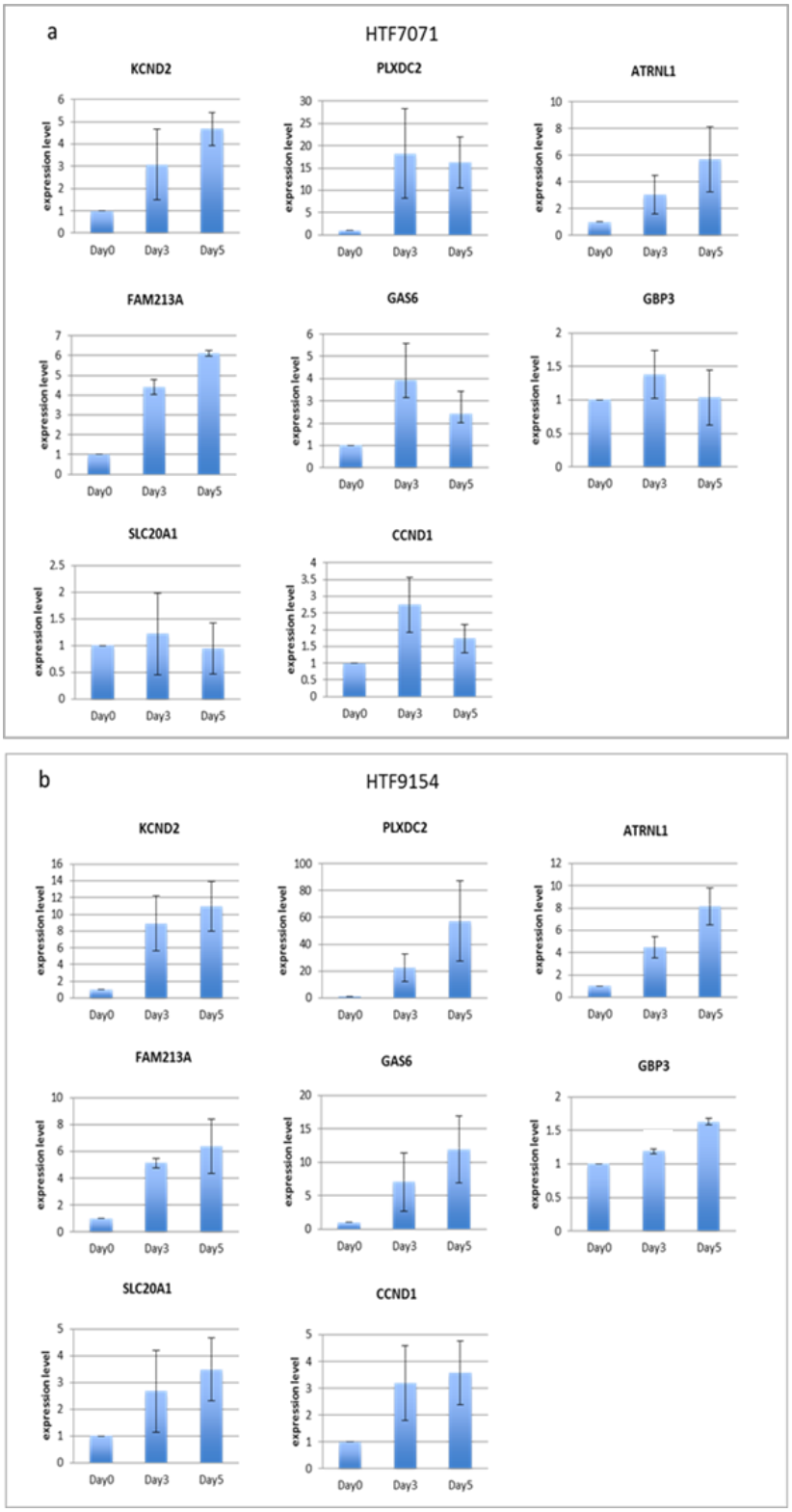

Figure 3.15 Validation of the in vitro late contraction profile signatures by qPCR. *qPCR validation of late contraction candidates in two human conjunctival fibroblasts (a) HTF7071 and (b) HTF9154 (n≥2 experiments ± SEM). In HTF9154 all the genes were upregulated from day0 to 3, and increased further from day3 to 5; whilst in HTF7071 they*

were upregulated from day0 to 3, and most of which kept around the similar expression levels from day3 to 5, suggesting that the expression levels of these genes can vary between fibroblasts from different donors.

3.8 Discussion

A comprehensive analysis was performed on the full gene expression profile of fibroblast-mediated contraction *in vitro* with the purpose of understanding the molecular mechanisms involved in fibroblast-mediated tissue contraction. The *in vitro* contraction was characterised by a dramatic, but transient, hyperactive early phase that initiated the entire contractile activity, and as the contraction slowed down at the later stage, the "activation" profile receded to a more "resting" phenotype. The dynamically regulated process reflected and matched the actual wound healing process *in vivo*, as after fibroblasts being activated in response to the injury and breach of the local tissue tension, the activation calms down and eventually terminates (Brown et al., 1998). In addition, the treatment with NSC23766 efficiently blocked the activation phase of contraction, and arrested the cells in the quiescent stage directly, suggesting that the signalling through Rac1 activity is critical in the early stage of contraction, as supported by the previous study (Tovell et al., 2012).

The genes that were significantly upregulated during the early contraction involved many inflammatory mediators. For example IL1RN and F2RL1, which positively modulate immune and inflammatory responses (Tamassia et al., 2010, Carvalho et al., 2010), CXCR4 that plays an essential role in vascularisation and endows potent chemotactic activity for lymphocytes (Rahimi et al., 2010, Pavlasova et al., 2016),

SERPINB2, a coagulation factor that contributes to the regulation of adaptive immunity (Kruithof et al., 1995, Medcalf and Stasinopoulos, 2005, Heit et al., 2013), IL8, a major inflammation regulator that attracts neutrophils, basophils and T-cells (Larsen et al., 1989, Baggiolini, 2015), and HBEGF that displays mitogenic and migratory effects to both fibroblasts and keratinocytes, as well as promoting angiogenesis (Shirakata et al., 2005). These stimuli are involved in intercellular signalling *in vivo* (Iyer et al., 1999), not only for the fibroblasts to interpret, amplify and broadcast signals that provoke inflammation, but also purposing to recruit other participant cells such as lymphocytes and macrophages. These cells enter the wounding site to provide both innate and antigen-specific defences against wound infection, and recruit the phagocytic cells to clear out the debris during the remodelling of the wound. The fact that the profile was captured in the *in vitro* profile demonstrated that our collagen contraction model is a good system to replicate at least partly some of the pathways of local inflammation in the wound healing response *in vivo*. Furthermore, the most downregulated gene clusters in the early contraction were the ones that related to sterol metabolic process and cofactor binding, which were activated again in the late contraction. The suppression of these pathways in the early contraction might be explained as a feedback response of fibroblasts to serum stimulation (that provided external lipid and cholesterol), which in turns brought down the endogenous cholesterol biosynthesis (Iyer et al., 1999).

The application of NSC23766 reversed the gene expression profile of early contraction as the activation of immune response, wound healing and transcription activity was suppressed, and the pathways controlling oxidation reduction, cofactor binding and lipid metabolism were promoted. The same pattern was observed in the late contraction, in which the cells were rested or appeared to have reduced

contraction status, suggesting that the upregulation of redox reaction, coenzyme activity and sterol metabolism signalling might be associated with reduction of contractile properties. Indeed, it has been reported that dermal fibroblasts expressing a strong upregulation of lipid and fatty acid metabolism signature genes exhibited a ‘normal-like’ non-fibrotic feature compared to the fibrotic ones in systemic sclerosis pathogenesis (Milano et al., 2008, Johnson et al., 2015), which hypothesised a potential anti-fibrotic function linked to these pathways. However, the detailed mechanisms are awaiting further investigation.

A coordinated and multi-faced gene program that modulates tissue homeostasis, cell migration, inflammation and angiogenesis, is induced by fibroblast in response to serum stimulation (Iyer et al., 1999, Chang et al., 2004). In the *in vitro* early contraction profile, the serum-responsive genes captured matched the gene groups that were significantly upregulated between 4-8hrs after serum stimulation (Iyer et al., 1999), including those implicated in inflammation (IL8, PTGS2, ICAM1, IL6), coagulation and homeostasis (THBD, TFPI2, PLAUR), angiogenesis (VEGFA, FGF2) and tissue remodelling (PLOD2, CDH2), as well as the downregulated ones, such as those related to lipid synthesis (ACACA, FADS2, SQLE, PSAT1), cell adhesion (SVEP1, THBS2, FAT4), cell cycle arrest (CDKN1C, CDKN2C, ARHGAP20) and actin cytoskeleton binding (SPTBN1, DAAM1, EPB41L2), suggesting that the fibroblast-mediated contractile activity is at least partially induced by an early response to serum stimuli. In total about two thirds of the serum response genes were expressed during the *in vitro* contraction, demonstrating that our *in vitro* model well replicated the physiological response of fibroblasts to serum stimulation. However, as our study was using fibroblasts from a different tissue (conjunctiva vs. foreskin), harvesting at different time points (5-day period vs. 24hr period) and culturing in a different experimental environment (3D collagen gel vs.

2D tissue culture flask), our serum response profile was expected to be slightly different from the one of the previous study of fibroblast in response to serum (Iyer et al., 1999). Most importantly, majority of the genes expressed in our profile are not related to serum stimulation, which are possibly linked to contractile activity.

Whilst the *in vitro* microarray has provided an in depth understanding of the gene modulation during fibroblast-mediated tissue contraction, numerous other cells contribute to the wound healing process *in vivo*, such as neutrophils, macrophages and lymphocytes (Clark, 1996, Martin, 1997). The in parallel pilot study of the *in vivo* wounding model in rabbit has given an insight into the inflammatory exponents of wound healing. Our collagen gel contraction assay can be used as an accelerated model of the wound healing program *in vivo*, which is a much longer process. In the rabbit eye undergoing glaucoma filtration surgery, the time point accessed in this study (5-day) represents an early stage of the tissue repair when the bleb is closed by filled granulation tissue and the contraction by migratory fibroblasts being observed (Geggel et al., 1984, Miller et al., 1989). Thus we expected the *in vivo* gene expression profiling to match closely the *in vitro* contraction profile. Indeed, we have shown that one third of the genes regulated in the *in vivo* contraction were altered in the same manner in the *in vitro* assay, and the ones that were not presented in the *in vitro* profile were likely related to other cellular participants (such as epithelial cells and inflammatory cells). Moreover, our *in vitro* array recapitulated many more of the genes regulated *in vivo* than the assay of the fibroblasts in response to serum stimulation (Iyer et al., 1999), indicating that the 3D collagen contraction model is a better match to the *in vivo* wound healing behaviour than the 2D serum stimulation model. Notably, ACTA2, which encodes α-SMA that is a major constituent of the contractile apparatus and commonly used as a marker of myofibroblast formation (Sappino et al., 1990, Desmouliere, 1995), was upregulated

exclusively in the *in vivo* profile. The differentiation of the myofibroblast population at the wound site usually occurs in a later stage of the wound healing (Miller et al., 1989, Midwood et al., 2004). The fact that ACTA2 was not found regulated in the *in vitro* contraction suggested that the *in vitro* assay, as expected, does not recapitulate all aspects of the contraction.

Through the comparison of the gene expression profiles of trachoma and thyroid-associated orbitopathy (TED), we have shown that some of the genes identified as associating to the fibrotic features were captured in our *in vitro* assay, with the expression profile slightly leaning towards late contraction. It suggested that the late contraction may represent the cells leading towards the progression of fibrosis. Moreover, more trachoma signature genes were expressed in the *in vitro* profile than that of TED, which is possibly because trachoma is a conjunctival fibrotic disease (Abu el-Asrar et al., 1998) that is much closer to our model, whilst the study of TED was using orbital fibroblasts rather than the conjunctival ones. Besides, the causes of the TED involve not only fibrosis but also adipogenesis (Naik et al., 2010). Nevertheless, the fact that there were still some common genes being identified between the TED and the *in vitro* contraction profile indicated that TED may be fundamentally associated with fibrosis, independent of the cause of the disease.

Finally, the signature genes verified in the study of the *in vitro* contraction are not only limited to the ocular fibrotic diseases, but also applied to a wide variety of fibrotic associated pathogenesis from different locations (**Table 3.15**). It is recognised that these candidates represent only a part of the gene signatures of the *in vitro* contraction, and more studies are needed to understand the gene interactions and signalling pathways underlying fibroblast-driven matrix contraction

and tissue repair. Moreover, the downregulated gene signatures of the contraction will need to be characterised in the future work. Nevertheless, the comprehensive analysis presented has provided a 'molecular portrait' of the fibroblast-mediated contraction *in vitro*, which will be a powerful tool assisting future anti-scaring and fibrosis research in a wide range of fibrotic related diseases.

Table 3.15 Examples of the implications of the in vitro contraction signature genes in various fibrotic diseases and cancers. The early contraction signature genes are coloured in blue, and the late contraction signature genes are coloured in pink. MMP1 and MMP3 are highlighted in yellow as they were upregulated throughout the whole contraction process.

Genes	Diseases	References
MMP1	Idiopathic pulmonary fibrosis (IPF)	(Pardo and Selman, 2006, Herrera et al., 2013)
MMP3	Peyronie's disease	(Gelfand et al., 2015)
MMP10	Cardiac fibrosis	(Turner et al., 2010)
IL8	Cystic fibrosis	(Furlan et al., 2016)
HBEGF	Heart and pancreatic fibrosis	(Means et al., 2003, Blaine et al., 2009, Lian et al., 2012)
IL1A	Lung fibrosis	(Sohn et al., 2015)
PMEPA1	Tumorigenesis and metastasis in cancers	(Brunschwig et al., 2003, Bai et al., 2014, E et al., 2014)
TNFAIP6	Inflammatory diseases	(Wisniewski et al., 1996, Yu et al., 2016, Wang et al., 2015, Qi et al., 2014)
KCND2	Differentiation of vascular adventitial myofibroblasts	(Guo et al., 2006)
PLXDC2	Colon tumour progression and angiogenesis	(Greening et al., 2013)
GAS6	Inflammation and myofibroblast activation in liver	(Fourcot et al., 2011)
CCND1	Liver, renal and skin fibrosis	(Fan et al., 2014, Cuevas et al., 2015, Han et al., 2016)

Chapter 4 The involvement of the Rho GTPases in contraction

4.1 The variable response of fibroblasts to NSC23766 treatment

In the previous chapter, we have discussed how Rac1 appeared to be a major regulator in fibroblast-mediated tissue contraction, as a transient 24hrs downregulation of Rac1 by its inhibitor NSC23766 altered gene expression and prevented the initiation of the contraction. The original results were obtained with one conjunctival fibroblast line (HTF7071) from one donor. During the validation of the *in vitro* microarray candidates by qPCR, we used an additional line from a different donor (HTF9154), which showed a different response to the treatment with NSC23766. Thus, in the current chapter, the effects of NSC23766 and other commercially available Rac inhibitors on the contractile activity of a few primary conjunctival fibroblasts that originated from different donors were characterised. We also investigated the modulations of contraction by other Rho GTPases and MAPK signalling. The results would provide useful information in assisting the future study of Rac-mediated cellular functions in the *in vivo* models of ocular scarring, and also for the development of anti-scarring therapeutics in the clinics.

The primary human conjunctival fibroblast cells used in this study and their donor information were recorded in **Chapter 2** (**2.1.1**). The differential responses of fibroblasts to NSC23766 treatment were firstly evaluated in the collagen contraction experiment using HTF7071, HTF9154, HTF2489 and HTF2493 treated with 50μM NSC23766 for the first 24hrs (**Figure 4.1**). The results showed that at day2,

NSC23766 treatment led to a 50% reduction of contraction in HTF7071, HTF2489 and HTF2493, and about 30% reduction of contraction in HTF9154 comparing to the untreated contraction. At day7, NSC23766 treatment suppressed 30% contraction in HTF7071, and about 10% contraction in HTF9154, HTF2489 and HTF2493 comparing to the untreated contraction, suggesting a variable response of fibroblasts to the treatment of NSC23766. In particular, HTF9154 was not sensitive to the NSC23766 treatment, suggesting that it might utilise other signalling pathways rather than Rac1 to sustain contraction.

4.2 The Characterisation of other Rac inhibitors

NSC23766 was initially identified as a small molecule that binds to a putative binding pocket in the surface groove of Rac1. It interacts with the Rac-specific GEFs Trio and Tiam1 without affecting the closely related Cdc42 or RhoA binding or activation by their respective GEFs (Gao et al., 2004). Although NSC23766 was widely used in *in vitro* studies as a moderately active Rac inhibitor, its relatively high IC50 of 50-100μM in fibroblasts restricts its potential of being used as a therapeutic agent in the clinic. Therefore, for the purpose of evaluating alternative Rac inhibitors, especially with the focus on their short transient inhibitory ability that will benefit the potential future clinical application, four commercially available compounds were selected. They included W56, which selectively inhibits Rac1 interaction with Rac1-specific GEFs TrioN, GEF-H1 and Tiam1 (Gao et al., 2001), Z62954982, a cell-permeable isoxazolyl-benzamide compound that interferes Rac1-Tiam1 interaction, while exhibiting no effect toward cellular Cdc42 and RhoA activation or Rac1 interaction to its effector Pak1 (Ferri et al., 2009), EHT1864, an inhibitor of Rac family GTPases by direct binding to Rac1, Rac1b, Rac2 and Rac3

(Shutes et al., 2007), and Ehop-016, which was synthesized based on the structure of NSC23766 but with an IC50 of 1.1μM that is 100 times lower than NSC23766 (Montalvo-Ortiz et al., 2012). Also, Simvastatin, a clinical proved cholesterol-lowering drug that is widely used in the prevention and treatment of atherosclerotic cardiovascular disease, was selected for its ability of blocking Rac1-mediated signalling events by depletion of the lipid attachments that are required by the Rho GTPases (Negre-Aminou et al., 2001, Miller et al., 2011). The Rho-associated protein kinase (ROCK) inhibitor H1152 and the broad MMP inhibitor GM6001 were applied for their known effect of preventing fibroblast-mediated matrix contraction (Martin-Martin et al., 2011), and NSC23766 was used as a base line control. The inhibitors were added to the collagen contraction medium of fibroblast HTF9154, which did not respond well to 50μM 24hrs NSC23766 treatment. The concentrations of the inhibitors applied were set to be 10μM for 7 days and 50μM for 24hrs respectively (except GM6001 that was used at a concentration of 100μM (Martin-Martin et al., 2011)), as in comparison with the standard 50μM 24hrs dosage of NSC23766 (**Figure 4.2**). As a result, 10 and 20μM of 7-day application of W56, and 10, 25μM 7-day and 50μM 24hrs applications of Z62954982 barely affected the contraction, whilst 50μM of Simvastatin and EHT1864 notably inhibited 1/3 of the contraction respectively with a transient 24hrs application. Significantly, the 7-day 10μM or 50μM 24hrs application of Ehop-016 completely suppressed the whole contraction activity for 7 days, making it the most efficient Rac inhibitor among all. Furthermore, as expected, the ROCK inhibitor and broad MMP inhibitor both had good inhibitory effect on the contractile activity of HTF9154 with a consistent 7-day application of 10μM and 100μM concentrations respectively.

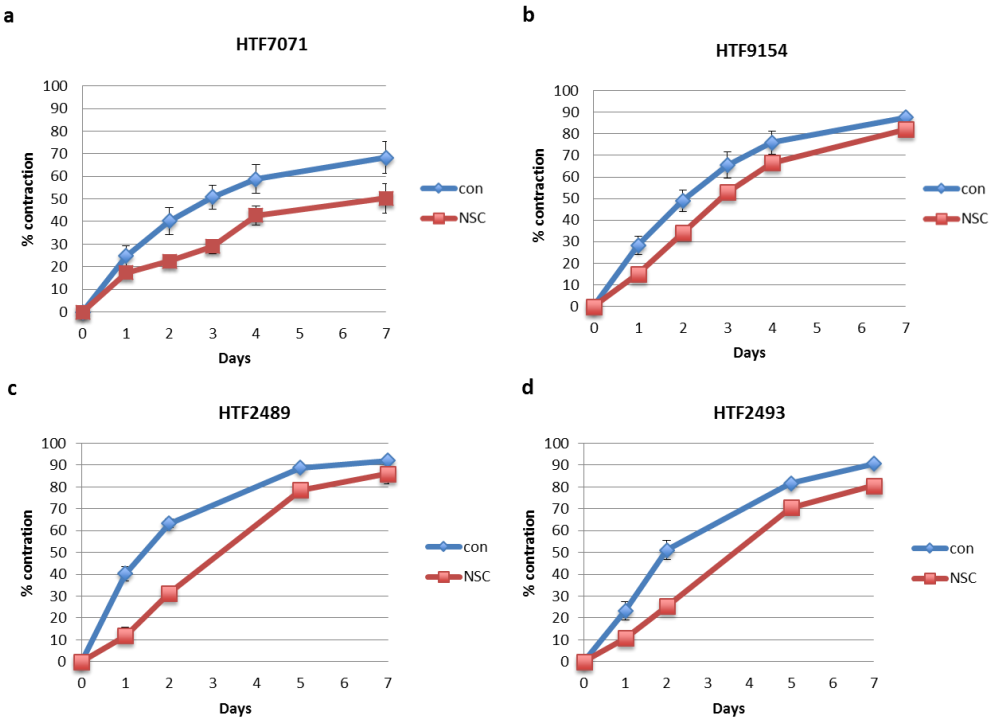

Figure 4.1 The variable responses of fibroblasts to NSC23766 treatment.

Collagen contraction kinetics of four primary conjunctival fibroblasts HTF7071 (a), HTF9154 (b), HTF2489 (c) and HTF2493 (d) treated with NSC23766 for the first 24hrs ((a), (b): mean ± SEM, n=3 experiments with triplicate wells; (c), (d): mean ± SEM, n=2 experiment with triplicate wells). The primary fibroblast line of HTF7071 was going to an end at the time of performing the experiment, thus its contraction curve was lower than the others.

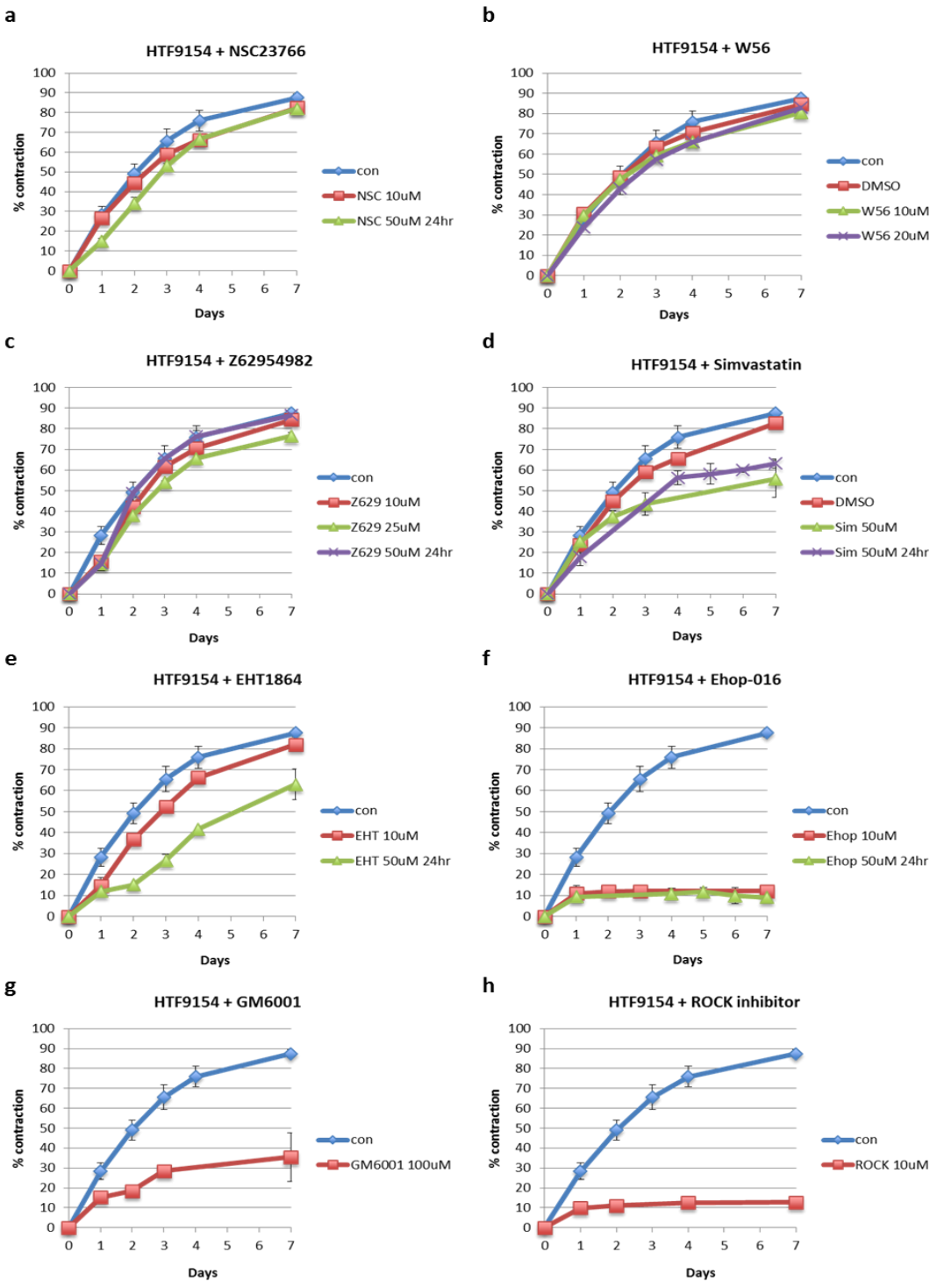

Figure 4.2 Characterisation of the inhibitory efficiency of a range of Rac inhibitors including NSC23766, W56, Z62954982, EHT1864 and Ehop-016, as well as the broad MMP inhibitor GM6001 and the Rho-associated protein kinase (ROCK) inhibitor H1152 (labelled as 'ROCK') on fibroblast-mediated collagen gel contraction.

7-day contraction kinetics of HTF9154 treated with a range of Rac inhibitors including (a) NSC23766 10μM and 50μM, for 7 days and 24hrs respectively; (b) W56 10μM and 20μM, for 7 days; (c) Z62954982 10μM and 25μM for 7 days, and 50μM for 24hrs; (d) Simvastatin

50μM, for 7 days and 24hrs; (e) EHT1864 10μM and 50μM, for 7 days and 24hrs respectively; and (f) Ehop-016 10μM and 50μM, for 7 days and 24hrs respectively. The broad MMP inhibitor GM6001 (g) and the Rho-associated protein kinase (ROCK) inhibitor H1152 (h) were also applied for 100μM and 10μM respectively, both for 7 days (Mean ± SEM, n=3 experiments with triplicate wells). DMSO was used as solvent control in the W56 and Simvastatin treated groups, and its concentrations used was kept the same with W56 or Simvastatin respectively.

Moreover, Simvastatin, EHT1864 and Ehop-016 were further tested in the collagen contraction assay with seven primary fibroblast cell lines originated from different donors, with unrelated age and sex spectrum respectively. We used 50μM 24hrs treatment for Simvastatin and EHT1864, and 10μM 24hrs treatment for Ehop-016, as 10μM of Ehop-016 already showed a great efficiency in inhibiting contraction (**Figure 4.2**). The ROCK inhibitor, GM6001 and NSC23766 were also used as reference (**Figure 4.3**). The results showed that 24hrs treatment of 50μM Simvastatin reduced 20-30% contraction of most of the fibroblasts, with HTF7071 being the most sensitive one to the drug, and HTF1818 and HTF0748-1 being the most insensitive ones. HTF7071 and HTF1785R were sensitive to the NSC23766 treatment, which managed to reduce 40% of the contraction on HTF0104 and HTF2320 but only for the first three days, suggesting that a reapplication of the inhibitor for these cells may be necessary. Furthermore, treatment with 50μM of EHT1864 resulted in a good suppression of contraction of all the fibroblasts for the first two to three days, which indicated that a reapplication of the drug at day3 would be desirable as the efficiency gradually drew back afterwards. By contrast, 24hrs treatment of 10μM Ehop-016 significantly blocked the contractile activity of most of the fibroblasts tested, especially for the ones that were not responsive to

NSC23766, such as HTF9154 and HTF1818. HTF0748-1 only responded well to the ROCK inhibitor, suggesting that it may use a different mechanism for contraction.

To determine whether the inhibitory effect of the inhibitors was due to their effect on contraction or toxicity, the cell viability upon the treatment was evaluated using AlamarBlue reagent in the culture medium of four contracting fibroblasts including HTF7071, HTF9154, HTF1785R and HTF0041 at day2 and day7 respectively (**Figure 4.4**). The results showed that the inhibitors had variable effects on different fibroblasts. Broadly, Simvastatin, NSC23766, the ROCK inhibitor H1152 and GM6001 did not result in much reduction on cell viability of all the cells, whereas EHT1864 and Ehop-016 appeared to be more toxic. They caused a 20% drop of the cell viability at day2 and a 30% drop at day7 on HTF9154, HTF1785R and HTF0041, and a 50% decrease of the cell viability on HTF7071 at both day2 and day7, suggesting that HTF7071 was extremely sensitive to the treatment, and also the inhibitory effect of EHT1864 and Ehop-016 on contraction may partly due to their toxicity to the cells.

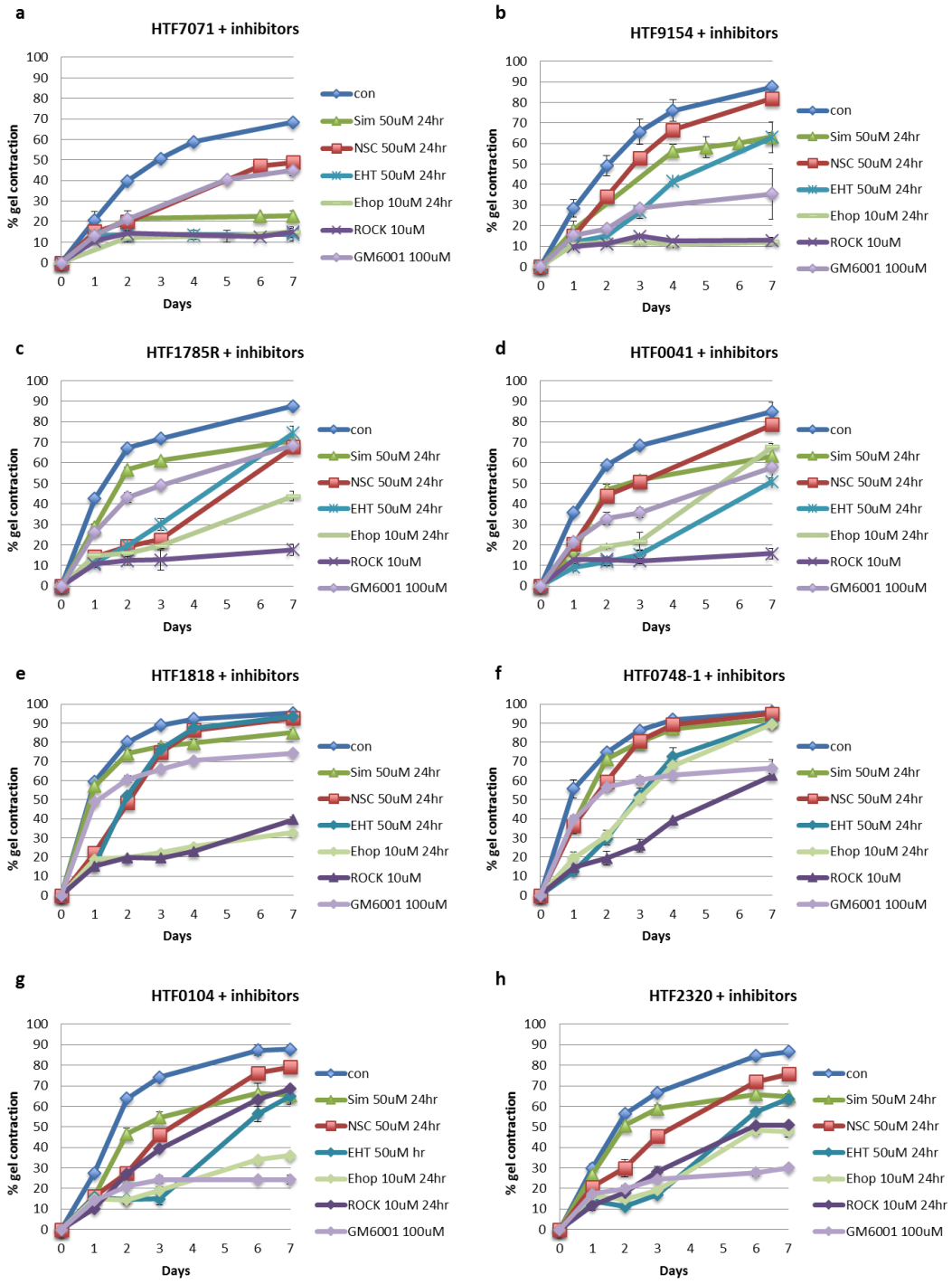

Figure 4.3 Characterisation of the inhibition efficiency of the Rac inhibitors Simvastatin, NSC23766, EHT1864 and Ehop-016, as well as the broad MMP inhibitor GM6001 and the Rho-associated protein kinase (ROCK) inhibitor H1152 (labelled as 'ROCK') on collagen contraction with eight different conjunctival fibroblasts.

Collagen contraction assay of fibroblasts HTF7071 (a), HTF9154 (b), HTF1785R (c), HTF0041 (d), HTF1818 (e), HTF0748-1 (f), HTF0104 (g) and HTF2320 (h) were treated with inhibitors including Simvastatin 50μM, NSC23766 50μM, EHT1864 50μM and Ehop-016 10μM respectively for 24hrs, or ROCK inhibitor H1152 10μM for 7 days, or the broad MMP

inhibitor GM6001 100μM for 7 days (Mean ± SEM, (a)-(b), n=3 experiments with triplicate wells, (c)-(h), n=2 experiments with triplicate wells).

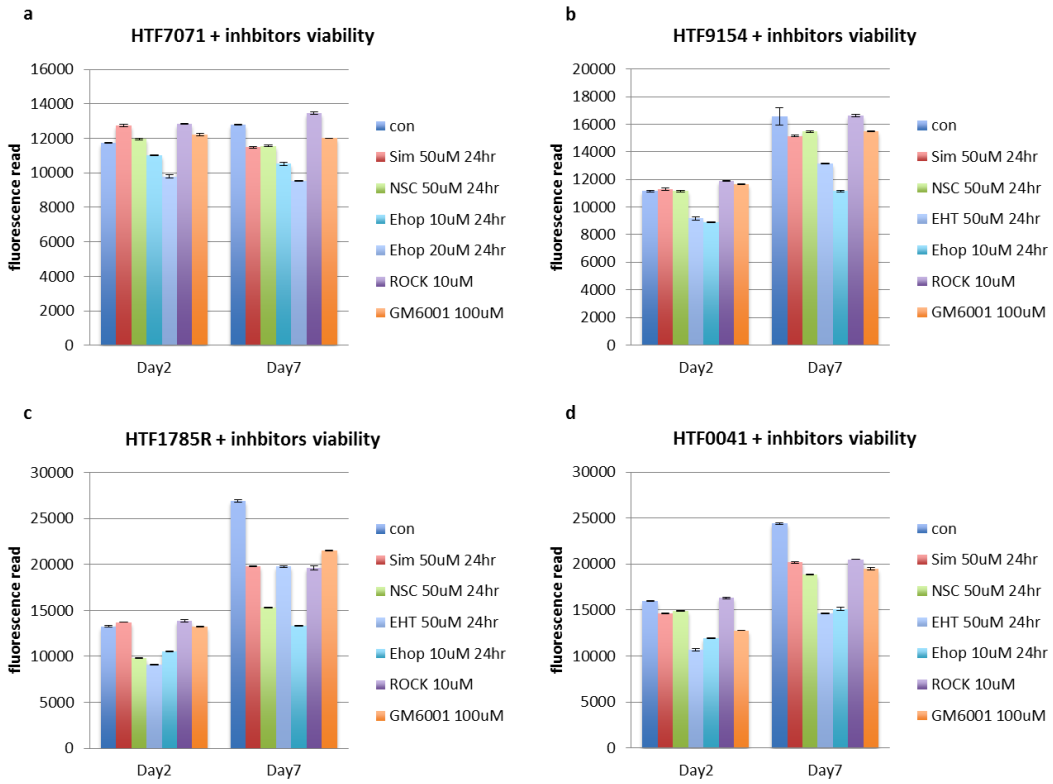

Figure 4.4 Cell viability assay performed on the inhibitors treated contracting fibroblasts at day2 and day7.

Cell viability assay was performed by adding alamarBlue dye in the day2 and day7 contraction medium of fibroblasts HTF7071 (a), HTF9154 (b), HTF1785R (c) and HTF0041 (d) treated with inhibitors including Simvastatin 50μM, NSC23766 50μM, EHT1864 50μM, Ehop-016 10μM respectively for 24hrs, or the ROCK inhibitor H1152 10μM and the broad MMP inhibitor GM6001 100μM respectively for 7 days (mean ± SEM, n=2 experiments with triplicate wells). The fluorescence read was normalised to the read of day2 control sample. The inhibitors caused variable effects on the cell viability of these fibroblasts. EHT1864 and Ehop-016 appeared to reduce more viability than other inhibitors, especially at day7.

4.3 The role of Rho GTPases Rac1, Cdc42 and RhoA in contraction

In the previous study, the involvement of Rac1 in serum-stimulated matrix contraction by human conjunctival fibroblast was investigated by siRNA knockdown and treatment with NSC23766, both of which significantly reduced the contraction by 70% in HTF7071 (Tovell et al., 2012). However, we have found that fibroblasts from different donors responded variably to the NSC23766 treatment, suggesting that the cells may apply other mechanisms to regulate contractile activity. We explored the contribution of Rac1, Cdc42 and RhoA in contraction by depleting the individual gene by siRNA technology, and seeding these knockdown cells into collagen contraction assay for three days. To verify the specificity of NSC23766 to Rac1, and also the modulation of Rac1 on contraction in the absence of Cdc42 or RhoA, we applied the 50μM NSC23766 treatment in the contraction medium for the first 24hrs (**Figure 4.5**). The experiment was performed with conjunctival fibroblasts HTF1785R, which were sensitive to the NSC23766 treatment, and exhibited a moderate sensitivity to other Rac inhibitors. The knockdown of Rac1, Cdc42 or RhoA in the cells was validated by Western blot, which proved a good depletion of the target proteins (**Figure 4.5d**). Surprisingly, depletion majority of the Rac1 protein by siRNA barely reduced the contraction, whilst the treatment of NSC23766 decreased 30% of the contraction in both control and Rac1 knockdown cells, suggesting that the cells may use other signalling pathways to regulate contraction in the absence of Rac1, and NSC23766 may have other targets that played a role in contraction. Meanwhile, knocking down of Cdc42 or RhoA resulted in a significant 30% or 25% of reduction of contraction respectively, indicating that Cdc42 and RhoA both played a regulatory role in contraction. However, treatment with NSC23766 further decreased the contractile activity of the Cdc42 or RhoA knockdown cells, suggesting that Cdc42 and RhoA partially regulated contraction, and they were not targeted by NSC23766.

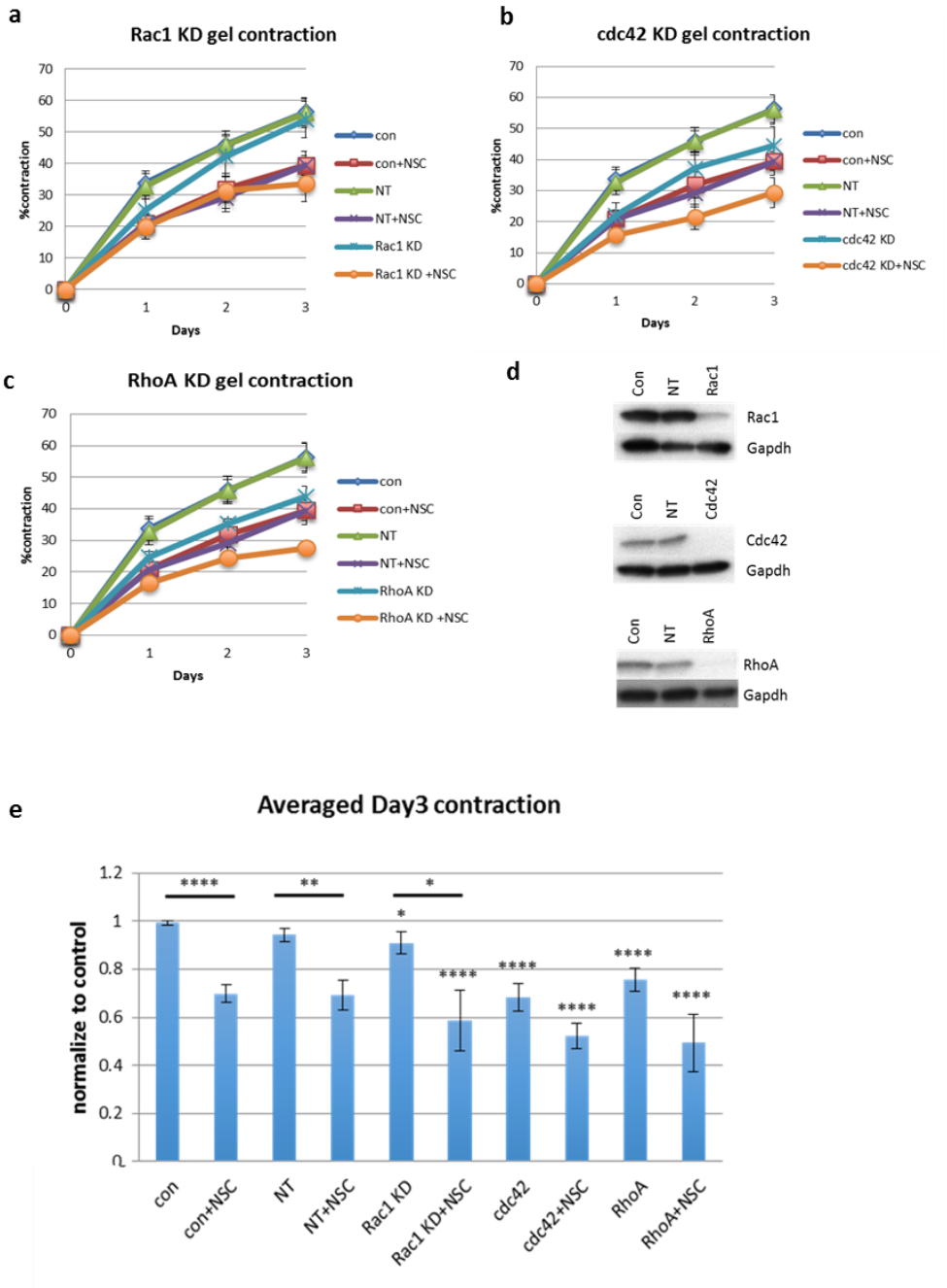

Figure 4.5 Small Rho GTPases Rac1, Cdc42 and RhoA differently regulated the contractile activity of human conjunctival fibroblast HTF1785R.

Fibroblast HTF1785R cells were treated with siRNA for Rac1, Cdc42 and RhoA respectively and then seeded into collagen contraction assay with transient treatment with NSC23766 for the first 24hrs. The 3-day contraction curve was plotted for Rac1 (a), Cdc42 (b) and RhoA (c) knockdown cells respectively (NT: non-targeting siRNA control. Mean ± SEM, n=3 experiments with triplicate wells). (d) The validation of the Rac1, Cdc42 or RhoA siRNA-knockdown cells by Western blot showed a good depletion of the target protein. The figure is

*a representative of reproducible results (n≥3 experiments for each knockdown). (e) Averaged day3 contraction normalised to control contraction (Mean ± SEM, n=3 experiments with triplicate wells, t test between siRNA treated samples and control contraction, ****p<0.0001, *p<0.05; t test between NSC23766 treated and non-treated samples within the same group, ****p<0.0001, **p<0.01, *p<0.05).*

4.4 Role of ERK, P38 MAPK and PI3K signalling in contraction

After identifying that small Rho GTPases (mainly Cdc42 and RhoA) play a regulatory role in fibroblast-mediated contraction, we further explored the regulation of other signalling pathways in contraction, specifically the MAPK signalling including ERK and P38 MAPK, and the PI3K signalling pathway, and their links to GTPase activation. Rac1, Cdc42 or RhoA knockdown HTF1785R cells were seeded into 3-day collagen contraction assay and treated with the ERK inhibitor U0126 10μM, P38 MAPK inhibitor SB203580 10μM and PI3K inhibitor Ly294002 25μM, respectively. The percentage of contraction was monitored daily, and the kinetics are shown in (**Figure 4.6**). The results demonstrated that the PI3K signalling played an important role in contraction, as treatment with Ly294002 depleted at least 40% of contraction in all the cells. Blocking of the P38 MAPK by SB203580 barely affected contraction, however upon inactivation of Cdc42, it significantly reduced 20-30% of contraction, suggesting that the P38 MAPK signalling was downstream of Cdc42 and its participation in contraction was Cdc42 dependent. Notably, application of U0126 increased contraction in all the cells, indicating that the ERK signalling played an inhibitory role in contraction. The fact that inhibition of ERK counteracted the effect brought by inactivation of Cdc42 suggested that the modulation of contraction by Cdc42 was likely mediated through the suppression of

the ERK signalling. The prospective roles of these participators in contraction are modelled in **Figure 4.7**.

4.5 Role of Rac2, Racgap1, Arhgap5 and Arhgef3 in contraction

During the analysis of the *in vitro* microarray, we found that many regulators of the Rho GTPases were expressed differently in different stages of contraction, including the GTPase-activating proteins (GAPs) and Guanine nucleotide exchange factors (GEFs). Other members of the Rac superfamily, for example Rac2, was also found being regulated. We hypothesised that these genes may perform differential regulatory functions in different stages of the contraction via GTPase activity (Rac members), and activation (GEFs) or inactivation (GAPs) of the Rho GTPases that involved in the contraction modulation (such as Cdc42 and RhoA). Therefore, we selected four candidates for exploration, which included Rho GTPase Rac2 (Ras-related C3 botulinum toxin substrate 2), Arhgap5 (Rho GTPase Activating Protein 5) whose GAP activity is preferentially towards RhoA (Matheson et al., 2006), Racgap1 (Rac GTPase Activating Protein 1) that strongly interacts with Cdc42 and Rac1 (Bastos et al., 2012) and Arhgef3 (Rho Guanine Nucleotide Exchange Factor 3) that selectively activates RhoA and RhoB (Arthur et al., 2002). Both Rac2 and Arhgap5 were upregulated in the early contraction from day0 to 3, and then downregulated in the late contraction from day3 to 5, whilst Racgap1 and Arhgef3 were downregulated from day0 to 3, and upregulated oppositely from day3 to 5 (**Table 4.1**). Notably, the expression patterns of all four genes' were completely reversed by the NSC23766 treatment at day3, suggesting that Rac2 and Arhgap5 might be functional in promoting contraction, whereas Racgap1 and Arhgef3 played a negatively part. Herein, to verify the roles of these genes in contraction, we

inactivated the individual gene in HTF1785R using siRNA technology (**Figure 4.8**), and seeded the knockdown cells in 3-day collagen contraction assay with/without the treatment of NSC23766 (**Figure 4.9**). As a result, knocking down of Rac2 significantly blocked contraction, indicating that its activity performed a vital function in mediating contraction. Depletion of Racgap1 increased contractile activity, suggesting that it suppressed the contraction possibly via inactivation of Cdc42 and Rac1. Blocking of Arhgap5 significantly inhibited contraction, which matched its expression profile in the *in vitro* microarray. We supposed that Arhgap5 might be required for contraction through other signalling pathways, as its modulation on contraction cannot be explained by its GAP activity towards RhoA. Inhibition of Arhgef3 completely inhibited contraction. We did not find Arhgef3 knockdown to be lethal to the cells, thus speculated that similar to Arhgap5, Arhgef3 was possibly involved in other signalling event whose activity was needed for the activation of contraction. Moreover, no statistical difference was found between the NSC23766 treated and untreated Rac2 knockdown cells, which suggested that these cells mainly utilised Rac2 to mediate contraction. Also, it was possible that the sensitivity of the fibroblasts in response to NSC23766 treatment was a reflection of the ratio of Rac1/Rac2 within them. The fact that suppression of Racgap1 counteracted the effect of NSC23766 treatment, suggesting that Racgap1 negatively regulated the contraction mainly through inactivation of Cdc42.

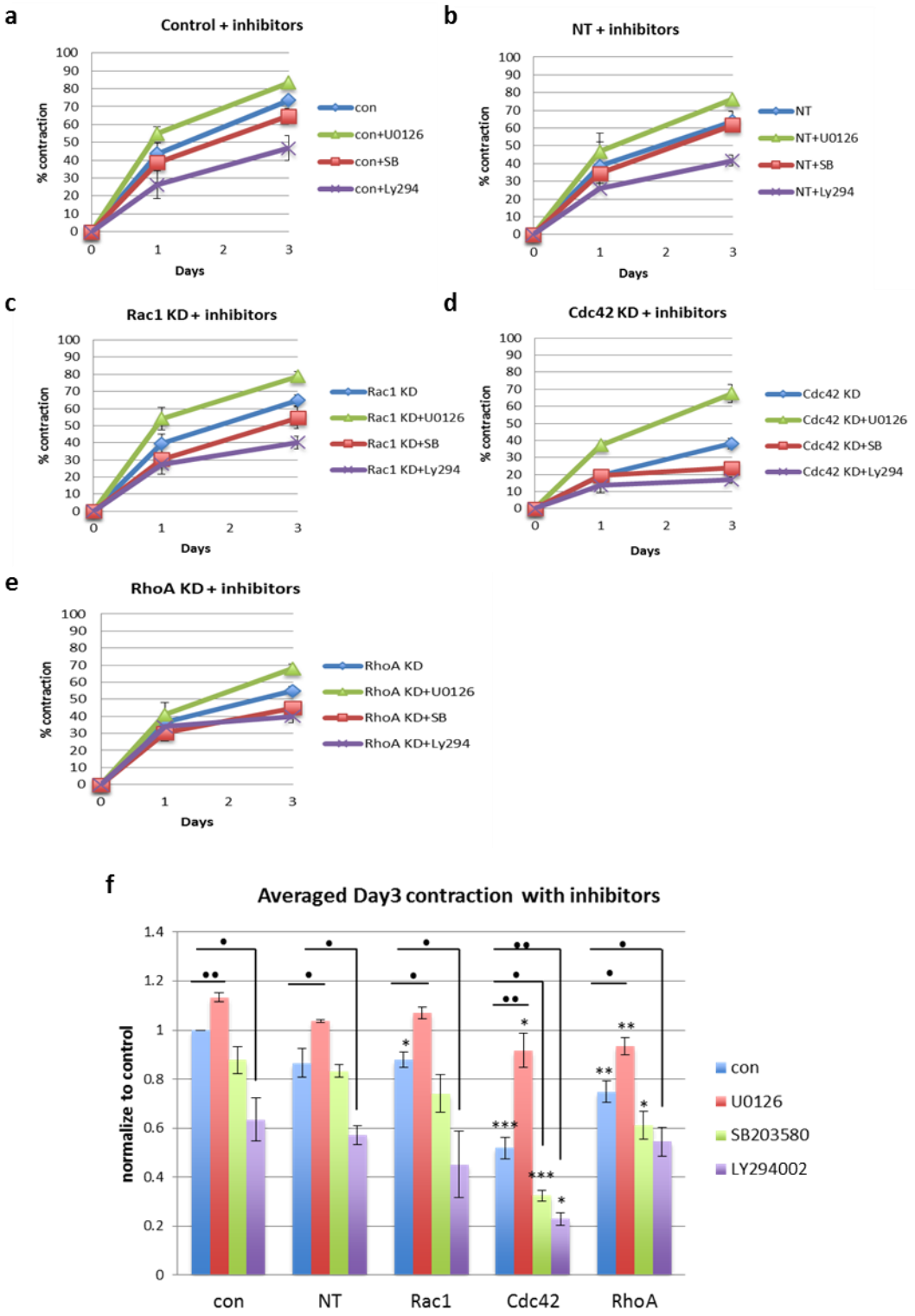

Figure 4.6 The ERK, P38 MAPK and PI3K signalling differently regulated the contractile activity of human conjunctival fibroblast HTF1785R.

(a)-(e) 3-day contraction kinetics of Rac1, Cdc42 or RhoA-knockdown HTF1785R cells treated with the ERK inhibitor U0126 10μM, P38 MAPK inhibitor SB203580 10μM and PI3K inhibitor Ly294002 25μM, respectively (NT: non-targeting siRNA control. Mean ± SEM, n=3

*experiments with triplicate wells). (f) Averaged day3 contraction normalised to the control contraction (Mean ± SEM, n=3 experiments with triplicate wells, t test between the same inhibitor treated samples in the siRNA knockdown group and control group, ***p<0.001, **p<0.01, *p<0.05; t test between non-treated and inhibitor-treated samples within the same group, ••p<0.01, •p<0.05).*

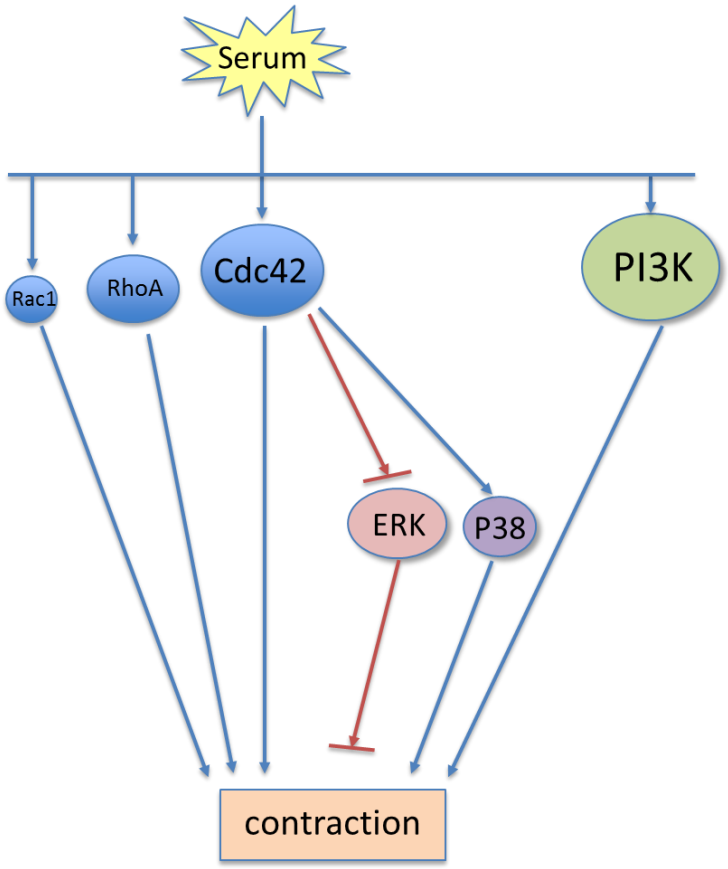

Figure 4.7 Illustrative diagram showing the potential regulatory roles of Rac1, Cdc42 and RhoA, and ERK, PI3K and P38 signalling in contraction.

The prospective roles of Rac1, Cdc42 and RhoA, and ERK, P38 MAPK and PI3K signalling in contraction were showed in the illustration. The size of the protein icon represents the importance of the protein to contraction. Upon serum stimulation, Cdc42, RhoA and PI3K signalling are activated to promote contraction, whilst the contribution of active Rac1 to contraction is small. The activation of ERK plays an inhibitory role, which is suppressed by Cdc42 activity. The P38 MAPK signalling positively regulates contraction downstream of Cdc42.

Table 4.1 Gene expression fold changes of Rac2, Racgap1, Arhgap5 and Arhgef3 in the in vitro microarray of fibroblast-mediated contraction at day0-3, day3-5 and NSC23766 treated samples at day3 (p<0.05).

	fold change (p<0.05)		
Gene	day0-3	day3-5	NSC day3
Rac2	1.78	-2.12	-1.37
Racgap1	-1.89	1.79	1.79
Arhgap5	1.89	-2.35	-2.60
Arhgef3	-5.8	1.67	2.29

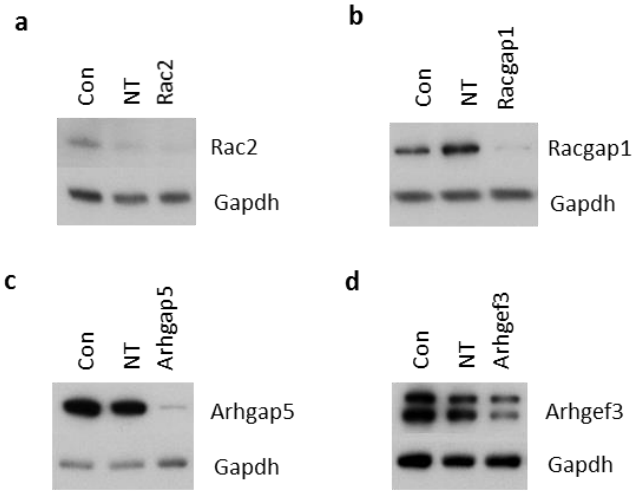

Figure 4.8 Validation of the siRNA knockdown of Rac2, Racgap1, Arhgap5 and Arhgef3 respectively in HTF1785R using Western blot.

Western blot results confirmed that the protein expression of (a) Rac2, (b) Racgap1, (c) Arhgap5 and (d) Arhgef3 respectively was successfully depleted following the siRNA treatment in human conjunctival fibroblast HTF1785R (NT: non-targeting siRNA control. Figure represented reproducible results n≥3).

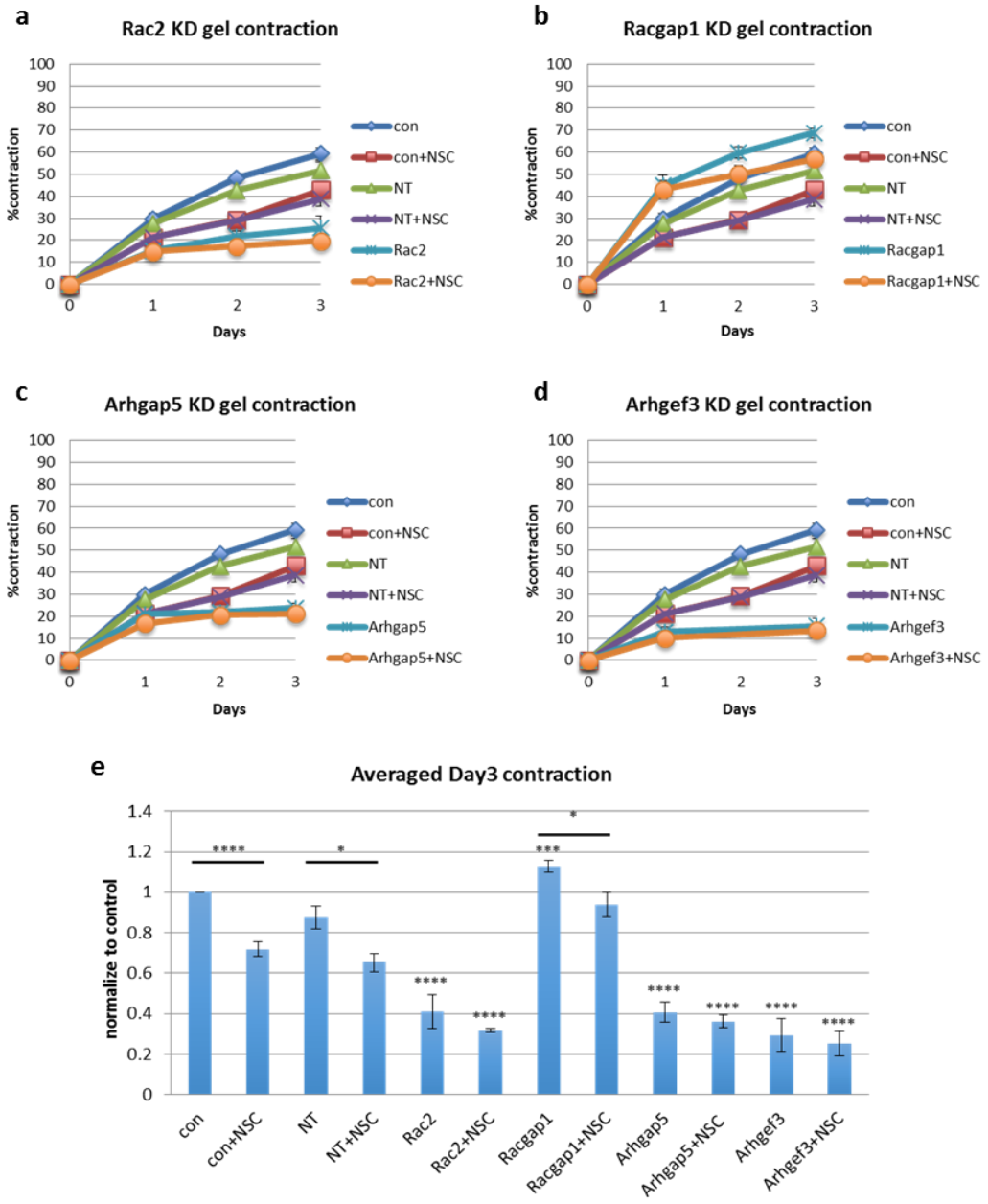

Figure 4.9 Collagen gel contraction kinetics of the Rac2, Racgap1, Arhgap5 and Arhgef3 knockdown HTF1785R cells respectively treated with/without NSC23766.

*3-day collagen contraction curves of fibroblast HTF1785R treated with siRNA for Rac2 (a), Racgap1 (b), Arhgap5 (c) and Arhgef3 (d) respectively, with/without treatment with NSC23766 for the first 24hrs (NT: non-targeting siRNA control. Mean ± SEM, n=3 experiments with triplicate wells). (e) Averaged day3 contraction normalised to the control contraction (Mean ± SEM, n=3 experiments with triplicate wells, t test between siRNA treated samples and control contraction, ****p<0.0001, ***p<0.001; t test between NSC23766 treated and non-treated samples within the same group, ****p<0.0001, *p<0.05).*

4.6 Discussion

We have demonstrated that a transient application of Rac1 inhibitor NSC23766 on human conjunctival fibroblast cells HTF7071 altered gene expression, which prevented the cells from entering the contractile phenotype as a whole, suggesting that inhibition of Rac1 activity could be a promising approach in the treatment of conjunctival scaring after glaucoma surgery. However, by enlarging the sample size for validation in this study, it was shown that approximately half of the fibroblasts from different donors did not respond to the NSC23766 treatment, suggesting that these cells utilised additional signalling pathways to mediate contraction. Also, the sensitivity of the fibroblasts to the NSC23766 treatment were not related to the sex or age of the donors.

We have evaluated the efficiency of a range of Rac inhibitors in contraction, and found that treatment with Z62954982 or W56 barely suppressed contraction. By contrast, transient treatment with 50μM Simvastatin had a moderate inhibitory effect that decreased 30% of the contraction at day7 of most of the fibroblasts, whilst a consistent exposure to the drug at the same concentration showed better results, suggesting a persistent administration was required. The advantage of using Simvastatin is that it has already been proved to use clinically for treating atherosclerosis. Also, its pleiotropic effects including regulating actin cytoskeleton dynamics via Rac or RhoA/ Rac1 pathways (Kang et al., 2016, Serra et al., 2015, Baba et al., 2008, Caceres et al., 2011), which make it potentially to be beneficial in a wide range of therapeutic settings.

Transient treatment with 50μM of EHT1864 exhibited a good inhibitory effect on gel contraction, especially within the first 3 days, suggesting that a reapplication of the

drug at day3 will be desirable. However, a study has reported that the application of EHT1864 and NSC23766 at 100μM respectively affected directly the activation of the Rac1 effectors PAK1 (p21-activated kinase 1) and PAK2 (p21-activated kinase 2) (Dutting et al., 2015), which raised questions about the off-target effects at such concentration.

Significantly, Ehop-016, with an application of 10μM for 24hrs, completely blocked the contractile activity, which makes it the most efficient drug among all. It has been demonstrated to block Rac activity in MDA-MB-231 cells, as well as inhibiting mammary tumour growth and metastasis in a nude mice model (Dharmawardhane et al., 2013, Castillo-Pichardo et al., 2014), and recently been patented for Rac1 inhibition in treating metastatic breast cancer cells (https://www.google.com/patents/US8884006), showing that it could be a promising agent in the prevention of contractile scarring. Ehop-016 was reported to have no effect on the cell viability of mammary epithelial cells (MCF-10A) and reduced only 20% of cell viability of MDA-MB-435 cells at concentrations of < 5 μM (Montalvo-Ortiz et al., 2012). We used a higher concentration (10 μM) in our assay and observed about 40% reduction of cell viability at day7, suggesting that a transient 10μM treatment of Ehop-016 was tolerable to our cells, though the effect of the drug on gel contraction might be partly due to toxicity.

One surprising finding of the study was that depletion majority of the Rac1 protein in the cells by siRNA knockdown did not suppress fibroblast-mediated contraction. It explained the reason by which Rac1 specific inhibitors (Z62954982 and W56) had no effect in reducing contraction, whilst the effective ones may have achieved the target by inhibiting other regulators of contraction. For example, Simvastatin impairs

the RhoA/Rho-kinase signalling pathway (Serra et al., 2015, Laufs et al., 2002), EHT1864 blocks the closely related Rac1b, Rac2 and Rac3 isoforms and the Rac-dependent transformation caused by Tiam1 or Ras (Shutes et al., 2007), and Ehop-016 inhibits Cdc42 at concentrations above 10μM (Dharmawardhane et al., 2013), whilst Rac2, Cdc42 and ROCK signalling were all showed to play important regulatory roles during contraction in the study. Rac1 inhibition has been shown to reverse the phenotype of fibrotic fibroblasts cultured from lesional areas of scleroderma (Xu et al., 2009), and delayed cutaneous wound closure *in vivo* with reduced collagen production and myofibroblast formation (Liu et al., 2009). Its inefficacy in our model might be explained as the fibroblasts we used are from normal conjunctival tissue rather than fibrotic origins, or it is due to a tissue specific effect of conjunctiva. Moreover, our results suggested that NSC23766 is not Rac1 specific. It may suppress contraction via inhibition of other effectors, such as Rac2 or even RhoA, as NSC23766 was found to be a competitive antagonist at muscarinic acetylcholine receptors (mAChRs), which concomitantly suppressed the carbachol-induced RhoA activation (Levay et al., 2013).

We found that Cdc42 and RhoA were both involved in regulating fibroblast-mediated contraction, especially Cdc42, which activated the contraction possibly through suppression of ERK signalling. The regulatory role of Cdc42 in ERK pathway was also reported by recent studies in human keratinocytes and pulmonary endothelial cells (Rohani et al., 2014, Lv et al., 2017). Interestingly, we showed that activation of ERK signalling negatively regulated contraction, which was different from that observed in other models, such as scleroderma fibroblasts, proximal epithelial cells and osteoblast-like MG-63 cells, in which ERK pathway contributed to the overexpression of fibrotic proteins and enhanced contractile activity (Chen et al., 2008, Saenz-Morales et al., 2009, Parreno and Hart, 2009), suggesting that ERK

signalling performs differential functions in contraction in different cells. Furthermore, some studies pointed out that Cdc42 deficiency decreased collagen gel contraction of primary mouse embryonic fibroblasts, which associated with altered cell-matrix interaction and reduced focal adhesion complex formation. This was linked to the interaction between Cdc42 and p21-activated kinase (PAK) that was known to affect contraction (Sipes et al., 2011, Rhee and Grinnell, 2006), suggesting that Cdc42 have more downstream effectors to regulate contraction apart from ERK. By contrast, the participation of RhoA in contraction was observed to be consistent in different models. For example, it was reported to mediate lysophosphatidic acid (LPA) induced retraction of fibroblast dendritic network (Grinnell et al., 2003), and was shown to regulate airway smooth muscle contraction through modulating actin polymerisation, via catalysing the assembly and activation of membrane adhesome signalling modules, such as paxillin, vinculin and focal adhesion kinase (FAK) (Zhang et al., 2015, Zhang et al., 2010).

Meanwhile, the intervention of the p38 MAPK signalling only subtly reduced contraction. However, treatment with SB203580 in the Cdc42 knockdown cells significantly reduced contraction comparing to the untreated control, suggesting that the activation of the pathway positively contributed to contraction in a Cdc42-dependent way. The P38 signalling was also reported to play a modest regulatory role in contraction in osteoblasts-like cells (Parreno and Hart, 2009). Furthermore, we found that the PI3K signalling was vitally involved in the activation of contraction. Consistently, PI3K was shown to mediate human recombinant basic fibroblast growth factor (bFGF)-stimulated matrix contraction of dermal fibroblasts, and platelet-derived growth factor (PDGF)-mediated contraction of retinal pigment epithelial (RPE) cells (Abe et al., 2007, Bando et al., 2006). Although its downstream mechanisms are awaiting further investigation, the intervention of the

PI3K signalling pathway could be of therapeutic benefit in preventing fibroblast-mediated contraction.

Lastly, our study characterised that Rac2 may be a master regulator of conjunctival fibroblast-mediated contraction, which has not been mentioned by any other study before. The activity of Rac2 was linked to integrin-directed migration in macrophages, although in fibroblasts this signalling was thought to be compensated by Rac1 (Pradip et al., 2003). Rac2 was required for the postnatal neovascular response and αvβ3/ α4β1/α5β1 integrin-dependent migration in endothelial cells (De et al., 2009), however its function in the three-dimensional cultured cells has not yet been studied. Our results demonstrated that conjunctival fibroblasts utilised Rac2 to mediate contraction, and we proposed that Rac2 can be a promising target in the prevention of conjunctival scarring. We also for the first time explored the regulatory roles of a few regulators of Rho GTPases' in contraction. Racgap1 that is functional critically in driving cytokinesis and cell proliferation (Warga et al., 2016, Sahin et al., 2016, Neubauer et al., 2016), was found to negatively regulate contraction possibly via inactivation of Cdc42. Arhgap5, which regulates fibroblast focal adhesion, cytoskeletal organisation and migration, and maintains the tensional homeostasis and functional composition of the mesenchymal microenvironment through inactivating of RhoA (Barker et al., 2004, Ponik et al., 2013, Raman et al., 2013), and Arhgef3 that activates RhoA and RhoB (Arthur et al., 2002), may be both required by independent signalling pathways that were compulsory for contraction activation. Arhgap5 is regulated by β3 integrin/EGFR pathway (Balanis et al., 2011), and it interacts with focal adhesion kinase (FAK) and p120RasGAP (Tomar et al., 2009) to regulate cell polarity. Arhgef3 regulates a number of genes in bone cells including ACTA2 (Mullin et al., 2014), and interacts with mTORC2 (Mammalian target of rapamycin complex 2) and Akt (Khanna et al., 2013) independently of its

GEF activity. The detailed mechanisms by which they modulated contraction are awaiting further characterisation. Nevertheless, our study has provided novel prospective roles for these regulators of Rho GTPases' in contraction, which offers new possibilities for the future therapeutic interventions.

Chapter 5 Matrix metalloproteinase 1 (MMP1) in the contraction

5.1 The expression of matrix metalloproteinases (MMPs) during *in vitro* contraction

Matrix metalloproteinases (MMPs) play a vital part in all major cell behaviours such as proliferation, migration and differentiation, due to their essential ability to degrade extracellular matrix (ECM) proteins. MMP1 (collagenase I) cleaves fibrillar collagens type I, II and III, and is upregulated in many diseases and cancers that associated with dysregulation of ECM degradation. Previous work showed that transient treatment with Rac1 inhibitor NSC23766 efficiently prevented matrix degradation *in vitro* and *ex vivo,* and led to a significant reduction of MMP1 mRNA and protein expression during the *in vitro* contraction of HTF7071 (Tovell et al., 2012). Therefore, we proceeded to explore the link between Rho GTPase activation and MMP1 expression in contracting conjunctival fibroblasts.

MMP family members were found to be strongly upregulated during *in vitro* contraction, especially MMP1, 3 and 10 in early contraction from day0 to 3, and MMP1 and 3 in late contraction from day3 to 5. Other MMPs, such as MMP16, 14, 27, 12 and 2 were all found upregulated (**Table 5.1**), suggesting they perform important roles during the process. Only MMP10 was found downregulated in the late contraction. However, despite the observation that transient NSC23766 treatment significantly reduced tissue contraction and matrix degradation in both *in vitro* and *ex vivo* models (Tovell et al., 2012), the *in vitro* microarray profile showed

that the inhibitor did not suppress the upregulation of MMPs but further increased their expression levels (**Table 5.2**).

Table 5.1 The gene expression fold changes of Matrix metalloproteinases (MMPs) regulated during (a) early contraction from day0 to 3 and (b) late contraction from day3 to 5.

a

Ensembl	Symbol	FoldChange	p value
ENSG00000196611	MMP1	38.73	0.000
ENSG00000166670	MMP10	22.09	0.000
ENSG00000149968	MMP3	5.31	0.001
ENSG00000156103	MMP16	2.19	0.002

b

Ensembl	Symbol	FoldChange	p value
ENSG00000149968	MMP3	4.40	0.000
ENSG00000196611	MMP1	2.78	0.003
ENSG00000157227	MMP14	2.35	0.005
ENSG00000137675	MMP27	1.90	0.025
ENSG00000156103	MMP16	1.89	0.010
ENSG00000110347	MMP12	1.77	0.007
ENSG00000087245	MMP2	1.43	0.019
ENSG00000166670	MMP10	-4.19	0.002

Table 5.2 The gene expression fold changes of MMPs regulated in the NSC23766 treated samples at (a) day3 and (b) day5 compared to untreated control samples.

a

Ensembl	Symbol	FoldChange	p value
ENSG00000149968	MMP3	5.54	0.000
ENSG00000110347	MMP12	4.66	0.000
ENSG00000166670	MMP10	3.91	0.001
ENSG00000118113	MMP8	3.34	0.004
ENSG00000196611	MMP1	3.26	0.000
ENSG00000157227	MMP14	2.23	0.001
ENSG00000123342	MMP19	1.85	0.020
ENSG00000156103	MMP16	1.38	0.030

b

Ensembl	Symbol	FoldChange	p value
ENSG00000118113	MMP8	2.23	0.021
ENSG00000110347	MMP12	1.62	0.011
ENSG00000129270	MMP28	1.39	0.042
ENSG00000166670	MMP10	-2.13	0.011

5.2 Effect of NSC23766 treatment on MMPs' expression and enzymatic activity

To validate the gene expression profile of MMPs during contraction, the mRNA levels of the most upregulated MMPs including MMP1, 3 and 10 were quantified using qPCR with two conjunctival fibroblasts HTF7071 and HTF9154, which were originated from different donors (**Figure 5.1**). The results showed the gene expressions of MMP1, 3 and 10 were significantly upregulated during fibroblast-mediated gel contraction, especially in HTF9154 that the mRNA levels of MMP1 and 10 both increased over 100 times at day3 peak contraction rate. The expression patterns of these MMPs varied between the two fibroblasts. MMP1 and 10 in HTF7071, and MMP3 in HTF9154 further upregulated after day3, whereas MMP3 in HTF7071, and MMP10 in HTF9154 dropped back in late contraction at day5, suggesting a natural variation between the two fibroblasts. However, the treatment with NSC23766 did not suppress the overexpression of these MMPs.

To determine the effect of NSC23766 treatment on MMPs secretion and activity, we measured the MMPs' enzymatic activities released in the culture medium during contraction at day0, 3 and 5 with/without 24hrs transient treatment with NSC23766 using HTF7071, HTF9154, HTF1785R and HTF0041 (**Figure 5.2**). The total amount of MMPs activity released was measured by incubating the samples with APMA (4-aminophenylmercuric acetate) for 3hrs at 37ºC to active all the MMPs. The results confirmed that a large amount of MMPs were released in the medium throughout the contraction, matching the *in vitro* microarray profile. However, comparing to the total MMPs produced, only a small portion of MMPs were released in their active form, which only significantly increased at day5. For all the fibroblasts tested,

treatment with NSC23766 significantly abrogated total MMPs activity in the medium from day3 to day5, and active MMPs activity at day5.

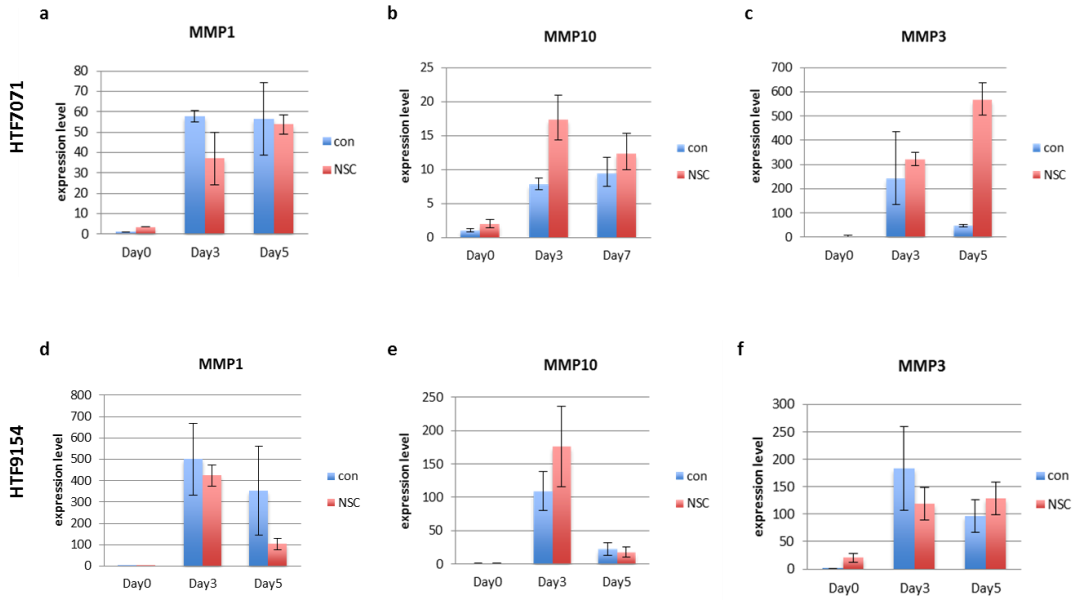

Figure 5.1 mRNA expression levels of MMP1, 3 and 10 were upregulated during contraction, independently of treatment with NSC23766.

The mRNA expressions for MMP1, 3 and 10 during contraction (with/without transient treatment with NSC23766) were validated using qPCR. Two different primary human conjunctival fibroblasts were used: HTF7071 (a, b, c) and HTF9154 (d, e, f) (n=2 experiments, mean ± SEM).

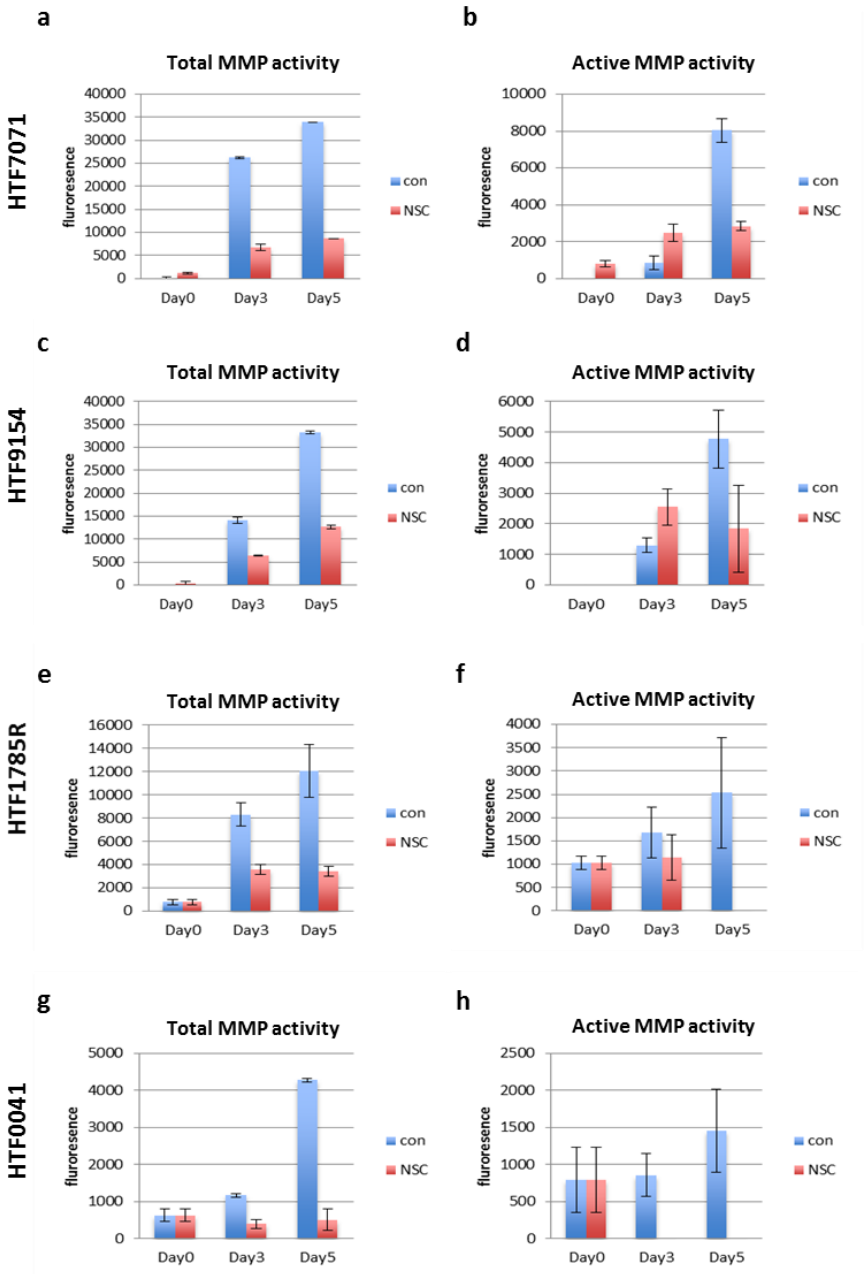

Figure 5.2 Transient treatment with NSC23766 significantly inhibited total MMP activity in the contraction medium.

Measurements of total (a, c, e, g) and active (b, d, f, h) MMP enzymatic activities in the medium of fibroblasts HTF7071 (a, b), HTF9154 (c, d), HTF1785R (e, f) and HTF0041 (g, h) contracting at day0, 3 and 5 with/without transient treatment with NSC23677. The activities were measured using MMP activity assay, and APMA (4-aminophenylmercuric acetate) was applied to stimulate all the MMPs in the medium (for total activity) (Mean ± SEM, n=2 experiments with triplicate wells). The active MMP activity of NSC23766 treated cells at day5 of HTF1785R (f) and day3 and 5 of HTF0041 (h) were under detectable level.

5.3 Treatment with NSC23766 altered MMP1 expression and secretion

The above results demonstrated that NSC23766 treatment regulated MMP expression on protein release, rather than a direct inhibition on the gene expression. As MMP1 was the most upregulated MMP in the *in vitro* early contraction, whose significant upregulation at mRNA level was validated by qPCR in different fibroblasts, it was selected as an example to study the relation between its intracellular protein expression and extracellular secretion upon NSC23766 treatment. The protein expressions of MMP1 in contracting fibroblasts HTF7071 and HTF1785R was detected by performing Western blot on cell lysates extracted from collagen gels at day0, 3 and 5 with/without transient NSC23766 treatment for the first 24hrs. The amount of MMP1 protein secreted into the contraction medium at the matching time points was identified using MMP1 ELISA. The results confirmed that MMP1 was massively secreted into the extracellular medium during contraction of both fibroblasts tested, and treatment with NSC23766 significantly suppressed its secretion (**Figure 5.3**). By contrast, MMP1 intracellular protein levels were increased following NSC23766 treatment, matching the previously observed increase in mRNA expression (**Figure 5.4**). This suggested that treatment with NSC23766 did not affect MMP protein levels in the cells but rather prevented its release to the extracellular space.

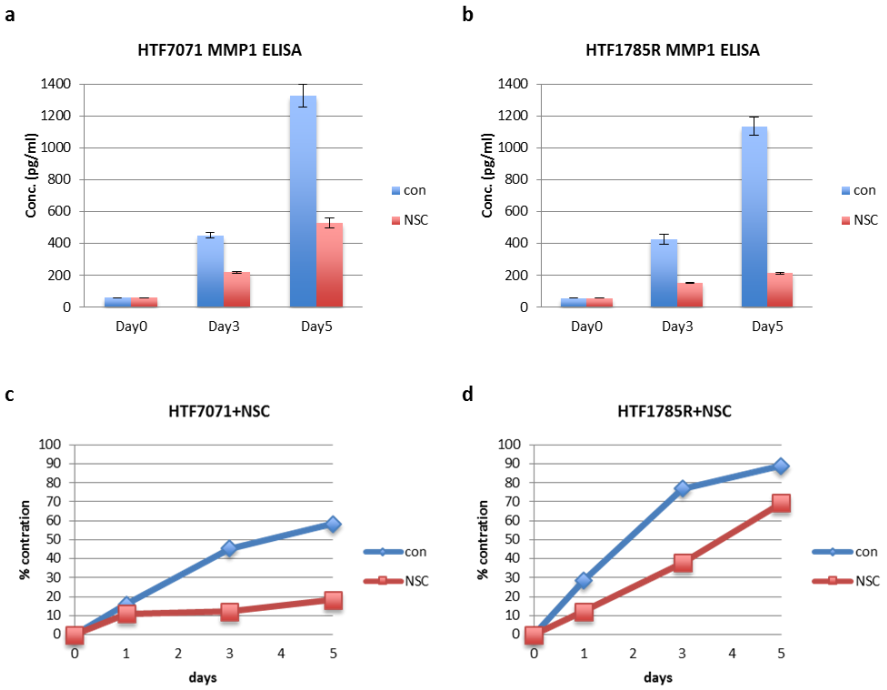

Figure 5.3 NSC23766 significantly blocked MMP1 protein released in the culture medium during contraction.

MMP1 protein released in the medium of gel contraction at day 0, 3 and 5 (with/without transient NSC23766 treatment) of two human conjunctival fibroblasts HTF7071 (a) and 1785R (b) was detected by MMP1 ELISA (mean ± SEM, n=2 experiments with triplicate wells). (c), (d) showing the matching contraction kinetics.

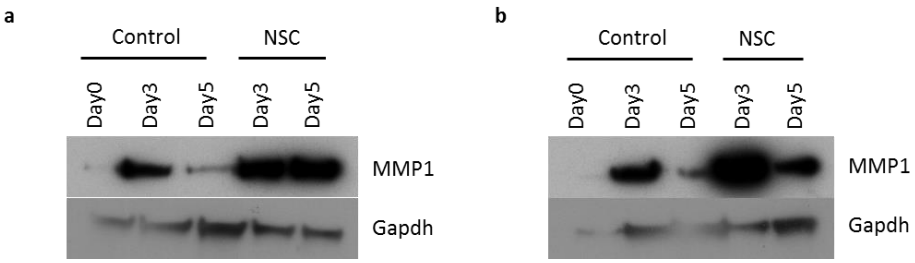

Figure 5.4 NSC23766 increased MMP1 intracellular protein expression.

Detection of MMP1 protein expression in fibroblasts HTF7071 (a) and 1785R (b) extracted from contraction gels at day 0, 3 and 5 (with/without transient NSC23766 treatment) by Western blot. (representative figures of reproducible results, n≥3 experiments).

5.4 NSC23766 treatment led to intracellular accumulation of MMP1 in both 2D- and 3D-cultured cells

5.4.1 MMP1 expression and secretion in 2D- and 3D-cultured fibroblasts

We used fluorescence staining to detect where MMP1 was localised in the cells. Due to the complexity of processing and quantifying fluorescence signal from fibroblasts embedded in 3D collagen matrices in projected images, the alternative model of 2D cell culture was investigated. We firstly determined whether the transient application of NSC23766 inhibited the extracellular secretion of MMP1 in monolayer-cultured fibroblasts to the same extent as in 3D culture using HTF1785R. MMP1 intracellular protein levels were detected using Western blot on cell lysates extracted from 3D and 2D cell cultures respectively, and the release of MMP1 in the culture medium was measured in parallel using ELISA (**Figure 5.5**). The results suggested that NSC23766 treatment led to accumulation of MMP1 within the cells under both culturing conditions. Although the effect was less profound in monolayers, there was still over 3 times more MMP1 protein detected in the NSC23766 treated cells comparing to the untreated control, suggesting that the modulation of NSC23766 on MMP1 expression and secretion in fibroblasts could be alternatively studied in the 2D cell culture.

To confirm this result using immunofluorescence staining, human conjunctival fibroblast HTF1785R cells seeded on coverslips with/without transient treatment with NSC23766 were fixed at day3 and stained for MMP1. The fluorescence signal was measured using ImageJ. The cells were traced manually for the calculation of the integrated density and cell size. The corrected integrated density (CID) was calculated based on the equation listed on **Chapter 2** (**2.11.1**) (**Figure 5.6**). NSC23766 treated cells had about 2 times more MMP1 fluorescence signal than

control ones, which was consistent with the Western blot measurements in **Figure 5.5**. Besides, treatment with NSC23766 led to a significant increase of cells size, which was about 1.5 times bigger than the untreated ones.

5.4.2 The localisation of MMP1 in the cells

Next we used immunofluorescence staining to localise MMP1 in the cells during contraction. Collagen contraction gels of fibroblasts HTF7071 and HTF9154 treated with/without transient NSC23766 treatment respectively were fixed at day3 and double-stained for MMP1 (Abcam ab38929 anti-MMP1 antibody) and actin cytoskeleton. The gels were imaged using Biorad Radiance laser scanning confocal microscope with a long working distance objective (ZEISS LD plan- Neofluoar 63x0.75). The untreated control cells were in starlike shape that reflected a strong protrusive activity, whereas the NSC23766 treated ones were sat in a more quiescent stage. The difference was shown more obviously in HTF7071, which matched its sensitivity to NSC23766 treatment, as discussed in the previous chapter. A significant amount of MMP1 released into the extracellular matrix by control fibroblasts were captured in the image, shown as hazy-green little dots surrounding the cell. The secretion of MMP1 was almost completely suppressed in the NSC23766 treated cells (**Figure 5.7**).

This experiment, using the Abcam anti-MMP1 antibody Ab38929, revealed a unspecific staining in centre of the cells (**Figure 5.7** top panel), which was unexpected. To investigate whether MMP1 was localised in the nucleus, we changed to use an in-house produced anti-MMP1 primary antibody that was kindly provided by Dr. Yoshi Itoh from Oxford University. We fixed the collagen contraction gels of fibroblast HTF1785R treated with/without transient NSC23766 at day3 and

stained them with this antibody. The imaging was performed using Nikon Eclipse Ti confocal microscope with 20x objective (20x S Plan Fluor ELWD 0.45 Ph1). The images were acquired with z-stacks of 2µm per layer and projected using Nikon NIS elements software (**Figure 5.8**). The images showed that NSC23766 treated fibroblasts had brighter fluorescence signal comparing to untreated control, which suggested that the cells treated with NSC23766 had more intracellular MMP1. Also, MMP1 was found to be localised mostly in the cytoplasm area. Furthermore, the accumulation of MMP1 in 2D-cultured cells was determined by Western blot performed on fractionated cytoplasm and nuclear lysates of monolayer-cultured HTF1785R cells with/without transient NSC23766 treatment (**Figure 5.9**). The results suggested that the accumulation of intracellular MMP1 led by NSC23766 treatment was mostly cytoplasmic, which was consistent with the observation in 3D.

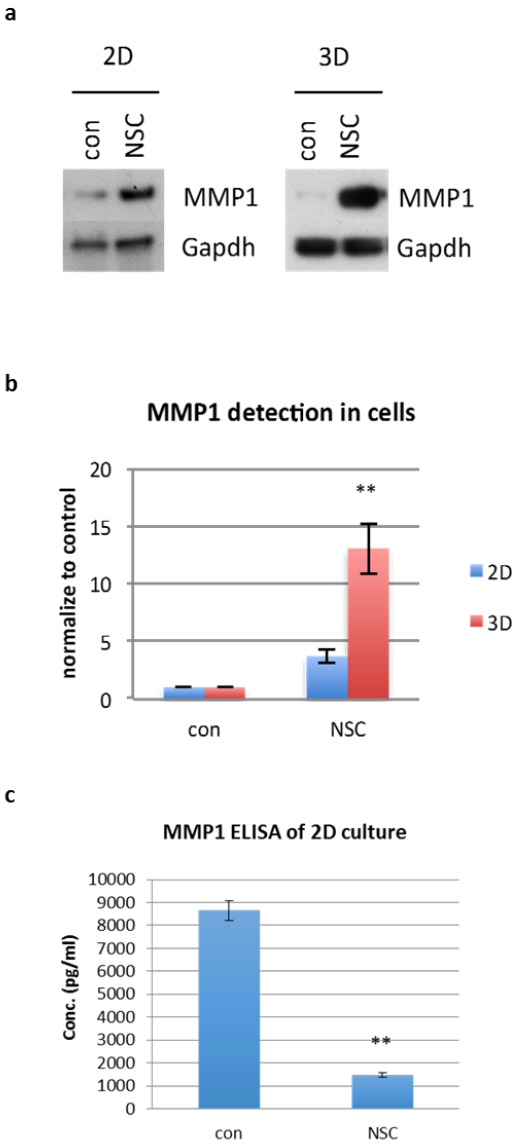

Figure 5.5 NSC23766 treatment led to accumulation of intracellular MMP1 in HTF1785R, which was stronger in collagen gels (3D) comparing to monolayers (2D).

*(a) Western blot results showing MMP1 protein expression in fibroblast HTF1785R cells extracted from collagen gels (3D) at day3 contraction or tissue culture of monolayer (2D) at day3 both with/without treatment with 50uM NSC23766 at first 24hr. (b) The quantitation of the Western blot results (mean ± SEM, n=5 experiments, t test between 3D and 2D cultured NSC23766-treated samples, **p<0.05). (c) MMP1 ELISA of culture medium from 2D-cultured control and NSC23766 treated cells at day3 (mean ± SEM, n=2 experiments, **p<0.05).*

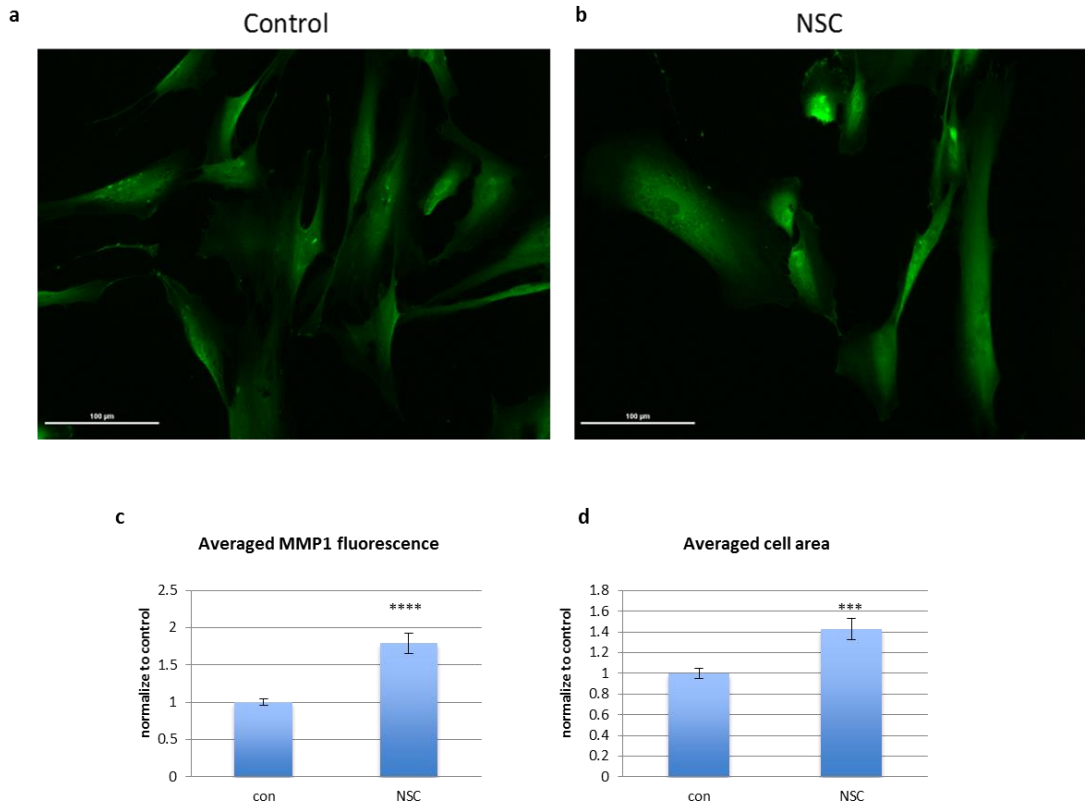

Figure 5.6 Immunofluorescence staining of MMP1 expression in HTF1785R cells cultured on tissue culture flask (2D).

*Immunofluorescence staining of MMP1 expression in the non-treated control (a) or 24hrs NSC23766 treated (b) fibroblast cells HTF1785R cultured on coverslips at day3 (scale bar=100um). (c) Averaged fluorescence corrected integrated density (CID) for MMP1 in control and NSC23766 treated cells (mean ± SEM, n=4 experiments, 3 of which used Abcam ab38929 anti-MMP1 antibody, and 1 used the in-house produced anti-MMP1 antibody provided by Dr. Y. Itoh from Oxford University. Totally more than 200 cells were counted, ****p<0.0001). (d) Corresponding averaged cell area of control and NSC23766 treated cells (mean ± SEM, n=4 experiments, with more than 200 cells were counted, ***p<0.001).*

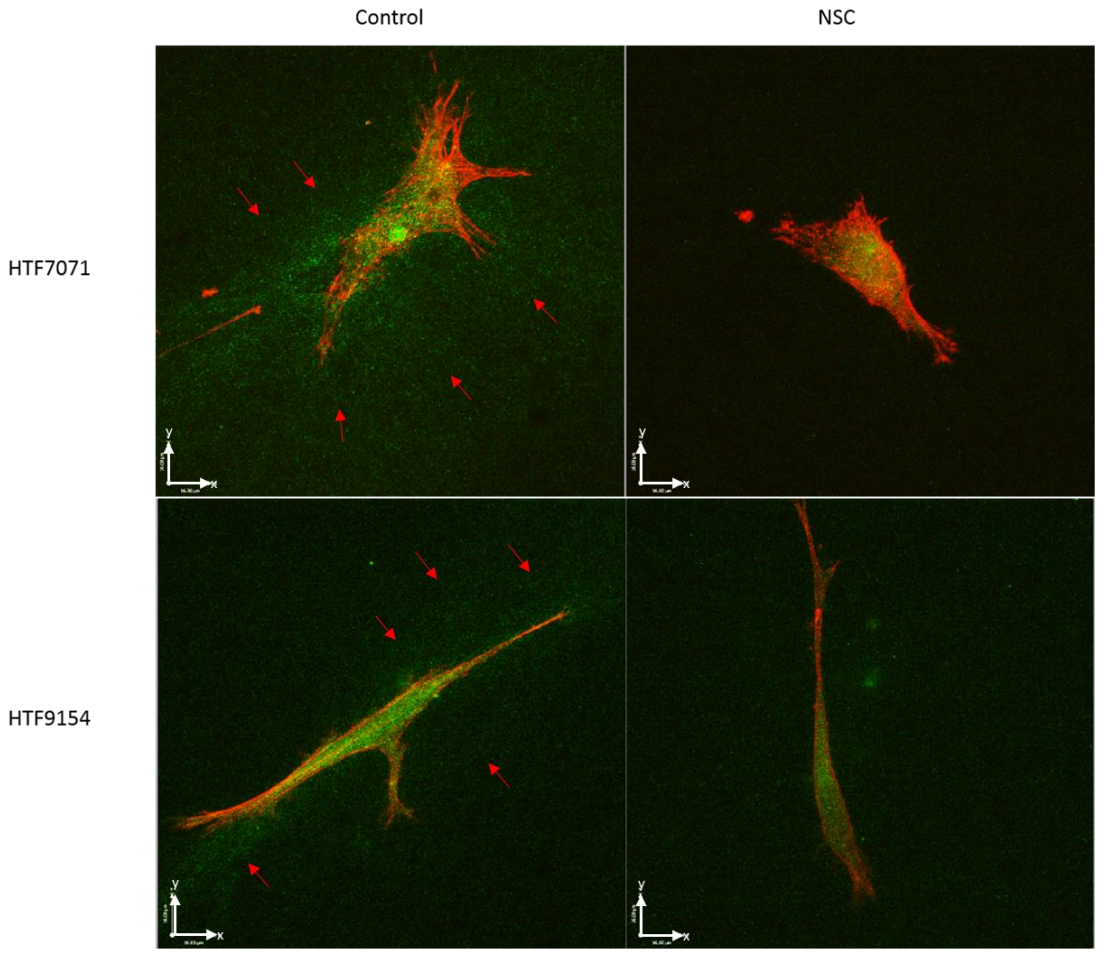

Figure 5.7 Immunofluorescence staining of MMP1 in fibroblast cells HTF7071 and HTF9154 contracting in collagen gels at day3.

Contracting fibroblasts HTF7071 and HTF9154 in collagen gels at day3 with/without 24hrs transient NSC23766 treatment were fixed and stained with Abcam ab38929 anti-MMP1 antibody (green) for MMP1 and Phalloidin (red) for actin cytoskeleton (scale bar x axis=16 µm, y axis=36 µm). The red arrows pointed out MMP1 release in the extracellular space. The images were taken using Biorad Radiance confocal microscope with a long working distance objective (ZEISS LD plan- Neofluoar 63x0.75), and the projections were made using Velocity software.

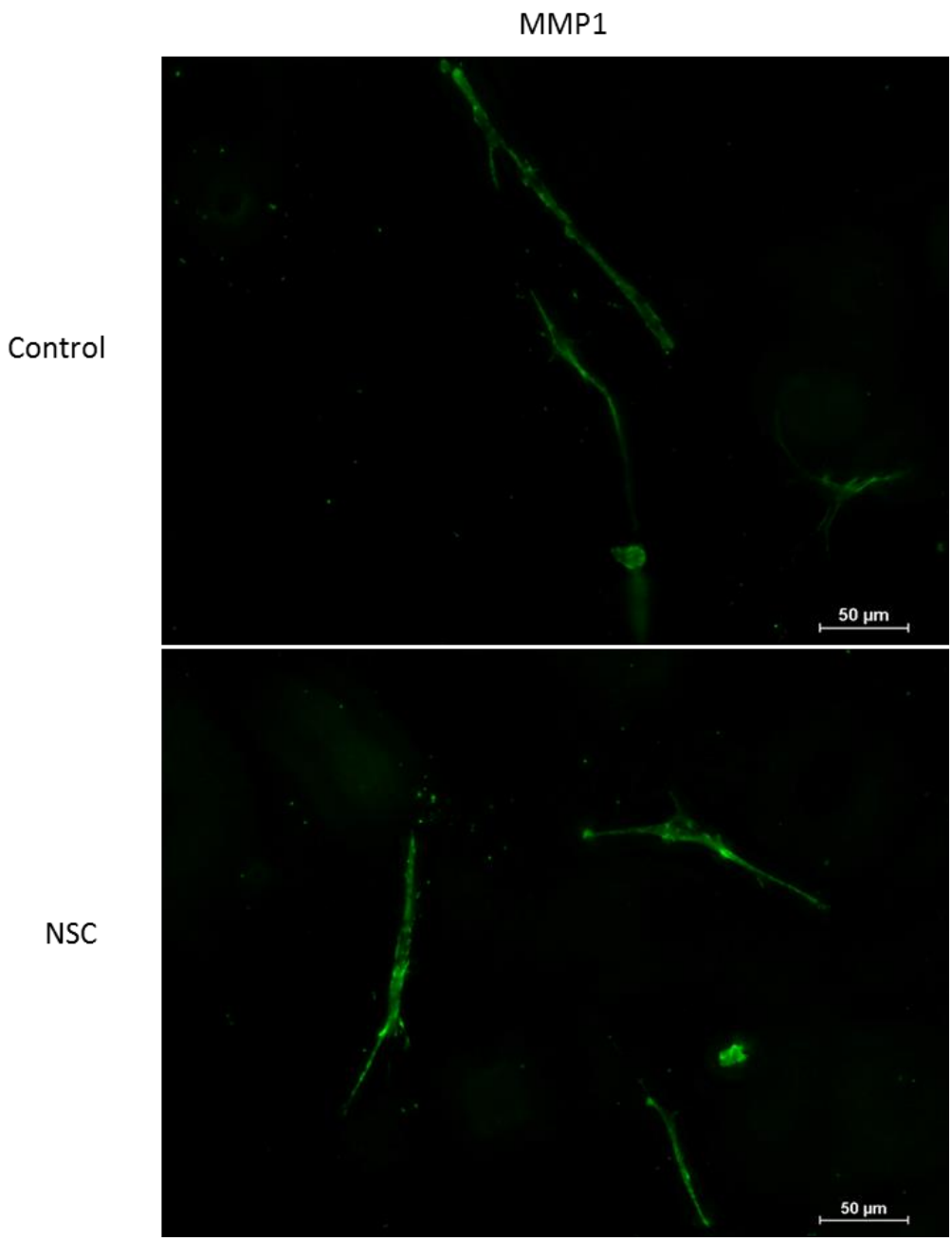

Figure 5.8 Immunofluorescence staining of MMP1 in fibroblast cells HTF1785R contracting in the collagen gels at day3.

Contracting fibroblast cells HTF1785R in day3 collagen gels with/without transient NSC23766 treatment were fixed and stained with an in-house produced anti-MMP1 antibody (green) that was kindly provided by Dr. Y. Itoh from Oxford University. The images were taken with z-stacks of 2µm per layer using Nikon Eclipse Ti confocal microscope with 20x objective (20x S Plan Fluor ELWD 0.45 Ph1), and projected using the Nikon NIS elements software (scale bar=50µm).

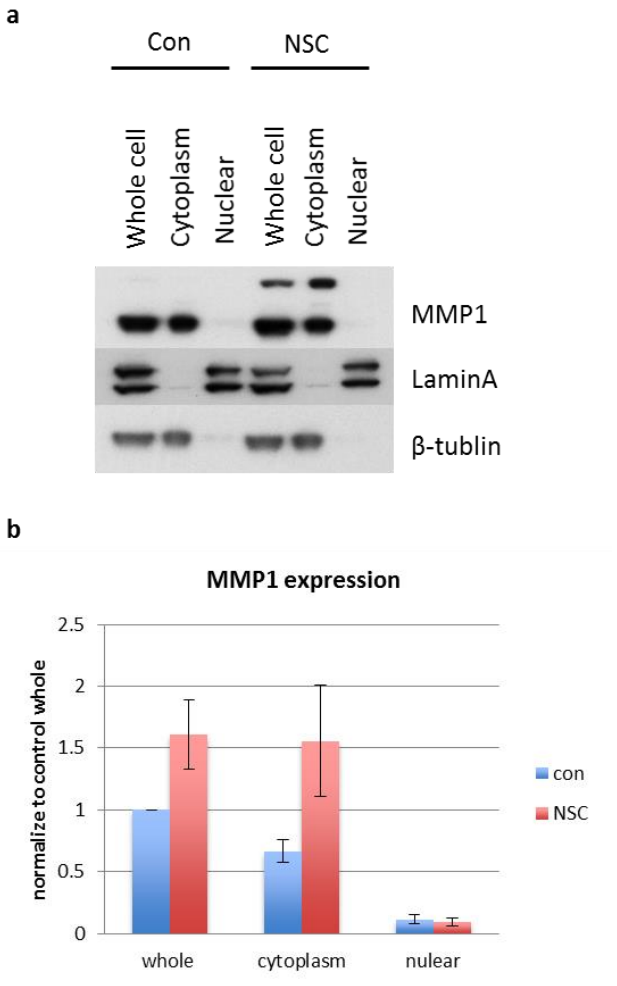

Figure 5.9 NSC23766 treatment led to MMP1 accumulation in the cytoplasm.

(a) The protein expression of MMP1 detected by Western blot on fractionated cytoplasm and nuclear lysates of monolayer-cultured fibroblast cells HTF1785R with/without transient treatment with NSC23766 at day3. The untreated whole cell lysates were used as control. LaminA and β-tublin were used as markers of the nuclear and cytoplasm proteins respectively. The extra bands of MMP1 in the NSC23766 treated samples might be dimerised full length and active form of MMP1, and were both counted in the measurements. The figure is a representative of reproducible results (n=3 experiments). (b) Quantitation of the fractionation Western blot results (the cytoplasmic MMP1 was normalised to β-tublin, and then normalised to β-tublin-normalised whole cell control. The nuclear MMP1 was normalised to LaminA, and then normalised to LaminA-normalised whole cell control. Mean ± SEM, n=3 experiments).

5.5 The effect of NSC23766 treatment on MMP1 secretion was not due to a direct inhibition of GTPase dynamin

In a recent study, a novel invadopodia-independent matrix degradation process was identified in stromal fibroblast. It reported that inhibition of dynamin family member 2 (Dyn2) caused a marked upregulation of stromal matrix degradation, which was mediated by augmented surface expression of MT1-MMP that stimulated MMP2 activity (Cao et al., 2016). Dynamin is a GTPase responsible for endocytosis in the eukaryotic cells. It is a member of the 'dynamin superfamily', which includes classical dynamins, dynamin-like proteins (Dlps), Myxovirus resistance proteins, Atlastins, mitofusins, Optic atrophy 1 (OPA1) and the guanylate-binding proteins (GBPs) (Faelber et al., 2013). Dynamins are principally involved in the scission of newly formed vesicles both at the membrane as well as at the Golgi apparatus (Urrutia et al., 1997, Henley et al., 1999), and they have been extensively studied in the context of clathrin-coated vesicle budding from the cell membrane (Praefcke and McMahon, 2004). It was the first time that Cao et al revealed that the deactivation of a dynamin member triggered upregulation of fibroblast-mediated matrix degradation, suggesting a link between the dynamins and the modulation of MMP release. Coincidentally, another member of dynamins, dynamin 1 like (DNM1L), was found 1.4 times upregulated from day3 to 5 in our *in vitro* contraction expression profile. Also, it was 1.54 times upregulated following the NSC23766 treatment at day3. Therefore, we hypothesised that the upregulation of DNM1L by NSC23766 might contribute to the regulation of MMP1 secretion. Herein, we used a dynamin inhibitor Dynasore that interferes with GTPase activity of dynamin 1, dynamin 2 and DNM1L (Macia et al., 2006) to investigate the possible modulation of dynamin/DNM1L on MMP1 expression and secretion.

Fibroblast cells HTF1785R were embedded in gels and contraction was allowed to proceed following the treatment with NSC23766 (24hr), Dynasore (24hr and 5-day respectively) and NSC23766 (24hr) plus Dynasore (24hr and 5-day respectively), respectively. The day3 and 5 contraction gels were analysed for the examination of in-cell MMP1 expression by Western blot. The culture medium was harvested at the same time points for the detection of MMP1 secretion by ELISA (**Figure 5.10**). The results showed that treatment with Dynasore did not interfere with the contraction kinetics of the fibroblasts, but it significantly suppressed MMP1 protein release in the medium, whether used for only 24hr or continuously for 5 days. The inhibitory effect was not as strong as that of NSC23766 treatment, and applying both inhibitors together did not result in a further reduction of MMP1 release. However, Dynamin inhibition did not lead to any increase of MMP1 protein expression, suggesting that the pathways that NSC23766 and Dynasore applied to modulate MMP1 secretion partially overlapped. Moreover, there were a lot more MMP1 expressed following NSC23766 treatment than that of treatment with Dynasore alone, suggesting that NSC23766 targeted more pathways than just inhibiting dynamin.

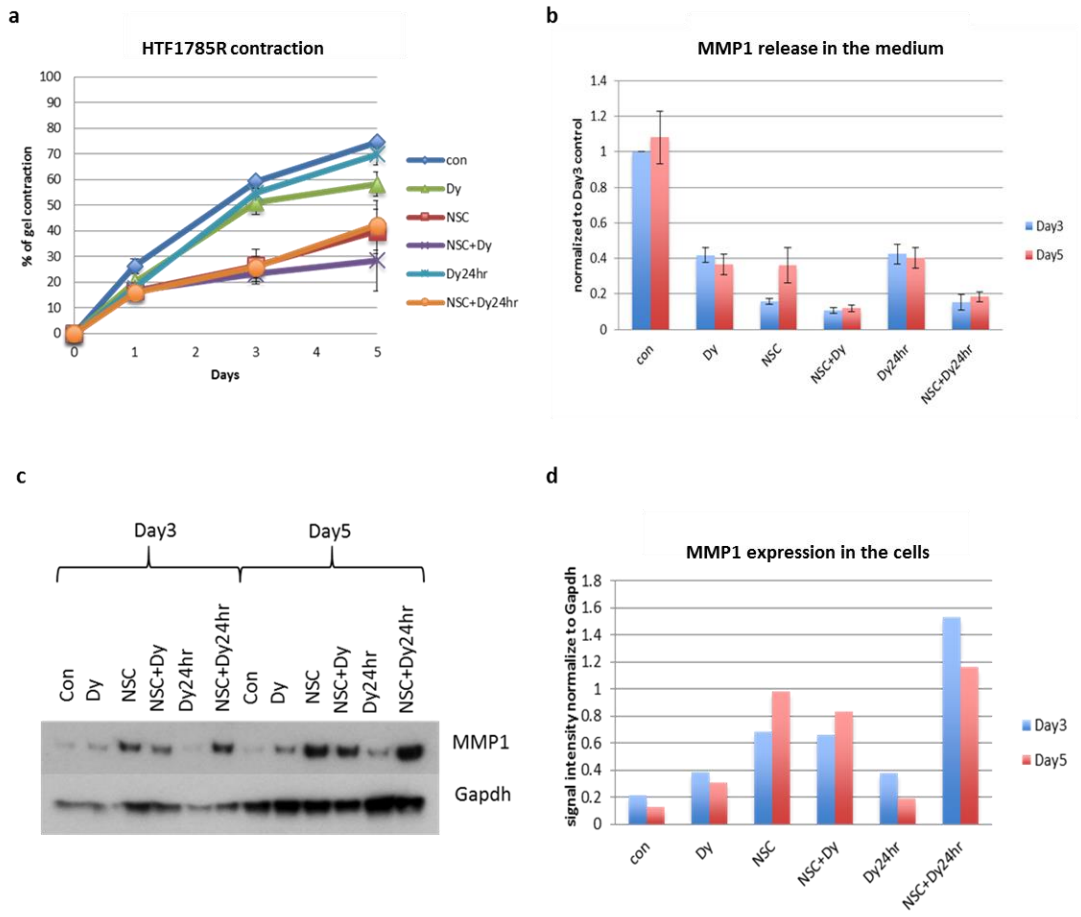

Figure 5.10 Dynamin inhibition significantly suppressed MMP1 protein secretion. *Fibroblast cells HTF1785R were treated with NSC23766 (50μM for 24hr), Dynasore (80μM for 24hr and 5-day respectively), and NSC23766 (50μM for 24hr) plus Dynasore (80μM for 24hr and 5-day respectively) respectively in collagen contraction assay. MMP1 protein expression in the cells and secretion in the culture medium at day3 and 5 were detected by Western blot and ELISA respectively. (a) 5-day gel contraction kinetics (mean ± SEM, n=3 experiments with triplicate wells). (b) MMP1 ELISA assay on contraction medium at day3 and 5 (mean ± SEM, n=2 experiments with triplicate wells). (c) The detection of MMP1 in-cell protein expression in the HTF1785R cells extracted from contraction gels at day3 and 5, normalised to protein expression of Gapdh loading control. (d) Quantitation of the Western blot results. (c) and (d) are representative figures of reproducible results (n=3 experiments).*

5.6 Small Rho GTPases Rac1, Cdc42 and RhoA differentially regulated MMP1 expression and secretion

To investigate the role of small Rho GTPases on MMP1 production in human conjunctival fibroblasts, immunofluorescence staining was performed to evaluate MMP1 protein expression in Rac1, Cdc42 or RhoA knockdown HTF1785R cells cultured on 2D cover slips. Silencing of the Rho GTPases led to a 1.5 (Rac1 or Cdc42, $p<0.0001$) to 2 times (RhoA, $p<0.0001$) fold increase of MMP1 fluorescence in the cells. In addition, RhoA inhibition led to a 1.5 times increase in cell size (**Figure 5.11**).

We next explored the regulation of MMP1 protein expression and extracellular release by Rho GTPases in fibroblasts cultured in 3D collagen gels. The Rac1, Cdc42 or RhoA siRNA knockdown fibroblast cells HTF1785R were seeded in collagen contraction assay with/without 24hrs transient treatment with NSC23766. The cells were extracted from the gels at day3 and lysed for the extraction of RNA and protein respectively. The culture medium was collected at the same time for the detection of MMP1 release by MMP1 ELISA. The mRNA levels of MMP1 in the Rho GTPase knockdown cells were quantified by qPCR, whilst the protein expression levels of MMP1 were determined by Western blot. Silencing each of Rac1, Cdc42 or RhoA resulted in a significant upregulation of MMP1 mRNA expression in contracting fibroblasts, which was not affected by NSC23766 treatment (**Figure 5.12a**). Moreover, knockdown of Rac1, Cdc42 or RhoA respectively led to a significant increase of MMP1 protein expression in the cells (from 5 (Rac1, $p<0.01$) to 10 times (RhoA, $p<0.01$)) (**Figure 5.12b**). Silencing of Rac1 did not suppress the release of MMP1 statistically. However, considering that more MMP1 were produced intracellularly upon Rac1 inhibition, it was likely that the release was

affected to some extent. Knockdown of Cdc42 remarkably augmented MMP1 secretion by 2 fold ($p<0.001$), whereas inhibition of RhoA radically depleted MMP1 release in the medium by almost 70% ($p<0.0001$) (**Figure 5.12c**). NSC23766 treatment counteracted the overexpression of MMP1 in the cells led by silencing of Cdc42, which also brought the MMP1 protein release back to normal, suggesting that the regulation of MMP1 expression by Cdc42 was possibly reliant on signalling through Rac. By contrast, NSC23766 treatment on the Rac1-knockdown cells notably reduced MMP1 release in the medium, suggesting that other targets of NSC23766 (for example Rac2, as discussed in **Chapter 4**) played a regulatory role in controlling the release of MMP1. Moreover, in the RhoA-knockdown cells, NSC23766 further increased MMP1 expression and suppressed its release, suggesting that the signalling through RhoA also contributed vitally to the modulation of MMP1 expression and release, which did not overlap with the one that NSC23766 applied.

In addition, inhibition of the Rho-associated protein kinase (ROCK), a downstream effector of RhoA in contracting HTF1785R cells using the ROCK inhibitor H1152 also increased MMP1 protein production in the cells, but had no effect on its secretion (**Figure 5.13**). It suggested that MMP1 expression might be triggered by a major downstream signalling event led by ROCK inhibition (such as changes in actin polymerisation), although signalling through ROCK was not essential for the extracellular release of MMP1.

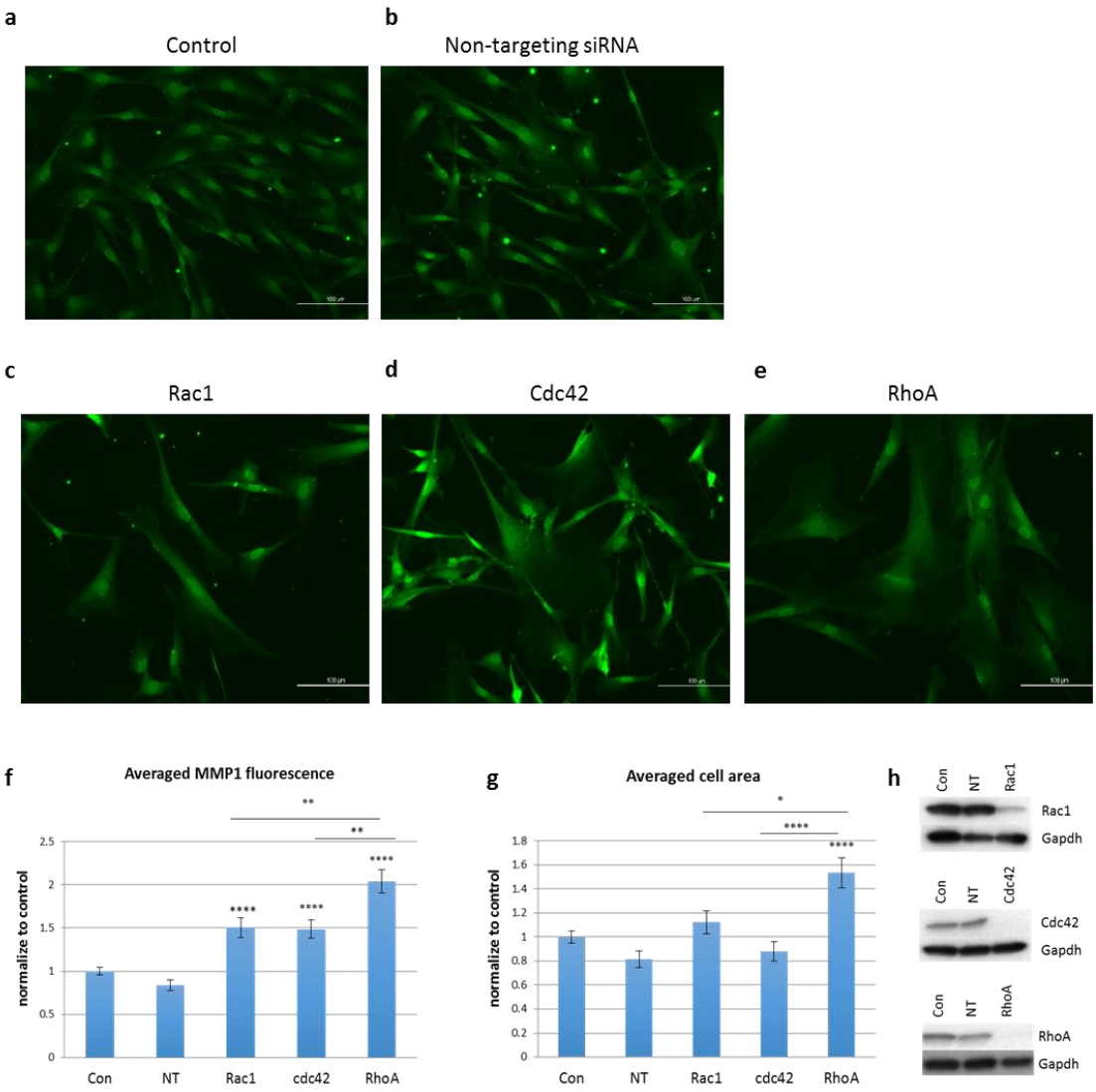

Figure 5.11 Silencing of Rac1, Cdc42 or RhoA increased MMP1 expression.

*(a-e) Immunofluorescence staining of MMP1 in Rac1, Cdc42 or RhoA knockdown HTF1785R cells cultured on coverslips respectively (scale bar=100μm, used Abcam Ab38929 anti-MMP1 antibody). (f) Averaged fluorescence corrected integrated density (CID) for MMP1 in the Rac1, Cdc42 or RhoA knockdown cells and (g) corresponding cell area (n=4 experiments counting in total >200 cells per group, t test between control and knockdown cells, and between knockdown cells ****p<0.0001, ***p<0.001, **p<0.01, *p<0.05). (h) The validation of the protein depletion of Rac1, Cdc42 or RhoA following siRNA treatment by Western blot (figure is a representative of repeatable results, n=4 experiments).*

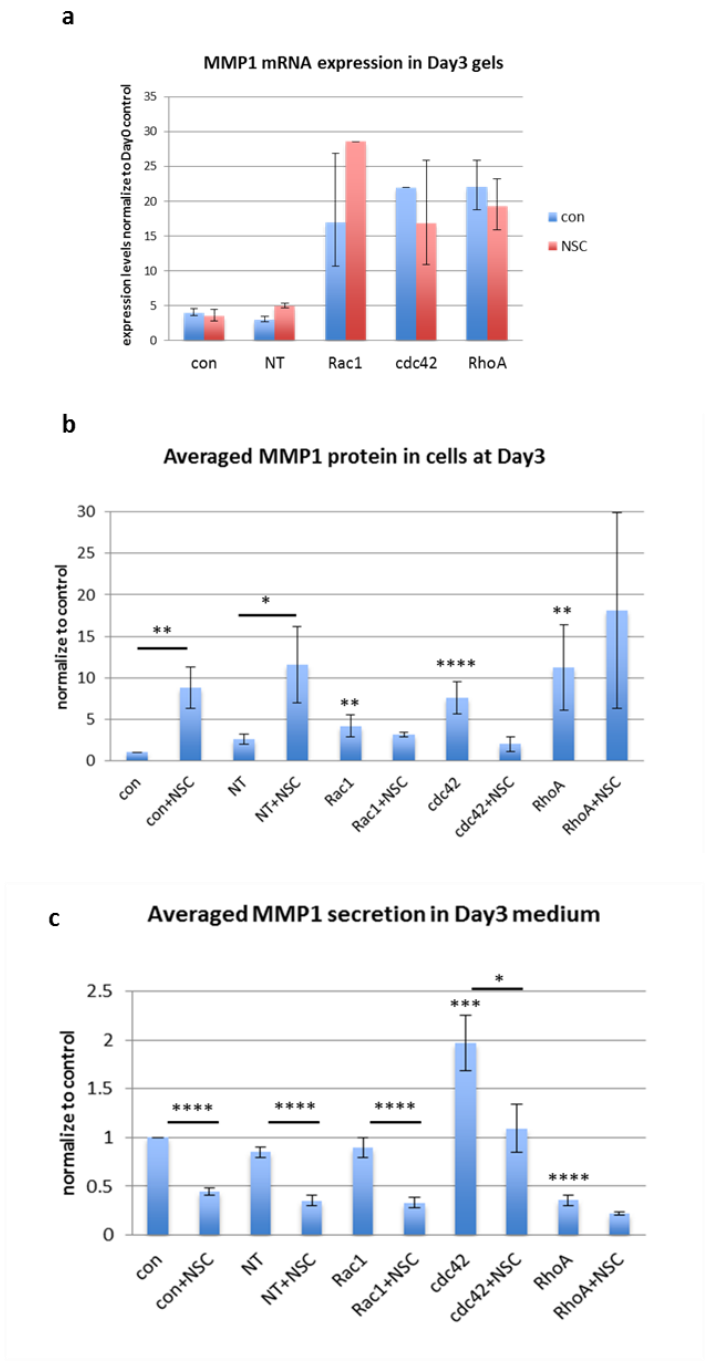

Figure 5.12 Downregulation of Rac1, Cdc42 or RhoA increased MMP1 production, whilst only RhoA inhibition significantly prevented MMP1 secretion.

*(a) MMP1 mRNA expression levels of Rac1, Cdc42 or RhoA knockdown cells extracted from day3 contraction gels measured by qPCR. (b) MMP1 protein expression in Rac1, Cdc42 or RhoA knockdown cells extracted from day3 contraction gels measured by Western blot (n>3 experiments, t test between control and knockdown expression, and NSC23766 treated and non-treated samples. *p<0.05, **p<0.01, ****p<0.0001). (c) Detection of MMP1 protein secreted in the day3 contraction medium by MMP1 ELISA (n=3 experiments with triplicate*

*wells, t test between control and knockdown secretion, and NSC23766 treated and non-treated samples. *p<0.05, ***p<0.001, ****p<0.0001).*

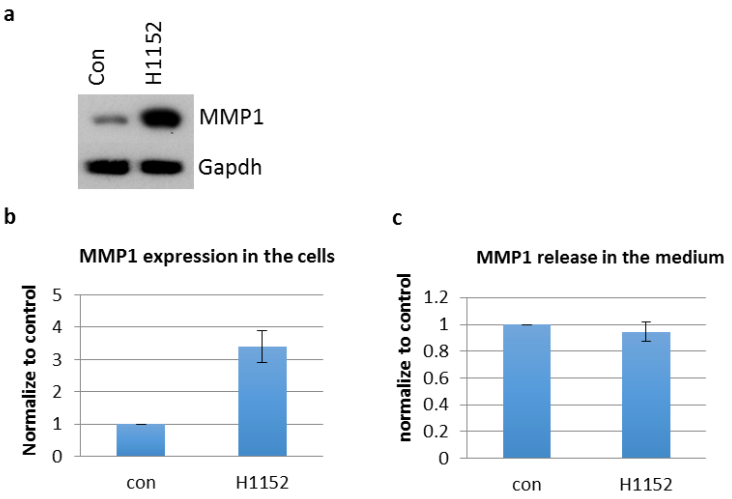

Figure 5.13 The inhibition of ROCK, a downstream mediator of RhoA, also increased MMP1 protein production in the cells, but had no effect on its secretion.

(a) MMP1 detection by Western blot on HTF1785R cells extracted from day3 collagen contraction gels treated with/without 10μM ROCK inhibitor H1152. (b) Quantitation of the Western blot results (mean ± SEM, n=2 experiments). (c) MMP1 ELISA performed on day3 control and ROCK inhibitor treated gel contraction medium (mean ± SEM, n=2 experiments with triplicate wells).

5.7 ERK, P38 MAPK and PI3K signalling differentially regulated MMP1 expression and secretion

The small Rho GTPases are activated by signalling downstream of activated integrins and growth factors, so are the mitogen-activated protein kinases (MAPKs), which are involved in regulating various major cell functions (Miyamoto et al., 1995). It has been reported that activation of ERK1/2 or P38 MAP kinase pathway was

able to induce transcription from MMP1 promoter in human primary fibroblasts (Brauchle et al., 2000). The activation of ERK1/2 stimulated MMP1 production in human skin fibroblasts and keratinocytes, which was shown to be Cdc42 dependent (Deroanne et al., 2005, Rohani et al., 2014), consistently with our results in **Figure 5.12**. In addition, the PI3K (phosphoinositide-3-kinase) signalling pathway was also reported to be involved in the regulation of MMPs in fibroblasts (Liao et al., 2003), suggesting that these signalling pathways potentially participated in the regulation of MMP production. Here we aimed to identify the implication of ERK, P38 MAPK and PI3K signalling on MMP1 expression and secretion in contracting human conjunctival fibroblasts with relation to the Rho GTPases activation.

We investigated the role of the ERK1/2, p38 MAPK and PI3K pathways in mediating MMP1 expression and secretion in the Rho GTPases-silenced fibroblasts using pharmacological inhibition. The Rac1, Cdc42 or RhoA siRNA knockdown HTF1785R cells were seeded in collagen contraction gels and treated with U0126 (ERK inhibitor), SB203580 (P38 MAPK inhibitor) and Ly294002 (PI3K inhibitor) respectively. The cells and culture medium were harvested at day3 for MMP1 immunoblotting and ELISA respectively (**Figure 5.14**). The results demonstrated that inhibition of ERK1/2 significantly reduced MMP1 release in the medium of all experiment conditions, which was possibly due to the deactivation of MMP1 promoter (Brauchle et al., 2000), implying that MMP1 secretion was ERK-dependent. By contrast, inhibition of P38 MAPK signalling did not lead to significant changes in MMP1 expression or secretion, suggesting that it did not perform a major role in regulating MMP1 production. Furthermore, inhibition of PI3K notably increased MMP1 accumulation in the cells but remarkably suppressed its secretion in all conditions, indicating that it played an important role in the modulation of MMP1 expression and secretion.

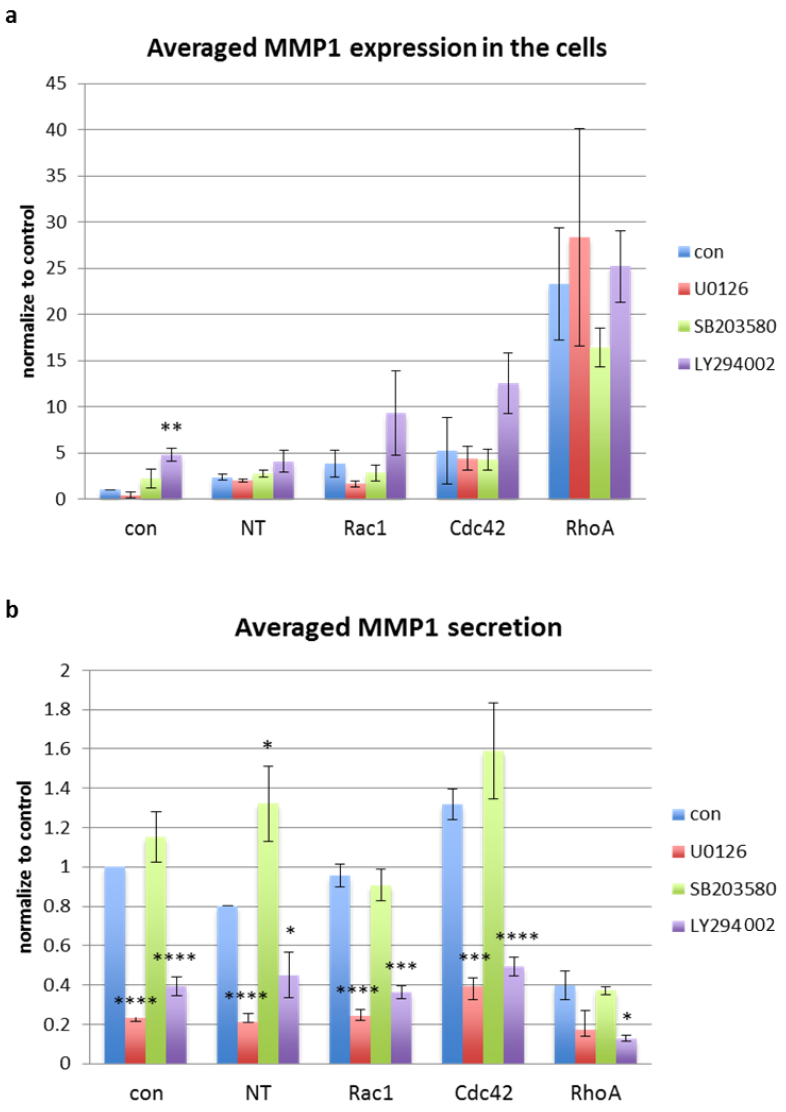

Figure 5.14 The ERK, P38 MAPK and PI3K signalling differentially regulated MMP1 expression and secretion.

*(a) Averaged MMP1 expression in Rac1, Cdc42 or RhoA knockdown fibroblast cells HTF1785R extracted from day3 contraction gels treated with ERK inhibitor U0126 10μM, P38 MAPK inhibitor SB203580 10μM or PI3K inhibitor Ly294002 25μM respectively (normalised to day3 untreated control expression, n=3 experiments, mean ± SEM, t test against non-treated control within the same sample group, **p<0.01). (b) Averaged MMP1 secretion at day3 of Rac1, Cdc42 or RhoA knockdown fibroblast cells HTF1785R treated with the ERK inhibitor U0126 10μM, P38 MAPK inhibitor SB203580 10μM or PI3K inhibitor Ly294002 25μM respectively (normalised to day3 untreated control secretion, n=3 experiments with duplicate wells, mean ± SEM, t test against non-treated control within the same sample group, ****p<0.0001, ***p<0.001, *p<0.05).*

5.8 Regulation of GTPases activation in MMP1 secretion

In the previous chapter, it has been demonstrated Arhgap5, Racgap1, Arhgef3 and Rac2 were expressed differently during the *in vitro* contraction (**Figure 4.8**) and performed differential regulatory roles in contractile activity (**Figure 4.9**). To further characterise signalling pathways that regulate MMP1 expression and secretion, HTF1785R were transfected with siRNA targeting Rac2, Arhgap5, Racgap1 or Arhgef3 to silence their respective gene expressions, and then seeded into collagen gels with/without transient treatment with NSC23766. The gels were terminated at day3, following with the extraction of the cells for the detection of MMP1 expression using Western blot. The culture medium was collected at the same time for measuring MMP1 release by ELISA (**Figure 5.15**). Silencing each of the gene caused a significant increase of MMP1 protein expression in the cells, suggesting that MMP1 production might be induced as a result of changes in actin polymerisation caused by activation/deactivation of Rho GTPases. Silencing of Rac2, Racgap1 or Arhgef3 notably increased MMP1 secretion in the culture medium, whereas with NSC23766 treatment the effect was counteracted, suggesting that none of the gene was functional in controlling MMP1 release. By contrast, inhibition of Argap5 significantly suppressed MMP1 secretion, which was further reduced by NSC23766 treatment, suggesting that Arhgap5 was vital in regulating the extracellular release of MMP1.

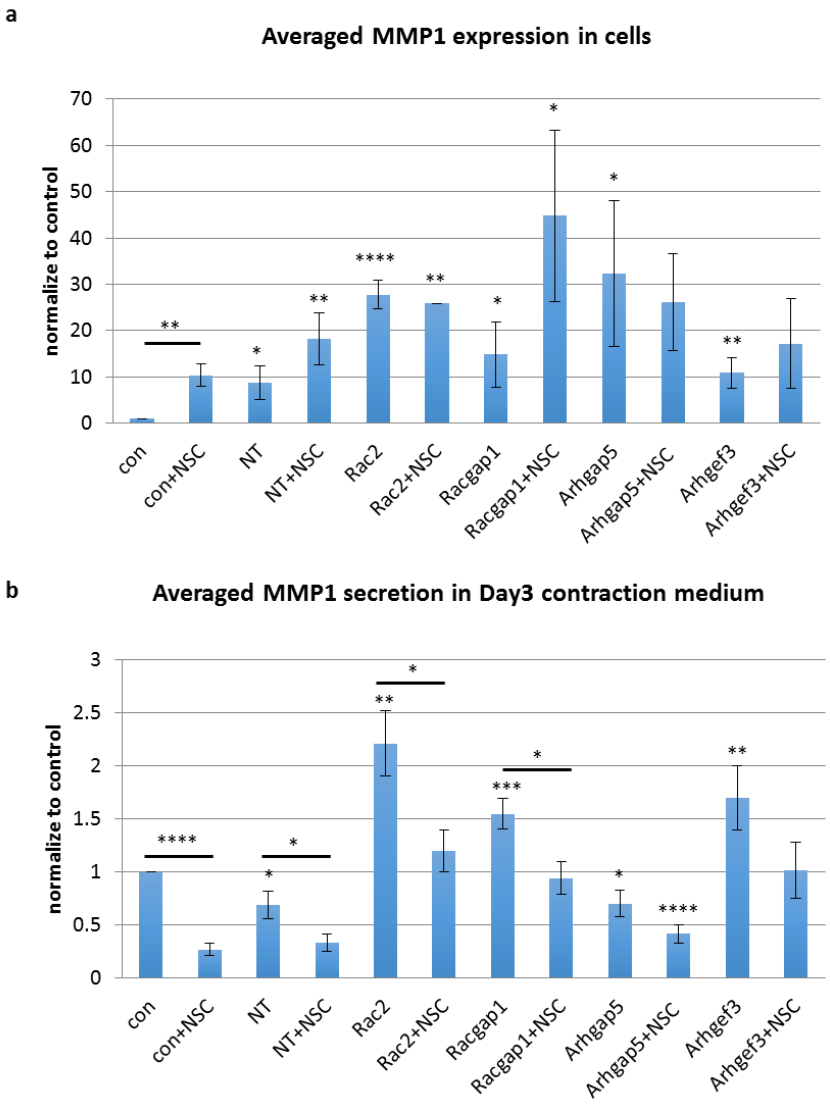

Figure 5.15 Silencing of Rac2, Arhgap5, Racgap1 or Arhgef3 increased MMP1 expression in the cells but differently regulated its release in the medium.

*(a) Averaged MMP1 protein expression in the Rac2, Racgap1, Arhgap5 or Arhgef3 knockdown HTF1785R cells extracted from day3 collagen contraction gels with/without transient NSC23766 treatment for the first 24hrs (normalised to day3 control expression, n≥3 experiments mean ± SEM, t test between knockdown expression and control expression, and also between NSC23766 treated and non-treated samples within same group. ****p<0.0001, **p<0.01, *p<0.05). (b) Averaged MMP1 secretion in the day3 contraction medium of Rac2, Racgap1, Arhgap5 or Arhgef3 knockdown HTF1785R cells with/without transient NSC23766 treatment for the first 24hrs (normalised to day3 control secretion, n≥3 experiments with triplicate wells, mean ± SEM. t test against control secretion, and n****p<0.0001, ***p<0.001, **p<0.01, *p<0.05).*

5.9 Discussion

Members of the MMPs family were among the most upregulated gene groups during conjunctival fibroblast-mediated *in vitro* contraction, especially MMP1, which was expressed over 38 times on gene level in early contraction, and upregulated all the way throughout the whole contraction process. Elevated expression of MMP1 has been reported in many diseases associated with dysregulation of ECM remodelling, as well as tumour invasion and metastasis (Lemaitre and D'Armiento, 2006). Multiple studies showed that in addition to degrading ECM, MMP1 cleaves signalling molecule precursors, such as pro-TGFα, EGF-like ligands, and TGFβ from cell surfaces or extracellular matrix. It processes several important mediators including pro-TNFα, IL-1β, L-selectin (CD62L), α1-antiprotease inhibitor, C1q, connective tissue growth factor (CTGF), and insulin growth factor-binding proteins 1 (IGFBP1) and 3 (IGFBP3) (Rajah et al., 1995, Hatfield et al., 2010, Page-McCaw et al., 2007, Kessenbrock et al., 2010). MMP1 also activates PAR-1, which is a proteinase-activated receptor that promotes migration and invasion of tumour-infiltrating fibroblasts in the model of breast carcinoma (Boire et al., 2005), vascular smooth muscle cell dedifferentiation and arterial stenosis (Austin et al., 2013). These findings suggest that by working in both proteolytic and non-proteolytic manners, MMP1 has important and complex roles in regulating matrix turnover, disease progression and signal transduction. However, knockdown of MMP1 by siRNA that caused an 85% decrease of the protein release in the medium only reduced 50% contraction at day2 and 20% contraction at day7 (**Figure 5.16**). It suggests that a small amount of MMP1 secreted in the medium may be enough to stimulate contraction, or MMP1 may not play a major functional role in contraction. Alternatively, other MMPs, such as MMP3 or 10, may cover the role of MMP1 in its absence.

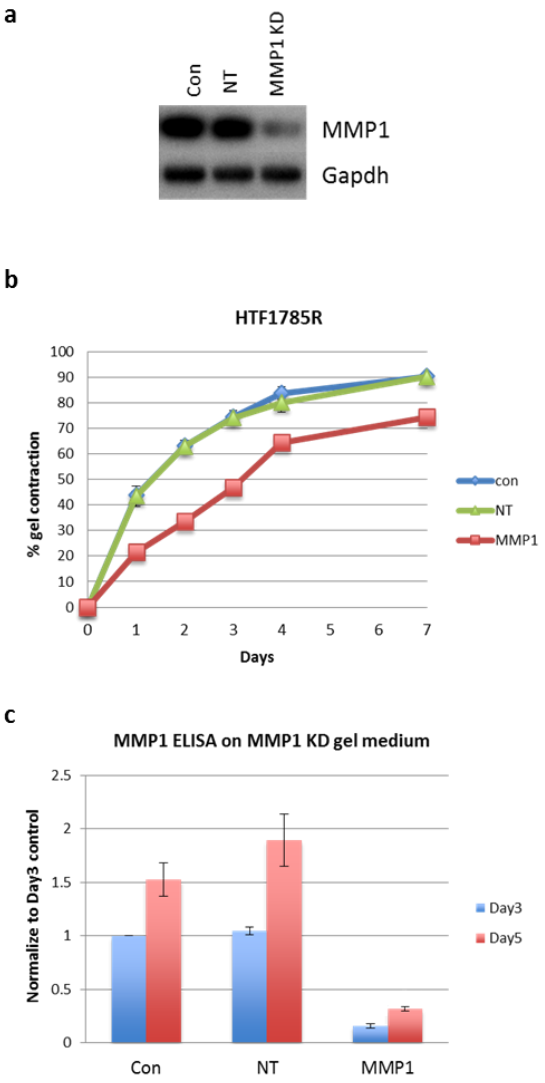

Figure 5.16 Silencing of MMP1 by siRNA in conjunctival fibroblasts only mildly affected contraction.

Fibroblast HTF1785R cells were treated with siRNA targeting MMP1 for 72hrs, and then seeded into collagen contraction gels for 7 days. The culture medium at day3 and 5 were collected for the application of MMP1 ELISA. (a) Western blot results showing after 72hr of siRNA treatment, MMP1 protein expression was significantly decreased in the cells. (NT: non-targeting control siRNA). (b) 7-day contraction kinetics of the control and MMP1-knockdown HTF1785R cells (mean ± SEM, assay performed with triplicate wells). (c) ELISA results demonstrated that MMP1 secretion was significantly reduced in day3 and 5 contraction medium of MMP1 knockdown cells (mean ± SEM, n=2 experiments with duplicate wells). (a), (b) are representative figures of reproducible results (n=2 experiments).

The large quantity of MMP1 produced during the contraction process makes it a good model to investigate the post-translational modulation of its secretion by the Rho GTPases. However, it was difficult to locate where MMP1 was produced within the cells, due to the lack of reliable anti-MMP1 primary antibody for immunofluorescence staining. The subsequent quantification of MMP1 signal intensity in fibroblasts embedded in 3D collagen matrix had technical restriction as well. The anti-MMP1 antibody used for most of the study was the commercially available Abcam ab38929, which worked efficiently in Western blotting but showed a strong non-specific nucleus signal in immunofluorescence staining that was dependent on batch variations. Although MMP1 was reported to accumulate in the mitochondria and nuclei within the cells during the mitotic phase of the cell cycle (Limb et al., 2005), and in the nuclei of breast tumour cells with a slight additional staining in the cytoplasm (Kohrmann et al., 2009), by performing Western blot on fractionated cytoplasm and nuclear lysates of contracting fibroblasts, we confirmed MMP1 localised mainly cytoplasmic in our model. The application of a more specific in-house produced anti-MMP1 antibody, which was kindly provided by Dr. Itoh from Oxford University, confirmed the results. Also, the experiments performed on the 2D-cultured fibroblasts showed that they exhibited an identical expression pattern of MMP1 comparing to the 3D-cultured cells, but with a less profound production of the protein.

The mechanisms by which MMP1 is expressed and released in the cells are yet unclear. Previous studies showed that disruption of actin cytoskeleton, initiated by binding of soluble antibody to α5β1 integrin, led to an increased expression of MMP1 gene in rabbit synovial fibroblasts that was dependent on Rac1 activation (Kheradmand et al., 1998). The Rho family of small GTPases are activated downstream of integrin activation, which tightly control the organisation and

dynamics of the various structures that constitute the actin cytoskeleton. Rac1, Cdc42 and RhoA are reported to differently regulate MMP1 expression in several cell types from different origins (Kheradmand et al., 1998, Deroanne et al., 2005, Rohani et al., 2014, Ferri et al., 2007, Igata et al., 2010). However, our work is the first study that investigated the role of Rho GTPases in regulating MMP1 protein expression and extracellular release.

The modulation of Rho GTPases on MMP1 production varies depending on different cell types. In our model, inhibition of Cdc42 significantly augmented MMP1 secretion that was caused by overexpression of the protein in the cells, which was possibly through the activation of ERK1/2, consistently with previous findings (Kheradmand et al., 1998, Rohani et al., 2014). Notably, the treatment with NSC23766 abolished Cdc42-dependent MMP1 overexpression and secretion, suggesting that NSC23766 may suppress ERK activity, which was also mentioned in the study of human skin fibroblasts (Deroanne et al., 2005).

The regulatory roles that Rac1 and RhoA performed on MMP1 expression and release are distinct in our cells from the ones of other cell types. The activation of Rac1 was required for the production of MMP1, and blocking of Rac1 resulted in a reduction of MMP1 expression at both gene and protein levels in the rabbit synovial fibroblasts, human smooth muscle cells and the *in vivo* mice model (Kheradmand et al., 1998, Ferri et al., 2007, Bopp et al., 2013). In conjunctival fibroblasts, we found that Rac1 downregulation did not greatly interfered with the secretion of MMP1, but increased its expression in the cells. Furthermore, we showed that downregulation of RhoA significantly reduced MMP1 secretion, which was very different from the results found in keratinocytes and dermal fibroblasts (Deroanne et al., 2005, Rohani

et al., 2014). RhoA inhibition led to a remarkable accumulation of MMP1 within the cells, whereas blocking of the RhoA downstream effector ROCK pathway failed to prevent MMP1 from being released, suggesting that signalling through activated RhoA but not ROCK, is essential for MMP1 protein secretion in conjunctival fibroblasts (**Table 5.3**).

Table 5.3 Summary of the changes of MMP1 protein expression and secretion upon siRNA knockdown (KD) of small Rho GTPases Rac1, Cdc42, RhoA and Rac2, and GAPs and GEFs including Arhgap5, Racgap1 and Arhgef3. '≈' represents no statistically significant change detected. '↑' and '↓' represent up and downregulation respectively, '↑↑' represents over 2 times upregulation in protein secretion characterised and '↓↓' represents a significant reduction of contraction kinetics.

Gene KD	MMP1 expression	MMP1 secretion
Rac1	↑	≈
Cdc42	↑	↑↑
RhoA	↑	↓
Rac2	↑	↑↑
Arhgap5	↑	↓
Racgap1	↑	↑
Arhgef3	↑	↑

Several studies have demonstrated the involvement of MARK signalling in MMP1 expression. Activation of the ERK1/2 or P38 MAP kinase pathway was found to induce transcription from MMP1 promoter in primary human fibroblasts (Brauchle et al., 2000), and activation of ERK1/2 signalling induced MMP1 protein expression in human dermal fibroblasts, keratinocytes and epithelial cells, as well as in the *ex vivo* model of lung tissue (Mercer et al., 2004, Deroanne et al., 2005, Rohani et al., 2014, Jian et al., 2011). Inhibition of the p38 MAP kinase increased MMP1 expression in dermal fibroblasts but had no effects in keratinocytes (Deroanne et al., 2005, Rohani et al., 2014), suggesting that the modulation of the P38 MAPK signalling on

MMP1 expression is cell-type and model dependent. It was reported that the divergent regulatory role that P38 MAPK played in MMP1 expression in contracting human fibroblasts was depend on the level of p38α kinase activity in response to biomechanical signals (Xu et al., 2001). In our model, inhibition of ERK signalling remarkably reduced MMP1 produced by the cells, whilst blocking of P38 MAPK signalling had no significant effect on MMP1 expression and secretion, suggesting that it did not play a key role in the regulation (**Table 5.4**).

Furthermore, inhibition of the PI3K signalling by its inhibitor LY294002 was reported to suppress the secretion of MMP2 and 9 in mouse embryo fibroblasts, colorectal cancer cells and macrophages (Liao et al., 2003, Ordonez et al., 2016, Ren et al., 2016), but had no effect on MMP1 expression in dermal fibroblasts (Rohani et al., 2014). We showed that treatment with LY294002 significantly increased MMP1 expression but reduced its secretion (**Table 5.4**), which led to a great accumulation of MMP1 within the cells that was similar to the effect of downregulating RhoA. PI3K signalling (specific PI3Kα, Akt1 and Akt2 isoforms) was reported to act as upstream regulator of RhoA in osteosarcoma MG-63 and U2OS cells (Zhang et al., 2017), suggesting that its regulation on MMP1 expression and secretion may be (at least) partially through modulating of RhoA activity.

Table 5.4 Summary of the regulation of the inhibitors of ERK (U0126), P38 MAPK (SB203580) and PI3K (LY294002) pathways on MMP1 expression and secretion respectively in contracting conjunctival fibroblasts HTF1785R. '≈' represents no statistically changes detected, ' ↑ ' and ' ↓ ' represent up and downregulation respectively.

Inhibitors	Pathway	MMP1 expression	MMP1 secretion
U0126	ERK	↓	↓
SB203580	P38 MAPK	≈	≈
LY294002	PI3K	↑	↓

Besides, our results showing that fibroblasts cultured in 3D collagen gels produced significantly more MMP1 than 2D monolayer-cultured cells is consistent with the previous studies, suggesting that fibroblasts spread on a rigid substrate express low levels of MMP1 than cells grown on polymerized collagen or in-gel (Kheradmand et al., 1998, Ferri et al., 2007, Lambert et al., 2001). The possible explanations are that contracting floating collagen lattices induced the expression of Nuclear factor-kappaB (NF-κB), a previously identified positive regulator of MMP1 expression (Xu et al., 1998), and ligation to collagen induced the activation of ERK signalling, which triggered the expression of MMP1 (Rohani et al., 2014).

Our study for the first time characterised the role of Rac2, Racgap1, Arhgap5 and Arhgef3 in regulating MMP1 expression and secretion (**Table 5.3**). We found that silencing any of these genes led to an upregulation of MMP1 expression in the cells. Unlike Rac1, downregulation of Rac2 significantly increased MMP1 secretion, showing that Rac2 activity may participate in the rate-limiting control of MMP1 release. Arhgap5 (P190BRhoGAP) is an important regulator of RhoGTPase activity in mammalian cells, with a catalytic activity preferentially towards RhoA (Matheson et al., 2006). It was reported to regulate proteolysis through MMP14 and MMP2 expression in endothelial cells, via modulating on these MMPs' mRNA levels (Guegan et al., 2008), suggesting that its regulation on MMP1 expression might be on the mRNA level. Silencing of Arhgap5 decreased MMP1 secretion, suggesting that its activity may be required for signalling pathways that regulate MMP1 secretion. Racgap1 is a crucial modulator in cytokinesis that shows strong GAP activity towards Rac1 and Cdc42, and less towards RhoA (Bastos et al., 2012, Warga et al., 2016). Blocking of Racgap1 resulted in an augmented MMP1 release led by increased protein expression, suggesting that Racgap1 was involved in

signalling pathways that regulate MMP1 expression. Lastly, Arhgef3 is a RhoGEF that selectively activate RhoA and RhoB (Arthur et al., 2002). It was reported to regulate transferrin uptake in erythroid cells through activation of RhoA (Serbanovic-Canic et al., 2011), suggesting that it plays a role in the secretory processes. In our model, inhibition of Arhgef3 did not result in the same result as that of inhibiting RhoA, suggesting that Arhgef3 is functional in modulating MMP1 release that is independent of its GEF activity towards RhoA. In addition, treatment with NSC23766 counteracted the secretion of MMP1 to the level of control in Rac2, Racgap1 and Arhgef3 knockdown cells, and further reduced MMP1 release in Arhgap5 knockdown cells. In correlation with the changes in MMP1 expression, it suggested that Rac1 activity is required for the expression of MMP1 (in Rac2 and Arhgap5 knockdown cells); or for the rate-limiting regulation of MMP1 release into the extracellular space (in Racgap1 and Arhgef3 knockdown cells).

In summary, this study demonstrated that inactivation of small Rho GTPases and their modulators induced the production of MMP1 in the cells, though only RhoA or Arhgap5 downregulation significantly inhibited MMP1 secretion (**Table 5.3, Table 5.4**), suggesting their important and differential roles in the regulation of MMP1 manufacture in contracting conjunctival fibroblasts. It is proposed that the rate-limiting step for modulating MMP1 during the tissue contraction is the release of the protein in the extracellular medium rather than its expression levels. Also, it is highly possible that this mechanism is applicable to other MMPs that exhibited upregulation during the contraction, hence drawing some interesting new prospects for future therapies.

Chapter 6 Discussion and future directions

To characterise the molecular pathways underlying conjunctival fibrosis and scarring, we utilised a genome wide microarray study to investigate gene expression changes during human conjunctival fibroblast-mediated contraction. Unlike the previous microarray studies that have been carried out in animals or small cohort of patients with mixed cell populations (Esson et al., 2004, Popp et al., 2007, Mahale et al., 2015), our work is the first study that performed with *in vitro* 3D contraction model that contained only fibroblasts. Through a comprehensive analysis that combined a pilot parallel study of an *in vivo* wounding model in rabbit following glaucoma filtration surgery, and previously obtained microarray data of human ocular fibrotic diseases such as trachoma and thyroid-associated orbitopathy, we identified that the contraction process consisted of two phases: the early phase, exhibited a classic serum/wound response profile with upregulation of genes related to inflammation, matrix remodelling and transcription activation; and a late stage when the hyperactive signal receded and the gene profile progressed to promote fibrosis. Furthermore, we found that an early transient inhibition of Rac1 by its inhibitor NSC23766 was efficient to suppressed the gene expression changes that initiated the contraction in fibroblasts HTF7071. Importantly, our results demonstrated that small Rho GTPases Rac2, Cdc42 and RhoA, and their regulators including Arhgap5, Racgap1 and Arhgef3 differently regulated the contractile activity. They also differently regulated matrix remodelling by modulating the expression and secretion of MMP1. The uncovered regulators of the contraction that

we identified and the rate-limiting model of MMP1 secretion that we proposed will draw some interesting new prospects for the future research and therapies.

6.1 Signalling pathways characterised in contraction

Our analysis has provided novel insights into the signalling pathways that contributed to the activation or inhibition of the cellular contractile activity, by characterising the annotated functional gene clusters being dynamically modulated during the contraction *in vitro* and *in vivo* (**Figure 6.1**). We confirmed the participation of some expected signalling events such as 'Respond to wounding', 'transcription regulation' and 'cytokine activity' that are closely related to wound healing (Iyer et al., 1999). We also proposed the involvement of gene clusters that have not been directly linked to tissue contraction before, for example, the gene cluster of 'Cadmium ion binding' was found to be related to the upregulation of contraction. Cadmium was reported to induce translocation of proteins to cellular compartments, particularly cytoskeleton (Liu et al., 2014). It acted on the disruption of focal adhesions, as well as shifting the actin polymerisation-depolymerisation in favour of depolymerisation by activation of $Ca(^{2+})$-dependent proteins in the studies of rat, mouse, and human mesangial cells (Templeton and Liu, 2013), which suggested that the uptake of Cadmium ion potentially regulated actin cytoskeleton, which may facilitate the contraction.

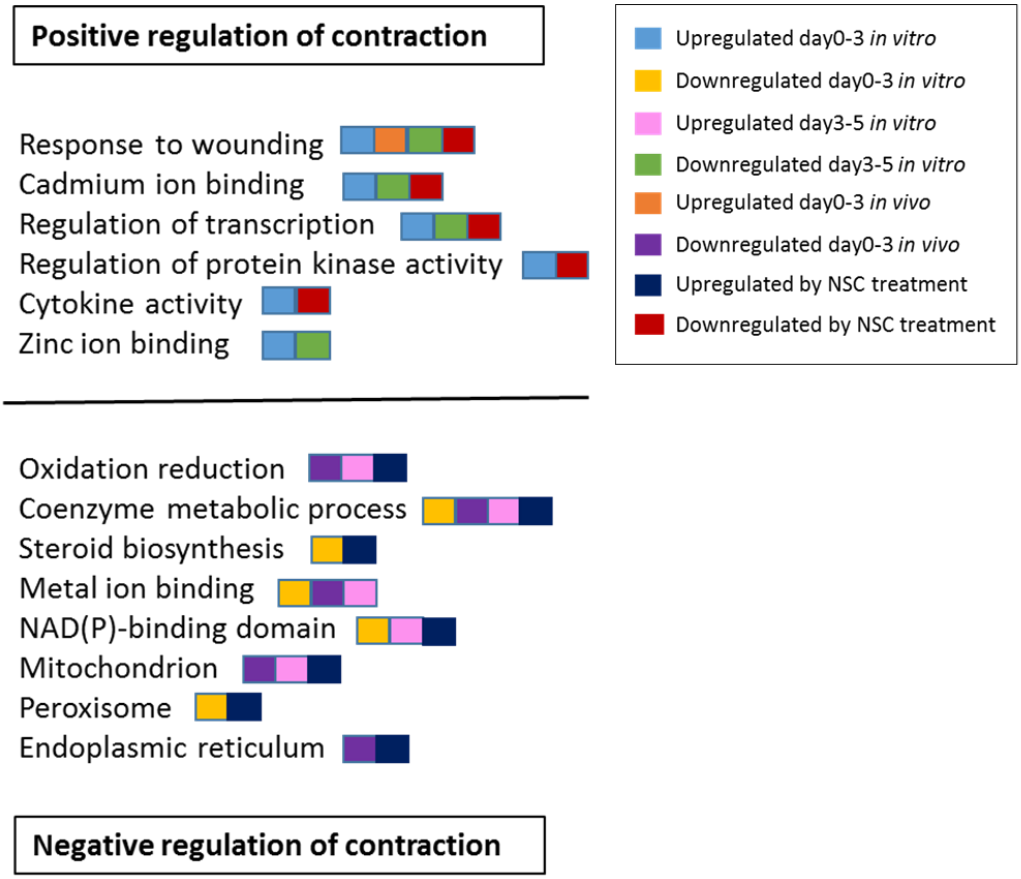

Figure 6.1 Conclusion of the annotated functional gene clusters that are associated with the activation or inhibition of the contractile activity.

The figure concludes the annotated functional gene clusters that are related to the positive regulation (activation) or negative regulation (inhibition) of the contractile activity. They are selected as they were among the top 10 up or downregulated gene clusters in the in vitro early contraction from day0-3 or late contraction from day3-5, day3 NSC23766 treated samples, or the in vivo contraction, and also being similarly regulated in at least two other sample groups that are identically related to the activation or inhibition of contraction. The different colour blocks following the cluster name represent its expression patterns in different sample groups. The explanation of each colour block is listed in the figure legend.

Similarly, functional clusters that were identified underlying negative regulation of the contraction, such as ‘oxidation reduction’, ‘coenzyme metabolic processes’ and ‘steroid biosynthesis’, have not been recognised by any other studies before. However, gene that regulate cholesterol biosynthesis were showed to be suppressed in the previous study of the transcriptional program of fibroblasts in response to serum (Iyer et al., 1999). Lately, the expression profile of strongly upregulated lipid and fatty acid metabolism signature genes was found to be associated with a less contractile phenotype in human dermal fibroblasts *in vitro* (Milano et al., 2008, Johnson et al., 2015). Also, rats with a higher body fat constituent were identified with a higher levels of lipid peroxidation and significantly delayed wound contraction (Paulino do Nascimento and Monte-Alto-Costa, 2011), suggesting that enhanced lipid metabolism may be linked to or result from the inhibition of the contractile activity. Still, the detailed mechanisms by which these signalling events affected contraction are awaiting further investigation, our work has expanded a wider view of the current event and suggested more possibilities for the future direction of the research.

6.2 A model for the role of small GTPases in contraction

One surprising finding of the study was that the small Rho GTPase Rac1 may not play an essential role in regulating conjunctival fibroblast-mediated contraction. Following the published study of Tovell et al (Tovell et al., 2012), it was hypothesised that Rac1 is a master regulator of tissue contraction in conjunctiva. However, our results suggested that Rac2, but not Rac1, may be a major regulator of contraction, indicating that Rac2 can be a promising target in the future therapeutics of conjunctival scarring. Similar to Rac1, Rac2 was found to regulate

actin dynamics through interacting with cofilin and Arp2/3 (Sun et al., 2007). It may also act with DIAP3 or other downstream effectors to perform a dominant regulatory role of actin despite the presence of Rac1.

Here we proposed a model by which the contractile activity of conjunctival fibroblast is regulated by the Rho GTPases and other regulators that we characterised in the study (**Figure 6.2**). Following serum stimulation, Rac2 is activated and performs a vital role in mediating contraction. Activation of Cdc42 promotes contraction via inhibition of the ERK signalling, whose activity suppresses contraction. Cdc42 may also facilitate contraction by activating the P38 MAPK signalling pathway. The activation of RhoA promotes contraction, whilst the contribution of active Rac1 to contraction is small. The PI3K signalling pathway plays an important role in promoting contraction. Activation of Racgap1 suppresses contraction through inactivation of Cdc42. The inhibition of Arhgap5 or Arhgef3 significantly decreases contraction, suggesting that their activities are required for the signalling pathways that are essential to the contraction, which makes them novel targets for the prevention of contraction. Our work revealed that Rho GTPases and numerous signalling pathways contribute to the contraction in which they perform distinct regulatory roles, and several GAPs and GEFs also play vital functions in regulating the process.

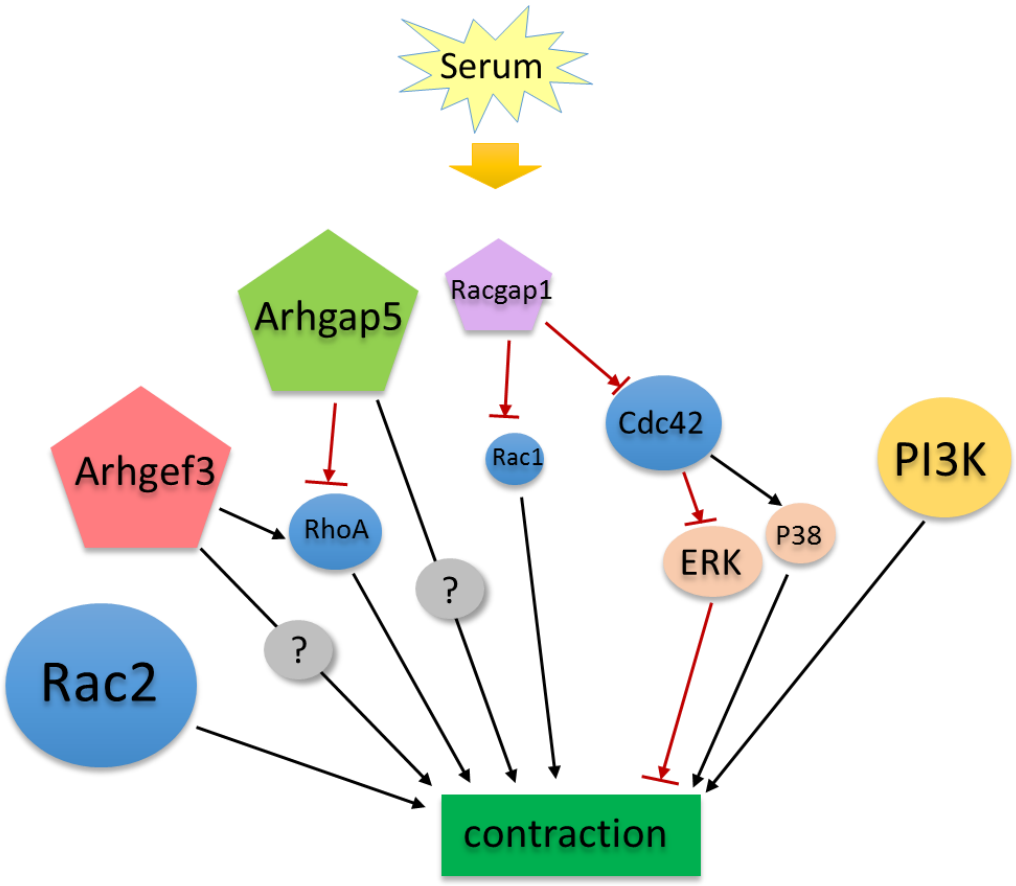

Figure 6.2 Illustrative diagram showing the potential regulatory roles of numerous modulators in the conjunctival fibroblast-mediated contraction.

The potential regulatory roles of small Rho GTPases Rac1, Cdc42, RhoA and Rac2, and their regulators including Racgap1, Arhgap5 and Arhgef3, and the ERK, P38 MAPK and PI3K signalling pathways are illustrated in the figure. The size of the icon represents the importance of the participator in the contraction. The black arrows represent positive regulation, and the red arrows represent inhibition. Upon serum stimulation, Rac2 is activated and performs a vital role in contraction. Cdc42 promotes contraction by inactivation of ERK. The P38 MAPK signalling facilitates contraction downstream of Cdc42. The PI3K signalling plays an important role in mediating contraction. The activation of RhoA or Rac1 promotes contraction, though the contribution of Rac1 is small. Activation of Racgap1 suppresses contraction through inactivation of Cdc42 and Rac1, especially Cdc42. The inhibition of Arhgap5 or Arhgef3 significantly decreases contraction, suggesting that their activities are required for the signalling pathways that are essential for the contraction.

Moreover, other Rho GTPases, for example RhoB and RhoD, were also found being differently regulated during the *in vitro* contraction. RhoB holds a conserved 'effector domain' like RhoA and has the potential to interact with the same downstream effectors (Ridley, 2013). RhoB was shown to regulate actin dynamics via modulating β1 integrin surface levels and activity, thereby stabilising lamellipodial protrusions (Alfano et al., 2012, Vega et al., 2012). RhoB was downregulated 1.5 times by NSC23766 treatment at day3, and downregulated 2.1 times from day3 to 5, suggesting that it may be functional in a way to promote early contraction. RhoD was thought to have cellular functions that are antagonistic to RhoA, as introduction of constitutively active form of RhoD into fibroblasts resulted in disassembly of actin stress fibres and focal adhesions (Tsubakimoto et al., 1999). RhoD was downregulated 2 times from day0 to 3, and upregulated 3 times from day3 to 5, suggesting that RhoD-dependent pathways may negatively affect the contraction. It will be interesting to further investigate the roles that RhoB and RhoD perform in contraction.

6.3 A model for the regulation of MMP1 expression and secretion during contraction

Another surprising result suggested by the study was that 85% depletion in the level of MMP1 protein released in the culture medium was not able to stop contraction. It is suspected a small amount of MMP1 was enough to facilitate contraction, or that other MMPs, such as MMP3 and MMP10 that were also significantly upregulated during the contraction, shared the same function with MMP1. It will be interesting to explore that if a complete suppression of MMP1, or depleting MMP1, 3 and 10 altogether could prevent the contraction. Also, overproduction of MMP1 was not

able to overcome the loss of cellular contractility led by deactivation of vital regulators of contraction, such as Rac2 in our model, suggesting that cell-mediated protrusive activity and MMP1-mediated matrix degradation are independent events in conjunctival fibroblast-mediated contraction.

We for the first time proposed a model of potential mechanisms by which the expression and release of MMP1 are regulated during contraction in conjunctival fibroblasts (**Figure 6.3**). We found that the expression of MMP1 is triggered by inactivation of the small Rho GTPases Rac2, RhoA, Cdc42 or Rac1. Cdc42 inhibits MMP1 expression by suppression of the ERK signalling, which upon activation promotes MMP1 production. The activation of ERK may require the participation of active Rac1. The PI3K signalling negatively regulate MMP1 expression possibly via activating RhoA, whose downstream effector ROCK serves to inhibit MMP1 expression. Arhgef3 also reduces MMP1 expression via activation of RhoA, whilst Racgap1 and Arhgap5 inhibit MMP1 expression through other signalling pathways other than their GAP activity towards Cdc42, Rac1 or RhoA. In terms of the export of MMP1, RhoA, Rac1 and Arhgap5 perform important regulatory roles in controlling the release of MMP1 to the extracellular spaces. Our work revealed that the rate-limiting regulation of MMP1 is on the protein release rather than its expression levels, suggesting some promising new strategies for the future therapeutics.

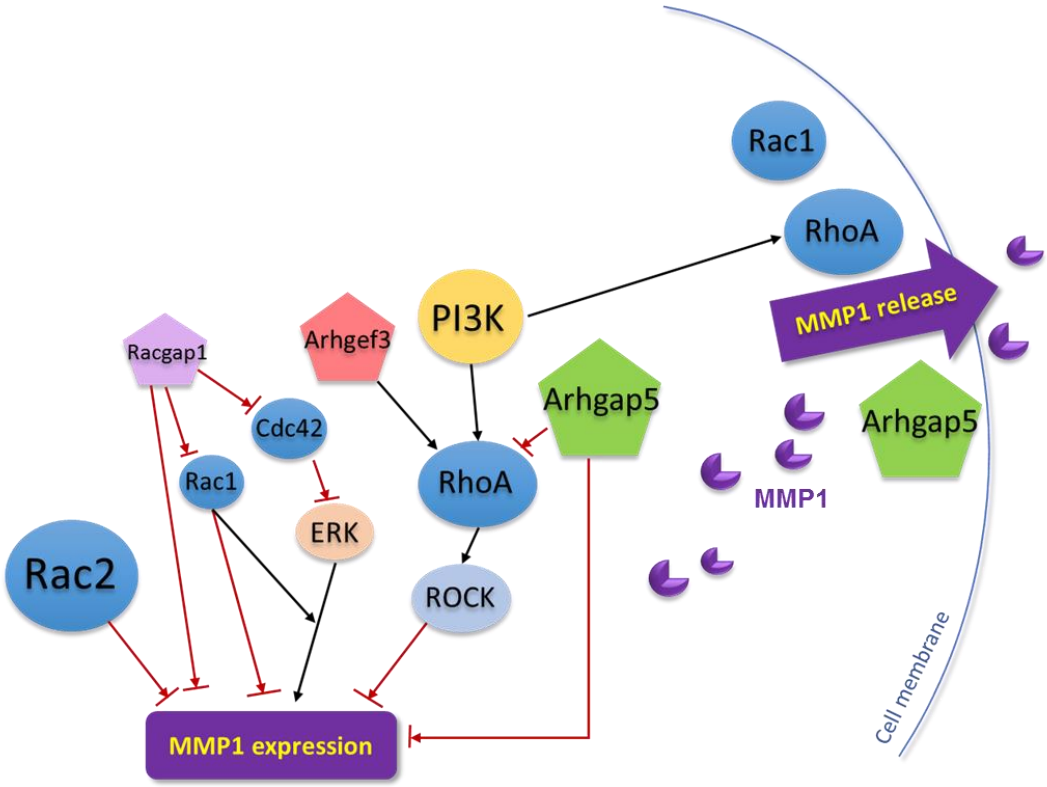

Figure 6.3 A model for the potential mechanisms by which the expression and release of MMP1 are regulated during the conjunctival fibroblast-mediated contraction.

The expression of MMP1 is triggered by inactivation of the small Rho GTPases Rac2, RhoA, Cdc42 or Rac1. Cdc42 suppresses MMP1 expression by inhibition of the ERK signalling, which upon activation promotes MMP1 production, and may require the participation of active Rac1. The PI3K signalling negatively regulate MMP1 expression possibly by activating RhoA, whose downstream effector ROCK serves to inhibit MMP1 expression. Arhgef3 reduces MMP1 expression via activation of RhoA, whilst Racgap1 and Arhgap5 inhibit MMP1 expression through unknown signalling pathways other than their GAP activity towards Cdc42, Rac1 or RhoA. RhoA, Rac1 and Arhgap5 perform important regulatory roles in controlling the release of MMP1 to the extracellular spaces.

6.4 Future direction

The mechanisms by which the small Rho GTPases especially RhoA and Rac1 controlled the rate-limiting secretion of MMP1 during the contraction are worth being further characterised. The Rho GTPases are known to be critical players in the process of vesicle trafficking. Together with their regulators, Rho GTPases modulate and/or trigger exocytosis, and induce the squeezing of the post-exocytic vesicles through promoting the remodelling of the cytoskeleton around the fused vesicle (de Curtis and Meldolesi, 2012). Although most of the molecular pathways involved in the process are still unclear, emerging evidence suggest that RhoA may be an important regulator. RhoA controls the coordination of actin and microtubule cytoskeleton modulation, as well as vesicle trafficking and fusion, via interacting with the exocyst complex, which is a multi-subunit tethering complex involved in the regulation of cell-surface transport and cell polarity in various cell systems (Pathak and Dermardirossian, 2013). Rac1 is also reported to participate in the modulation of actin cytoskeleton for vesicle release (Williams et al., 2009, Humeau et al., 2002). Other vital regulators of exocytosis, such as the Rab and Ral family of GTPases that are functional in exocyst assembly and vesicle-tethering processes (Wu et al., 2008), are also found to be dynamically regulated during the *in vitro* contraction. We hypothesise that RhoA and to a less extent of Rac1, modulate MMP1 secretion through their regulatory roles in vesicle trafficking in cooperation with other small G proteins like Rab and Ral family of proteins (**Figure 6.4**). The interactions between these regulators in MMP1 exocytosis are waiting to be further characterised.

In summary, this study has provided comprehensive and in-depth views of the gene expression patterns and signalling pathways underlying conjunctival fibroblast-mediated contraction, which will assist as a powerful tool in the research of preventing conjunctival fibrosis and scarring. Also, the characterisation of the

regulatory roles that Rho GTPases and their regulators performed on cellular contractile activity and MMP1-mediated matrix remodelling has offered unique insights and novel targets for the future development of new therapeutics.

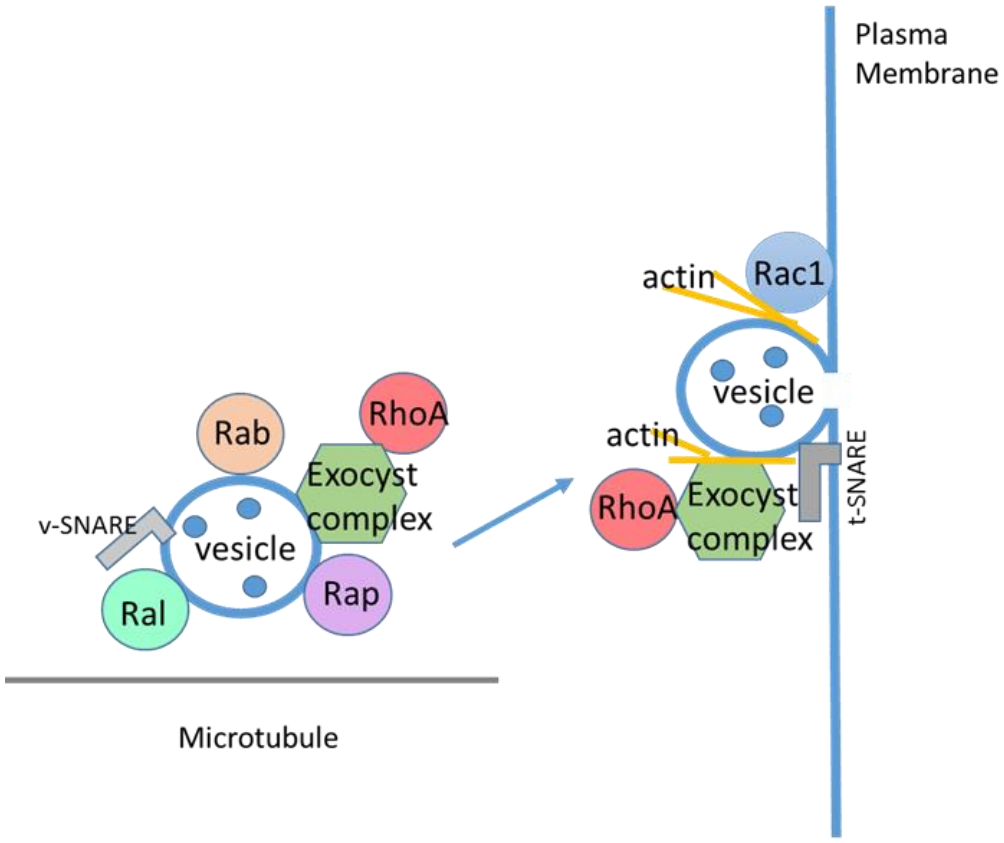

Figure 6.4 A putative model for the regulation of MMP1 trafficking by RhoA and Rac1, in cooperation with the Rab, Ral and Rap family of proteins.

MMP1 vesicles that bound with Rab, Ral and/or Rap families of proteins and exocyst components are transported to the plasma membrane using microtubule as tracks. At the plasma membrane, RhoA is activated and recruited to the exocyst complex. With the aid of Rac1, RhoA regulates the exocyst function by affecting the complex formation which promotes the opening of actin filaments and fusion of the vesicles with the membrane.

Bibliography

ABE, M., SOGABE, Y., SYUTO, T., YOKOYAMA, Y. & ISHIKAWA, O. 2007. Evidence that PI3K, Rac, Rho, and Rho kinase are involved in basic fibroblast growth factor-stimulated fibroblast-Collagen matrix contraction. *J Cell Biochem,* 102**,** 1290-9.

ABU EL-ASRAR, A. M., GEBOES, K., TABBARA, K. F., AL-KHARASHI, S. A., MISSOTTEN, L. & DESMET, V. 1998. Immunopathogenesis of conjunctival scarring in trachoma. *Eye (Lond),* 12 (Pt 3a)**,** 453-60.

AKIRA, S. & TAKEDA, K. 2004. Toll-like receptor signalling. *Nat Rev Immunol,* 4**,** 499-511.

ALEXANDER, C. M., HANSELL, E. J., BEHRENDTSEN, O., FLANNERY, M. L., KISHNANI, N. S., HAWKES, S. P. & WERB, Z. 1996. Expression and function of matrix metalloproteinases and their inhibitors at the maternal-embryonic boundary during mouse embryo implantation. *Development,* 122**,** 1723-36.

ALFANO, D., RAGNO, P., STOPPELLI, M. P. & RIDLEY, A. J. 2012. RhoB regulates uPAR signalling. *J Cell Sci,* 125**,** 2369-80.

ANDRAE, J., GALLINI, R. & BETSHOLTZ, C. 2008. Role of platelet-derived growth factors in physiology and medicine. *Genes Dev,* 22**,** 1276-312.

ARORA, P. D. & MCCULLOCH, C. A. 1994. Dependence of collagen remodelling on alpha-smooth muscle actin expression by fibroblasts. *J Cell Physiol,* 159**,** 161-75.

ARTHUR, W. T., ELLERBROEK, S. M., DER, C. J., BURRIDGE, K. & WENNERBERG, K. 2002. XPLN, a guanine nucleotide exchange factor for RhoA and RhoB, but not RhoC. *J Biol Chem,* 277**,** 42964-72.

AUSTIN, K. M., NGUYEN, N., JAVID, G., COVIC, L. & KULIOPULOS, A. 2013. Noncanonical matrix metalloprotease-1-protease-activated receptor-1 signaling triggers vascular smooth muscle cell dedifferentiation and arterial stenosis. *J Biol Chem,* 288**,** 23105-15.

BABA, T. T., NEMOTO, T. K., MIYAZAKI, T. & OIDA, S. 2008. Simvastatin suppresses the differentiation of C2C12 myoblast cells via a Rac pathway. *J Muscle Res Cell Motil,* 29**,** 127-34.

BAGGIOLINI, M. 2015. CXCL8 - The First Chemokine. *Front Immunol,* 6**,** 285.

BALANIS, N., YOSHIGI, M., WENDT, M. K., SCHIEMANN, W. P. & CARLIN, C. R. 2011. beta3 integrin-EGF receptor cross-talk activates p190RhoGAP in mouse mammary gland epithelial cells. *Mol Biol Cell,* 22**,** 4288-301.

BANDO, H., IKUNO, Y., HORI, Y., SAYANAGI, K. & TANO, Y. 2006. Mitogen-activated protein kinase (MAPK) and phosphatidylinositol-3 kinase (PI3K) pathways differently regulate retinal pigment epithelial cell-mediated collagen gel contraction. *Exp Eye Res,* 82**,** 529-37.

BASTOS, R. N., PENATE, X., BATES, M., HAMMOND, D. & BARR, F. A. 2012. CYK4 inhibits Rac1-dependent PAK1 and ARHGEF7 effector pathways during cytokinesis. *J Cell Biol,* 198**,** 865-80.

BATALLER, R., SCHWABE, R. F., CHOI, Y. H., YANG, L., PAIK, Y. H., LINDQUIST, J., QIAN, T., SCHOONHOVEN, R., HAGEDORN, C. H., LEMASTERS, J. J. & BRENNER, D. A. 2003. NADPH oxidase signal transduces angiotensin II in hepatic stellate cells and is critical in hepatic fibrosis. *J Clin Invest,* 112**,** 1383-94.

BEJJANI, B. A., LEWIS, R. A., TOMEY, K. F., ANDERSON, K. L., DUEKER, D. K., JABAK, M., ASTLE, W. F., OTTERUD, B., LEPPERT, M. & LUPSKI, J. R. 1998. Mutations in CYP1B1, the gene for cytochrome P4501B1, are the predominant cause of primary congenital glaucoma in Saudi Arabia. *Am J Hum Genet,* 62**,** 325-33.

BELL, E., IVARSSON, B. & MERRILL, C. 1979. Production of a tissue-like structure by contraction of collagen lattices by human fibroblasts of different proliferative potential *in vitro*. *Proc Natl Acad Sci U S A,* 76**,** 1274-8.
BELPERIO, J. A., DY, M., BURDICK, M. D., XUE, Y. Y., LI, K., ELIAS, J. A. & KEANE, M. P. 2002. Interaction of IL-13 and C10 in the pathogenesis of bleomycin-induced pulmonary fibrosis. *Am J Respir Cell Mol Biol,* 27**,** 419-27.
BIRBRAIR, A., ZHANG, T., FILES, D. C., MANNAVA, S., SMITH, T., WANG, Z. M., MESSI, M. L., MINTZ, A. & DELBONO, O. 2014. Type-1 pericytes accumulate after tissue injury and produce collagen in an organ-dependent manner. *Stem Cell Res Ther,* 5**,** 122.
BLEASE, K., JAKUBZICK, C., WESTWICK, J., LUKACS, N., KUNKEL, S. L. & HOGABOAM, C. M. 2001. Therapeutic effect of IL-13 immunoneutralization during chronic experimental fungal asthma. *J Immunol,* 166**,** 5219-24.
BLEASE, K., MEHRAD, B., STANDIFORD, T. J., LUKACS, N. W., KUNKEL, S. L., CHENSUE, S. W., LU, B., GERARD, C. J. & HOGABOAM, C. M. 2000. Airway remodeling is absent in CCR1-/- mice during chronic fungal allergic airway disease. *J Immunol,* 165**,** 1564-72.
BOIRE, A., COVIC, L., AGARWAL, A., JACQUES, S., SHERIFI, S. & KULIOPULOS, A. 2005. PAR1 is a matrix metalloprotease-1 receptor that promotes invasion and tumorigenesis of breast cancer cells. *Cell,* 120**,** 303-13.
BOPP, A., WARTLICK, F., HENNINGER, C., KAINA, B. & FRITZ, G. 2013. Rac1 modulates acute and subacute genotoxin-induced hepatic stress responses, fibrosis and liver aging. *Cell Death Dis,* 4**,** e558.
BORDER, W. A., NOBLE, N. A., YAMAMOTO, T., HARPER, J. R., YAMAGUCHI, Y., PIERSCHBACHER, M. D. & RUOSLAHTI, E. 1992. Natural inhibitor of transforming growth factor-beta protects against scarring in experimental kidney disease. *Nature,* 360**,** 361-4.
BOTTINGER, E. P. & BITZER, M. 2002. TGF-beta signaling in renal disease. *J Am Soc Nephrol,* 13**,** 2600-10.
BRAUCHLE, M., GLUCK, D., DI PADOVA, F., HAN, J. & GRAM, H. 2000. Independent role of p38 and ERK1/2 mitogen-activated kinases in the upregulation of matrix metalloproteinase-1. *Exp Cell Res,* 258**,** 135-44.
BRODEUR, T. Y., ROBIDOUX, T. E., WEINSTEIN, J. S., CRAFT, J., SWAIN, S. L. & MARSHAK-ROTHSTEIN, A. 2015. IL-21 Promotes Pulmonary Fibrosis through the Induction of Profibrotic CD8+ T Cells. *J Immunol,* 195**,** 5251-60.
BROWN, R. A., PRAJAPATI, R., MCGROUTHER, D. A., YANNAS, I. V. & EASTWOOD, M. 1998. Tensional homeostasis in dermal fibroblasts: mechanical responses to mechanical loading in three-dimensional substrates. *J Cell Physiol,* 175**,** 323-32.
BURTON, M. J., BAILEY, R. L., JEFFRIES, D., RAJAK, S. N., ADEGBOLA, R. A., SILLAH, A., MABEY, D. C. & HOLLAND, M. J. 2010. Conjunctival expression of matrix metalloproteinase and proinflammatory cytokine genes after trichiasis surgery. *Invest Ophthalmol Vis Sci,* 51**,** 3583-90.
CACERES, M., ROMERO, A., COPAJA, M., DIAZ-ARAYA, G., MARTINEZ, J. & SMITH, P. C. 2011. Simvastatin alters fibroblastic cell responses involved in tissue repair. *J Periodontal Res,* 46**,** 456-63.
CAO, H., EPPINGA, R. D., RAZIDLO, G. L., KRUEGER, E. W., CHEN, J., QIANG, L. & MCNIVEN, M. A. 2016. Stromal fibroblasts facilitate cancer cell invasion by a novel invadopodia-independent matrix degradation process. *Oncogene,* 35**,** 1099-110.
CARVALHO, R. F., NILSSON, G. & HARVIMA, I. T. 2010. Increased mast cell expression of PAR-2 in skin inflammatory diseases and release of IL-8 upon PAR-2 activation. *Exp Dermatol,* 19**,** 117-22.

CASTILLO-PICHARDO, L., HUMPHRIES-BICKLEY, T., DE LA PARRA, C., FORESTIER-ROMAN, I., MARTINEZ-FERRER, M., HERNANDEZ, E., VLAAR, C., FERRER-ACOSTA, Y., WASHINGTON, A. V., CUBANO, L. A., RODRIGUEZ-ORENGO, J. & DHARMAWARDHANE, S. 2014. The Rac Inhibitor EHop-016 Inhibits Mammary Tumor Growth and Metastasis in a Nude Mouse Model. *Transl Oncol,* 7**,** 546-55.

CERIONE, R. A. & ZHENG, Y. 1996. The Dbl family of oncogenes. *Curr Opin Cell Biol,* 8**,** 216-22.

CHANG, H. Y., CHI, J. T., DUDOIT, S., BONDRE, C., VAN DE RIJN, M., BOTSTEIN, D. & BROWN, P. O. 2002. Diversity, topographic differentiation, and positional memory in human fibroblasts. *Proc Natl Acad Sci U S A,* 99**,** 12877-82.

CHANG, H. Y., SNEDDON, J. B., ALIZADEH, A. A., SOOD, R., WEST, R. B., MONTGOMERY, K., CHI, J. T., VAN DE RIJN, M., BOTSTEIN, D. & BROWN, P. O. 2004. Gene expression signature of fibroblast serum response predicts human cancer progression: similarities between tumors and wounds. *PLoS Biol,* 2**,** E7.

CHEN, Y., LEASK, A., ABRAHAM, D. J., PALA, D., SHIWEN, X., KHAN, K., LIU, S., CARTER, D. E., WILCOX-ADELMAN, S., GOETINCK, P., DENTON, C. P., BLACK, C. M., PITSILLIDES, A. A., SARRAF, C. E. & EASTWOOD, M. 2008. Heparan sulfate-dependent ERK activation contributes to the overexpression of fibrotic proteins and enhanced contraction by scleroderma fibroblasts. *Arthritis Rheum,* 58**,** 577-85.

CHOI, I., KANG, H. S., YANG, Y. & PYUN, K. H. 1994. IL-6 induces hepatic inflammation and collagen synthesis *in vivo*. *Clin Exp Immunol,* 95**,** 530-5.

CLARK, R. 1996. *The molecular and cellular biology of wound repair,* New York, NY, Plenum Press.

COLEMAN, A. L. & BRIGATTI, L. 2001. The glaucomas. *Minerva Med,* 92**,** 365-79.

CORDEIRO, M. F., BHATTACHARYA, S. S., SCHULTZ, G. S. & KHAW, P. T. 2000. TGF-beta1, -beta2, and -beta3 *in vitro*: biphasic effects on Tenon's fibroblast contraction, proliferation, and migration. *Invest Ophthalmol Vis Sci,* 41**,** 756-63.

COTE, J. F. & VUORI, K. 2002. Identification of an evolutionarily conserved superfamily of DOCK180-related proteins with guanine nucleotide exchange activity. *J Cell Sci,* 115**,** 4901-13.

CUCORANU, I., CLEMPUS, R., DIKALOVA, A., PHELAN, P. J., ARIYAN, S., DIKALOV, S. & SORESCU, D. 2005. NAD(P)H oxidase 4 mediates transforming growth factor-beta1-induced differentiation of cardiac fibroblasts into myofibroblasts. *Circ Res,* 97**,** 900-7.

CURRIE, J. C., FORTIER, S., SINA, A., GALIPEAU, J., CAO, J. & ANNABI, B. 2007. MT1-MMP down-regulates the glucose 6-phosphate transporter expression in marrow stromal cells: a molecular link between pro-MMP-2 activation, chemotaxis, and cell survival. *J Biol Chem,* 282**,** 8142-9.

DAHLMANN-NOOR, A. H., MARTIN-MARTIN, B., EASTWOOD, M., KHAW, P. T. & BAILLY, M. 2007. Dynamic protrusive cell behaviour generates force and drives early matrix contraction by fibroblasts. *Exp Cell Res,* 313**,** 4158-69.

DAHLMANN, A. H., MIRESKANDARI, K., CAMBREY, A. D., BAILLY, M. & KHAW, P. T. 2005. Current and future prospects for the prevention of ocular fibrosis. *Ophthalmol Clin North Am,* 18**,** 539-59.

DALLON, J. C. & EHRLICH, H. P. 2008. A review of fibroblast-populated collagen lattices. *Wound Repair Regen,* 16**,** 472-9.

DANIELS, J. T., CAMBREY, A. D., OCCLESTON, N. L., GARRETT, Q., TARNUZZER, R. W., SCHULTZ, G. S. & KHAW, P. T. 2003. Matrix metalloproteinase inhibition modulates fibroblast-mediated matrix contraction and collagen production *in vitro*. *Invest Ophthalmol Vis Sci,* 44**,** 1104-10.

DE CURTIS, I. & MELDOLESI, J. 2012. Cell surface dynamics - how Rho GTPases orchestrate the interplay between the plasma membrane and the cortical cytoskeleton. *J Cell Sci,* 125**,** 4435-44.
DENK, P. O., HOPPE, J., HOPPE, V. & KNORR, M. 2003. Effect of growth factors on the activation of human Tenon's capsule fibroblasts. *Curr Eye Res,* 27**,** 35-44.
DEODHAR, A. K. & RANA, R. E. 1997. Surgical physiology of wound healing: a review. *J Postgrad Med,* 43**,** 52-6.
DEROANNE, C. F., HAMELRYCKX, D., HO, T. T., LAMBERT, C. A., CATROUX, P., LAPIERE, C. M. & NUSGENS, B. V. 2005. Cdc42 downregulates MMP-1 expression by inhibiting the ERK1/2 pathway. *J Cell Sci,* 118**,** 1173-83.
DESMOULIERE, A. 1995. Factors influencing myofibroblast differentiation during wound healing and fibrosis. *Cell Biol Int,* 19**,** 471-6.
DESMOULIERE, A., GEINOZ, A., GABBIANI, F. & GABBIANI, G. 1993. Transforming growth factor-beta 1 induces alpha-smooth muscle actin expression in granulation tissue myofibroblasts and in quiescent and growing cultured fibroblasts. *J Cell Biol,* 122**,** 103-11.
DESMOULIERE, A., GUYOT, C. & GABBIANI, G. 2004. The stroma reaction myofibroblast: a key player in the control of tumor cell behavior. *Int J Dev Biol,* 48**,** 509-17.
DHARMAWARDHANE, S., HERNANDEZ, E. & VLAAR, C. 2013. Development of EHop-016: a small molecule inhibitor of Rac. *Enzymes,* 33 Pt A**,** 117-46.
DO, N. N. & EMING, S. A. 2016. Skin fibrosis: Models and mechanisms. *Curr Res Transl Med,* 64**,** 185-193.
DUTTING, S., HEIDENREICH, J., CHERPOKOVA, D., AMIN, E., ZHANG, S. C., AHMADIAN, M. R., BRAKEBUSCH, C. & NIESWANDT, B. 2015. Critical off-target effects of the widely used Rac1 inhibitors NSC23766 and EHT1864 in mouse platelets. *J Thromb Haemost,* 13**,** 827-38.
EASTWOOD, M., MCGROUTHER, D. A. & BROWN, R. A. 1998. Fibroblast responses to mechanical forces. *Proc Inst Mech Eng H,* 212**,** 85-92.
EBIHARA, Y., MASUYA, M., LARUE, A. C., FLEMING, P. A., VISCONTI, R. P., MINAMIGUCHI, H., DRAKE, C. J. & OGAWA, M. 2006. Hematopoietic origins of fibroblasts: II. *In vitro* studies of fibroblasts, CFU-F, and fibrocytes. *Exp Hematol,* 34**,** 219-29.
EGEBLAD, M. & WERB, Z. 2002. New functions for the matrix metalloproteinases in cancer progression. *Nat Rev Cancer,* 2**,** 161-74.
EHRLICH, H. P. & RAJARATNAM, J. B. 1990. Cell locomotion forces versus cell contraction forces for collagen lattice contraction: an *in vitro* model of wound contraction. *Tissue Cell,* 22**,** 407-17.
EHRMANN, R. L. & GEY, G. O. 1956. The growth of cells on a transparent gel of reconstituted rat-tail collagen. *J Natl Cancer Inst,* 16**,** 1375-403.
EMAD, A. & EMAD, Y. 2008. Relationship between eosinophilia and levels of chemokines (CCL5 and CCL11) and IL-5 in bronchoalveolar lavage fluid of patients with mustard gas-induced pulmonary fibrosis. *J Clin Immunol,* 28**,** 298-305.
EMIG, D., SALOMONIS, N., BAUMBACH, J., LENGAUER, T., CONKLIN, B. R. & ALBRECHT, M. 2010. AltAnalyze and DomainGraph: analyzing and visualizing exon expression data. *Nucleic Acids Res,* 38**,** W755-62.
ESSON, D. W., POPP, M. P., LIU, L., SCHULTZ, G. S. & SHERWOOD, M. B. 2004. Microarray analysis of the failure of filtering blebs in a rat model of glaucoma filtering surgery. *Invest Ophthalmol Vis Sci,* 45**,** 4450-62.
EZRA, D. G., ELLIS, J. S., BEACONSFIELD, M., COLLIN, R. & BAILLY, M. 2010. Changes in fibroblast mechanostat set point and mechanosensitivity: an adaptive response to mechanical stress in floppy eyelid syndrome. *Invest Ophthalmol Vis Sci,* 51**,** 3853-63.

EZRA, D. G., KRELL, J., ROSE, G. E., BAILLY, M., STEBBING, J. & CASTELLANO, L. 2012. Transcriptome-level microarray expression profiling implicates IGF-1 and Wnt signalling dysregulation in the pathogenesis of thyroid-associated orbitopathy. *J Clin Pathol,* 65**,** 608-13.

FAELBER, K., GAO, S., HELD, M., POSOR, Y., HAUCKE, V., NOE, F. & DAUMKE, O. 2013. Oligomerization of dynamin superfamily proteins in health and disease. *Prog Mol Biol Transl Sci,* 117**,** 411-43.

FALANGA, V. 2005. Wound healing and its impairment in the diabetic foot. *Lancet,* 366**,** 1736-43.

FERRI, N., COLOMBO, G., FERRANDI, C., RAINES, E. W., LEVKAU, B. & CORSINI, A. 2007. Simvastatin reduces MMP1 expression in human smooth muscle cells cultured on polymerized collagen by inhibiting Rac1 activation. *Arterioscler Thromb Vasc Biol,* 27**,** 1043-9.

FERRI, N., CORSINI, A., BOTTINO, P., CLERICI, F. & CONTINI, A. 2009. Virtual screening approach for the identification of new Rac1 inhibitors. *J Med Chem,* 52**,** 4087-90.

FERTIN, C., NICOLAS, J. F., GILLERY, P., KALIS, B., BANCHEREAU, J. & MAQUART, F. X. 1991. Interleukin-4 stimulates collagen synthesis by normal and scleroderma fibroblasts in dermal equivalents. *Cell Mol Biol,* 37**,** 823-9.

FREYMAN, T. M., YANNAS, I. V., PEK, Y. S., YOKOO, R. & GIBSON, L. J. 2001. Micromechanics of fibroblast contraction of a collagen-GAG matrix. *Exp Cell Res,* 269**,** 140-53.

FRIEDL, P. & WOLF, K. 2008. Tube travel: the role of proteases in individual and collective cancer cell invasion. *Cancer Res,* 68**,** 7247-9.

FRIEDLANDER, M. 2007. Fibrosis and diseases of the eye. *J Clin Invest,* 117**,** 576-86.

GABBIANI, G. 1992. The biology of the myofibroblast. *Kidney Int,* 41**,** 530-2.

GABBIANI, G. 1999. Some historical and philosophical reflections on the myofibroblast concept. *Curr Top Pathol,* 93**,** 1-5.

GABBIANI, G., RYAN, G. B. & MAJNE, G. 1971. Presence of modified fibroblasts in granulation tissue and their possible role in wound contraction. *Experientia,* 27**,** 549-50.

GAO, J. L., WYNN, T. A., CHANG, Y., LEE, E. J., BROXMEYER, H. E., COOPER, S., TIFFANY, H. L., WESTPHAL, H., KWON-CHUNG, J. & MURPHY, P. M. 1997. Impaired host defense, hematopoiesis, granulomatous inflammation and type 1-type 2 cytokine balance in mice lacking CC chemokine receptor 1. *J Exp Med,* 185**,** 1959-68.

GAO, Y., DICKERSON, J. B., GUO, F., ZHENG, J. & ZHENG, Y. 2004. Rational design and characterization of a Rac GTPase-specific small molecule inhibitor. *Proc Natl Acad Sci U S A,* 101**,** 7618-23.

GAO, Y., XING, J., STREULI, M., LETO, T. L. & ZHENG, Y. 2001. Trp(56) of rac1 specifies interaction with a subset of guanine nucleotide exchange factors. *J Biol Chem,* 276**,** 47530-41.

GEGGEL, H. S., FRIEND, J. & THOFT, R. A. 1984. Conjunctival epithelial wound healing. *Invest Ophthalmol Vis Sci,* 25**,** 860-3.

GENTLEMAN, R. 2005. *Bioinformatics and computational biology solutions using R and Bioconductor,* New York ; London, Springer.

GHARAEE-KERMANI, M. & PHAN, S. H. 1997. Lung interleukin-5 expression in murine bleomycin-induced pulmonary fibrosis. *Am J Respir Cell Mol Biol,* 16**,** 438-47.

GORELIK, L. & FLAVELL, R. A. 2002. Transforming growth factor-beta in T-cell biology. *Nat Rev Immunol,* 2**,** 46-53.

GREENHALGH, D. G. 1998. The role of apoptosis in wound healing. *Int J Biochem Cell Biol,* 30**,** 1019-30.

GRINNELL, F. 1994. Fibroblasts, myofibroblasts, and wound contraction. *J Cell Biol,* 124**,** 401-4.
GRINNELL, F. 2003. Fibroblast biology in three-dimensional collagen matrices. *Trends Cell Biol,* 13**,** 264-9.
GRINNELL, F., HO, C. H., TAMARIZ, E., LEE, D. J. & SKUTA, G. 2003. Dendritic fibroblasts in three-dimensional collagen matrices. *Mol Biol Cell,* 14**,** 384-95.
GRINNELL, F., ZHU, M., CARLSON, M. A. & ABRAMS, J. M. 1999. Release of mechanical tension triggers apoptosis of human fibroblasts in a model of regressing granulation tissue. *Exp Cell Res,* 248**,** 608-19.
GROSS, J. & LAPIERE, C. M. 1962. Collagenolytic activity in amphibian tissues: a tissue culture assay. *Proc Natl Acad Sci U S A,* 48**,** 1014-22.
GUEGAN, F., TATIN, F., LESTE-LASSERRE, T., DRUTEL, G., GENOT, E. & MOREAU, V. 2008. p190B RhoGAP regulates endothelial-cell-associated proteolysis through MT1-MMP and MMP2. *J Cell Sci,* 121**,** 2054-61.
HALL, A. 1998. Rho GTPases and the actin cytoskeleton. *Science,* 279**,** 509-14.
HALL, A. 2005. Rho GTPases and the control of cell behaviour. *Biochem Soc Trans,* 33**,** 891-5.
HANNINK, M. & DONOGHUE, D. J. 1989. Structure and function of platelet-derived growth factor (PDGF) and related proteins. *Biochim Biophys Acta,* 989**,** 1-10.
HATFIELD, K. J., REIKVAM, H. & BRUSERUD, O. 2010. The crosstalk between the matrix metalloprotease system and the chemokine network in acute myeloid leukemia. *Curr Med Chem,* 17**,** 4448-61.
HEIT, C., JACKSON, B. C., MCANDREWS, M., WRIGHT, M. W., THOMPSON, D. C., SILVERMAN, G. A., NEBERT, D. W. & VASILIOU, V. 2013. Update of the human and mouse SERPIN gene superfamily. *Hum Genomics,* 7**,** 22.
HELDIN, C. H. 1992. Structural and functional studies on platelet-derived growth factor. *Embo j,* 11**,** 4251-9.
HENLEY, J. R., CAO, H. & MCNIVEN, M. A. 1999. Participation of dynamin in the biogenesis of cytoplasmic vesicles. *Faseb j,* 13 Suppl 2**,** S243-7.
HERRERA, I., CISNEROS, J., MALDONADO, M., RAMIREZ, R., ORTIZ-QUINTERO, B., ANSO, E., CHANDEL, N. S., SELMAN, M. & PARDO, A. 2013. Matrix metalloproteinase (MMP)-1 induces lung alveolar epithelial cell migration and proliferation, protects from apoptosis, and represses mitochondrial oxygen consumption. *J Biol Chem,* 288**,** 25964-75.
HILLS, C. E. & SQUIRES, P. E. 2011. The role of TGF-beta and epithelial-to mesenchymal transition in diabetic nephropathy. *Cytokine Growth Factor Rev,* 22**,** 131-9.
HINZ, B. 2006. Masters and servants of the force: the role of matrix adhesions in myofibroblast force perception and transmission. *Eur J Cell Biol,* 85**,** 175-81.
HINZ, B. 2015. The extracellular matrix and transforming growth factor-beta1: Tale of a strained relationship. *Matrix Biol,* 47**,** 54-65.
HONJO, M., TANIHARA, H., KAMEDA, T., KAWAJI, T., YOSHIMURA, N. & ARAIE, M. 2007. Potential role of Rho-associated protein kinase inhibitor Y-27632 in glaucoma filtration surgery. *Invest Ophthalmol Vis Sci,* 48**,** 5549-57.
HOOPER, S., GAGGIOLI, C. & SAHAI, E. 2010. A chemical biology screen reveals a role for Rab21-mediated control of actomyosin contractility in fibroblast-driven cancer invasion. *Br J Cancer,* 102**,** 392-402.
HUANG DA, W., SHERMAN, B. T. & LEMPICKI, R. A. 2009a. Bioinformatics enrichment tools: paths toward the comprehensive functional analysis of large gene lists. *Nucleic Acids Res,* 37**,** 1-13.
HUANG DA, W., SHERMAN, B. T. & LEMPICKI, R. A. 2009b. Systematic and integrative analysis of large gene lists using DAVID bioinformatics resources. *Nat Protoc,* 4**,** 44-57.

HUMEAU, Y., POPOFF, M. R., KOJIMA, H., DOUSSAU, F. & POULAIN, B. 2002. Rac GTPase plays an essential role in exocytosis by controlling the fusion competence of release sites. *J Neurosci,* 22**,** 7968-81.

IGATA, T., JINNIN, M., MAKINO, T., MORIYA, C., MUCHEMWA, F. C., ISHIHARA, T. & IHN, H. 2010. Up-regulated type I collagen expression by the inhibition of Rac1 signaling pathway in human dermal fibroblasts. *Biochem Biophys Res Commun,* 393**,** 101-5.

IMAI, K., DALAL, S. S., CHEN, E. S., DOWNEY, R., SCHULMAN, L. L., GINSBURG, M. & D'ARMIENTO, J. 2001. Human collagenase (matrix metalloproteinase-1) expression in the lungs of patients with emphysema. *Am J Respir Crit Care Med,* 163**,** 786-91.

IREDALE, J. P. 2007. Models of liver fibrosis: exploring the dynamic nature of inflammation and repair in a solid organ. *J Clin Invest,* 117**,** 539-48.

IRIZARRY, R. A., HOBBS, B., COLLIN, F., BEAZER-BARCLAY, Y. D., ANTONELLIS, K. J., SCHERF, U. & SPEED, T. P. 2003. Exploration, normalization, and summaries of high density oligonucleotide array probe level data. *Biostatistics,* 4**,** 249-64.

IYER, V. R., EISEN, M. B., ROSS, D. T., SCHULER, G., MOORE, T., LEE, J. C., TRENT, J. M., STAUDT, L. M., HUDSON, J., JR., BOGUSKI, M. S., LASHKARI, D., SHALON, D., BOTSTEIN, D. & BROWN, P. O. 1999. The transcriptional program in the response of human fibroblasts to serum. *Science,* 283**,** 83-7.

JAKUBZICK, C., KUNKEL, S. L., PURI, R. K. & HOGABOAM, C. M. 2004. Therapeutic targeting of IL-4- and IL-13-responsive cells in pulmonary fibrosis. *Immunol Res,* 30**,** 339-49.

JIAN, J., PELLE, E., YANG, Q., PERNODET, N., MAES, D. & HUANG, X. 2011. Iron sensitizes keratinocytes and fibroblasts to UVA-mediated matrix metalloproteinase-1 through TNF-alpha and ERK activation. *Exp Dermatol,* 20**,** 249-54.

JOHNSON, M. E., MAHONEY, J. M., TARONI, J., SARGENT, J. L., MARMARELIS, E., WU, M. R., VARGA, J., HINCHCLIFF, M. E. & WHITFIELD, M. L. 2015. Experimentally-derived fibroblast gene signatures identify molecular pathways associated with distinct subsets of systemic sclerosis patients in three independent cohorts. *PLoS One,* 10**,** e0114017.

JOSHI, B. H., HOGABOAM, C., DOVER, P., HUSAIN, S. R. & PURI, R. K. 2006. Role of interleukin-13 in cancer, pulmonary fibrosis, and other T(H)2-type diseases. *Vitam Horm,* 74**,** 479-504.

KALLURI, R. & NEILSON, E. G. 2003. Epithelial-mesenchymal transition and its implications for fibrosis. *J Clin Invest,* 112**,** 1776-84.

KANE, C. J., HEBDA, P. A., MANSBRIDGE, J. N. & HANAWALT, P. C. 1991. Direct evidence for spatial and temporal regulation of transforming growth factor beta 1 expression during cutaneous wound healing. *J Cell Physiol,* 148**,** 157-73.

KANG, S., KIM, K., NOH, J. Y., JUNG, Y., BAE, O. N., LIM, K. M. & CHUNG, J. H. 2016. Simvastatin induces the apoptosis of normal vascular smooth muscle through the disruption of actin integrity via the impairment of RhoA/Rac-1 activity. *Thromb Haemost,* 116**,** 496-505.

KECHAGIA, J. Z., EZRA, D. G., BURTON, M. J. & BAILLY, M. 2016. Fibroblasts profiling in scarring trachoma identifies IL-6 as a functional component of a fibroblast-macrophage pro-fibrotic and pro-inflammatory feedback loop. *Sci Rep,* 6**,** 28261.

KESSENBROCK, K., PLAKS, V. & WERB, Z. 2010. Matrix metalloproteinases: regulators of the tumor microenvironment. *Cell,* 141**,** 52-67.

KHANNA, N., FANG, Y., YOON, M. S. & CHEN, J. 2013. XPLN is an endogenous inhibitor of mTORC2. *Proc Natl Acad Sci U S A,* 110**,** 15979-84.

KHAW, P. T., CHIANG, M., SHAH, P., SII, F., LOCKWOOD, A. & KHALILI, A. 2012. Enhanced trabeculectomy: the Moorfields Safer Surgery System. *Dev Ophthalmol,* 50**,** 1-28.
KHERADMAND, F., WERNER, E., TREMBLE, P., SYMONS, M. & WERB, Z. 1998. Role of Rac1 and oxygen radicals in collagenase-1 expression induced by cell shape change. *Science,* 280**,** 898-902.
KLEE, S., LEHMANN, M., WAGNER, D. E., BAARSMA, H. A. & KONIGSHOFF, M. 2016. WISP1 mediates IL-6-dependent proliferation in primary human lung fibroblasts. *Sci Rep,* 6**,** 20547.
KOBAYASHI, T., TANAKA, K., FUJITA, T., UMEZAWA, H., AMANO, H., YOSHIOKA, K., NAITO, Y., HATANO, M., KIMURA, S., TATSUMI, K. & KASUYA, Y. 2015. Bidirectional role of IL-6 signal in pathogenesis of lung fibrosis. *Respir Res,* 16**,** 99.
KOHRMANN, A., KAMMERER, U., KAPP, M., DIETL, J. & ANACKER, J. 2009. Expression of matrix metalloproteinases (MMPs) in primary human breast cancer and breast cancer cell lines: New findings and review of the literature. *BMC Cancer,* 9**,** 188.
KONDO, T. & ISHIDA, Y. 2010. Molecular pathology of wound healing. *Forensic Sci Int,* 203**,** 93-8.
KOTTLER, U. B., JUNEMANN, A. G., AIGNER, T., ZENKEL, M., RUMMELT, C. & SCHLOTZER-SCHREHARDT, U. 2005. Comparative effects of TGF-beta 1 and TGF-beta 2 on extracellular matrix production, proliferation, migration, and collagen contraction of human Tenon's capsule fibroblasts in pseudoexfoliation and primary open-angle glaucoma. *Exp Eye Res,* 80**,** 121-34.
KOZMA, R., AHMED, S., BEST, A. & LIM, L. 1995. The Ras-related protein Cdc42Hs and bradykinin promote formation of peripheral actin microspikes and filopodia in Swiss 3T3 fibroblasts. *Mol Cell Biol,* 15**,** 1942-52.
KRUITHOF, E. K., BAKER, M. S. & BUNN, C. L. 1995. Biological and clinical aspects of plasminogen activator inhibitor type 2. *Blood,* 86**,** 4007-24.
KUMAR, S., COENEN, M. J., SCHERER, P. E. & BAHN, R. S. 2004. Evidence for enhanced adipogenesis in the orbits of patients with Graves' ophthalmopathy. *J Clin Endocrinol Metab,* 89**,** 930-5.
LAMBERT, C. A., COLIGE, A. C., MUNAUT, C., LAPIERE, C. M. & NUSGENS, B. V. 2001. Distinct pathways in the over-expression of matrix metalloproteinases in human fibroblasts by relaxation of mechanical tension. *Matrix Biol,* 20**,** 397-408.
LARSEN, C. G., ANDERSON, A. O., APPELLA, E., OPPENHEIM, J. J. & MATSUSHIMA, K. 1989. The neutrophil-activating protein (NAP-1) is also chemotactic for T lymphocytes. *Science,* 243**,** 1464-6.
LAUFS, U., KILTER, H., KONKOL, C., WASSMANN, S., BOHM, M. & NICKENIG, G. 2002. Impact of HMG CoA reductase inhibition on small GTPases in the heart. *Cardiovasc Res,* 53**,** 911-20.
LEASK, A. 2010. Potential therapeutic targets for cardiac fibrosis: TGFbeta, angiotensin, endothelin, CCN2, and PDGF, partners in fibroblast activation. *Circ Res,* 106**,** 1675-80.
LEASK, A. & ABRAHAM, D. J. 2004. TGF-beta signaling and the fibrotic response. *Faseb j,* 18**,** 816-27.
LEI, L., ZHONG, X. N., HE, Z. Y., ZHAO, C. & SUN, X. J. 2015. IL-21 induction of CD4+ T cell differentiation into Th17 cells contributes to bleomycin-induced fibrosis in mice. *Cell Biol Int,* 39**,** 388-99.
LEMAITRE, V. & D'ARMIENTO, J. 2006. Matrix metalloproteinases in development and disease. *Birth Defects Res C Embryo Today,* 78**,** 1-10.
LETTERIO, J. J. & ROBERTS, A. B. 1998. Regulation of immune responses by TGF-beta. *Annu Rev Immunol,* 16**,** 137-61.

LEVAY, M., KROBERT, K. A., WITTIG, K., VOIGT, N., BERMUDEZ, M., WOLBER, G., DOBREV, D., LEVY, F. O. & WIELAND, T. 2013. NSC23766, a widely used inhibitor of Rac1 activation, additionally acts as a competitive antagonist at muscarinic acetylcholine receptors. *J Pharmacol Exp Ther,* 347**,** 69-79.

LI, H., EZRA, D. G., BURTON, M. J. & BAILLY, M. 2013. Doxycycline prevents matrix remodeling and contraction by trichiasis-derived conjunctival fibroblasts. *Invest Ophthalmol Vis Sci,* 54**,** 4675-82.

LIAO, J., WOLFMAN, J. C. & WOLFMAN, A. 2003. K-ras regulates the steady-state expression of matrix metalloproteinase 2 in fibroblasts. *J Biol Chem,* 278**,** 31871-8.

LIAO, P., GEORGAKOPOULOS, D., KOVACS, A., ZHENG, M., LERNER, D., PU, H., SAFFITZ, J., CHIEN, K., XIAO, R. P., KASS, D. A. & WANG, Y. 2001. The *in vivo* role of p38 MAP kinases in cardiac remodeling and restrictive cardiomyopathy. *Proc Natl Acad Sci U S A,* 98**,** 12283-8.

LIM, Y. S. & KIM, W. R. 2008. The global impact of hepatic fibrosis and end-stage liver disease. *Clin Liver Dis,* 12**,** 733-46, vii.

LIMB, G. A., MATTER, K., MURPHY, G., CAMBREY, A. D., BISHOP, P. N., MORRIS, G. E. & KHAW, P. T. 2005. Matrix metalloproteinase-1 associates with intracellular organelles and confers resistance to lamin A/C degradation during apoptosis. *Am J Pathol,* 166**,** 1555-63.

LIU, S., KAPOOR, M. & LEASK, A. 2009. Rac1 expression by fibroblasts is required for tissue repair *in vivo*. *Am J Pathol,* 174**,** 1847-56.

LIU, Y., XIAO, W. & TEMPLETON, D. M. 2014. Cadmium-induced aggregation of iron regulatory protein-1. *Toxicology,* 324**,** 108-15.

LOHI, J., WILSON, C. L., ROBY, J. D. & PARKS, W. C. 2001. Epilysin, a novel human matrix metalloproteinase (MMP-28) expressed in testis and keratinocytes and in response to injury. *J Biol Chem,* 276**,** 10134-44.

LV, J., ZENG, J., ZHAO, W., CHENG, Y., ZHANG, L., CAI, S., HU, G. & CHEN, Y. 2017. Cdc42 regulates LPS-induced proliferation of primary pulmonary microvascular endothelial cells via ERK pathway. *Microvasc Res,* 109**,** 45-53.

MA, B., ZHU, Z., HOMER, R. J., GERARD, C., STRIETER, R. & ELIAS, J. A. 2004. The C10/CCL6 chemokine and CCR1 play critical roles in the pathogenesis of IL-13-induced inflammation and remodeling. *J Immunol,* 172**,** 1872-81.

MACIA, E., EHRLICH, M., MASSOL, R., BOUCROT, E., BRUNNER, C. & KIRCHHAUSEN, T. 2006. Dynasore, a cell-permeable inhibitor of dynamin. *Dev Cell,* 10**,** 839-50.

MAHALE, A., OTHMAN, M. W., AL SHAHWAN, S., AL JADAAN, I., OWAYDHA, O., KHAN, Z. & EDWARD, D. P. 2015. Altered expression of fibrosis genes in capsules of failed Ahmed glaucoma valve implants. *PLoS One,* 10**,** e0122409.

MAJNO, G., GABBIANI, G., HIRSCHEL, B. J., RYAN, G. B. & STATKOV, P. R. 1971. Contraction of granulation tissue *in vitro*: similarity to smooth muscle. *Science,* 173**,** 548-50.

MANTRAVADI, A. V. & VADHAR, N. 2015. Glaucoma. *Prim Care,* 42**,** 437-49.

MARCHENKO, G. N. & STRONGIN, A. Y. 2001. MMP-28, a new human matrix metalloproteinase with an unusual cysteine-switch sequence is widely expressed in tumors. *Gene,* 265**,** 87-93.

MARTIN-MARTIN, B., TOVELL, V., DAHLMANN-NOOR, A. H., KHAW, P. T. & BAILLY, M. 2011. The effect of MMP inhibitor GM6001 on early fibroblast-mediated collagen matrix contraction is correlated to a decrease in cell protrusive activity. *Eur J Cell Biol,* 90**,** 26-36.

MARTIN, P. 1997. Wound healing--aiming for perfect skin regeneration. *Science,* 276**,** 75-81.

MARTIN, P. & LEIBOVICH, S. J. 2005. Inflammatory cells during wound repair: the good, the bad and the ugly. *Trends Cell Biol,* 15**,** 599-607.
MATEOS, J., LOURIDO, L., FERNANDEZ-PUENTE, P., CALAMIA, V., FERNANDEZ-LOPEZ, C., OREIRO, N., RUIZ-ROMERO, C. & BLANCO, F. J. 2012. Differential protein profiling of synovial fluid from rheumatoid arthritis and osteoarthritis patients using LC-MALDI TOF/TOF. *J Proteomics,* 75**,** 2869-78.
MATHESON, S. F., HU, K. Q., BROUNS, M. R., SORDELLA, R., VANDERHEIDE, J. D. & SETTLEMAN, J. 2006. Distinct but overlapping functions for the closely related p190 RhoGAPs in neural development. *Dev Neurosci,* 28**,** 538-50.
MCCOLGAN, P. & SHARMA, P. 2009. Polymorphisms of matrix metalloproteinases 1, 2, 3 and 9 and susceptibility to lung, breast and colorectal cancer in over 30,000 subjects. *Int J Cancer,* 125**,** 1473-8.
MEDCALF, R. L. & STASINOPOULOS, S. J. 2005. The undecided serpin. The ins and outs of plasminogen activator inhibitor type 2. *Febs j,* 272**,** 4858-67.
MENEGHIN, A. & HOGABOAM, C. M. 2007. Infectious disease, the innate immune response, and fibrosis. *J Clin Invest,* 117**,** 530-8.
MENG, X. M., HUANG, X. R., XIAO, J., CHEN, H. Y., ZHONG, X., CHUNG, A. C. & LAN, H. Y. 2012. Diverse roles of TGF-beta receptor II in renal fibrosis and inflammation *in vivo* and *in vitro*. *J Pathol,* 227**,** 175-88.
MERCER, B. A., KOLESNIKOVA, N., SONETT, J. & D'ARMIENTO, J. 2004. Extracellular regulated kinase/mitogen activated protein kinase is up-regulated in pulmonary emphysema and mediates matrix metalloproteinase-1 induction by cigarette smoke. *J Biol Chem,* 279**,** 17690-6.
MESHEL, A. S., WEI, Q., ADELSTEIN, R. S. & SHEETZ, M. P. 2005. Basic mechanism of three-dimensional collagen fibre transport by fibroblasts. *Nat Cell Biol,* 7**,** 157-64.
MEZZANO, S. A., RUIZ-ORTEGA, M. & EGIDO, J. 2001. Angiotensin II and renal fibrosis. *Hypertension,* 38**,** 635-8.
MIDWOOD, K. S., WILLIAMS, L. V. & SCHWARZBAUER, J. E. 2004. Tissue repair and the dynamics of the extracellular matrix. *Int J Biochem Cell Biol,* 36**,** 1031-7.
MILANO, A., PENDERGRASS, S. A., SARGENT, J. L., GEORGE, L. K., MCCALMONT, T. H., CONNOLLY, M. K. & WHITFIELD, M. L. 2008. Molecular subsets in the gene expression signatures of scleroderma skin. *PLoS One,* 3**,** e2696.
MILLARD, T. H., SHARP, S. J. & MACHESKY, L. M. 2004. Signalling to actin assembly via the WASP (Wiskott-Aldrich syndrome protein)-family proteins and the Arp2/3 complex. *Biochem J,* 380**,** 1-17.
MILLER, M. H., GRIERSON, I., UNGER, W. I. & HITCHINGS, R. A. 1989. Wound healing in an animal model of glaucoma fistulizing surgery in the rabbit. *Ophthalmic Surg,* 20**,** 350-7.
MILLER, T., YANG, F., WISE, C. E., MENG, F., PRIESTER, S., MUNSHI, M. K., GUERRIER, M., DOSTAL, D. E. & GLASER, S. S. 2011. Simvastatin stimulates apoptosis in cholangiocarcinoma by inhibition of Rac1 activity. *Dig Liver Dis,* 43**,** 395-403.
MIRASTSCHIJSKI, U., HAAKSMA, C. J., TOMASEK, J. J. & AGREN, M. S. 2004. Matrix metalloproteinase inhibitor GM 6001 attenuates keratinocyte migration, contraction and myofibroblast formation in skin wounds. *Exp Cell Res,* 299**,** 465-75.
MIYAMOTO, S., TERAMOTO, H., COSO, O. A., GUTKIND, J. S., BURBELO, P. D., AKIYAMA, S. K. & YAMADA, K. M. 1995. Integrin function: molecular hierarchies of cytoskeletal and signaling molecules. *J Cell Biol,* 131**,** 791-805.

MONTALVO-ORTIZ, B. L., CASTILLO-PICHARDO, L., HERNANDEZ, E., HUMPHRIES-BICKLEY, T., DE LA MOTA-PEYNADO, A., CUBANO, L. A., VLAAR, C. P. & DHARMAWARDHANE, S. 2012. Characterization of EHop-016, novel small molecule inhibitor of Rac GTPase. *J Biol Chem,* 287**,** 13228-38.

MOORE, B. B., KOLODSICK, J. E., THANNICKAL, V. J., COOKE, K., MOORE, T. A., HOGABOAM, C., WILKE, C. A. & TOEWS, G. B. 2005. CCR2-mediated recruitment of fibrocytes to the alveolar space after fibrotic injury. *Am J Pathol,* 166**,** 675-84.

MORTON, L. M. & PHILLIPS, T. J. 2016. Wound healing and treating wounds: Differential diagnosis and evaluation of chronic wounds. *J Am Acad Dermatol,* 74**,** 589-605; quiz 605-6.

MOZAFFARIEH, M., GRIESHABER, M. C. & FLAMMER, J. 2008. Oxygen and blood flow: players in the pathogenesis of glaucoma. *Mol Vis,* 14**,** 224-33.

MULLIN, B. H., MAMOTTE, C., PRINCE, R. L. & WILSON, S. G. 2014. Influence of ARHGEF3 and RHOA knockdown on ACTA2 and other genes in osteoblasts and osteoclasts. *PLoS One,* 9**,** e98116.

NAGASE, H. & WOESSNER, J. F., JR. 1999. Matrix metalloproteinases. *J Biol Chem,* 274**,** 21491-4.

NAIK, V. M., NAIK, M. N., GOLDBERG, R. A., SMITH, T. J. & DOUGLAS, R. S. 2010. Immunopathogenesis of thyroid eye disease: emerging paradigms. *Surv Ophthalmol,* 55**,** 215-26.

NEARY, R., WATSON, C. J. & BAUGH, J. A. 2015. Epigenetics and the overhealing wound: the role of DNA methylation in fibrosis. *Fibrogenesis Tissue Repair,* 8**,** 18.

NEGRE-AMINOU, P., VAN ERCK, M., VAN LEEUWEN, R. E., COLLARD, J. G. & COHEN, L. H. 2001. Differential effect of simvastatin on various signal transduction intermediates in cultured human smooth muscle cells. *Biochem Pharmacol,* 61**,** 991-8.

NGUYEN, C. H., SENFTER, D., BASILIO, J., HOLZNER, S., STADLER, S., KRIEGER, S., HUTTARY, N., MILOVANOVIC, D., VIOLA, K., SIMONITSCH-KLUPP, I., JAGER, W., DE MARTIN, R. & KRUPITZA, G. 2015. NF-kappaB contributes to MMP1 expression in breast cancer spheroids causing paracrine PAR1 activation and disintegrations in the lymph endothelial barrier *in vitro*. *Oncotarget,* 6**,** 39262-75.

NOBES, C. D. & HALL, A. 1995. Rho, rac, and cdc42 GTPases regulate the assembly of multimolecular focal complexes associated with actin stress fibers, lamellipodia, and filopodia. *Cell,* 81**,** 53-62.

NOBES, C. D. & HALL, A. 1999. Rho GTPases control polarity, protrusion, and adhesion during cell movement. *J Cell Biol,* 144**,** 1235-44.

NUZZI, R. & TRIDICO, F. 2017. Glaucoma: Biological Trabecular and Neuroretinal Pathology with Perspectives of Therapy Innovation and Preventive Diagnosis. *Front Neurosci,* 11**,** 494.

OHUCHI, E., IMAI, K., FUJII, Y., SATO, H., SEIKI, M. & OKADA, Y. 1997. Membrane type 1 matrix metalloproteinase digests interstitial collagens and other extracellular matrix macromolecules. *J Biol Chem,* 272**,** 2446-51.

ORDONEZ, M., RIVERA, I. G., PRESA, N. & GOMEZ-MUNOZ, A. 2016. Implication of matrix metalloproteinases 2 and 9 in ceramide 1-phosphate-stimulated macrophage migration. *Cell Signal,* 28**,** 1066-74.

ORGILL, D. 2009. Biomaterials for treating skin loss.

PAGE-MCCAW, A., EWALD, A. J. & WERB, Z. 2007. Matrix metalloproteinases and the regulation of tissue remodelling. *Nat Rev Mol Cell Biol,* 8**,** 221-33.

PALLISTER, C. & WATSON, M. 2011. *Haematology,* Banbury, Scion.

PARDO, A. & SELMAN, M. 2006. Matrix metalloproteases in aberrant fibrotic tissue remodeling. *Proc Am Thorac Soc,* 3**,** 383-8.

PARIKH, R. S., PARIKH, S. R., NAVIN, S., ARUN, E. & THOMAS, R. 2008. Practical approach to medical management of glaucoma. *Indian J Ophthalmol,* 56**,** 223-30.
PARKS, W. C., WILSON, C. L. & LOPEZ-BOADO, Y. S. 2004. Matrix metalloproteinases as modulators of inflammation and innate immunity. *Nat Rev Immunol,* 4**,** 617-29.
PARRENO, J. & HART, D. A. 2009. Molecular and mechano-biology of collagen gel contraction mediated by human MG-63 cells: involvement of specific intracellular signaling pathways and the cytoskeleton. *Biochem Cell Biol,* 87**,** 895-904.
PATHAK, R. & DERMARDIROSSIAN, C. 2013. GEF-H1: orchestrating the interplay between cytoskeleton and vesicle trafficking. *Small GTPases,* 4**,** 174-9.
PAULINO DO NASCIMENTO, A. & MONTE-ALTO-COSTA, A. 2011. Both obesity-prone and obesity-resistant rats present delayed cutaneous wound healing. *Br J Nutr,* 106**,** 603-11.
PAVLASOVA, G., BORSKY, M., SEDA, V., CERNA, K., OSICKOVA, J., DOUBEK, M., MAYER, J., CALOGERO, R., TRBUSEK, M., POSPISILOVA, S., DAVIDS, M. S., KIPPS, T. J., BROWN, J. R. & MRAZ, M. 2016. Ibrutinib inhibits CD20 upregulation on CLL B cells mediated by the CXCR4/SDF-1 axis. *Blood,* 128**,** 1609-13.
PEPPER, M. S. 2001. Extracellular proteolysis and angiogenesis. *Thromb Haemost,* 86**,** 346-55.
PHILLIPS, R. J., BURDICK, M. D., HONG, K., LUTZ, M. A., MURRAY, L. A., XUE, Y. Y., BELPERIO, J. A., KEANE, M. P. & STRIETER, R. M. 2004. Circulating fibrocytes traffic to the lungs in response to CXCL12 and mediate fibrosis. *J Clin Invest,* 114**,** 438-46.
PIETRUSZEWSKA, W., BOJANOWSKA-POZNIAK, K. & KOBOS, J. 2016. Matrix metalloproteinases MMP1, MMP2, MMP9 and their tissue inhibitors TIMP1, TIMP2, TIMP3 in head and neck cancer: an immunohistochemical study. *Otolaryngol Pol,* 70**,** 32-43.
PILCHER, B. K., DUMIN, J., SCHWARTZ, M. J., MAST, B. A., SCHULTZ, G. S., PARKS, W. C. & WELGUS, H. G. 1999. Keratinocyte collagenase-1 expression requires an epidermal growth factor receptor autocrine mechanism. *J Biol Chem,* 274**,** 10372-81.
PILCHER, B. K., DUMIN, J. A., SUDBECK, B. D., KRANE, S. M., WELGUS, H. G. & PARKS, W. C. 1997. The activity of collagenase-1 is required for keratinocyte migration on a type I collagen matrix. *J Cell Biol,* 137**,** 1445-57.
POPP, M. P., LIU, L., TIMMERS, A., ESSON, D. W., SHIROMA, L., MEYERS, C., BERCELI, S., TAO, M., WISTOW, G., SCHULTZ, G. S. & SHERWOOD, M. B. 2007. Development of a microarray chip for gene expression in rabbit ocular research. *Mol Vis,* 13**,** 164-73.
PORTER, R. A., BROWN, R. A., EASTWOOD, M., OCCLESTON, N. L. & KHAW, P. T. 1998. Ultrastructural changes during contraction of collagen lattices by ocular fibroblasts. *Wound Repair Regen,* 6**,** 157-66.
PRAEFCKE, G. J. & MCMAHON, H. T. 2004. The dynamin superfamily: universal membrane tubulation and fission molecules? *Nat Rev Mol Cell Biol,* 5**,** 133-47.
RAHIMI, M., GEORGE, J. & TANG, C. 2010. EGFR variant-mediated invasion by enhanced CXCR4 expression through transcriptional and post-translational mechanisms. *Int J Cancer,* 126**,** 1850-60.
RAJAH, R., KATZ, L., NUNN, S., SOLBERG, P., BEERS, T. & COHEN, P. 1995. Insulin-like growth factor binding protein (IGFBP) proteases: functional regulators of cell growth. *Prog Growth Factor Res,* 6**,** 273-84.
RAJAK, S. N., COLLIN, J. R. & BURTON, M. J. 2012. Trachomatous trichiasis and its management in endemic countries. *Surv Ophthalmol,* 57**,** 105-35.

RASCHE, H. 2001. Haemostasis and thrombosis: an overview. *European Heart Journal Supplements,* 3**,** Q3-Q7.
RATTNER, A. & NATHANS, J. 2006. Macular degeneration: recent advances and therapeutic opportunities. *Nat Rev Neurosci,* 7**,** 860-72.
REN, H., WANG, Z., ZHANG, S., MA, H., WANG, Y., JIA, L. & LI, Y. 2016. IL-17A Promotes the Migration and Invasiveness of Colorectal Cancer Cells Through NF-kappaB-Mediated MMP Expression. *Oncol Res,* 23**,** 249-56.
RESNIKOFF, S., PASCOLINI, D., ETYA'ALE, D., KOCUR, I., PARARAJASEGARAM, R., POKHAREL, G. P. & MARIOTTI, S. P. 2004. Global data on visual impairment in the year 2002. *Bull World Health Organ,* 82**,** 844-51.
REUNANEN, N., WESTERMARCK, J., HAKKINEN, L., HOLMSTROM, T. H., ELO, I., ERIKSSON, J. E. & KAHARI, V. M. 1998. Enhancement of fibroblast collagenase (matrix metalloproteinase-1) gene expression by ceramide is mediated by extracellular signal-regulated and stress-activated protein kinase pathways. *J Biol Chem,* 273**,** 5137-45.
RHEE, S. & GRINNELL, F. 2006. P21-activated kinase 1: convergence point in PDGF- and LPA-stimulated collagen matrix contraction by human fibroblasts. *J Cell Biol,* 172**,** 423-32.
RIDLEY, A. J. 2006. Rho GTPases and actin dynamics in membrane protrusions and vesicle trafficking. *Trends Cell Biol,* 16**,** 522-9.
RIDLEY, A. J. 2013. RhoA, RhoB and RhoC have different roles in cancer cell migration. *J Microsc,* 251**,** 242-9.
RIDLEY, A. J. 2015. Rho GTPase signalling in cell migration. *Curr Opin Cell Biol,* 36**,** 103-12.
RIDLEY, A. J. & HALL, A. 1992. The small GTP-binding protein rho regulates the assembly of focal adhesions and actin stress fibers in response to growth factors. *Cell,* 70**,** 389-99.
RIDLEY, A. J., PATERSON, H. F., JOHNSTON, C. L., DIEKMANN, D. & HALL, A. 1992. The small GTP-binding protein rac regulates growth factor-induced membrane ruffling. *Cell,* 70**,** 401-10.
RITCHIE, M. E., PHIPSON, B., WU, D., HU, Y., LAW, C. W., SHI, W. & SMYTH, G. K. 2015. limma powers differential expression analyses for RNA-sequencing and microarray studies. *Nucleic Acids Res,* 43**,** e47.
ROHANI, M. G., PILCHER, B. K., CHEN, P. & PARKS, W. C. 2014. Cdc42 inhibits ERK-mediated collagenase-1 (MMP-1) expression in collagen-activated human keratinocytes. *J Invest Dermatol,* 134**,** 1230-7.
ROSENKRANZ, S. 2004. TGF-beta1 and angiotensin networking in cardiac remodeling. *Cardiovasc Res,* 63**,** 423-32.
ROSENKRANZ, S., FLESCH, M., AMANN, K., HAEUSELER, C., KILTER, H., SEELAND, U., SCHLUTER, K. D. & BOHM, M. 2002. Alterations of beta-adrenergic signaling and cardiac hypertrophy in transgenic mice overexpressing TGF-beta(1). *Am J Physiol Heart Circ Physiol,* 283**,** H1253-62.
ROY, P., PETROLL, W. M., CAVANAGH, H. D., CHUONG, C. J. & JESTER, J. V. 1997. An *in vitro* force measurement assay to study the early mechanical interaction between corneal fibroblasts and collagen matrix. *Exp Cell Res,* 232**,** 106-17.
ROY, P., PETROLL, W. M., CHUONG, C. J., CAVANAGH, H. D. & JESTER, J. V. 1999. Effect of cell migration on the maintenance of tension on a collagen matrix. *Ann Biomed Eng,* 27**,** 721-30.
RUSSO, F. P., ALISON, M. R., BIGGER, B. W., AMOFAH, E., FLOROU, A., AMIN, F., BOU-GHARIOS, G., JEFFERY, R., IREDALE, J. P. & FORBES, S. J. 2006. The bone marrow functionally contributes to liver fibrosis. *Gastroenterology,* 130**,** 1807-21.

RUSZCZAK, Z. 2003. Effect of collagen matrices on dermal wound healing. *Adv Drug Deliv Rev,* 55**,** 1595-611.
SAARIALHO-KERE, U., KERKELA, E., JAHKOLA, T., SUOMELA, S., KESKI-OJA, J. & LOHI, J. 2002. Epilysin (MMP-28) expression is associated with cell proliferation during epithelial repair. *J Invest Dermatol,* 119**,** 14-21.
SAARIALHO-KERE, U. K., KOVACS, S. O., PENTLAND, A. P., OLERUD, J. E., WELGUS, H. G. & PARKS, W. C. 1993. Cell-matrix interactions modulate interstitial collagenase expression by human keratinocytes actively involved in wound healing. *J Clin Invest,* 92**,** 2858-66.
SAENZ-MORALES, D., CONDE, E., ESCRIBESE, M. M., GARCIA-MARTOS, M., ALEGRE, L., BLANCO-SANCHEZ, I. & GARCIA-BERMEJO, M. L. 2009. ERK1/2 mediates cytoskeleton and focal adhesion impairment in proximal epithelial cells after renal ischemia. *Cell Physiol Biochem,* 23**,** 285-94.
SAPPINO, A. P., SCHURCH, W. & GABBIANI, G. 1990. Differentiation repertoire of fibroblastic cells: expression of cytoskeletal proteins as marker of phenotypic modulations. *Lab Invest,* 63**,** 144-61.
SATO, M., MURAGAKI, Y., SAIKA, S., ROBERTS, A. B. & OOSHIMA, A. 2003. Targeted disruption of TGF-beta1/Smad3 signaling protects against renal tubulointerstitial fibrosis induced by unilateral ureteral obstruction. *J Clin Invest,* 112**,** 1486-94.
SAWHNEY, R. K. & HOWARD, J. 2002. Slow local movements of collagen fibers by fibroblasts drive the rapid global self-organization of collagen gels. *J Cell Biol,* 157**,** 1083-91.
SAWHNEY, R. K. & HOWARD, J. 2004. Molecular dissection of the fibroblast-traction machinery. *Cell Motil Cytoskeleton,* 58**,** 175-85.
SCHMIDT, A. & HALL, A. 2002. Guanine nucleotide exchange factors for Rho GTPases: turning on the switch. *Genes Dev,* 16**,** 1587-609.
SERBANOVIC-CANIC, J., CVEJIC, A., SORANZO, N., STEMPLE, D. L., OUWEHAND, W. H. & FRESON, K. 2011. Silencing of RhoA nucleotide exchange factor, ARHGEF3, reveals its unexpected role in iron uptake. *Blood,* 118**,** 4967-76.
SERRA, N., ROSALES, R., MASANA, L. & VALLVE, J. C. 2015. Simvastatin Increases Fibulin-2 Expression in Human Coronary Artery Smooth Muscle Cells via RhoA/Rho-Kinase Signaling Pathway Inhibition. *PLoS One,* 10**,** e0133875.
SETHI, K. K., YANNAS, I. V., MUDERA, V., EASTWOOD, M., MCFARLAND, C. & BROWN, R. A. 2002. Evidence for sequential utilization of fibronectin, vitronectin, and collagen during fibroblast-mediated collagen contraction. *Wound Repair Regen,* 10**,** 397-408.
SHIPLEY, J. M., WESSELSCHMIDT, R. L., KOBAYASHI, D. K., LEY, T. J. & SHAPIRO, S. D. 1996. Metalloelastase is required for macrophage-mediated proteolysis and matrix invasion in mice. *Proc Natl Acad Sci U S A,* 93**,** 3942-6.
SHIRAKATA, Y., KIMURA, R., NANBA, D., IWAMOTO, R., TOKUMARU, S., MORIMOTO, C., YOKOTA, K., NAKAMURA, M., SAYAMA, K., MEKADA, E., HIGASHIYAMA, S. & HASHIMOTO, K. 2005. Heparin-binding EGF-like growth factor accelerates keratinocyte migration and skin wound healing. *J Cell Sci,* 118**,** 2363-70.
SHUTES, A., ONESTO, C., PICARD, V., LEBLOND, B., SCHWEIGHOFFER, F. & DER, C. J. 2007. Specificity and mechanism of action of EHT 1864, a novel small molecule inhibitor of Rac family small GTPases. *J Biol Chem,* 282**,** 35666-78.
SINGER, A. J. & CLARK, R. A. 1999. Cutaneous wound healing. *N Engl J Med,* 341**,** 738-46.

SIPES, N. S., FENG, Y., GUO, F., LEE, H. O., CHOU, F. S., CHENG, J., MULLOY, J. & ZHENG, Y. 2011. Cdc42 regulates extracellular matrix remodeling in three dimensions. *J Biol Chem,* 286**,** 36469-77.
SMITH, R. E., STRIETER, R. M., ZHANG, K., PHAN, S. H., STANDIFORD, T. J., LUKACS, N. W. & KUNKEL, S. L. 1995. A role for C-C chemokines in fibrotic lung disease. *J Leukoc Biol,* 57**,** 782-7.
SPUUL, P., CIUFICI, P., VEILLAT, V., LECLERCQ, A., DAUBON, T., KRAMER, I. J. & GENOT, E. 2014. Importance of RhoGTPases in formation, characteristics, and functions of invadosomes. *Small GTPases,* 5**,** e28195.
STADELMANN, W. K., DIGENIS, A. G. & TOBIN, G. R. 1998. Physiology and healing dynamics of chronic cutaneous wounds. *Am J Surg,* 176**,** 26s-38s.
STERNLICHT, M. D. & WERB, Z. 2001. How matrix metalloproteinases regulate cell behavior. *Annu Rev Cell Dev Biol,* 17**,** 463-516.
STRIETER, R. M., GOMPERTS, B. N. & KEANE, M. P. 2007. The role of CXC chemokines in pulmonary fibrosis. *J Clin Invest,* 117**,** 549-56.
SUZUKI, K., ENGHILD, J. J., MORODOMI, T., SALVESEN, G. & NAGASE, H. 1990. Mechanisms of activation of tissue procollagenase by matrix metalloproteinase 3 (stromelysin). *Biochemistry,* 29**,** 10261-70.
TAKAI, Y., SASAKI, T., TANAKA, K. & NAKANISHI, H. 1995. Rho as a regulator of the cytoskeleton. *Trends Biochem Sci,* 20**,** 227-31.
TAMASSIA, N., CASTELLUCCI, M., ROSSATO, M., GASPERINI, S., BOSISIO, D., GIACOMELLI, M., BADOLATO, R., CASSATELLA, M. A. & BAZZONI, F. 2010. Uncovering an IL-10-dependent NF-kappaB recruitment to the IL-1ra promoter that is impaired in STAT3 functionally defective patients. *Faseb j,* 24**,** 1365-75.
TAO, L., LI, Z., LIN, L., LEI, Y., HONGYUAN, Y., HONGWEI, J., YANG, L. & CHUIZE, K. 2015. MMP1, 2, 3, 7, and 9 gene polymorphisms and urinary cancer risk: a meta-analysis. *Genet Test Mol Biomarkers,* 19**,** 548-55.
TAYLOR, M. P., KOYUNCU, O. O. & ENQUIST, L. W. 2011. Subversion of the actin cytoskeleton during viral infection. *Nat Rev Microbiol,* 9**,** 427-39.
TCHERKEZIAN, J. & LAMARCHE-VANE, N. 2007. Current knowledge of the large RhoGAP family of proteins. *Biol Cell,* 99**,** 67-86.
TEMPLETON, D. M. & LIU, Y. 2013. Effects of cadmium on the actin cytoskeleton in renal mesangial cells. *Can J Physiol Pharmacol,* 91**,** 1-7.
THANNICKAL, V. J., LEE, D. Y., WHITE, E. S., CUI, Z., LARIOS, J. M., CHACON, R., HOROWITZ, J. C., DAY, R. M. & THOMAS, P. E. 2003. Myofibroblast differentiation by transforming growth factor-beta1 is dependent on cell adhesion and integrin signaling via focal adhesion kinase. *J Biol Chem,* 278**,** 12384-9.
THOMSON, A. W. & LOTZE, M. T. 2003. The cytokine handbook.
TOMAR, A., LIM, S. T., LIM, Y. & SCHLAEPFER, D. D. 2009. A FAK-p120RasGAP-p190RhoGAP complex regulates polarity in migrating cells. *J Cell Sci,* 122**,** 1852-62.
TOMASEK, J. J., GABBIANI, G., HINZ, B., CHAPONNIER, C. & BROWN, R. A. 2002. Myofibroblasts and mechano-regulation of connective tissue remodelling. *Nat Rev Mol Cell Biol,* 3**,** 349-63.
TOVELL, V. E., CHAU, C. Y., KHAW, P. T. & BAILLY, M. 2012. Rac1 inhibition prevents tissue contraction and MMP mediated matrix remodeling in the conjunctiva. *Invest Ophthalmol Vis Sci,* 53**,** 4682-91.
TOVELL, V. E., DAHLMANN-NOOR, A. H., KHAW, P. T. & BAILLY, M. 2011. Advancing the treatment of conjunctival scarring: a novel ex vivo model. *Arch Ophthalmol,* 129**,** 619-27.
TROJANOWSKA, M. 2009. Noncanonical transforming growth factor beta signaling in scleroderma fibrosis. *Curr Opin Rheumatol,* 21**,** 623-9.

TSUBAKIMOTO, K., MATSUMOTO, K., ABE, H., ISHII, J., AMANO, M., KAIBUCHI, K. & ENDO, T. 1999. Small GTPase RhoD suppresses cell migration and cytokinesis. *Oncogene,* 18**,** 2431-40.
TYBULEWICZ, V. L. & HENDERSON, R. B. 2009. Rho family GTPases and their regulators in lymphocytes. *Nat Rev Immunol,* 9**,** 630-44.
URRUTIA, R., HENLEY, J. R., COOK, T. & MCNIVEN, M. A. 1997. The dynamins: redundant or distinct functions for an expanding family of related GTPases? *Proc Natl Acad Sci U S A,* 94**,** 377-84.
VAN STEENSEL, L., PARIDAENS, D., DINGJAN, G. M., VAN DAELE, P. L., VAN HAGEN, P. M., KUIJPERS, R. W., VAN DEN BOSCH, W. A., DREXHAGE, H. A., HOOIJKAAS, H. & DIK, W. A. 2010. Platelet-derived growth factor-BB: a stimulus for cytokine production by orbital fibroblasts in Graves' ophthalmopathy. *Invest Ophthalmol Vis Sci,* 51**,** 1002-7.
VEGA, F. M., COLOMBA, A., REYMOND, N., THOMAS, M. & RIDLEY, A. J. 2012. RhoB regulates cell migration through altered focal adhesion dynamics. *Open Biol,* 2**,** 120076.
VERSTEEG, H. H., HEEMSKERK, J. W., LEVI, M. & REITSMA, P. H. 2013. New fundamentals in hemostasis. *Physiol Rev,* 93**,** 327-58.
VISSE, R. & NAGASE, H. 2003. Matrix metalloproteinases and tissue inhibitors of metalloproteinases: structure, function, and biochemistry. *Circ Res,* 92**,** 827-39.
WALAKOVITS, L. A., MOORE, V. L., BHARDWAJ, N., GALLICK, G. S. & LARK, M. W. 1992. Detection of stromelysin and collagenase in synovial fluid from patients with rheumatoid arthritis and posttraumatic knee injury. *Arthritis Rheum,* 35**,** 35-42.
WALKER, H. K., HALL, W. D. & HURST, J. W. 1990. *Clinical methods : the history, physical, and laboratory examinations,* Boston, Butterworths.
WANG, W., KOKA, V. & LAN, H. Y. 2005. Transforming growth factor-beta and Smad signalling in kidney diseases. *Nephrology (Carlton),* 10**,** 48-56.
WARGA, R. M., WICKLUND, A., WEBSTER, S. E. & KANE, D. A. 2016. Progressive loss of RacGAP1/ogre activity has sequential effects on cytokinesis and zebrafish development. *Dev Biol,* 418**,** 307-22.
WATANABE, T., BARKER, T. A. & BERK, B. C. 2005. Angiotensin II and the endothelium: diverse signals and effects. *Hypertension,* 45**,** 163-9.
WEI, J., FANG, F., LAM, A. P., SARGENT, J. L., HAMBURG, E., HINCHCLIFF, M. E., GOTTARDI, C. J., ATIT, R., WHITFIELD, M. L. & VARGA, J. 2012. Wnt/beta-catenin signaling is hyperactivated in systemic sclerosis and induces Smad-dependent fibrotic responses in mesenchymal cells. *Arthritis Rheum,* 64**,** 2734-45.
WEI, J., MELICHIAN, D., KOMURA, K., HINCHCLIFF, M., LAM, A. P., LAFYATIS, R., GOTTARDI, C. J., MACDOUGALD, O. A. & VARGA, J. 2011. Canonical Wnt signaling induces skin fibrosis and subcutaneous lipoatrophy: a novel mouse model for scleroderma? *Arthritis Rheum,* 63**,** 1707-17.
WELLS, A. P., BUNCE, C. & KHAW, P. T. 2004. Flap and suture manipulation after trabeculectomy with adjustable sutures: titration of flow and intraocular pressure in guarded filtration surgery. *J Glaucoma,* 13**,** 400-6.
WERB, Z., TREMBLE, P. M., BEHRENDTSEN, O., CROWLEY, E. & DAMSKY, C. H. 1989. Signal transduction through the fibronectin receptor induces collagenase and stromelysin gene expression. *J Cell Biol,* 109**,** 877-89.
WERNER, E., KHERADMAND, F., ISBERG, R. R. & WERB, Z. 2001. Phagocytosis mediated by Yersinia invasin induces collagenase-1 expression in rabbit synovial fibroblasts through a proinflammatory cascade. *J Cell Sci,* 114**,** 3333-43.

WERNER, E. & WERB, Z. 2002. Integrins engage mitochondrial function for signal transduction by a mechanism dependent on Rho GTPases. *J Cell Biol,* 158**,** 357-68.
WILLIAMS, J. A., CHEN, X. & SABBATINI, M. E. 2009. Small G proteins as key regulators of pancreatic digestive enzyme secretion. *Am J Physiol Endocrinol Metab,* 296**,** E405-14.
WILLIS, B. C., DUBOIS, R. M. & BOROK, Z. 2006. Epithelial origin of myofibroblasts during fibrosis in the lung. *Proc Am Thorac Soc,* 3**,** 377-82.
WINKLES, J. A. 1998. Serum- and polypeptide growth factor-inducible gene expression in mouse fibroblasts. *Prog Nucleic Acid Res Mol Biol,* 58**,** 41-78.
WONG, T. T., MEAD, A. L. & KHAW, P. T. 2003. Matrix metalloproteinase inhibition modulates postoperative scarring after experimental glaucoma filtration surgery. *Invest Ophthalmol Vis Sci,* 44**,** 1097-103.
WONG, T. T., SETHI, C., DANIELS, J. T., LIMB, G. A., MURPHY, G. & KHAW, P. T. 2002. Matrix metalloproteinases in disease and repair processes in the anterior segment. *Surv Ophthalmol,* 47**,** 239-56.
WU, H., ROSSI, G. & BRENNWALD, P. 2008. The ghost in the machine: small GTPases as spatial regulators of exocytosis. *Trends Cell Biol,* 18**,** 397-404.
WYNN, T. A. 2004. Fibrotic disease and the T(H)1/T(H)2 paradigm. *Nat Rev Immunol,* 4**,** 583-94.
WYNN, T. A. 2007. Common and unique mechanisms regulate fibrosis in various fibroproliferative diseases. *J Clin Invest,* 117**,** 524-9.
WYNN, T. A. 2008. Cellular and molecular mechanisms of fibrosis. *J Pathol,* 214**,** 199-210.
XU, J., CLARK, R. A. & PARKS, W. C. 2001. p38 mitogen-activated kinase is a bidirectional regulator of human fibroblast collagenase-1 induction by three-dimensional collagen lattices. *Biochem J,* 355**,** 437-47.
XU, J., ZUTTER, M. M., SANTORO, S. A. & CLARK, R. A. 1998. A three-dimensional collagen lattice activates NF-kappaB in human fibroblasts: role in integrin alpha2 gene expression and tissue remodeling. *J Cell Biol,* 140**,** 709-19.
XU, S. W., LIU, S., EASTWOOD, M., SONNYLAL, S., DENTON, C. P., ABRAHAM, D. J. & LEASK, A. 2009. Rac inhibition reverses the phenotype of fibrotic fibroblasts. *PLoS One,* 4**,** e7438.
YAN, W., WANG, P., ZHAO, C. X., TANG, J., XIAO, X. & WANG, D. W. 2009. Decorin gene delivery inhibits cardiac fibrosis in spontaneously hypertensive rats by modulation of transforming growth factor-beta/Smad and p38 mitogen-activated protein kinase signaling pathways. *Hum Gene Ther,* 20**,** 1190-200.
YU-WAI-MAN, C. & KHAW, P. T. 2015. Developing novel anti-fibrotic therapeutics to modulate post-surgical wound healing in glaucoma: big potential for small molecules. *Expert Rev Ophthalmol,* 10**,** 65-76.
YU-WAI-MAN, C. & KHAW, P. T. 2016. Personalized Medicine in Ocular Fibrosis: Myth or Future Biomarkers. *Adv Wound Care (New Rochelle),* 5**,** 390-402.
ZEISBERG, E. M., TARNAVSKI, O., ZEISBERG, M., DORFMAN, A. L., MCMULLEN, J. R., GUSTAFSSON, E., CHANDRAKER, A., YUAN, X., PU, W. T., ROBERTS, A. B., NEILSON, E. G., SAYEGH, M. H., IZUMO, S. & KALLURI, R. 2007. Endothelial-to-mesenchymal transition contributes to cardiac fibrosis. *Nat Med,* 13**,** 952-61.
ZHANG, A., YAN, T., WANG, K., HUANG, Z. & LIU, J. 2017. PI3Kalpha isoform-dependent activation of RhoA regulates Wnt5a-induced osteosarcoma cell migration. *Cancer Cell Int,* 17**,** 27.
ZHANG, W., DU, L. & GUNST, S. J. 2010. The effects of the small GTPase RhoA on the muscarinic contraction of airway smooth muscle result from its role in regulating actin polymerization. *Am J Physiol Cell Physiol,* 299**,** C298-306.

ZHANG, W., HUANG, Y., WU, Y. & GUNST, S. J. 2015. A novel role for RhoA GTPase in the regulation of airway smooth muscle contraction. *Can J Physiol Pharmacol,* 93**,** 129-36.

ZHAO, T., ZHAO, W., CHEN, Y., LI, V. S., MENG, W. & SUN, Y. 2013. Platelet-derived growth factor-D promotes fibrogenesis of cardiac fibroblasts. *Am J Physiol Heart Circ Physiol,* 304**,** H1719-26.

ZHAO, Z. & MANSER, E. 2015. Myotonic dystrophy kinase-related Cdc42-binding kinases (MRCK), the ROCK-like effectors of Cdc42 and Rac1. *Small GTPases,* 6**,** 81-8.

ZHU, Z., MA, B., ZHENG, T., HOMER, R. J., LEE, C. G., CHARO, I. F., NOBLE, P. & ELIAS, J. A. 2002. IL-13-induced chemokine responses in the lung: role of CCR2 in the pathogenesis of IL-13-induced inflammation and remodeling. *J Immunol,* 168**,** 2953-62.

ZUO, F., KAMINSKI, N., EUGUI, E., ALLARD, J., YAKHINI, Z., BEN-DOR, A., LOLLINI, L., MORRIS, D., KIM, Y., DELUSTRO, B., SHEPPARD, D., PARDO, A., SELMAN, M. & HELLER, R. A. 2002. Gene expression analysis reveals matrilysin as a key regulator of pulmonary fibrosis in mice and humans. *Proc Natl Acad Sci U S A,* 99**,** 6292-7.

ZURAWSKI, S. M., VEGA, F., JR., HUYGHE, B. & ZURAWSKI, G. 1993. Receptors for interleukin-13 and interleukin-4 are complex and share a novel component that functions in signal transduction. *Embo j,* 12**,** 2663-70.

Appendix

Gene symbols and descriptions

A2M	alpha-2-macroglobulin
ACACA	acetyl-CoA carboxylase alpha
ACE	angiotensin I converting enzyme
ACTA1	actin, alpha 1, skeletal muscle
ACTA2	actin, alpha 2, smooth muscle, aorta
ADAM22	ADAM metallopeptidase domain 22
ADH1B	alcohol dehydrogenase 1B (class I), beta polypeptide
AKR1B1	aldo-keto reductase family 1 member B
APBB1IP	amyloid beta precursor protein binding family B member 1 interacting protein
ARHGAP20	Rho GTPase activating protein 20
ARID5B	AT-rich interaction domain 5B
C14orf180	chromosome 14 open reading frame 180
C1R	complement C1r
CD34	CD34 molecule
CDH2	cadherin 2
CDKN1C	cyclin dependent kinase inhibitor 1C
CDKN2C	cyclin dependent kinase inhibitor 2C
CLEC11A	C-type lectin domain family 11 member A
CLEC3B	C-type lectin domain family 3 member B
CMBL	carboxymethylenebutenolidase homolog
COL12A1	collagen type XII alpha 1 chain
COL14A1	collagen type XIV alpha 1 chain
COLEC12	collectin subfamily member 12
CPM	carboxypeptidase M
CRABP2	cellular retinoic acid binding protein 2
CXCR4	C-X-C motif chemokine receptor 4
CYP1B1	cytochrome P450 family 1 subfamily B member 1
DAAM1	dishevelled associated activator of morphogenesis 1
DMD	dystrophin
DUXA	double homeobox A
EPB41L2	erythrocyte membrane protein band 4.1 like 2
ERAP2	endoplasmic reticulum aminopeptidase 2
F10	coagulation factor X
F2RL1	F2R like trypsin receptor 1
FABP4	fatty acid binding protein 4
FADS2	fatty acid desaturase 2
FAT4	FAT atypical cadherin 4
FGF2	fibroblast growth factor 2
FGFR2	fibroblast growth factor receptor 2
FLT1	fms related tyrosine kinase 1
FOS	Fos proto-oncogene, AP-1 transcription factor subunit

FOXL2	forkhead box L2
GATA6	GATA binding protein 6
GKN1	gastrokine 1
HBEGF	heparin binding EGF like growth factor
HLTF	helicase like transcription factor
HSPB8	heat shock protein family B (small) member 8
ICAM1	intercellular adhesion molecule 1
IFIT1	interferon induced protein with tetratricopeptide repeats 1
IGFBP6	insulin like growth factor binding protein 6
IGSF10	immunoglobulin superfamily member 10
IL11	interleukin 11
IL1R1	interleukin 1 receptor type 1
IL1RN	interleukin 1 receptor antagonist
IL36B	interleukin 36, beta
IL6	interleukin 6
IL7R	interleukin 7 receptor
ITGBL1	integrin subunit beta like 1
JUN	Jun proto-oncogene, AP-1 transcription factor subunit
KCND2	potassium voltage-gated channel subfamily D member 2
KCNT2	potassium sodium-activated channel subfamily T member 2
KIT	KIT proto-oncogene receptor tyrosine kinase
KRT6A	keratin 6A
LDLR	low density lipoprotein receptor
LECT1	leukocyte cell derived chemotaxin 1
LIF	leukemia inhibitory factor
LILRA4	leukocyte immunoglobulin like receptor A4
LPL	lipoprotein lipase
MAP6	microtubule associated protein 6
MASP1	mannan binding lectin serine peptidase 1
MATN2	matrilin 2
MID1	midline 1
MMP1	matrix metallopeptidase 1
MMP10	matrix metallopeptidase 10
MMP16	matrix metallopeptidase 16
MMP3	matrix metallopeptidase 3
MYL1	myosin light chain 1
MYOC	myocilin
NEFL	neurofilament, light polypeptide
NOG	noggin
OLR1	oxidized low density lipoprotein receptor 1
PARD3B	par-3 family cell polarity regulator beta
PCLO	piccolo presynaptic cytomatrix protein
PEX2	peroxisomal biogenesis factor 2
PLAUR	plasminogen activator, urokinase receptor
PLOD2	procollagen-lysine,2-oxoglutarate 5-dioxygenase 2
PLXDC2	plexin domain containing 2

PSAT1	phosphoserine aminotransferase 1
PTGER3	prostaglandin E receptor 3
PTGS2	prostaglandin-endoperoxide synthase 2
PTHLH	parathyroid hormone like hormone
PZP	PZP, alpha-2-macroglobulin like
RASGRF2	Ras protein specific guanine nucleotide releasing factor 2
SEMA6A	semaphorin 6A
SERPINA3	serpin family A member 3
SERPINB2	serpin family B member 2
SERPINE2	serpin family E member 2
SFRP4	secreted frizzled related protein 4
SGK1	serum/glucocorticoid regulated kinase 1
SLC20A1	solute carrier family 20 member 1
SLC2A14	solute carrier family 2 member 14
SMAD2	SMAD family member 2
SMAD3	SMAD family member 3
SPTBN1	spectrin beta, non-erythrocytic 1
SQLE	squalene epoxidase
ST8SIA4	ST8 alpha-N-acetyl-neuraminide alpha-2,8-sialyltransferase 4
SVEP1	sushi, von Willebrand factor type A, EGF and pentraxin domain containing 1
SYNPO2	synaptopodin 2
SYTL5	synaptotagmin like 5
TFPI2	tissue factor pathway inhibitor 2
TGFBR3	transforming growth factor beta receptor 3
THBD	thrombomodulin
THBS2	thrombospondin 2
TNFSF4	tumor necrosis factor superfamily member 4
TNNI2	troponin I2, fast skeletal type
TNXB	tenascin XB
TSHZ2	teashirt zinc finger homeobox 2
UCHL1	ubiquitin C-terminal hydrolase L1
VEGFA	vascular endothelial growth factor A
VEGFC	vascular endothelial growth factor C
WISP3	WNT1 inducible signaling pathway protein 3
ZFP36L2	ZFP36 ring finger protein like 2